UiT The Arctic University of Norway

Faculty of Science and Technology, Department of Chemistry

Antibiotic Resistance Breakers: Design and Synthesis of OXA-48 Inhibitors

Harald Magnussen

KJE-3900, Master's thesis in Molecular Sciences, May 2020

I. Abstract

Antibiotic resistance is threatening the achievements of modern medicine and will evidentially lead to a situation, in which we stand helpless against common bacterial infections. The largest and most widely used group of antibiotics are the β-lactams. One of the major resistance determinants against β-lactam antibiotics is the expression of hydrolytic enzymes, called β-lactamases (BLs). The main concern of BLs is that they are threatening the most important group of β-lactam antibiotics, carbapenems.

A plausible solution to overcome the resistance introduced by BLs is the combination of antibiotics and inhibitors. In this thesis efforts are made towards deactivation of a BL, more specifically a carbapenemase, called OXA-48 by the synthesis of inhibitors. The synthetic strategies and computational foundations for a new fragment library are presented within, using four main reactions: Suzuki-Miyaura cross coupling, reductive amination, tetrazole formation and ester hydrolysis.

New inhibitors were synthesized and tested towards the activity of OXA-48, the most promising showing IC_{50} value of 3.3 μM.

II. Acknowledgements

There are several people whom I would like to thank for contributing with invaluable help and support during my work on this thesis. First, I would like to thank my supervisor Prof. Annette Bayer for presenting me with an inspiring and challenging project. I am thankful for all the guidance and it has been a joy to work under your supervision.

Secondly, I would like to thank my co-supervisor Aya Hashim Mohammed Ismael and Manuel Karl Langer for the endless help you have provided, but primarily for all the good times.

I would also like to thank Prof. Hanna-Kirsti Schrøder Leiros and Susann Skagseth for the collaboration and your contribution to this project.

My appreciation further goes to the CHOCO group, in particular Marc Boomgaren and Alexandra Kondratieva for the patience and help you have given me. I would also like to thank the university's engineers Jostein Johansen and Truls Ingebrigtsen for your expertise.

A big thanks to all my friends and my fellow master students Aleksi Juhu Kosonen, Bente Barge, Martin Pettersen, Magnus Burkow and Unni Mette Nordang for the last years.

Lastly, I want to thank my amazing family, Kari, Morten, Espen and Olav for the unwavering support.

Harald Magnussen, Tromsø, May 2020

III. Abbreviation

^{13}C-NMR	Carbon-13 nuclear magnetic resonance
^{1}H-NMR	Proton nuclear magnetic resonance
BHT	Butylated hydroxytoluene
BL	β-lactamases
BMIM-PF_6	1-Butyl-3-methylimidazolium hexafluorophosphate
DBO	Diazabicyclooctanone
DCE	1,2-Dichloroethane
DCM	Dichloromethane
DIPEA	*N*,*N*-Diisopropylethylamine
DMF	Dimethylformamide
DMSO	Dimethylsulfoxid
EDG	Electron donating group
EH	Ester hydrolysis
EWG	Electron withdrawing group
FBDD	Fragment based drug discovery
FBLD	Fragment based lead discovery
GC-MS	Gas chromatography with mass spectrometry detector
HMBC	Heteronuclear multiple bond coherence
HPLC	High pressure/performance liquid chromatography
HR-MS	High resolution mass spectroscopy
IPA	Isopropyl alcohol
IR	Infrared spectroscopy
LLE	Lipophilic ligand efficiency
MBL	Metallo β-lactamases
MW	Microwave
NMR	Nuclear magnetic resonance
OTF	Trifluoromethanesulfonate
OXA	Oxacillinase
OXA-48	Oxacillinase-48

PDB	Protein data bank
RA	Reductive amination
R_f	Retention factor
Rt	Retention time
SBL	Serine β-lactamases
SFC	Supercritical fluid chromatography
SMC	Suzuki-Miyaura cross coupling
S_N2	Bimolecular nucleophilic substitution
STAB	Sodium triacetoxyborohydride
TF	Tetrazole formation
TFA	Trifluoroacetic acid
THF	Tetrahydrofuran
TLC	Thin layer chromatography
$TMSN_3$	Trimethyl silyl azide

IV. Table of Contents

I. Abstract i

II. Acknowledgements iii

III. Abbreviation v

IV. Table of Contents vii

V. List of Tables xi

VI. List of Figures xi

VII. List of Schemes xii

1. Introduction and aim of thesis 1

2. Background 3

2.1 General background 3

2.2 Computational software 10

2.2.1 SeeSAR 10

2.3 Relevant Reactions 10

2.3.1 Metal-catalysed Suzuki-Miyaura cross coupling 11

2.3.2 Reductive Amination 14

2.3.3 Tetrazole formation 16

2.3.4 Ester hydrolysis 17

3. Results and discussion 19

3.1 Computational Results 19

3.1.1 A note on SeeSAR 19

3.1.2 Exploration phase 20

3.1.3 N-alkyl substituents 21

3.1.4 Elongation 22

3.1.5 New *meta* substituents 23

3.2 Synthetic Strategy 24

3.2.1 Synthetic strategy for new *meta* substituents 27

3.2.2 Synthetic strategy for elongation 27
3.3 Synthetic results 28
3.3.1 Suzuki-Miyaura Cross coupling 28
3.3.2 Reductive Amination 32
3.3.3 Tetrazole formation 38
3.3.4 Hydrolysis of carboxylic esters 44
4. Biological Results 47
5. Future Outlook 51
6. Conclusion 55
7. References 57
8. Experimental Procedures 65
8.1 Suzuki-Miayura Cross coupling 66
8.1.1 General Procedure 1 66
8.2 Reductive Amination 68
8.2.1 Reductive Amination Screening Data 68
8.2.2 General Procedure 2 70
8.3 Tetrazole formation 73
8.3.1 General Procedure 3 73
8.4 Hydrolysis 77
8.4.1 General procedure 4 77
9. Appendices 81
9.1 Suzuki Miyaura cross coupling Spectra 81
9.1.1 4'-amino-3'-(methoxycarbonyl)-[1,1'-biphenyl]-4-sulfonic acid (16) 81
9.1.2 Methyl 4-amino-4'-cyano-[1,1'-biphenyl]-3-carboxylate (13) 83
9.1.3 Methyl 2-(benzylamino)-5-bromobenzoate (11) 85
9.2 Reductive amination Spectra 87
9.2.1 Methyl 4-(benzylamino)-4'-cyano-[1,1'-biphenyl]-3-carboxylate (18) 87

9.2.2 Methyl 4'-cyano-4-((3-methoxybenzyl)amino)-[1,1'-biphenyl]-3-carboxylate (22)…….. 89

9.2.3 Methyl 4'-cyano-4-((3,5-dimethoxybenzyl)amino)-[1,1'-biphenyl]-3-carboxylate (26) …….. 91

9.2.4 Methyl 4'-cyano-4-((thiophen-2-ylmethyl)amino)-[1,1'-biphenyl]-3-carboxylate (23) …….. 94

9.2.5 Methyl 4-((2-bromo-6-fluorobenzyl)amino)-4'-cyano-[1,1'-biphenyl]-3-carboxylate (25)..... 96

9.3 Tetrazole formation 98

9.3.1 Methyl 4-amino-4'-(1*H*-tetrazol-5-yl)-[1,1'-biphenyl]-3-carboxylate (14)..... 98

9.3.2 Methyl 4-((3,5-dimethoxybenzyl)amino)-4'-(1*H*-tetrazol-5-yl)-[1,1'-biphenyl]-3-carboxylate (27)..... 100

9.3.3 Methyl 4-(((1-methyl-1*H*-imidazol-5-yl)methyl)amino)-4'-(1*H*-tetrazol-5-yl)-[1,1'-biphenyl]-3-carboxylate (28) 104

9.3.4 Methyl 4'-(1*H*-tetrazol-5-yl)-4-((thiophen-2-ylmethyl)amino)-[1,1'-biphenyl]-3-carboxylate (28)..... 110

9.3.5 Methyl 4-((3-methoxybenzyl)amino)-4'-(1*H*-tetrazol-5-yl)-[1,1'-biphenyl]-3-carboxylate (29)..... 114

9.4 Hydrolysis Spectra..... 118

9.4.1 4-amino-4'-cyano-[1,1'-biphenyl]-3-carboxylic acid (35)..... 118

9.4.2 4-amino-4'-(1*H*-tetrazol-5-yl)-[1,1'-biphenyl]-3-carboxylic acid (34)..... 122

9.4.3 4-(benzylamino)-4'-(1*H*-tetrazol-5-yl)-[1,1'-biphenyl]-3-carboxylic acid (33) 125

9.4.4 4-((3,5-dimethoxybenzyl)amino)-4'-(1*H*-tetrazol-5-yl)-[1,1'-biphenyl]-3-carboxylic acid (32)..... 127

9.5 Suzuki-Miyaura Screening Spectra 131

9.6 SeeSAR experimental..... 134

V. List of Tables

Table 1. Screening results of Suzuki-Miyaura cross coupling. 29
Table 2. Reductive amination screening results. 34

VI. List of Figures

Figure 1. Overview of the new and previous work carried out on substituted benzoic acids as inhibitors for OXA-48. 2
Figure 2. Oxacillin (**2**) with highlighted β-lactam ring. 3
Figure 3. Overview of reported OXA-48 inhibitors. 7
Figure 4. Fragment in binding pocket, showing relevant interactions with residues in the binding site. 8
Figure 5. Interactions of 4'-(1H-tetrazol-5-yl)-[1,1'-biphenyl]-3-carboxylic acid (**1**, Y = H) in the binding site of OXA-48. Reprinted with permission from Akhter et al. Copyright 2018 European Journal of medical chemistry.[7] 8
Figure 6. Surface representation of 4'-(1H-tetrazol-5-yl)-[1,1'-biphenyl]-3-carboxylic acid in OXA-48, used with permission from S. Akther, doctoral thesis, [2018] 9
Figure 7. Examples of common Pd-catalysts and ligands used for SMC. 14
Figure 8. Scaffold (**1**) used for further exploration in the 2-ortho position 20
Figure 9. Secondary N-alkyl as 2-ortho extension. An unprecedented H-bond to Lys 116 via a water molecule was observed. 21
Figure 10. Promising N-alkyl substituted fragments as suggested by SeeSAR. 22
Figure 11. Investigated carbon chain linkers. R=aryls, heterocycles etc. 23
Figure 12. Scaffold with elongated ortho substituent in the binding site of OXA-48. 23
Figure 13. Target molecules for synthesis. 24
Figure 14. Methyl 2-amino-bromobenzoate (**9**); starting material for the synthetic plan. 25
Figure 15. Target for elongation of the 2-ortho popsition of scaffold **1** 27
Figure 16. Reductive amination results, n.d. = Not isolated as the crude was directly submitted for tetrazole formation. 37
Figure 17. Modified scaffold (**14**) with highlighted amphiphile characteristics and different ionization forms according to pH, red = Hydrophilic, blue = Hydrophobic. 39
Figure 18. Tetrazole carbon (blue circle), often not observed in ^{13}C NMR 43
Figure 19. 2D NMR of compound **25** showing missing tetrazole carbon. 44
Figure 20. Compounds for biological testing with corresponding IC50 graphs. 47

Figure 21.SeeSAR's evaluation of the two biologically tested fragments 48
Figure 22. SeeSAR representation of compound 51 in the binding site of OXA-48. 49
Figure 23. SeeSAR representation of compound 35 in the binding site of OXA-48. 50
Figure 24. Benzhydrylamine (**36**) scaffold transformation to new possible future fragment (**37**). 52
Figure 25. Benzhydrylamine (**36**) in the active site of OXA-48, showing interactions with ser 70 and ser 118. 52
Figure 26. Possible future fragment (**37**) based on benzhydrylamine in OXA-48 binding site, with nano-molar interaction. 53
Figure 27. GCMS result of reductive amination screening (entry 2, R_1 = H, R_2 = H) 69
Figure 28. Custom defined binding site around L43_D_301 inhibitor 134
Figure 29. Example list of SeeSAR results 135

VII. List of Schemes

Scheme 1. Proposed hydrolysis mechanism of Oxacillin.[14] 4
Scheme 2.Proposed mechanism for avibactam. (A) acylation of Ser70 (B) deacylation of Ser70. Reprinted with permission from Lahiri et al. (106). Copyright 2015 American Chemical Society.[32] 5
Scheme 3. General Suzuki-Miyaura cross coupling reaction. 11
Scheme 4. Suzuki-Miyaura cross coupling reaction of aryl halide with boronic acid/derivatives. 11
Scheme 5. Catalytic cycle of Suzuki-Miyaura cross-coupling. 12
Scheme 6. Overview of reductive amination. 14
Scheme 7. Reaction mechanism of reductive amination with $NaBH_3CN$. 15
Scheme 8. Overview of tetrazole formation starting from a nitrile. 16
Scheme 9. Catalytic cycle of tetrazole formation.[99] 17
Scheme 10. Overview of ester hydrolysis. 17
Scheme 11. Acid catalyzed hydrolysis.[74b] 18
Scheme 12. Base catalyzed hydrolysis.[74a] 18
Scheme 13. Synthetic strategy 1. 26
Scheme 14. Synthetic strategy 2. 26
Scheme 15. Proposed plan for synthesizing new meta-substituent. 27
Scheme 16. Proposed plan for carbon chain linkers. 28

Scheme 17. Synthesis of methyl 4-amino-4'-cyano-[1,1'-biphenyl]-3-carboxylate (**13**) using SMC. 30
Scheme 18. Synthesis of methyl 4-(benzylamino)-4'-cyano-[1,1'-biphenyl]-3-carboxylate (**18**) using SMC. 31
Scheme 19. Synthesis of new meta substituent - sulfonic acid (**16**). 31
Scheme 20. Attempted reductive amination on methyl 4-amino-4'-(1H-tetrazol-5-yl)-[1,1'-biphenyl]-3-carboxylate (**14**). 32
Scheme 21. Resonance structures of 3-hydroxy-4-methoxybenzaldehyde. 35
Scheme 22. Synthesis of methyl 4'-cyano-4-((3-methoxybenzyl) amino)-[1,1'-biphenyl]-3-carboxylate (**22**) as a control reaction of reductive amination screening results. on = overnight r.t = room temperature. 36
Scheme 23. Overview of reaction conditions for tetrazole formation. * = 13% impurities found for compound 27. N.d = not determined. 38
Scheme 24. Synthesis of methyl 4-(((1-methyl-1H-imidazol-5-yl)methyl)amino)-4'-(1H-tetrazol-5-yl)-[1,1'-biphenyl]-3-carboxylate (**20**). 41
Scheme 25. Attempted reductive amination on methyl 4-amino-4'-(1H-tetrazol-5-yl)-[1,1'-biphenyl]-3-carboxylate (**14**). 43
Scheme 26. Overview of ester hydrolysis reactions. 45
Scheme 27. Attempted synthesis of methyl 4-((3,5-dimethoxybenzyl)amino)-4'-(1H-tetrazol-5-yl)-[1,1'-biphenyl]-3-carboxylate (**32**) by acid catalyzed hydrolysis. 46
Scheme 28. Reductive amination screening, R1= H or MeOCH3, R2 = H or OH. 68

1. Introduction and aim of thesis

"*Without urgent action, we are heading for a post-antibiotic era, in which common infections and minor injuries can once again kill.*" – 2018, World Health Organization.[1]

The global need for rapid solutions to restore the potency of our last-line defense antibiotics is at an all-time high. A growing number of infections like tuberculosis, salmonellosis and pneumonia are becoming harder, and sometimes impossible, to treat.[2-4] Antibiotic resistance is a direct threat to the achievements of modern medicine. The spread of resistance will have profound impact on our society and will lead to a situation in which "*common infections and minor injuries can once again kill"*.

An important class of antibiotics are the β-lactam antibiotics. Members of this class include penicillins, carbapenems, monobactams and cephalosporins, all which share the common structural feature of a β-lactam ring.[5] Several carbapenems are our last line defense against bacterial infections but their efficiency is now threatened by emerging resistance.

An important cause of antibiotic resistance stems from continuous evolution of bacteria possessing antibiotic-deactivating enzymes. For ß-lactam antibiotics these are known as ß-lactamases (BL) and can be divided into two sub-classes, based on their mechanism of action: serine - and metallo-ß-lactamases (SBL and MBLs). Furthermore, a carbapenemase is a carbapenem hydrolysing β-lactamase and can be a SBL or a MBLs. The focus of this thesis is inhibition of a serine-carbapenemase: Oxacillinase-48 (OXA-48). OXA-48 can be found in carbapenem-resistant *Enterobacteriaceae* bacteria, which are on the high priority list of families of bacteria that pose the greatest threat to human health, partly due to its antibiotic resistance properties.

One approach to overcome the threat of β-lactamases (BL), is to synthesize new inhibitors to use in combination therapy with antibiotics. The goal of the inhibitor is to deactivate the β-lactamase (or carbapenemase), and thereby maintain the bactericidal properties of the antibiotic. The strategy of co-administration has been applied with some success in the battle of carbapenem resistance, using inhibitors like avibactam, deactivating OXA-48, and vaborbactam, deactivating KPC-2.[6]

It was previously reported by our group, that highly substituted benzoic acids show weak inhibition of OXA-48.[7] A fragment library of 3-substituted benzoic acids and 3,5-*meta*-disubstituted benzoic acids (Figure 1) was constructed, where the X-ray analysis of OXA-48: compound **1** (Protein Data Bank (PDB): 5QAV) complex shows that they bind in two overlapping binding pockets in the enzyme. The compounds showed affinity for one of the two binding pockets (from here on named INN and OUT pockets). However, no inhibitors with strong binding interaction in the OUT pocket has been reported thus far. Moreover, a docking study on X-ray structures of reported complexes indicated that an 2,5-substituted benzoic acid was more suited to occupy both pockets than the previously tested *meta*-disubstituted compounds. The fragment 4'-(1*H*-tetrazol-5-yl)-[1,1'-biphenyl]-3-carboxylic acid (**1**) (Figure 1) showed the best inhibition against OXA-48, and is the scaffold used in this thesis for the new potential 2,5-disubstituted benzoic acid inhibitors.

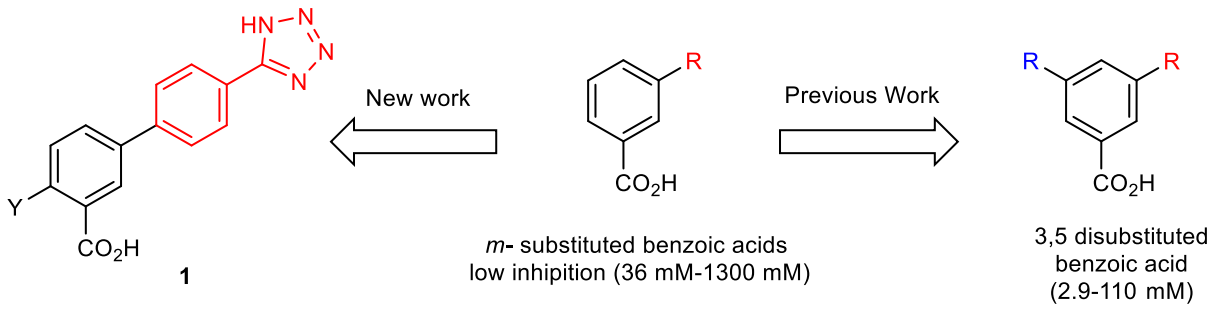

Figure 1. Overview of the new and previous work carried out on substituted benzoic acids as inhibitors for OXA-48.

In light of this, the aim of the work described in this thesis was:

- Design new fragments for OXA-48 inhibition, focusing mainly on the *ortho* position Y of 4'-(1*H*-tetrazol-5-yl)-[1,1'-biphenyl]-3-carboxylic acid (**1**).
- Develop a synthetic strategy to synthesize the fragments.
- Synthesize a library of fragments for testing performed in collaboration with The Norwegian Structural Biology Centre (NorStruct) and Universitetssykehyset Nord-Norge (UNN).

2. Background

2.1 General background

β-lactam antibiotics are the most prescribed antibiotics to date, having numerous clinical applications and uses.[8] The defining feature of all β-lactam antibiotics is the 3-carbon 1-nitrogen ring known as the β-lactam ring, outlined in Figure 2.

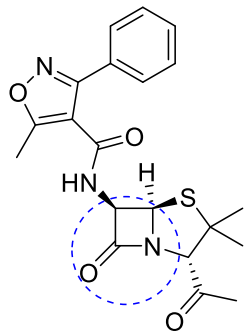

2

*Figure 2. Oxacillin (**2**) with highlighted β-lactam ring.*

The β-lactam ring allows the molecule to act as a substrate for the enzyme transpeptidase in bacteria (also known as penicillin-binding protein), instead of a natural substrate, thereby blocking the enzyme and hindering the cell wall biosynthesis.[9] The inhibition is covalent and thereby permanently blocks the enzyme.

Bacteria expresses resistance to antibiotics in several ways, one of the major resistance determinants against β-lactam antibiotics is the expression of hydrolytic enzymes.[10] These so-called β-lactamases function by hydrolysing the β-lactam ring and rendering the drug inactive. In 2018 almost 2800 unique β-lactamases had been identified.[11] They are classified into three or four groups, depending on the classification system. Namely, they are group 1 (class C) cephalosporinases; group 2 (classes A and D) broad-spectrum and extended-spectrum β-lactamases and serine carbapenemases; and group 3 (class B) metallo-β-lactamases.[12]

The focus of this thesis is on group 2, class D, the serine-carbapenemases. There are several proposed hydrolysis mechanisms for serine-carbapenemases, but all share the common feature of Serine 70 (according to DBL-numbering)[13] acting as a nucleophile (Scheme 1Scheme 1).[14, 15]

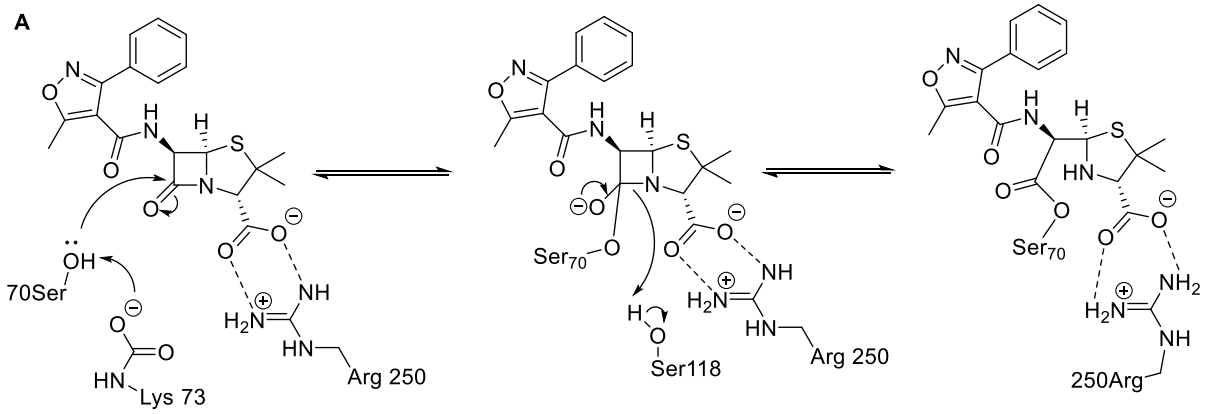

Scheme 1. Proposed hydrolysis mechanism of Oxacillin.[14]

As shown in Scheme 1, the hydroxyl group of Serine 70 acts as a nucleophile that attacks the carbonyl carbon of the β-lactam ring, cleaving the amide bond. The opening of the ring is irreversible and is common for all serine-β-lactamases. Lysine 73 is one of the neighbouring residues important to the reaction as it accepts the proton from the hydroxyl group of Serine 70. Other stabilizing residues include Arginine 250, which forms hydrogen bonds with the acid moiety of oxacillin.

One of the most important groups of BLs regarding antibiotic deactivation is class D, often referred to as the oxacillinases (OXAs). The importance is due to rapid transfers of high-level antibiotic-resistance genes to human pathogens such as *Escherichia Coli* and *Acinetobacter baumannii*.[16] OXAs hydrolyse penicillins, especially oxacillin (Figure 2, (**2**)), but are also known to inactivate carbapenem and some cephalosporins.[17]

The mechanism explained in Scheme 1 also applies to the specific class D enzyme - Oxacillinase-48, which is the main target in this thesis. OXA-48 was first identified in *Klebsiella pneumoniae*, a gram-negative bacterium in Turkey in 2001.[18] Since then, OXA-48 has been identified in several other countries, including Tunisia[19], Germany[20], Italy[21], India[22], as well as in other bacteria such as *E.Coli* and the high-risk, expanding *K. Pneumoniae* ST307.[23] Furthermore, both Turkey and Malta have reported a pandemic situation of OXA-48 producing *Enterobacteriaceae*, underlining the threat of the enzyme.[24]

In order to overcome the resistance caused by the activity of OXA-48, a combination therapy can be used.[25-27] Herein, two drugs are administered; one β-lactamase inhibitor to block OXA-48 and one known β-lactam antibiotic to carry out the clinical purposes, such as fighting the

bacteria causing an infection. The process of designing and finding new antibiotics can require a long time of development. In addition, designing new antibiotics can be a short-term solution as the bacteria could evolve and develop resistance against the new introduced antibiotic as well. Most of the drugs currently in the clinical pipeline are modifications on existing classes of antibiotics, and thereby more prone to resistance development.[28] Therefore, the combination therapy is a practical alternative that could extend the lifetime of the already known drugs.

Successful examples of combination therapy to inactivate carbapenemases or β-lactamases are meropenem/vaborbactam (deactivating KCP-2)[29] or ceftazidime/avibactam (deactivating OXA-48).[30,31] Avibactam is the first β-lactamase inhibitor without the characteristic β-lactam ring to reach the market as well as the first carbapenemase inhibitor to reach clinical use.[32] It is a diazabicyclooctanone (DBO) analogue and is approved for use in combination with ceftazidime.[33,34] Avibactam in combination with ceftazidime can be used to treat complicated intra-abdominal infections and urinary tract infections. In addition, avibactam is in phase three of clinical trials in combination with the β-lactam aztreonam.[6] It has shown inhibition for a range of β-lactamases, including OXA-48, with the proposed mechanism shown in Scheme 2.

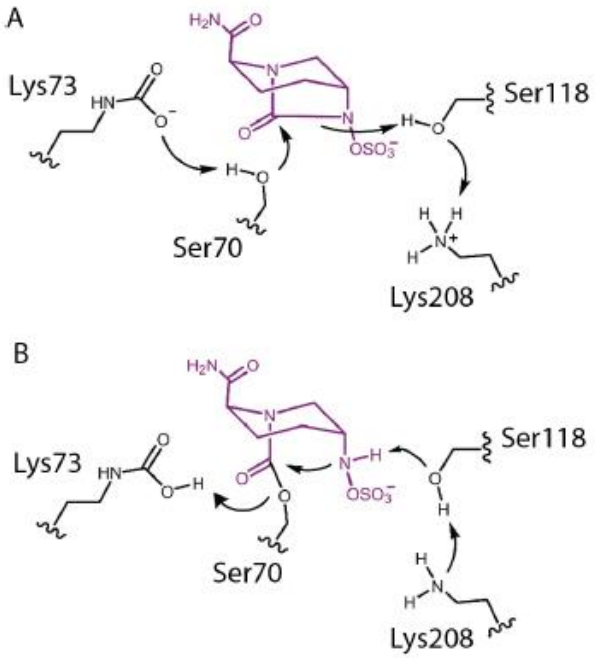

Scheme 2.Proposed mechanism for avibactam. (A) acylation of Ser70 (B) deacylation of Ser70. Reprinted with permission from Lahiri et al. (106). Copyright 2015 American Chemical Society.[32]

Lysine 73 activates Serine 70, allowing the nucleophilic attack on one of the carbonyls of avibactam (Scheme 2, A) resulting in the acylation of serine 70. Assistance from serine 118 is necessary as it acts as a proton shuttle. The reversed process, deacylation, is show in Scheme 2 B. Due to ring deacylation, the avibactam ring will be restored, which leaves the molecule intact and ready to inhibit a new enzyme.[35] Avibactam is a step in the right direction, but enzymatic resistance to the drug has already been reported, exemplifying the ongoing war on antibiotic resistance.[36]

There are also other molecules that show inhibition of OXA-48.[6] ETX2514 (**4**) seen in Figure 3, is a unique DBO that reached to clinical trials phase two in combination with sulbactam. It is important to note that these structures are not only interesting for OXA-48 inhibitor development but also show great potential for inhibition of several other β-lactamases.[6]

Another interesting group having reached clinical trials against OXA-48 are cyclic boronates.[37] Several of these have shown covalent interaction with the important Serine 70. The most noteworthy being the combination of VNRX-5133 (Figure 3 (**6**), Taniborbactam) and cefepime that has reached clinical trials phase one.[38] Vaborbactam is another cyclic boronates, which has reached clinical trials in the USA, but not against OXA-48.

Penicillanic acid sulfones derivates are promising inhibitors of OXA-48 as well but are yet to reach clinical trials. One example of these is LN-1-255 (Figure 3, (**7**)). To the best of our knowledge, there has been no crystal structures of OXA-48 with bound LN-1-255 so far. However, docking studies show that there are interactions between Arginine 250, Lysine 208, Tyrosine 211 and Threonine 209.[39] [40]

The same residue interactions were observed by Lund et al. after using a fragment based drug discovery (FBDD) approach [41] also known as fragment based lead discovery (FBLD). A FBDD approach uses small molecules (<300 Da) with favourable physiochemical properties (e.g high water solubility, high quality interactions) in order to probe a binding site for interactions. These small molecules could be developed further into bigger and more potent fragments that bind with higher affinity. Rapid determination of structure-activity relationships is one of FBDDs advantages.[42] It is commonly used in the early stages of enzyme inhibitor development as it can reveal information on moieties and structures that show inhibition, which can be further developed in combination with biological data. [43]

In 2020, Taylor et al. reported a new set of molecules based of their lead structure CDD-97 (Figure 3, (**3**)).[44] The hit molecule and its derivates has now been synthesized with two-fold increased activity compared with the initial hit. The results presented show the relevance of the topic and can be used for inspiration and ideas for new inhibitors.

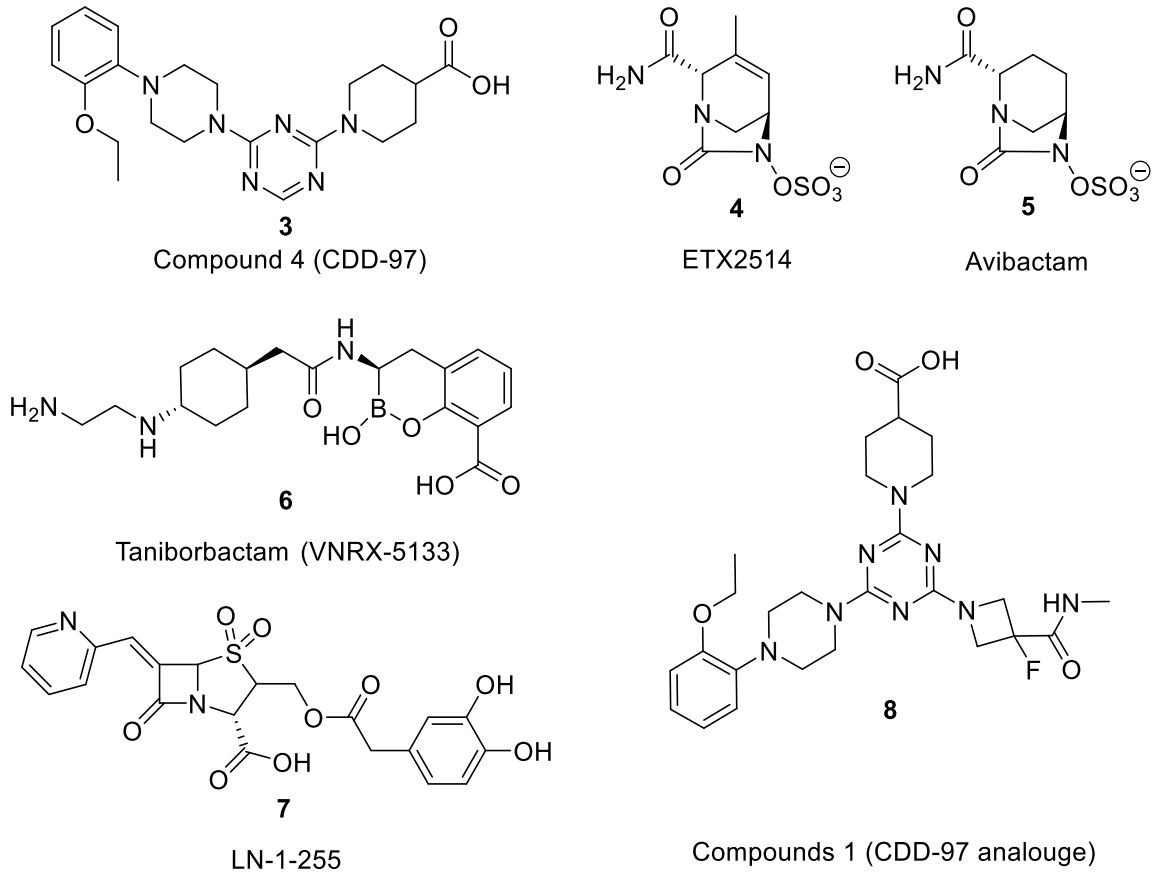

Figure 3. Overview of reported OXA-48 inhibitors.

Our group reported a fragment library consisting of 3-substituted benzoic acids and 3,5-disubstituted benzoic acids, showing inhibition of OXA-48.[7] The tested fragments showed inhibition in the micro molar range (the best disubstituted fragment had IC_{50} = 2.9 μM).[7] In 33 crystal structures of OXA-48 in complex with inhibitors, the fragments showed non-covalent bonding to Arg214, Arg250, Trp105 and Tyr211 in the binding site. As shown in Figure 4, the fragment does not bind directly to the important Ser70 but effectively blocks it from hydrolysing antibiotics by filling the binding site.

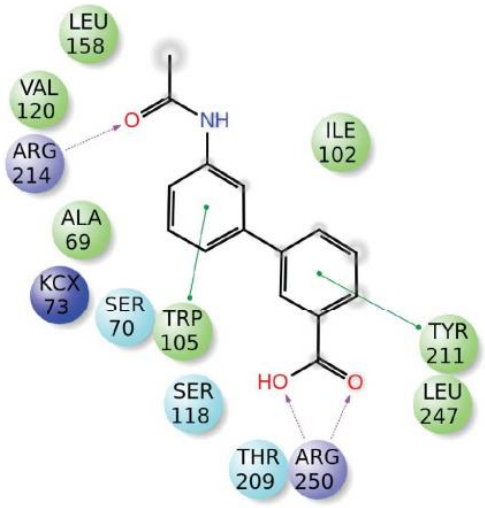

Figure 4. Fragment in binding pocket, showing relevant interactions with residues in the binding site. Reprinted with permission from Akhter et al. Copyright 2018 European Journal of medical chemistry.[7]

One of the most potent and promising fragments presented by out group was the benzoic acid with a tetrazol-5-ylphenyl substituent (IC_{50}= 36 μM) (Figure 5 (**1**, Y = H)). It showed, like most of the fragments, ionic bonding of the carboxylate group to the guanidine of Arg250 (Figure 5). The interaction resembles the observed function of the sulfamate in avibactam. Furthermore, the tetrazole substituent formed a hydrogen bond with the guanidine group of Arg214. Interestingly all other fragments showed π-π-stacking with Tyr211, which has previously been reported as an important interaction for the inhibition of OXA-48, but is not present in the case of the tetrazol-5-ylphenyl substituent.[45]

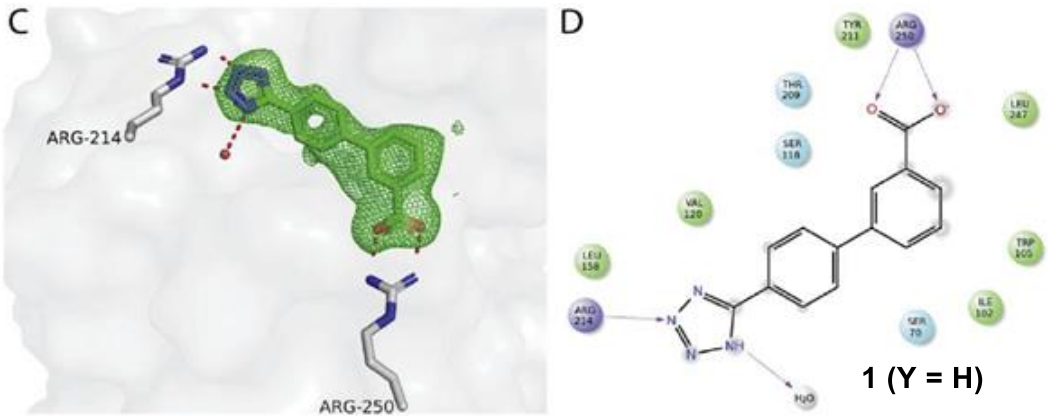

*Figure 5. Interactions of 4'-(1H-tetrazol-5-yl)-[1,1'-biphenyl]-3-carboxylic acid (**1**, Y = H) in the binding site of OXA-48. Reprinted with permission from Akhter et al. Copyright 2018 European Journal of medical chemistry.*[7]

Although having the lowest IC_{50} value in the mono-substituted series, fragment **1** (Y = H) shown in Figure 5 needs to be further improved for better inhibition. Structure based drug design (SBDD) can be further used to improve the fragment. SBDD includes selecting a structure and further evolving it to new potentially improved inhibitors based on previous enzyme:inhibitor complexes.

As mentioned, X-ray analysis of the OXA-48: compound **1** (Y = H) (PDB: 5QAV) complex showed that the substituted benzoic acids bind in two overlapping binding pockets in the enzyme (INN and OUT). An assortment of fragments with decent affinity for one of the two binding pockets (INN) had been identified, however, no inhibitors with a strong binding interaction in both pockets had been reported thus far.[7] Moreover, computational calculations based on the crystal structures performed by Akhter et al. indicated that a 2,5-substituted benzoic acid would be more suitable to accommodate both pockets than the previously tested *meta*-substituted compounds. Furthermore, Vallejo et al [40], and presented by Akhter et al (S. Akther, doctoral thesis, [2018]), suggested a future outlook for the study using 4'-(1*H*-tetrazol-5-yl)-[1,1'-biphenyl]-3-carboxylic acid (**1**, Y = H) as a scaffold and extending in the *ortho* position. The surface representation (Figure 6) shows the proposed scaffold in the active site of OXA-48 with an 2-*ortho* substituent.

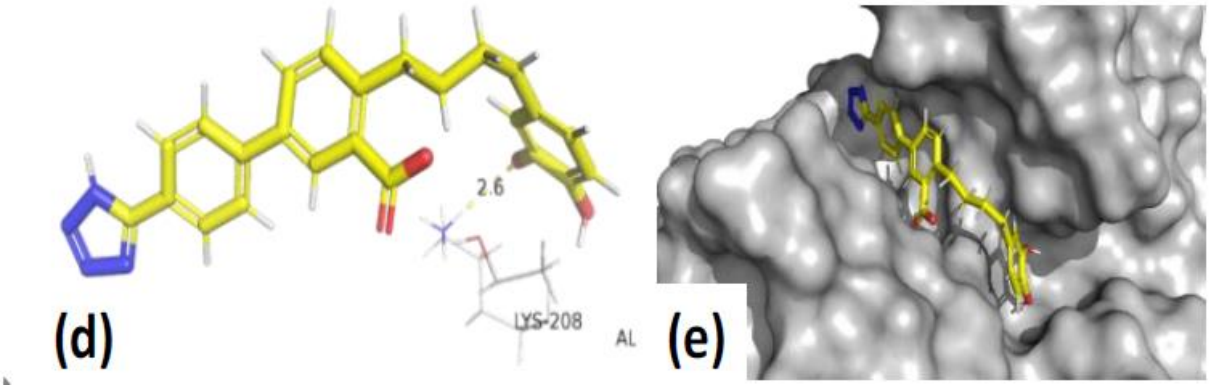

Figure 6. Surface representation of 4'-(1H-tetrazol-5-yl)-[1,1'-biphenyl]-3-carboxylic acid in OXA-48, used with permission from S. Akther, doctoral thesis, [2018]

2.2 Computational software

In silico methods are useful tools to identify new potential fragments and trends to guide the synthetic development of new inhibitors. One of the advantages of targeting an enzyme for modulating antibiotic resistance instead of looking for brand new antibiotics, is the possibility to build a suitable fragment library using structure-based drug design (SBDD) based on initial fragment-enzyme complexes. In SBDD, the next generation of potential inhibitors are designed in iterative cycles from the crystal structure data of an enzyme:inhibitor complex.

Computational modelling is a very useful tool in predicting the preferred orientation of a compound in a binding site and the associated estimated binding affinity or strength of dissociation of the compound. This strategy is known as molecular docking and is widely utilized in structure-based drug design, as well as a plethora of other fields.[46] [47]

There are many softwares available for molecular modelling and docking, each of them has different ways of predicting the estimated affinity and contribution to the overall inhibition. The most accurate programs often require heavy computational power, are complex and may demand a large set of knowledge to utilize them correctly.

2.2.1 SeeSAR

The software utilized in our SBDD study was SeeSAR, developed by BioSolveIt. It is a software designed to allow *"interactive, visual compound prioritization as well as compound evolution."*[48] This means that structures can be envisioned and inserted into the program, which not only allows to study the interactions in 3D, but also to get estimated affinity values, torsional properties, drug-likeliness and physicochemical parameters. SeeSAR has been used successfully in medicinal chemistry and other fields for similar purposes.[49] [50]

2.3 Relevant Reactions

Reactions employed during this thesis were reductive amination, Suzuki-Miayura cross coupling (SMC), tetrazole formation and ester hydrolysis. These four main reactions are briefly discussed in the following section.

2.3.1 Metal-catalysed Suzuki-Miyaura cross coupling

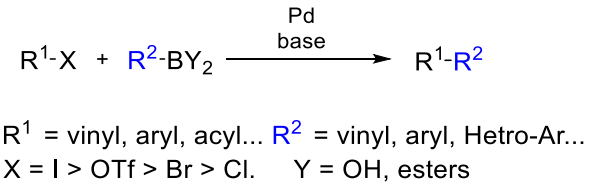

Scheme 3. General Suzuki-Miyaura cross coupling reaction.

Suzuki–Miyaura cross-coupling (SMC, Scheme 3), is the most extensively developed reaction to form C-C bonds and was originally reported by Akira Suzuki, Norio Miyaura and Kinji Yamada in 1979.[51] The reaction involves cross coupling between organoborons and organic halides, pseudo halides or acyl electrophiles (e.g. acyl halide, anhydride, ester, amide)[52], in presence of a nickel, iron or palladium catalyst and a base.[53] Palladium catalysts are by far the most utilized and explored, but the cheaper nickel has also shown wide application, albeit requiring higher catalyst loading. Iron is also an alternative.[54,55] Originally being an aryl-aryl connecting reaction, SMC has since been developed to facilitate a wide range of applications for C-C bond formation, including the synthesis of drugs, natural product and products of industrial value.[53] Even though there are many other cross coupling reactions such as Stille coupling, Ullman coupling, Negishi coupling, the Suzuki coupling is the most utilized. Mild reaction conditions (60-80 ^{o}C), commercially available and stable boronic acid derivatives and the reaction compatibility towards a broad range of functional groups are a few of its advantages.[56-58] Commonly, the reactions are performed in dioxane, DMF, toluene or water, often as biphasic solvent systems[59-61] or without solvents as a neat reaction.[62] Recently, water as a green medium for Suzuki couplings has attracted a noticeable attention, because of ecological, economical and safety reasons.[59,63] However, the focus of this thesis is palladium catalyzed SMC to form aryl-aryl bonds, which will be discussed further in the next section.

2.3.1.1 Palladium SMC of aryl halides

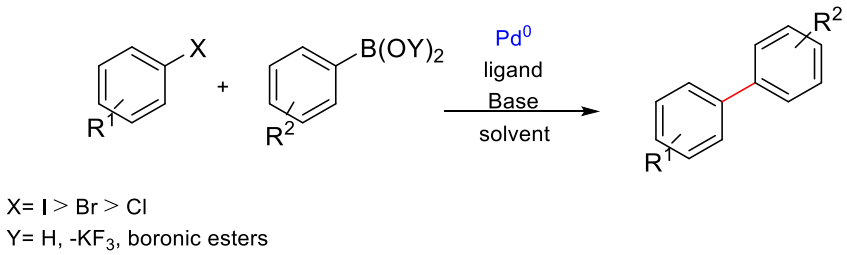

Scheme 4. Suzuki-Miyaura cross coupling reaction of aryl halide with boronic acid/derivatives.

The palladium-catalyzed SMC was originally used for the synthesis of biaryl compounds by coupling an aryl halide with a boronic acid/ acid derivative in presence of a palladium catalyst and a base, as shown in Scheme 4. The reaction mechanism follows a catalytic cycle of four steps (1, 2, 3, 4), as shown in Scheme 5, exemplified with palladium as catalyst for biaryl-coupling. Starting from the ligand (L_n) coordinated active species palladium (0), an aryl halide is added oxidatively to form an aryl-palladium (II) halide complex (A). The second step comprises ligand exchange between the base and the halogen to form (B) without changing the oxidation state of the Pd(II). The boronic acid is activated by the base to enhance polarization of the organic ligand and thus facilitate transmetalation (step 3). Transmetalation happens when the second organic moiety (Ar´) of the boron complex and the base on the palladium switch positions forming an aryl palladium (II) aryl complex (C) without changing the oxidation state. The last step (step 4) is reductive elimination. The two organic moieties are reductively eliminated from the Pd(II) complex and form a new C-C bond. The results is the desired Ar-Ar´ product, and the recovered active species Pd(0).

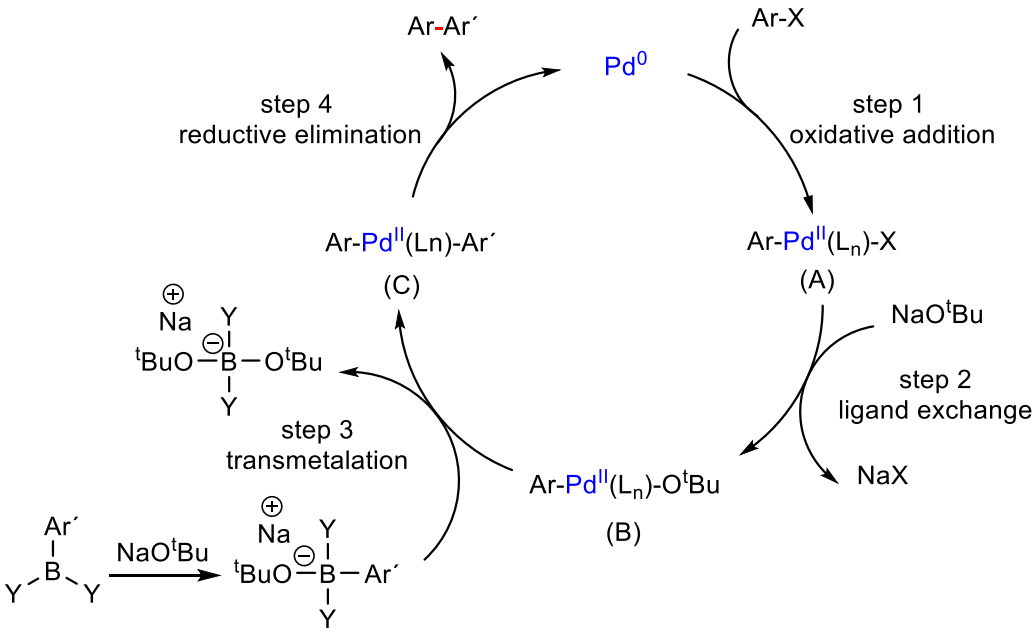

Scheme 5. Catalytic cycle of Suzuki-Miyaura cross-coupling.

The rate of reaction is normally dependent on the oxidative addition step, which is influenced by the nature of the Pd catalyst. Reactivity of aryl halides (Ar-X) are dependent on the bond dissociation energy of the C-X bond (I > Br >Cl).[55] A larger halogen will be a better leaving group and has a lower bond dissociation energy, thus increasing the reactivity.[64] Aryl iodide

has the lowest dissociation energy among the halides and will react the fastest. Bromides are also reactive and useful reactants as they are readily available. Even pseudo halides such as triflates (OTf) can be used as replacement for the halide in a Suzuki-Miyaura cross coupling. In addition, electron withdrawing substituents on the aryl halide increases their reactivity while electron donating substituents and presence of *ortho* substituents would decrease their activity towards the oxidative addition step.[65,66] Despite the slow oxidative addition in case of less reactive aryl halides, the choice of a suitable catalyst can help overcoming the low reaction rates.[67]

Initial reports were based on using triaryl phosphine as ligands for the catalyst. Since then, the applications of many new phosphines and phosphine free ligands (Figure 7) has improved the efficiency and selectivity in such cross-coupling reactions.[60,68] Generally, activity of the catalyst depends on the electronic and steric properties of the ligands around the metal center. Electron-donating and bulky ligands play a role in stabilizing the L_n-Pd (0) intermediate, which is the active species in the catalytic cycle. In addition, a smaller number of ligands coordinating to Pd (0) ensure faster oxidative addition of the organic halide moiety. In contrast higher number of ligands coordinating to Pd (0) complex leads to slower oxidative addition as the approach of the aryl halide is hampered. Reductive elimination has been proven to be faster in the case of less coordinated Pd complexes than the highly coordinated ones.[58]

Catalysts based on S-Phos or XPhos (Figure 7) showed great results with electron-deficient and sterically hindered boronic acids, producing the desired biaryls in high yields.[69] Aryl halides containing electron donating substituents such as NH_2 or NHR have shown to be difficult substrates as C-X bond is more electron rich and not cleaved as easily. Nevertheless, there are several studies reporting Suzuki-Miyaura coupling of systems containing free amines although the yields were relatively low.[70-72] Catalysts such as the Buchwald palladium pre-catalysts (e.g. Sphos G3, Xphos G2) have shown to be a good choice regarding the less active aryl halides as it easily creates the active palladium species at room temperature and it is both air and moisture stable.[73]

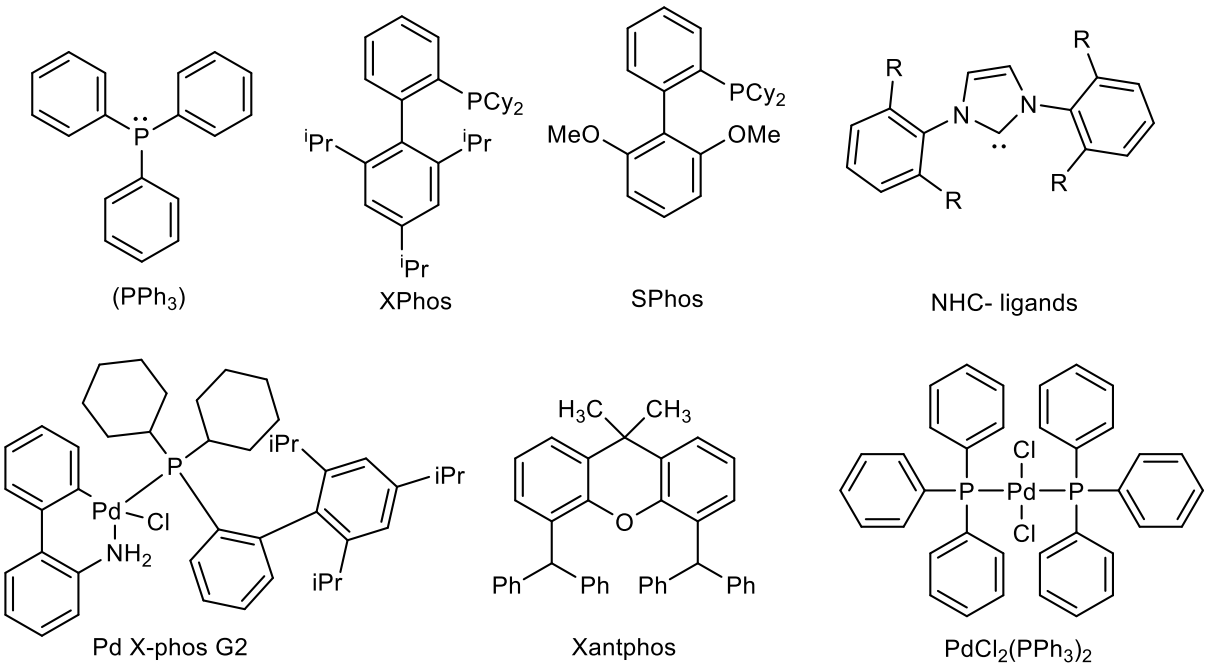

Figure 7. Examples of common Pd-catalysts and ligands used for SMC.

2.3.2 Reductive Amination

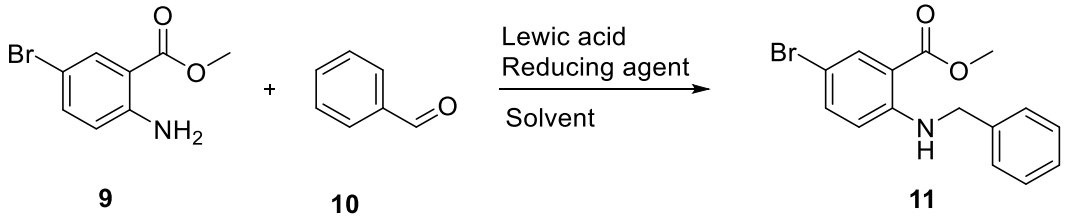

Scheme 6. Overview of reductive amination.

Reductive amination or reductive alkylation (Scheme 6) is a wide-spread and well-known reaction used to form nitrogen-carbon bonds.[74a,75] It proceeds via condensation of an aldehyde/ketone with an amine to form an iminium intermediate. The iminium is then reduced in the presence of a reducing agent and a mild acid, to yield the desired amines as shown in Scheme 7.

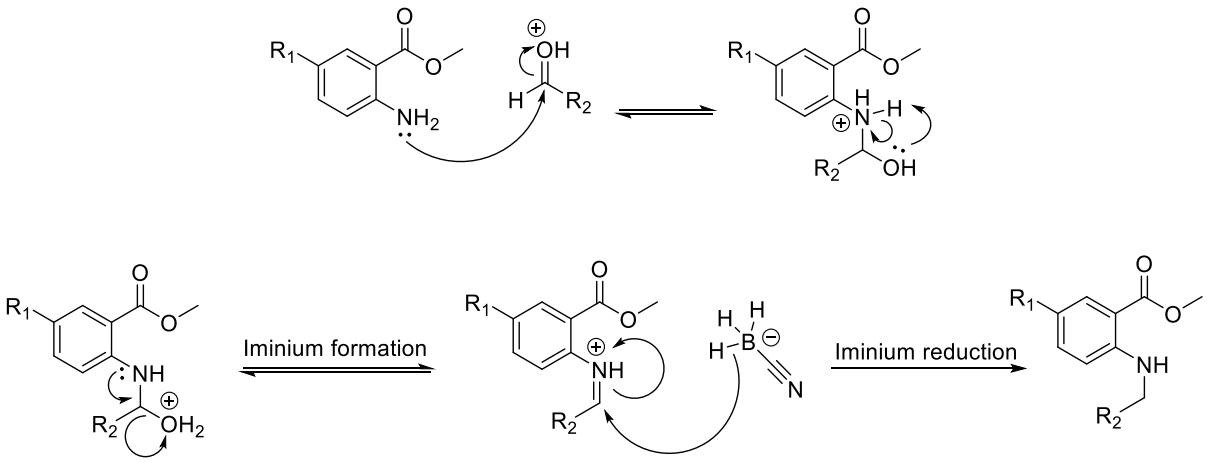

Scheme 7. Reaction mechanism of reductive amination with $NaBH_3CN$.

All the steps are reversible before the reduction of the imine. Choosing a suitable mild reducing agent that will readily reduce the imine is therefore important. The chemoselectivity of the reducing agent is the key, as the aldehydes/ketones could be reduced instead of the imine intermediate. The most commonly utilized reducing agents are borohydrides complexes, but also other agents have been reported. Examples of reducing agents are sodium triacetoxyborohydride (STAB)[76], sodium/zinc borohydride[77,78] and sodium cyanoborohydride.[79] Alternative reducing agents have also been employed including molecular hydrogen[79,80], silanes[81], formates[82], Hantzsch esters[83] and photochemical reductive amination.[84]

STAB is widely utilized as it is a mild hydride donor and reacts selectively with iminium ions. Sodium cyanoborohydride also reduces iminium ions selectively at pH 6[85], but at pH 3-4 will prefer to reduce carbonyl compounds to alcohols.[85] Moreover, cyanoborohydride generates HCN if the conditions are acidic enough, and is moisture and air sensitive.[76] Using a suitable reducing agent and monitoring the pH, the reaction can be carried out in a one-pot set up. Reduction of carbonyl groups can also be avoided by allowing enough time for the imine to form before adding the reducing agent. Even isolating the imine intermediate is a possibility, often referred to as indirect amination in comparison to the one-pot set up; direct amination.

The acid used in reductive amination can also be interchanged. AcOH and $ZnCl_2$ are used most commonly[76], but there is a wide variety to choose from, including, trifluoracetic acid (TFA)[86], HCl [87], $SnCl_2$ [88] and others.

Another aspect that makes reductive amination such a highly useful, robust and broadly employed method is the possibility to use a variety of solvents. The most common solvents for this reaction are chlorinated solvents such as 1,2-dichloroethene (DCE) and dichloromethane (DCM).[89] Non-halogenated solvents include DMF, MeOH and greener alternatives such as EtOAc.[89]

Electron poor aldehydes and electron rich amines increase the rate of reductive amination. Having an aldehyde with electron withdrawing substituents makes the carbonyl of the aldehyde more electrophilic and thereby react faster. An amine with electron donating groups is more nucleophilic and is thereby preferable. Electron withdrawing groups (EWG) and electron donating groups (EDG) can therefore have a significant effect on the reaction. Those factors should be considered when composing the synthetic sequence.

2.3.3 Tetrazole formation

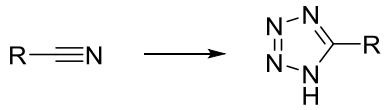

Scheme 8. Overview of tetrazole formation starting from a nitrile.

Tetrazoles are five membered rings containing four nitrogen atoms and are widely used in pharmaceuticals as lipophilic spacers and carboxylic acid surrogates.[90] They are commonly obtained by cycloaddition of azides and nitriles (shown in Scheme 8), but can also be synthesized from arylboronic acids[91], aldehydes with hydroxylamine and 1-butyl-3-methylimidazolium hexafluorophosphate (BMIM-PF_6)[92], or other starting materials.[93-96]

A common method for tetrazoles synthesis is combining nitrile and trimethyl silyl azide ($TMSN_3$) in presence of catalytic amounts of dimethyl tin oxide.[97] The catalytic cycle of tetrazole formation can be divided into three major steps (Scheme 9). First the trimethylsilyl azide and dimethyl tin oxide react to form complex **a**. This makes it possible for the azide to attack the nitrile carbon while the nitrile group (**b**) is stabilised by coordinating to the remaining tin complex providing **c**. Cyclization of **c** proceeds *via* an intramolecular nucleophilic attack by the nitrogen stemming from the azide, to give complex **d**. The catalytic cycle is then completed by a S_N2 intermolecular nucleophilic azide attack, yielding the final tetrazole product and

complex **a**. All the known methods for tetrazole formation from a nitrile group use organic solvents, in particular, dipolar aprotic solvents such as DMF.[98]

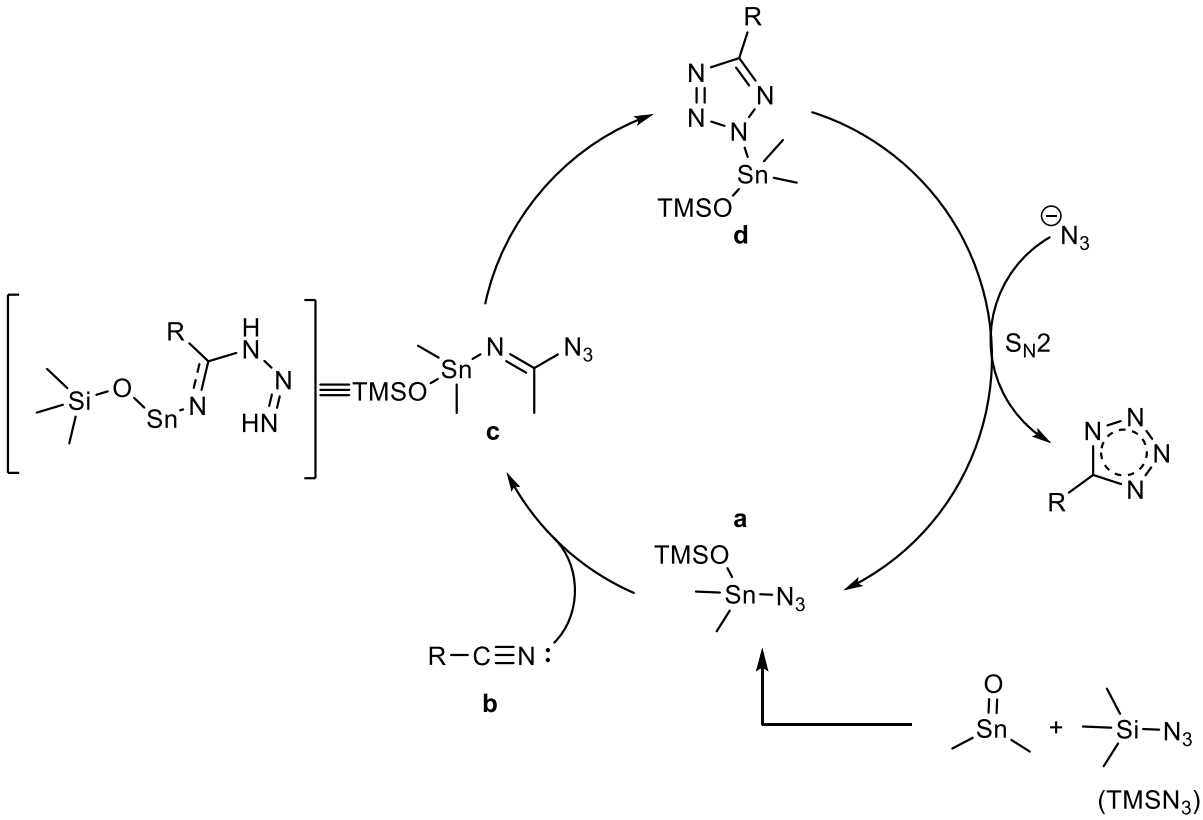

Scheme 9. Catalytic cycle of tetrazole formation.[99]

2.3.4 Ester hydrolysis

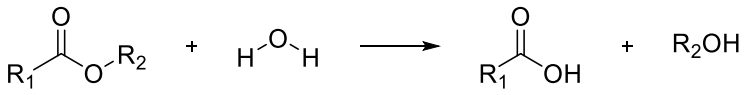

Scheme 10. Overview of ester hydrolysis.

Hydrolysis is a wide term used for any reaction where water cleaves one or more bonds, either through substitution or elimination, shown in Scheme 10. There is a plethora of examples of where hydrolysis occurs, but herein only acid/base catalysed ester hydrolysis is discussed. In the presence of water, hydrolysis of esters and amides can be performed by acid/base as catalysts.[74a] Acid- catalysed ester hydrolysis (Scheme 11) starts from an ester, excess of water

and an acid catalyst, yielding a carboxylic acid and a primary alcohol. The acid catalyzed hydrolysis works with several acids, e.g. HCl and is reversible.

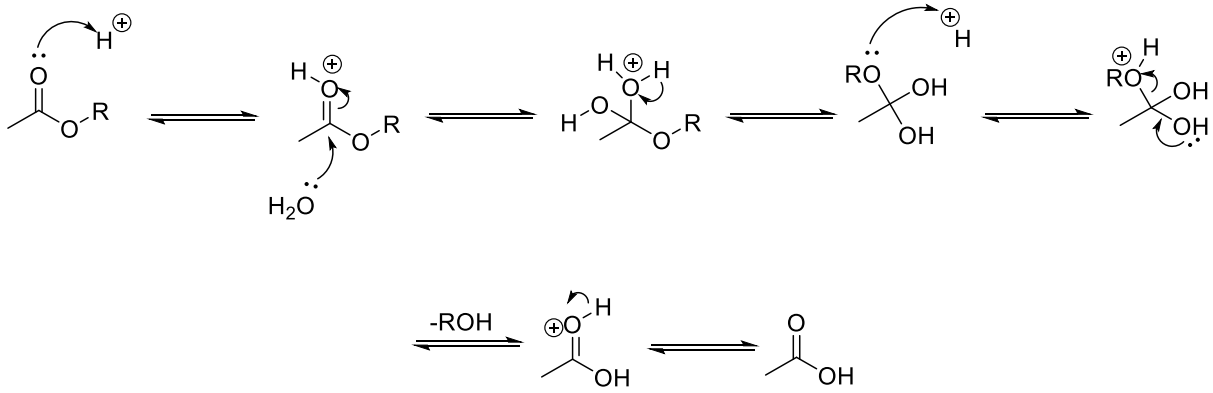

Scheme 11. Acid catalyzed hydrolysis.[74b]

Base catalysed hydrolysis on the other hand is not reversible. This is due to the carboxylic acid being deprotonated by the base. Additionally, the deprotonation will consume the base, making it important to have at least 1 equivalent. Nucleophilic attack of a hydroxyl group (base) on the carbonyl forces alkoxyl group to be kicked out, as it is a better leaving group than OH (Scheme 12), resulting in the salt adduct. The base catalyzed reaction is often run in aqueous sodium hydroxide, but using other salts is also possible, e.g. lithium- and potassium hydroxide.

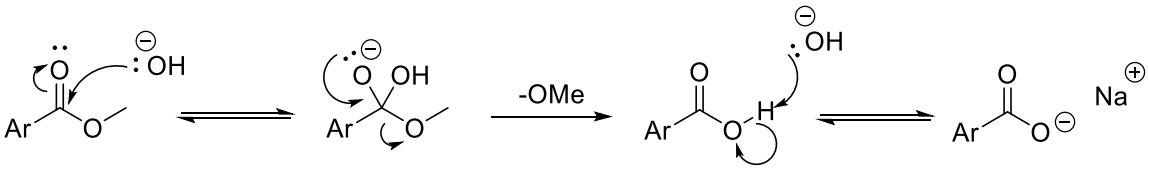

Scheme 12. Base catalyzed hydrolysis.[74a]

3. Results and discussion

3.1 Computational Results

Superimposing modelled structures proposed by Vallejo et al. [40] and the crystal structures of OXA-48 reported by Akhter et al. [7] inspired further investigation of possible modifications of the *ortho* position on scaffold **1**. We chose to use the enzyme: substrate complexes reported by our group as a starting point for *in silico* modification of the *ortho* position in SeeSAR. The program SeeSAR was used to identify target molecules with the caveat that a short and feasible synthetic strategy was accessible. The crystal structure utilized for all docking was OXA-48 in complex with compound **1** (Y = H, Figure 8) (PDB: 5QAV). The binding site was extended with 39 residues to cover region close to the 2-*ortho*-position.

3.1.1 A note on SeeSAR

SeeSAR was mainly used for generating ideas, inspiration and looking for trends. The version used lacked important features for substrate:enzyme interaction, such as the significant π-π stacking of the ligand with certain amino acids (*vide supra*). Additionally, SeeSAR does not account for the flexible nature of enzymes and induced fit mechanism. Therefore, the evaluations for specific molecules and the affinity ranking provided by SeeSAR should be considered with caution. Despite these limitations, the software can give valuable insight into the 3D properties of the binding site as well as spark imagination and identify potential crucial residues for interaction. Combined with a structure-based library approach, it can be productive when looking for new inhibitors and planning synthetic strategies.

3.1.2 Exploration phase

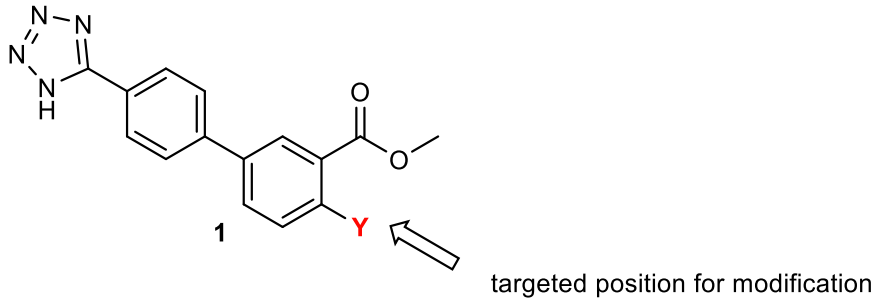

*Figure 8. Scaffold (**1**) used for further exploration in the 2-ortho position*

To find new potential binders a SBDD approach was utilized. First the unsubstituted scaffold **1** (Figure 8, Y = H) was inserted into the binding site of OXA-48 *in silico*, which revealed a further cavity next to the *ortho* position. To explore the sterically and electronical requirements of the 2-*ortho* substituent, an estimate of 1500 unique 2,5-substitued molecules were inserted. There were no common features between the 2-*ortho*-substituents added as the objective was to find new interactions and trends. From this "exploration-phase" three main trends were identified:

1) Extending the scaffold (**1**) with the *ortho* substituent being a nitrogen-alkyl group, showed positive contributions by an additional hydrogen bond between the fragment and the enzyme residues indirectly through a water bridge (shown in Figure 9).
2) Elongating the fragment in the 2-*ortho* position, by e.g. carbon chains, to reach further into the OUT pocket, showed more potential residue interactions and thereby overall higher estimated affinity.
3) Tetrazole in general had negative torsion contributions in the cavity. Substituting the tetrazole for other moieties gave more flexible conformations for the molecule in the binding pocket. The effect was especially clear when using sulfonic acid as a substituent, inspired by avibactam.

Those trends, together with synthetic accessibility comprised the basis for the design of the new library of inhibitors.

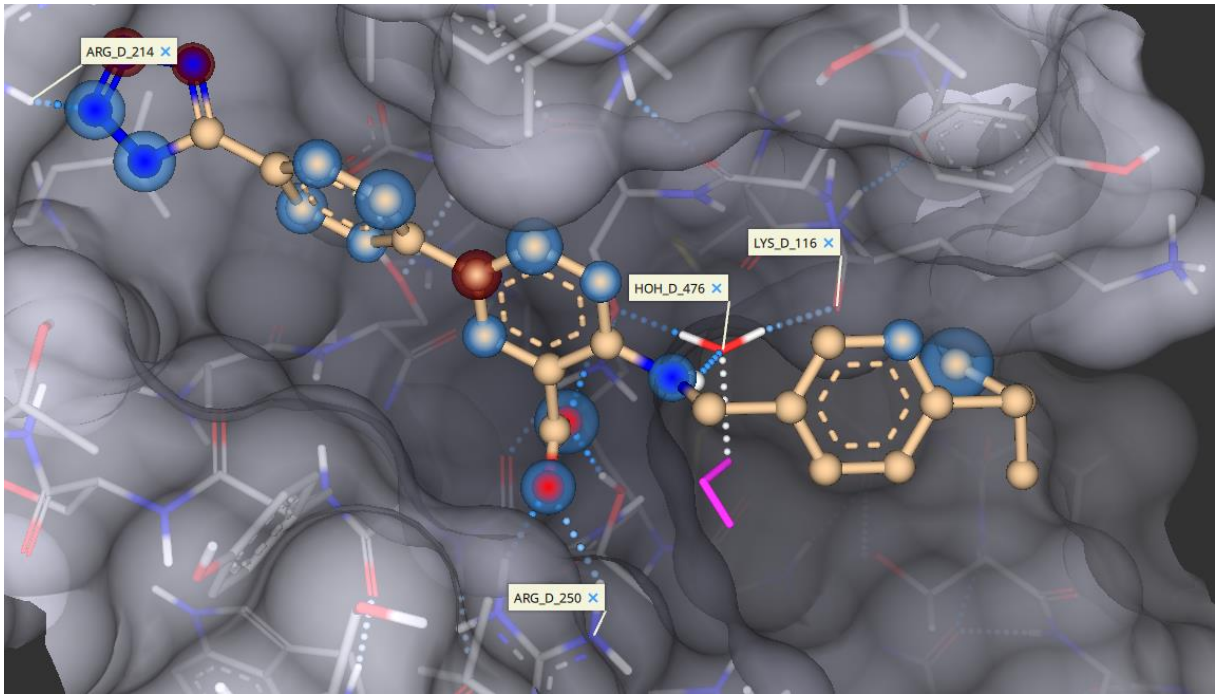

Figure 9. Secondary N-alkyl as 2-ortho extension. An unprecedented H-bond to Lys 116 via a water molecule was observed.

3.1.3 N-alkyl substituents

Having identified in trend 1 that nitrogen-alkyl groups increased the estimated affinity; scaffold **1**, Y = NH_2 became the new proposed and improved scaffold. From a synthetic point of view, the new scaffold could undergo reductive amination or Buchwald-Hartwig amination to functionalize the 2-*ortho* position, and thereby offer a plausible synthetic route for obtaining *N*-alkyl substituents. To limit the potential targets identified by SeeSAR and for a more practical approach, all aldehydes and aryl halides on the chemical list of our research group were drawn in ChemDraw. The collected aldehydes/aryl halides were drawn as connected to the new scaffold **1**, Y = NH2 through reductive amination or Buchwald-Hartwig amination before being docked in the binding site. The results of the hypothetical reactions and docking yielded a list of molecules with a plausible synthetic pathway and with new interactions in the OXA-48 binding site. The most promising fragments can be seen in Figure 10 and were targeted for synthesis.

.

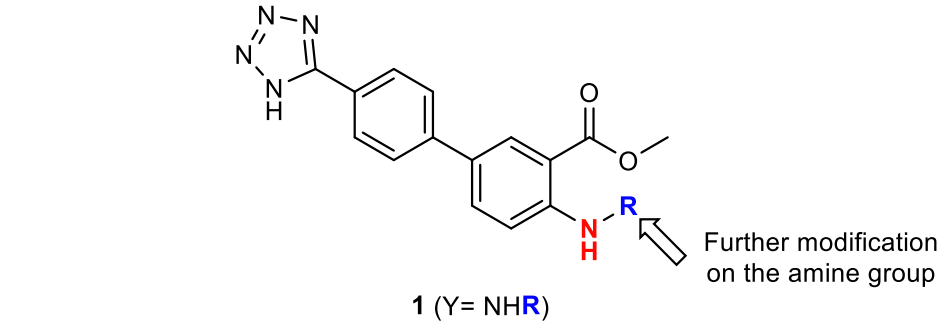

R =

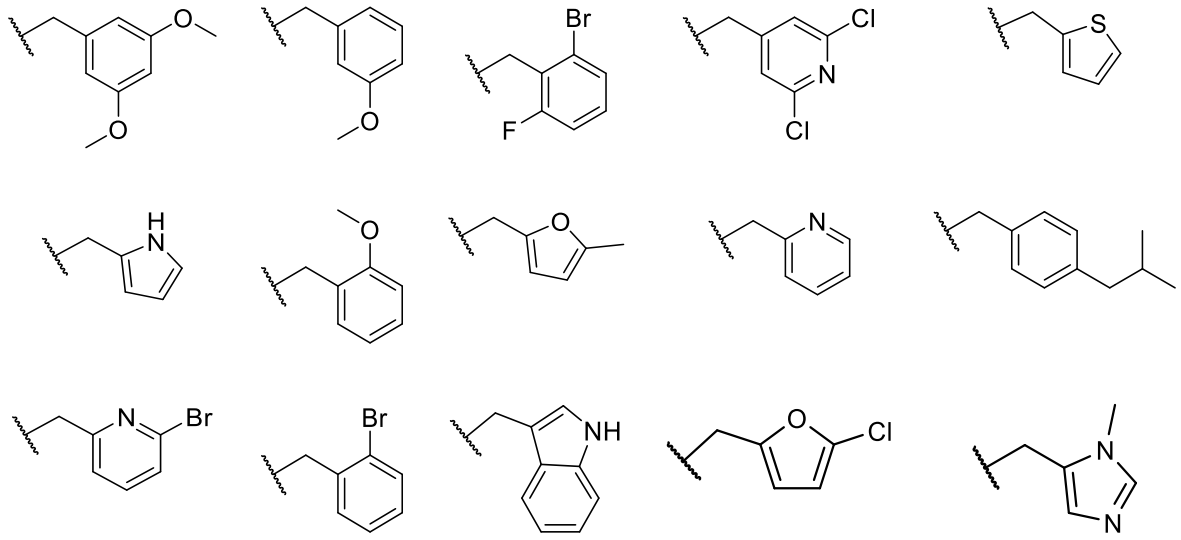

Figure 10. Promising N-alkyl substituted fragments as suggested by SeeSAR.

Other substituents such as N-acyls, ethers, esters alkane/alkene chains, thiols and more were also evaluated. None of these showed a trend towards a better estimated affinity in SeeSAR and did not offer for a clear synthetic route for further expansion.

3.1.4 Elongation

Elongating the chain to reach further into the pocket showed a trend of higher estimated affinity compared to those directly substituted. The goal was to keep the proposed scaffold **1**, Y = NH2, and add a linker chain and then functionalizing it with e.g. aryls, heterocycles etc. Six different possible chains were studied in detail (Figure 11) as a potential new series of inhibitors. The six elongation chains were added to the scaffold, and then some of the aldehydes from the N-alkylation step above were added. A total of 2780 elongated molecules were inserted.

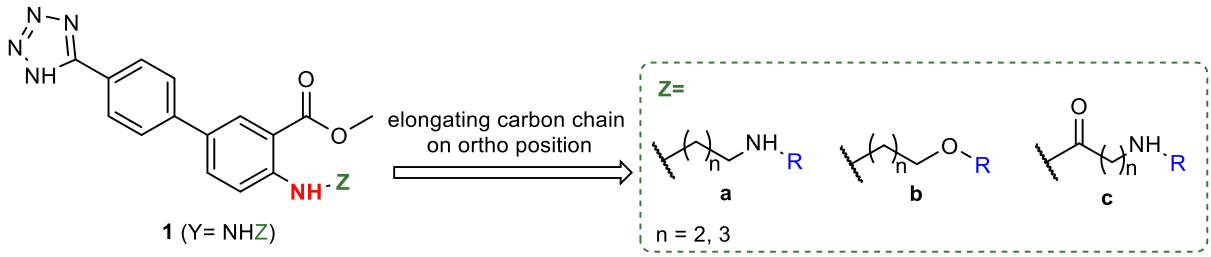

Figure 11. Investigated carbon chain linkers. R=aryls, heterocycles etc.

Out of these 6 chains, **a** with n = 2 was the most promising and showed a trend of higher estimated affinity whilst connected to different functionalities. It showed additional interaction with the ketone moiety of lysine 116 and allowed the molecules to reach other residues like threonine 104, shown in Figure 12. The computational data is not precise enough to state that certain fragments definitively bind stronger, especially as there are several factors impacting the affinity, but the trends observed with elongation were worth further investigation.

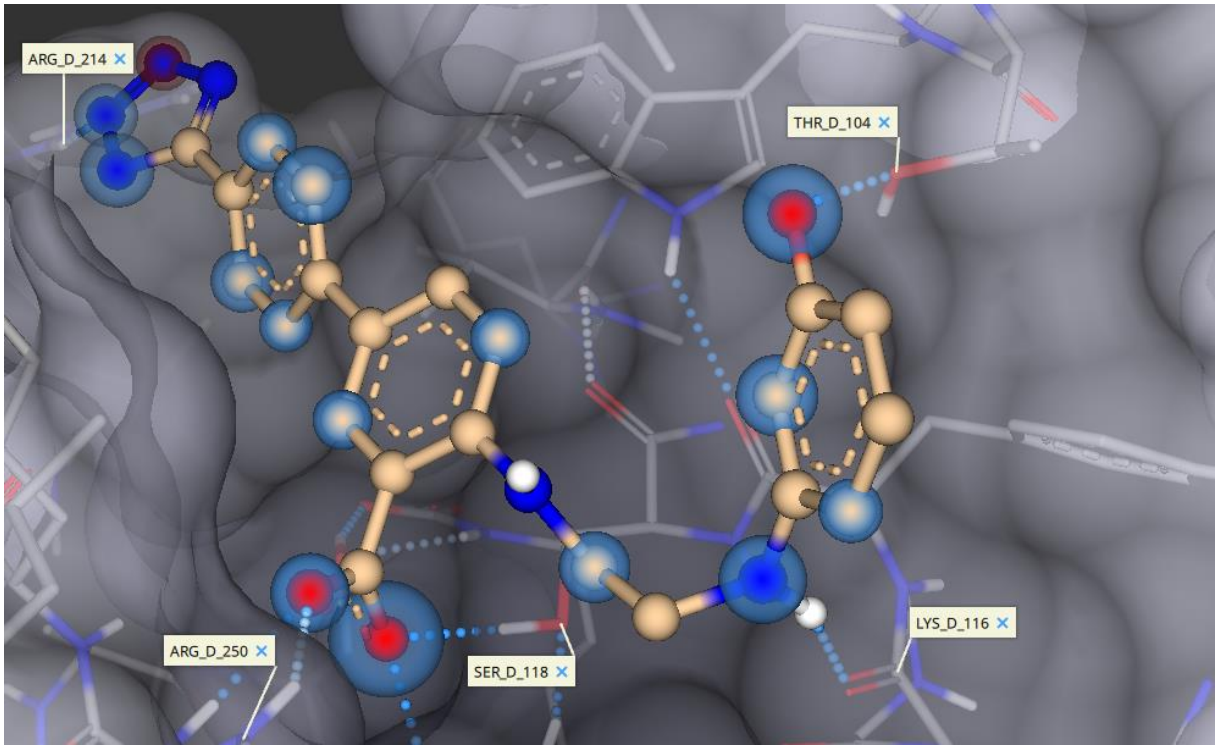

Figure 12. Scaffold with elongated ortho substituent in the binding site of OXA-48.

3.1.5 New *meta* substituents

A sulfonic acid moiety instead of tetrazole as the *meta* substituent showed a clear trend of higher estimated affinity in the docking results. The direct substitution with UiT's available aldehydes was carried out for both scaffold **1** (Y = NH_2) and the new sulfonic acid fragment and compared

(as for 3.2.2). Out of the top 50 hits for estimated affinity, 48 of the fragments were sulfonic acid variants. Based on these results the fragment without an additional 2-*ortho*-substituent was identified as a possible initial target structure similar to the previous work carried out by Akhter et al.

3.2 Synthetic Strategy

Based on the docking results and ideas generated by it, several molecules were identified as targets. The targets were separated into three part corresponding to the three trends identified during the computational work of this thesis and will be addressed as follows.

The compound series of *N*-alky substituted derivatives of scaffold **1** (Y = NHR) as shown in Figure 13 was the primary focus of our studies. The objective was to take scaffold **1** with a 2-*ortho* positioned amine and extending it with aryls/hetero aryls.

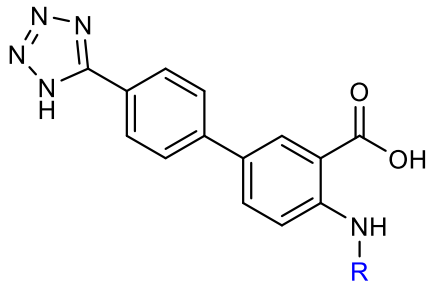

Scaffold **1** (Y = NH**R**)

N-alkyl substituents: **R** =

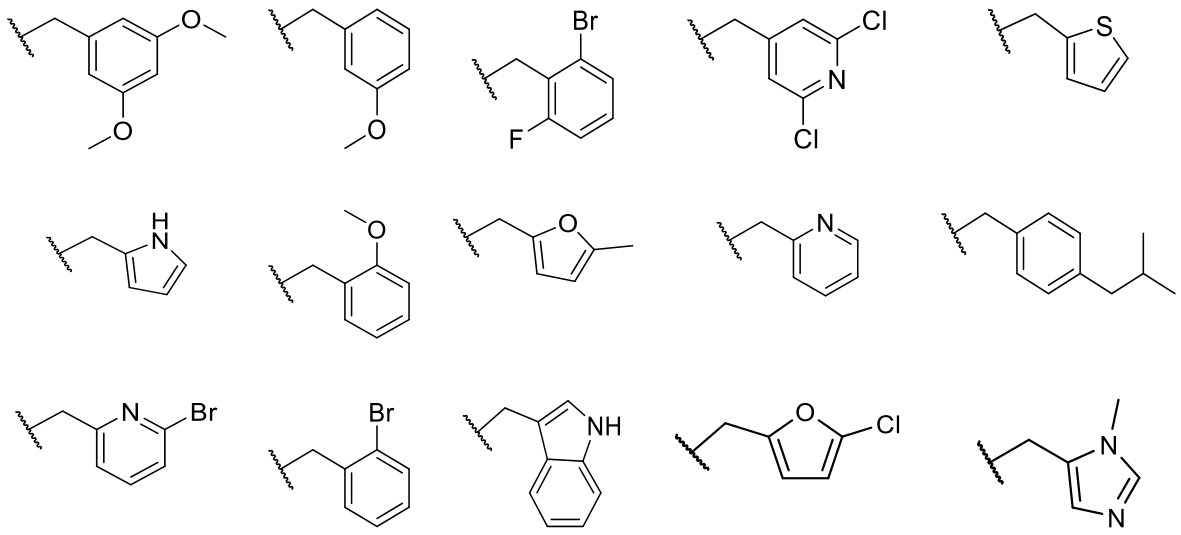

Figure 13. Target molecules for synthesis.

The extension with aryls/hetero aryls on the amine could be achieved following several possible synthetic strategies. Having an *ortho* positioned amine allowed for the use of reductive amination, which is a well-studied and reliable reaction. Other options were considered for the functionalization of the *ortho*-position, for example Buchwald-Hartwig amination. Buchwald-Hartwig aminations would, however, demand couplings with sp^3 carbons, which are generally more difficult substrates in coupling reactions.[100,101] Alternatively, the reaction could be started from a 2,4-dihalo benzoic acid, but this might lead to regioselectivity problems and the important secondary amine interaction would be excluded. Thereby reductive amination was preferred.

4-tetrazole-phenyl substituent in the *meta* position can be introduced by a sequence of Suzuki-Miyaura cross coupling with 4-cyano-phenylboronic acid followed by tetrazole formation from the cyano group. The SMC and tetrazole formation had been performed on similar structures in our group earlier[7] and was a natural synthetic choice considering the available experience. It also allowed us to utilize a two-step reaction reported by our group to obtain the final tetrazolecompound.[7] Furthermore, SMC is a robust method to achieve aryl-aryl bonds and has shown excellent yields.[52,55,57,62,67,69] Based on the reactions and the target compounds, the commercially available methyl 2-amino-5-bromobenzoate (**9**) (Figure 14) was used as starting material.

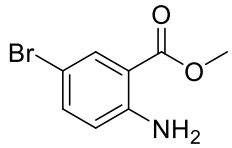

9

*Figure 14. Methyl 2-amino-bromobenzoate (**9**); starting material for the synthetic plan.*

The decision was made to start with an benzoate ester (**9**) instead of the free benzoic acid (Figure 14) since amino acids have zwitterionic characteristics and may be difficult to handle, isolate and purify.[102] This added an extra synthetic step in form of ester hydrolysis. The additional step seemed favourable being possibly material efficient and time saving as the intermediate compounds could be handled more easily.

When analysing the synthetic sequence, it became clear that the main diversification was achieved by reductive amination. Preferably, reductive amination should thereby be conducted

last to keep the synthetic route as efficient as possible (strategy 1, Scheme 13). Fewer synthetic steps when creating a library of molecules was favourable, but it implied to introduce zwitterionic characteristics once the tetrazole was build up. To avoid reactivity or work-up problems over several steps, an alternative idea was to form the tetrazole last (strategy 2, Scheme 14). Two synthetic routes where thereby identified, the preferred synthetic route 1 and back-up route 2, shown in Scheme 13 and 14, respectively.

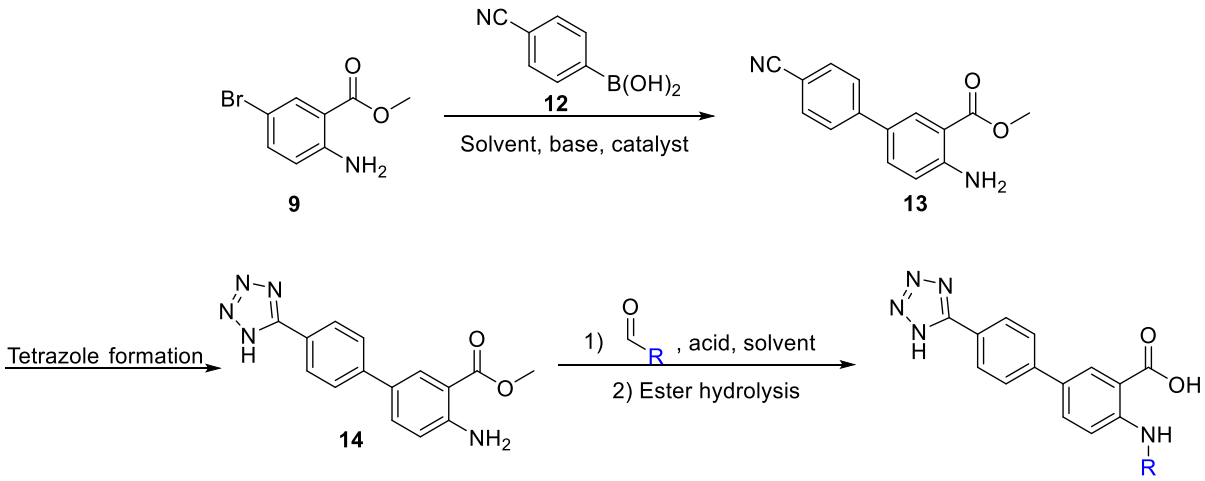

Scheme 13. Synthetic strategy 1.

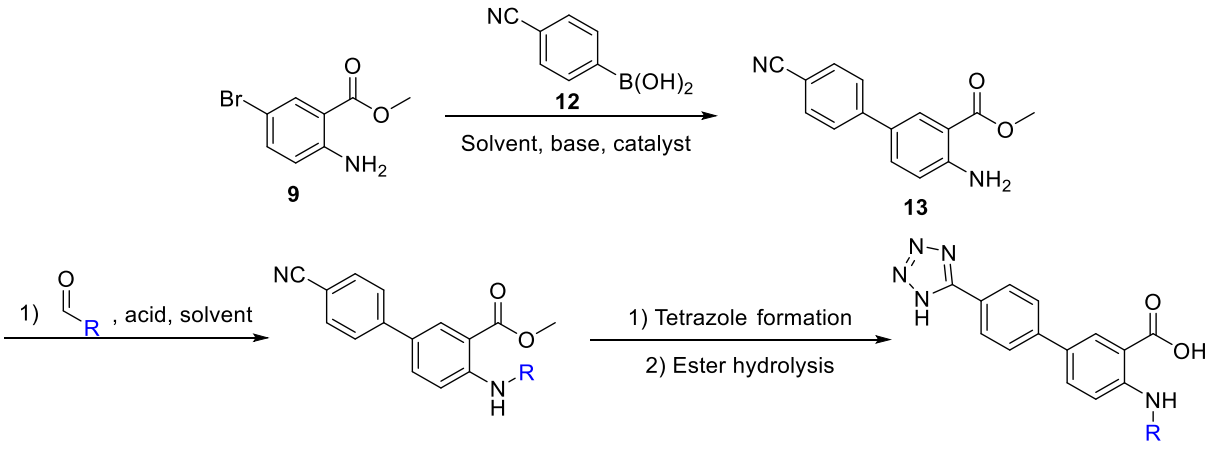

Scheme 14. Synthetic strategy 2.

Conducting tetrazole formation on the boronic acid (**12**) could additionally save time, but the reaction was tested by and group and proved ineffective.

3.2.1 Synthetic strategy for new *meta* substituents

Computational docking also pointed towards sulfonic acid fragment (**16**) with possible positive contributions of the sulfonic acid substituent instead of the tetrazole moiety. The sulfonic acid fragment (**16**) could be synthesized using SMC and a commercially available boronic acid, which was desirable and shown in Scheme 15.

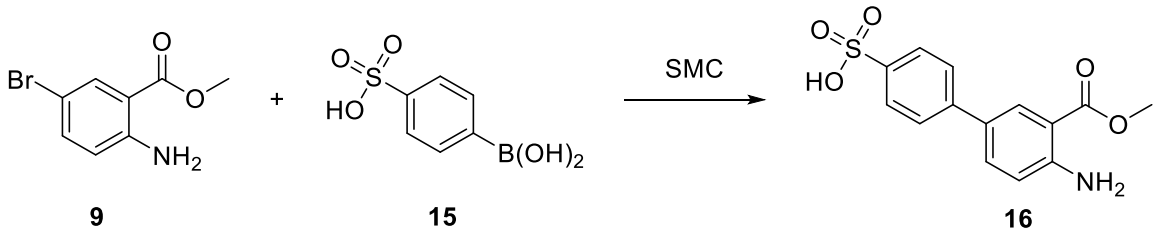

9 **15** **16**

Scheme 15. Proposed plan for synthesizing new meta-substituent.

Compound **16** could be the start of a new fragment series, much like the tetrazole series shown in Figure 13. The same synthetic strategies (1 and 2, scheme 13 and 14 respectively) could be applied to obtain the series, but biological results should back up the SeeSAR results before more time was invested. As discussed previously, SeeSAR results should be considered carefully, but if the biological results of compound **16** was promising, the new series could be continued.

3.2.2 Synthetic strategy for elongation

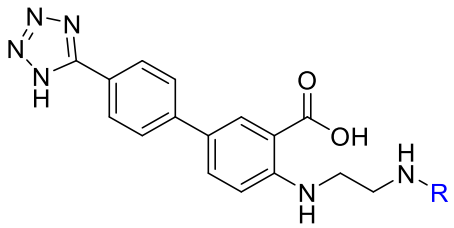

17

R = Substituents seen in Figure **14**

Figure 15. Target for elongation of the 2-ortho popsition of scaffold **1**

The last target molecule (Figure 15**,** (**17**)) was an elongated version of scaffold **1**. As with the sulfonic acid fragment, the elongated molecule (**17**) could be the start of a new series but obtaining some results to back up the SeeSAR prediction was the first priority. Compound **17** has a two-carbon spacer extending from the 2-*ortho* amine and could be synthesized by

reductive amination with *N*-Boc-2-aminoacetaldehyde. Choosing this route was considered a good alternative for elongation, as the reductive amination could simply be carried out twice; once for adding the carbon linkers, and a second time after removal of the Boc group to add new substituents (Scheme 16). The route to obtaining the elongated product could be adapted the synthetic plan 1 or 2 *vide supra*.

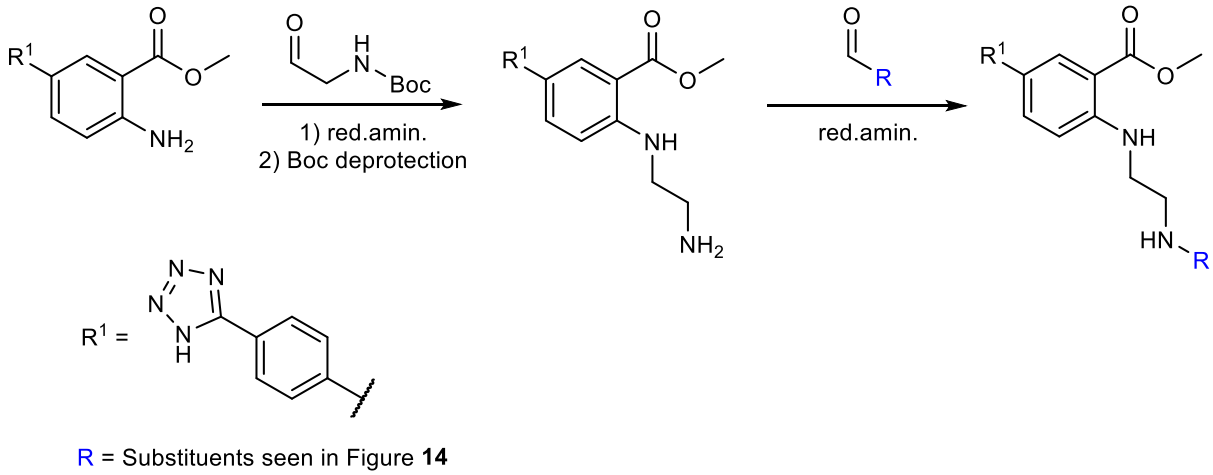

Scheme 16. Proposed plan for carbon chain linkers.

3.3 Synthetic results

3.3.1 Suzuki-Miyaura Cross coupling

As described previously, the first step of both the synthetic strategies was to carry out Suzuki-Miyaura cross coupling reactions before attempting reductive amination or tetrazole formation. Akhter et al. reported that Xphos-Pd G2 showed excellent result on a similar system to ours when used with K_3PO_4 as the base in dioxane/water at 60 ^oC overnight.[7] The reaction conditions used by Akhter et al. were not optimized for the starting materials used in this work, compound **9** or **13**. Therefore, a catalyst screening was performed in order to find tolerant reaction conditions for our system.

Table 1. Screening results of Suzuki-Miyaura cross coupling.

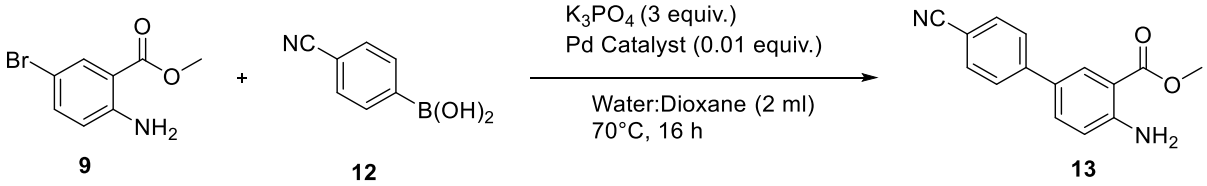

Entry	Catalyst (mol%)	Ratio SM:P[1]
1	$Pd(PPh_3)_4$	1:2.97
2	$Pd(OAc)_2$	1:3.30
3	$Pd(PPh_3)_2Cl_2$	1:3.01
4	XantPhos Pd G3	1:3.88
5	Xphos Pd G2	1: 4.02

General conditions: [1] = The ratios were determined by ^{1}H NMR without and internal standard, SM = Start material, P = Product.

Table 1 shows the results of the catalyst screening. The reaction model for the screening was set up with 1.0 equiv of methyl 2-amino-5-bromobenzoate (**9**) (0.2 mmol), 4-cyanophenyl boronic acid (**12**) (1.5 equiv), catalyst (1 mol%) and potassium phosphate (3.0 equiv) , in water: dioxane (1:1) at 70°C overnight. Low Catalyst loading (1 mol%) was used to test their general efficiency. Crude NMR analysis were used to estimate the initial conversion in order to compare the reactivity of catalysts.

$Pd(PPh_3)_4$ (Table 1. entry 1), showed the lowest ratio of starting material to product of (1:2.97) where $Pd(PPh_3)_2Cl_2$ (entry 3), was a close second with a ratio of 1:3.01 starting material to product. The ratios of XantPhos Pd G3 and X-phos Pd G2 (entry 4 and 5 respectively) were the highest in favour of the desired product according to ^{1}H NMR. This was to be expected as they are known to work excellently with electron deficient boronic acids as well as aryl halides containing electron donating substituents such as NH_2.[69]

Based on crude NMR, Xphos Pd G2 seemed to be the most promising catalyst. The reaction mixture of entry 5 was then worked up and the pure product **13** was isolated in 40% yield. The low isolated yield could have been caused and solubility problems for Xphos Pd G2 in

water:dioxane and we expected that ester hydrolysis may be an undesired side reaction in aqueous basic solution. Upon changing the solvent to anhydrous THF[58] the desired product was isolated in 72% yield after work up. Xphos Pd G2 proved to be the right choice when scaling up the reaction to 500 mg of methyl 2-amino-5-bromobenzoate, yielding 98% of **13** (Scheme 17). The catalyst loading was increased to 4 mol% to ensure full conversion. The use of THF also prevented possible solubility problems with future coupling partners as it is more diverse than the biphasic medium.

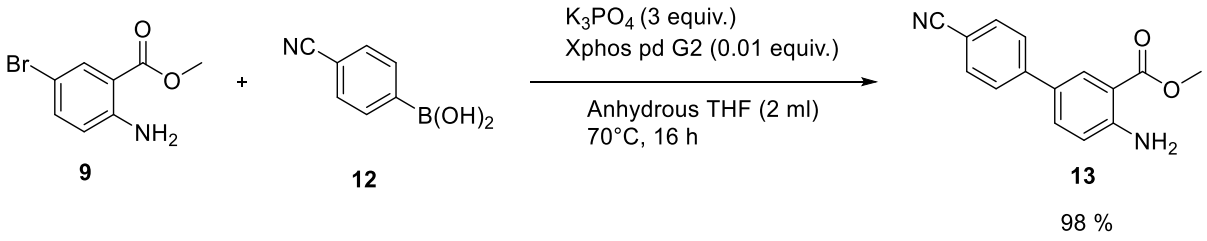

*Scheme 17. Synthesis of methyl 4-amino-4'-cyano-[1,1'-biphenyl]-3-carboxylate (**13**) using SMC.*

Methyl 4-amino-4'-cyano-[1,1'-biphenyl]-3-carboxylate **(13)** had previously reported by Georg Manolikakes and co-workers.[103] It was synthesized via Negishi cross-coupling between methyl 2-amino-5-bromobenzoate and 4-cyanophenylzinc iodine using $Pd(OAc)_2$ and S-Phos in anhydrous THF for 2 hours at 25°C, yielding 98%. The primary reason for choosing SMC was the increased scope it provided, the use of boronic acids instead of zinc iodine compounds is advantageous as boronic acids are more readily available and in a greater variation than zinc compounds, which was preferable considering the sulfonic acid moiety. In addition, boronic acids are safer to use and inhouse experiences with SMC reactions were present in the research group.

Having successfully determined efficient conditions for the SMC, the reaction was attempted with the *N*-benzylated compound **11**. The coupling of (4-cyanophenyl)boronic acid (1.5 equiv.) (**12**) with methyl 2-(benzylamino)-5-bromobenzoate (1 equiv.) (**11**) yielded **18** and was performed to compare the yields if reductive amination was carried out first, Scheme 18.

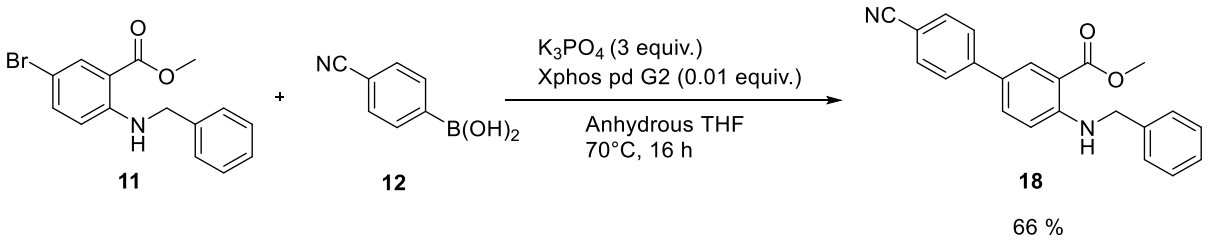

*Scheme 18. Synthesis of methyl 4-(benzylamino)-4'-cyano-[1,1'-biphenyl]-3-carboxylate (**18**) using SMC.*

As shown in the Scheme 18 the reaction only yielded 66% of product (**18**) but the reaction was only run with 1 mol% of catalyst, due to availability, which might explain the lower conversion and thus drop in the yield. Due to the lower yield and strategic unfavourable order of transformation this approach was not pursued further. To the best of our knowledge, **18** has not yet been reported and the synthesis of **11**, will be discussed later in the thesis.

Before the reaction was optimized with anhydrous THF, the SMC was performed in a mixture of dioxane and water (1:1) with methyl 2-amine-5-bromobenzoate (**9**) (1 equiv.) and 4-boronobenzenesulfonic acid (**15**) (1.5 equiv.) to obtain 4'-amino-3'-(methoxycarbonyl)-[1,1'-biphenyl]-4-sulfonic acid **16** (Scheme 19). The desired product was isolated in 49% yield. It was detected by HRMS that the methyl ester was partially hydrolysed after coupling. Additionally, the yield might have been affected by the water and running the reaction in THF would be a potential improvement, as shown with the cyano-coupled product. Furthermore, different charges on the moieties of the compound make it difficult to isolate and purify the product, leading to potential losses. This problem is well known for amphoteric compounds as their physicochemical properties are highly dependent on the pH (oppositely charged groups will be discussed in further detail under the tetrazole, results and discussion section of this thesis).

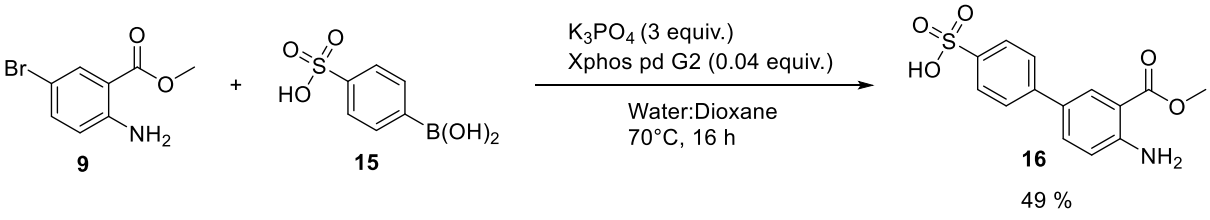

*Scheme 19. Synthesis of new meta substituent - sulfonic acid (**16**).*

3.3.2 Reductive Amination

Tetrazole formation with the nitrile containing starting material was the next step of the preferred synthetic plan (synthetic plan 1) followed by reductive amination. However, once the tetrazole moiety was introduced, the molecules became difficult to handle. Initial attempts of reductive amination on **14** (Scheme 20) were unsuccessful.

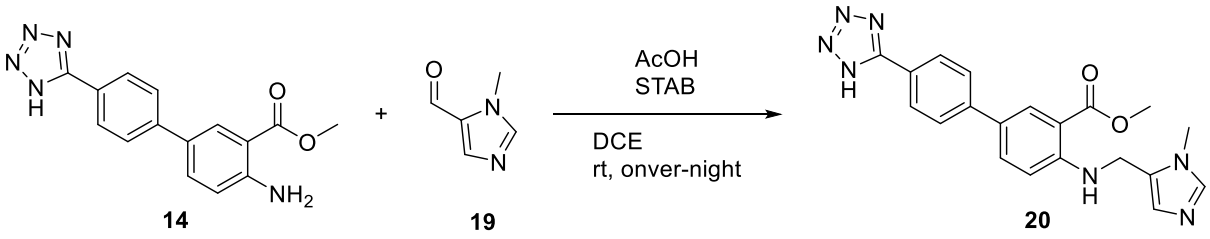

*Scheme 20. Attempted reductive amination on methyl 4-amino-4'-(1H-tetrazol-5-yl)-[1,1'-biphenyl]-3-carboxylate (**14**).*

The difficulties in handling the tetrazole compounds (**14**) and why the reactions were unsuccessful will be discussed under the tetrazole formation part of this thesis (**3.3.3**). The decision was made to use the second synthetic plan (2) from this stage on, thereby carrying out reductive amination right after SMC, in order to postpone introducing the tetrazole.

For screening and optimisation of the reaction conditions, readily available 2-amino-5-bromobenzoate was reacted with benzaldehyde or 3-hydroxy-4-methoxybenzaldehyde. Benzaldehyde was chosen as it is an aromatic compound without any electron withdrawing or donating groups, in hope that it would serve as a middle-way representative of all the different functionalities planned. For a more diverse substituent representative 3-hydroxy-4-methoxybenzaldehyde was used. AcOH and $ZnCl_2$ are both common acids used in reductive amination and were a natural choice. DCE is the most common solvent utilized, while EtOAc and IPA have both been reported to be good alternatives for a greener route.[89] Microwave irradiation was also utilized as it had been reported as successful with other reductive amination reactions (e.g. ketones and anilines) and could potentially shorten the reaction time.[104]

To side-step the safety aspect of using cyanoborohydride, the screening was done exclusively with sodium triacetoxyborohydride (STAB), a common and highly successful reducing agent for reductive amination.[76] Other reducing agents could also be considered, but the wide scope of STAB, the diverse and numerous applications and high tolerance of functional groups made it a good first choice considering the target molecules. Furthermore, STAB is simple to remove

in the workup process, has very few limitations compared to other reducing agents and allows for a one pot set-up.[76] Additionally, some reducing agents like NaH have been known to reduce nitriles in the presence of acids and were avoided due to possible side reactions with the nitrile.[105] The screening results are shown in Table 2. Interpretation of these results should go with the caveat that the ratios have been calculated from the starting material and product, excluding all by-products.

Table 2. Reductive amination screening results.

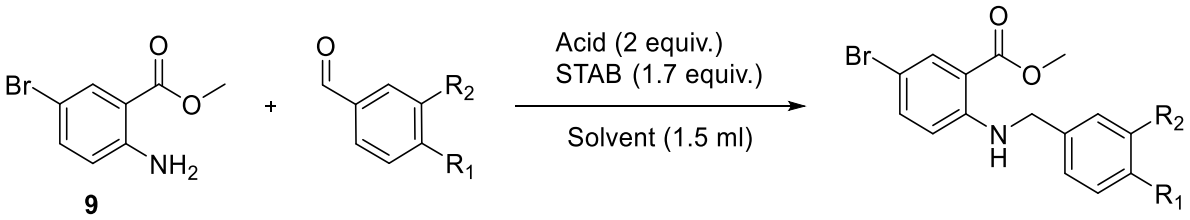

Entry	R_1	R_2	Acid (2 equiv.)	Solvent (1.5 ml)	Time [h]	Temp [°C]	Ratio (SM:P)[1]
1	H	H	AcOH	DCE	16	Ambient	Full conv
2	H	H	AcOH	EtOAc	16	Ambient	1:2
3	H	H	AcOH	IPA	16	Ambient	1:0.4
4	H	H	$ZnCl_2$	DCE	16	Ambient	Full conv
5	H	H	$ZnCl_2$	EtOAc	16	Ambient	Full conv
6	H	H	$ZnCl_2$	IPA	16	Ambient	1:0.3
7	H	H	AcOH	DCE	0.5	100, MW	1:2.3*
8	H	H	$ZnCl_2$	DCE	0.5	100, MW	1:1.9*
9	OMe	OH	AcOH	DCE	16	Ambient	No conv.
10	OMe	OH	AcOH	EtOAc	16	Ambient	No conv.
11	OMe	OH	AcOH	IPA	16	Ambient	No conv.
12	OMe	OH	$ZnCl_2$	IPA	16	Ambient	No conv.
13	OMe	OH	AcOH	DCE	0.5	100, MW	1: 0.2

*SM = Start Material, P = Product. * =Considerable amounts of biproducts. [1] Ratios were determined by GCMS after work-up.*

Entries 1 (DCE), 2 (EtOAc) and 3 (IPA) showed that entry 1 (DCE) was the most suitable solvent choice under the proposed conditions, having full conversion, whereas 2 (EtOAc) and 3 (IPA) only had partial conversion. Although not observed in the process, it has been reported

by Abdel-Magid[76] that the use of AcOH and STAB can form by-products like *N*-acetylated and *N*-ethylated aniline substrates. Based on the work by McGonagle et al.[89] it was thereby desirable to test $ZnCl_2$ as acid catalyst in combination with green solvents. Entries 4 (DCE), 5 (EtOAc) and 6 (IPA) were set up with $ZnCl_2$ as catalysts. The entries followed the same trend that was apparent with AcOH as mediator, only there was no discernible difference between DCE and EtOAc as both showed full conversion. IPA was clearly worse in both trials possibly due to it being a protic solvent. To reduce the reaction time microwave irradiation was employed (entries 7 and 8). The microwave reactions were only set up with DCE as it was showing good conversion for both acids. Entries 7 and 8 contained large amounts of by-products. Furthermore, MS analysis of 7 and 8 exhibited the presence of a peak that might be corresponding to the free acid of the desired product. The conditions might have been harsh enough for acidic hydrolysis, but further isolation/experiments are needed to prove this hypothesis.

Entries 9-12 showed no conversion using 3-hydroxy-4-methoxybenzaldehyde. Entry 13 showed some conversion. It is worth mentioning that for 3-hydroxy-4-methoxybenzaldehyde, the reaction was not screened with DCE and EtOAc with $ZnCl_2$, as it showed no conversion under the previous conditions.

The general method seemed very suitable for the benzaldehyde reductive amination, but not with 3-hydroxy-4-methoxybenzaldehyde. Increasing the temperature of the reaction to 40-60°C could have been a possibility, but as elevated temperatures under microwave irradiation showed ester hydrolysis, it was thereby not attempted. A potential reason for the sluggish reactivity might be the electronical nature of the compound or the free alcohol group. The two electron donating groups of 3-hydroxy-4-methoxybenzaldehyde, lowers the reactivity. The *meta*-methoxy group makes the carbon of the carbonyl group less electrophilic through resonance (Scheme 21), which may explain the low conversion.

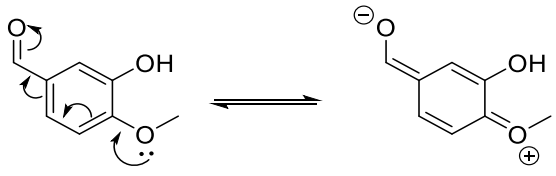

Scheme 21. Resonance structures of 3-hydroxy-4-methoxybenzaldehyde.

Entries 1, 4 and 5 all showed close to full conversion and no by-products. We therefore decided to use aldehyde (2 equiv.), STAB (1.7 equiv.) and $ZnCl_2$ (2 equiv.) in DCE at ambient temperature as a general method in the following work. Applying this general method to the synthetic plan meant that it was preferable to carry out on the cyano-coupled product and with diverse aldehydes. Therefore, a control reaction was set up using 3-methoxybenzaldehyde (**21**) (2.0 equiv.) and the cyano-coupled starting material (**13**, 1.0 equiv.) (Scheme 22), in belief that 3-hydroxy-4-methoxybenzaldehyde could be an especially difficult aldehyde and that aldehydes not as electron rich, might still work. The reaction yielded 96% of product (**22**) and the decision was made to continue the use of the method.

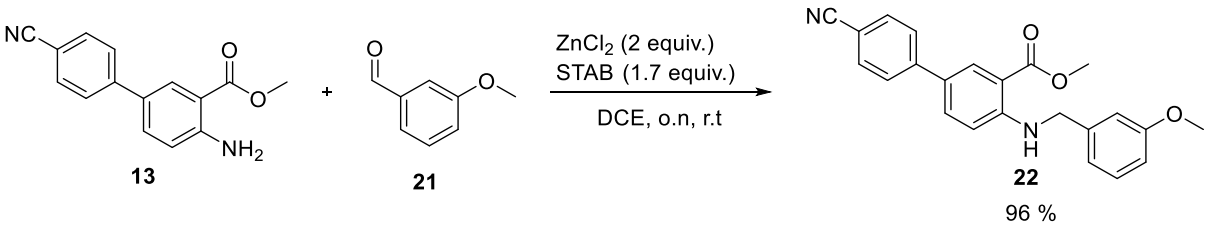

*Scheme 22. Synthesis of methyl 4'-cyano-4-((3-methoxybenzyl) amino)-[1,1'-biphenyl]-3-carboxylate (**22**) as a control reaction of reductive amination screening results. on = overnight r.t = room temperature.*

Using the optimized reaction conditions, compounds **11**, **22-26**, in Figure 16 were synthesized. The reaction of 2-amino-5-bromobenzoate (**9**) with benzaldehyde, sodium cyanoborohydride and zinc chloride in MeOH had previously been reported by Levesque and Fournier [106], yielding 99% of desired product **11**. In my hands, the conditions reported by Levesque and Fournier, the desired product was obtained with 70% yield. Similar reactions have been carried out by Zhao et al. [107] with methyl 2-aminobenzoate, substituted benzaldehydes (including non-substituted benzaldehyde), $ZnCl_2$ and $NaBH_3CN$. The yields were not reported as the product was an intermediate. The reaction with 3-hydroxy-4-methoxybenzaldehyde or any of the compounds **22-26** has to the best of our knowledge not yet been reported.

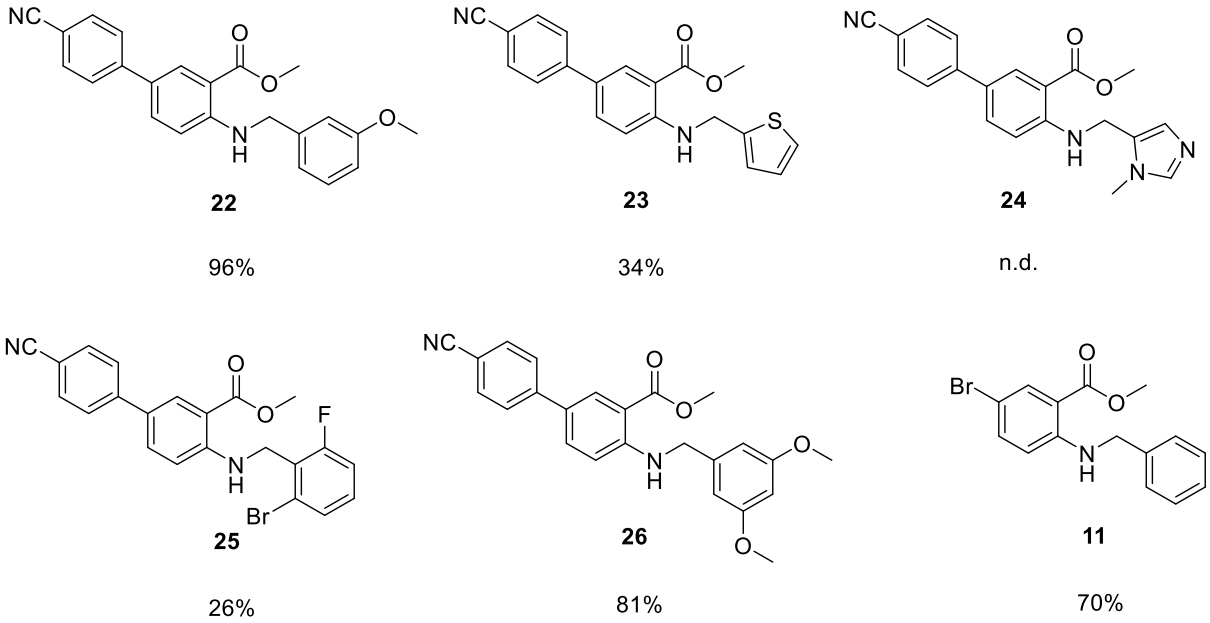

Figure 16. Reductive amination results, n.d. = Not isolated as the crude was directly submitted for tetrazole formation.

Compounds **11**, **22**, **26** had good to excellent yields (70-96%), whilst **23** and **25** showed significantly lower yields (26-34%). The low yield of compound **25** might be due to sterics of the bulky bromo substituent. Compound **23** has an electron donating sulfur in the heterocycle, which makes the carbonyl carbon of the aldehyde less electrophilic. Compound **22** has excellent yields using an aldehyde that has an electron donating group. The cause of the high yield might be that the electron donating group is in the *meta* position and thereby therefore can't donate electron density to the carbonyl group *via* mesomery. The same is true for compound **26**.

Compound **24** was not isolated as the R_f value of the aldehyde was indiscernible from the product. A very slow gradient on flash chromatography (DCM:MeOH) could not separate the two compounds. To remedy this, the crude was submitted directly for tetrazole formation in belief that the tetrazole functional group would impact the R_f value significantly. Other options could have been to use the aldehyde as the limiting reagent and make sure the reaction ran to completion or to swap the order of the reductive amination and the Suzuki-Miyaura coupling in hope of better separation at a later stage.

Due to time constrictions, elongating the *ortho* position with a carbon linker through reductive amination was not carried out.

3.3.3 Tetrazole formation

After reductive amination, the next step in the synthetic plan (2, Scheme 14) was tetrazole formation. The tetrazole formation from a cyano group is a well-studied reaction.[99,108-111] In this work, the conditions were based on our groups previous work with tetrazoles where those delivered excellent yields with similar systems.[7] The compounds synthesized in the previous step (**11**, **22**-**26**) were treated with dibutyltin (IV) oxide (0.1 eq) and trimethylsilyl azide (1.0 eq) in DCE to provide **20**, **27**-**31** as shown in Scheme 23. Compounds **20**, **27**-**21** have not been reported in literature.

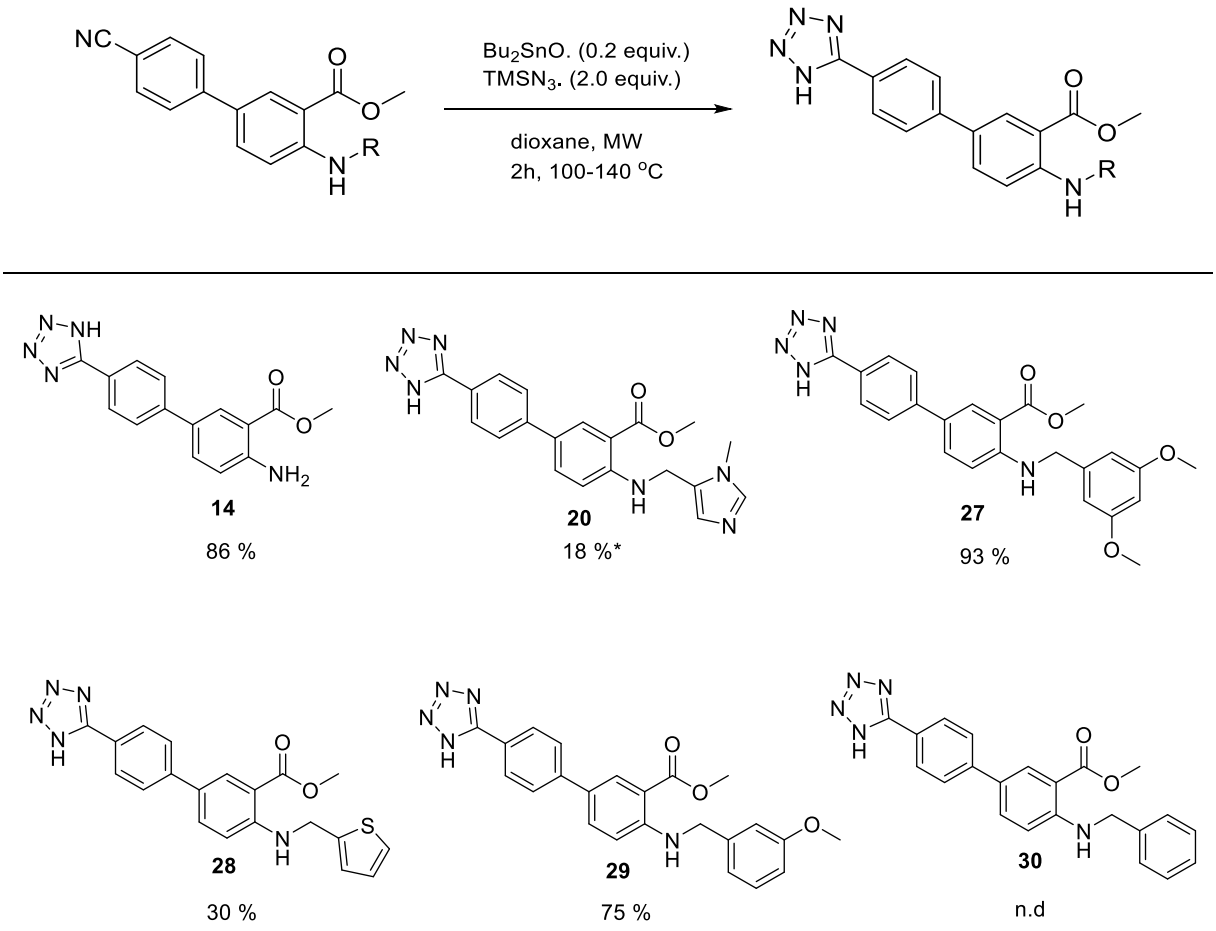

*Scheme 23. Overview of reaction conditions for tetrazole formation. * = 13% impurities found for compound 27. N.d = not determined.*

Compounds **14**, **27** and **29** were obtained with good to excellent yields (> 75%), whilst **20** and **28** were obtained with poor yields (< 30%). Compound **30** was submitted directly to hydrolysis and no yield for the tetrazole formation step was determined. Based on crude NMR (and

supported by TLC and HR-MS), the compounds showed good conversion under the given reaction conditions, thus the poor yield for some of the compounds are probably explained by work-up and purification problems. For compounds **14**, **20**, **27**, **29** the reaction was attempted at least twice and showed different behavior during work-up each time, making it difficult to devise a general work-up strategy. However, the yields increased during more attempts, which is likely due to a more comprehensive understanding of the structures.

The major difference between previous work in our group and the compounds presented in this work was the amine functional group. The combination of an acidic tetrazole moiety and a basic amine moiety results in the molecule always having a charge. The tetrazole or the amine groups were always ionised and the structures become amphiphilic with the hydrophobic bi-aryl scaffold. Aniline and tetrazole moieties have pKa of approximately 4.9. Thereby, if pH ≥ 7 the compounds will mainly exist in an ionized form with negatively charged tetrazole and neutral amine (**14c**, Figure 17). On the other hand, at low pH ≤ 3, the compound will be in an ionized form with neutral tetrazole while the amine group is protonated and positively charged (**14a,** Figure 17). At pH between 3-7 allows the compound will exhibit different ionized forms including double charged compound with zwitterionic nature (**14b**) as shown in Figure 17.

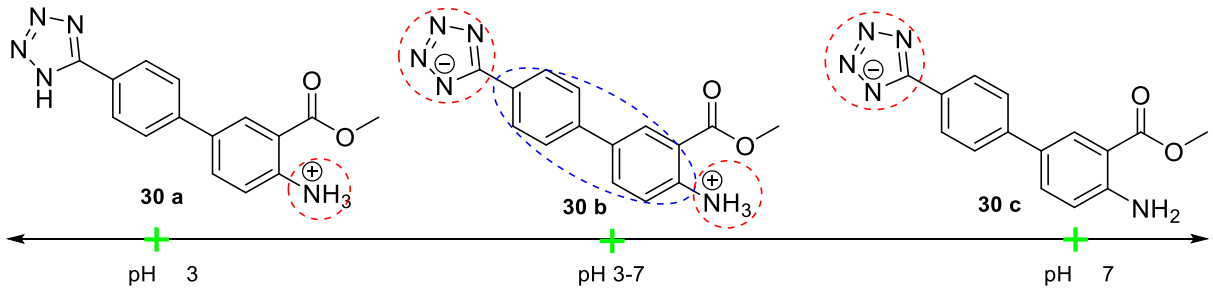

*Figure 17. Modified scaffold (**14**) with highlighted amphiphile characteristics and different ionization forms according to pH, red = Hydrophilic, blue = Hydrophobic.*

As a consequence, we encountered problems when attempting extraction, running TLCs and column chromatography or obtaining NMR data, and the general method proposed had to be adapted to each individual reaction.

Investigation towards a work-up procedure: One of the encountered problems was partial solubility, as some of the products precipitated in the reaction solvent and some were completely soluble. Compound **14**, **20**, **27** and **28** precipitated in dioxane during the tetrazole formation in the microwave, suggesting the solubility in dioxane was poor, which could be

exploited for an easy work-up. Only compound **29** did not precipitate in dioxane. Thereby, the compounds (**14**, **20**, **27**, **28**) were submitted to filtration directly upon reaction completion and washed with small amounts of cold dioxane to remove impurities/staring material. Unfortunately, it was not possible to fully isolate the pure product in form of a precipitate as a lot of product was observed in the filtrate as well. Several attempt of filtrating the crude with cold pentane and other non-polar solvents that were predicted to not dissolve the compounds took place. All filtration attempts with using different solvent were unsuccessful as it did not result in a maximum yield. Only compound **27** was able to be isolated by filtration as a pure precipitate with good yields (93%). The solubility inconveniences could be explained by the hydrophobic section of the molecule that takes precedence and partially dissolves the residue.

Extractive work-up was then attempted on compounds **14**, **20**, **28**-**29** to prevent the loss of the product that could result from filtration. THF had shown the ability to dissolve most of the compounds and it was believed that the compounds (**14**, **20**, **28**-**29**) would prefer the organic phase. As THF is partially miscible with water, 2-methyl THF was used for extraction instead. Extractive work-up showed the same limitation as in the filtration step as the products were observed in both aqueous and organic phases. This resulted in exclusion of extraction for being an ineffective work-up method if maximum yields were desirable. The conclusion thereby became to attempt purification of the reaction mixture without additional work-up.

Investigation towards a purification procedure: In the process to find a suitable chromatographic purification system, the first general trend noticed regarding finding suitable elution systems to the column chromatography for molecules **14**, **20**, **28**-**29** was TLC tailing. The compounds were unable to move on normal silica plates, due to the charges. Normal silica was exchanged with C-18 silica plates, but tailing was observed when using normal eluents such as water:acetonitrile. To mediate the tailing several eluent combinations were tested in order to control pH and/or deactivate the silica plates, including triethylamine, TFA, *N*,*N*-Diisopropylethylamine (DIPEA) in water:acetonitrile. As a result of the attempts 0.1 % TFA in water and acetonitrile was found to be the most effective in preventing tailing, creating estimate pH of around 2-3 with the purpose of protonating the amine and making a net positive charge on the molecule.

The method of purification for compounds **14**, **20**, **28**-**29** thereby became direct submission of the crude to C-18 flash chromatography with 0.1 % TFA in water and acetonitrile and flushing the pre-samplets with THF, if the product had solidified. Compound **29** partially solidified after the column chromatography within the pre-samplet whilst some was isolated from the column fractions. The product in the pre-sample was flushed out with THF, analysed by ^{1}H NMR and ^{13}C NMR and compared to the product found in the fractions after column. The analysis clearly showed the presence of the product **29** in both samples. The first hypothesis was that different protonation states caused this intriguing behaviour, but the protonated amine was visible in both NMRs. The difference in separation may be caused by different behaviour of the compound in the column as a result of its only partial solubility in water:acetonitrile. This purification method was generally successful despite that some of the compounds needed several columns to yield the pure product.

One particularly challenging molecule to separate in the C-18 column was compound **20,** shown in Scheme 24.

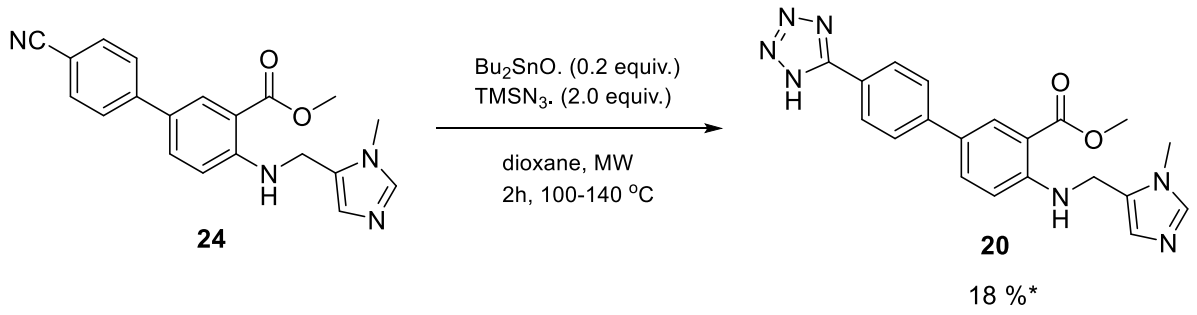

*Scheme 24. Synthesis of methyl 4-(((1-methyl-1H-imidazol-5-yl)methyl)amino)-4'-(1H-tetrazol-5-yl)-[1,1'-biphenyl]-3-carboxylate (**20**).*

Compound **20** was synthesized over two-steps, with 18 % yield. The compound behaved different than the other candidates when applied to the general eluent system C-18 flash chromatography with 0.1 % TFA in water and acetonitrile. Compound **20** did not show any tailing on C-18 TLC, but on the flash chromatography the compound tailed and exited the column over a large range of column volumes. In addition, the compound had to be submitted for purification several times, before it was finally isolated in 87% purity (SFC). Possible reasons for the column tailing are the additional charge of the imidazole ring but could also be that pH 2-3 was not enough to protonate the moieties consistently. Recrystallization could be

an alternative to limit purification problems as tetrazoles have a highly crystalline nature,[112-114] but recrystallization was not attempted due to time constraints.

Notes on analytical methods: After purification, finding a suitable NMR solvent also proved a challenge for compounds **14**, **20**, **27-29**. Dissolving the tetrazole containing compounds in classic NMR solvents such as $CDCl_3$, MeOD or D_2O was not possible. Alternatively, DMSO and *d*-THF were considered as they showed better solubility of this type of compounds. Despite that DMSO dissolved the majority of the compounds (**14**, **27**, **28**,), it was preferably the last option to spare the time required for regaining the product after dissolving it due its high boiling point. *d*-THF was also a good choice as NMR solvent and at least partially dissolved most of the compounds. Unfortunately, *d*-THF is expensive and not readily available. Compound **20** failed to dissolve in the given NMR solvents, which could be due to the 13 % of impurities that we did not manage to separate. *d*-Acetic acid was shown to be a suitable NMR solvent for compound **20** so, it was used to obtain the final analytical data.

Considering all the aforementioned challenges with work-up and purification, the general method that seemed most suitable for similar compounds was direct application of crude C-18 flash chromatography with 0.1 % TFA in water and acetonitrile. If solidification of product occurred within the pre-samplet, THF was applied successfully to elute the remaining residue.

Note on reductive amination after tetrazole formation (strategy 1): The synthetic strategy 1 (Scheme 13) suggests reductive amination on the tetrazole substrate **14** (Scheme 25). The reactions were attempted but failed due to the difficulties encountered while working with the charged/zwitterionic characteristics combined with the amphiphilic characteristic. The tetrazole-compounds could not dissolve in common solvents used for reductive amination (EtOAc, DCE, IPA) and the aldehyde solubility was an additional factor to consider in the reaction. A combination of the low conversion and general difficulties in purifications as explained above discouraged the continuing of synthetic strategy 1.

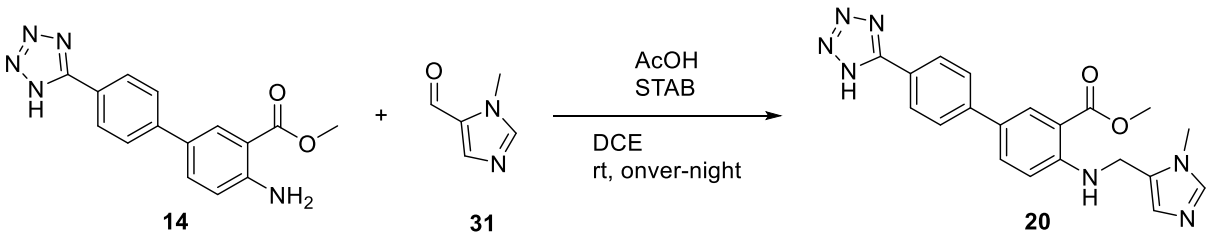

*Scheme 25. Attempted reductive amination on methyl 4-amino-4'-(1H-tetrazol-5-yl)-[1,1'-biphenyl]-3-carboxylate (**14**).*

Lastly, in ^{13}C NMR analysis of the tetrazole compounds, one carbon was often missing. More specifically the tetrazole carbon shown in Figure 18.

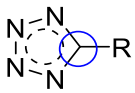

Figure 18. Tetrazole carbon (blue circle), often not observed in ^{13}C NMR

Weak or no signals of this carbon is common and has been reported previously.[7,115,116] The carbon can however be observed with the use of HMBC, shown for compound **29** (Figure 19). The signal labeled tetrazole carbon shows no interactions with any visible peak from the ^{13}C NMR but shows a clear interaction between a carbon and the hydrogens 2 and 6.

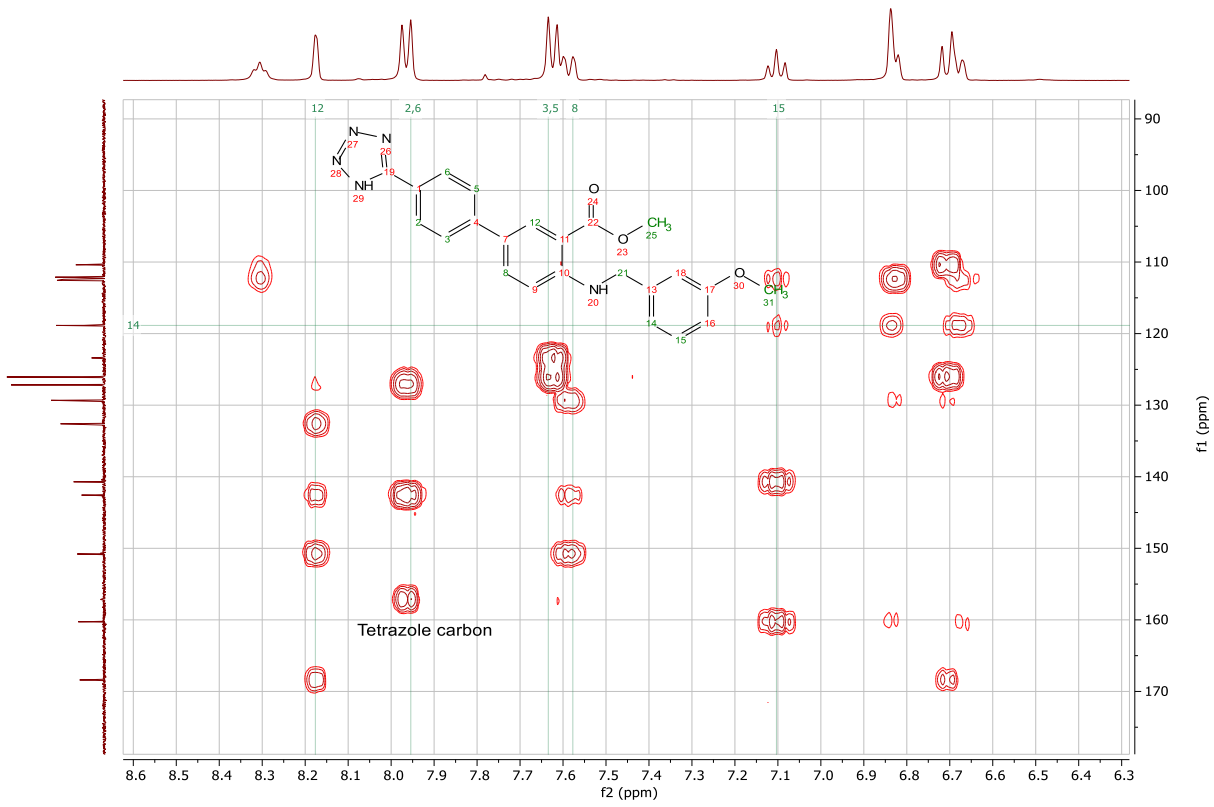

*Figure 19. 2D NMR of compound **25** showing missing tetrazole carbon.*

3.3.4 Hydrolysis of carboxylic esters

With the tetrazoles in hand, we continued the synthetic plan with hydrolysis to liberate the desired acid. The hydrolysis of carboxylic esters to carboxylic acids are well-studied.[117] The most common conditions for basic hydrolysis of carboxylic acids are sodium, lithium and/or potassium hydroxide [74a,118,119] in MeOH, water or THF at ambient temperature. The most common condition for acidic hydrolysis is using HCl with or without a solvent.[74a]

An overview of the reaction and results are given below in Scheme 26.

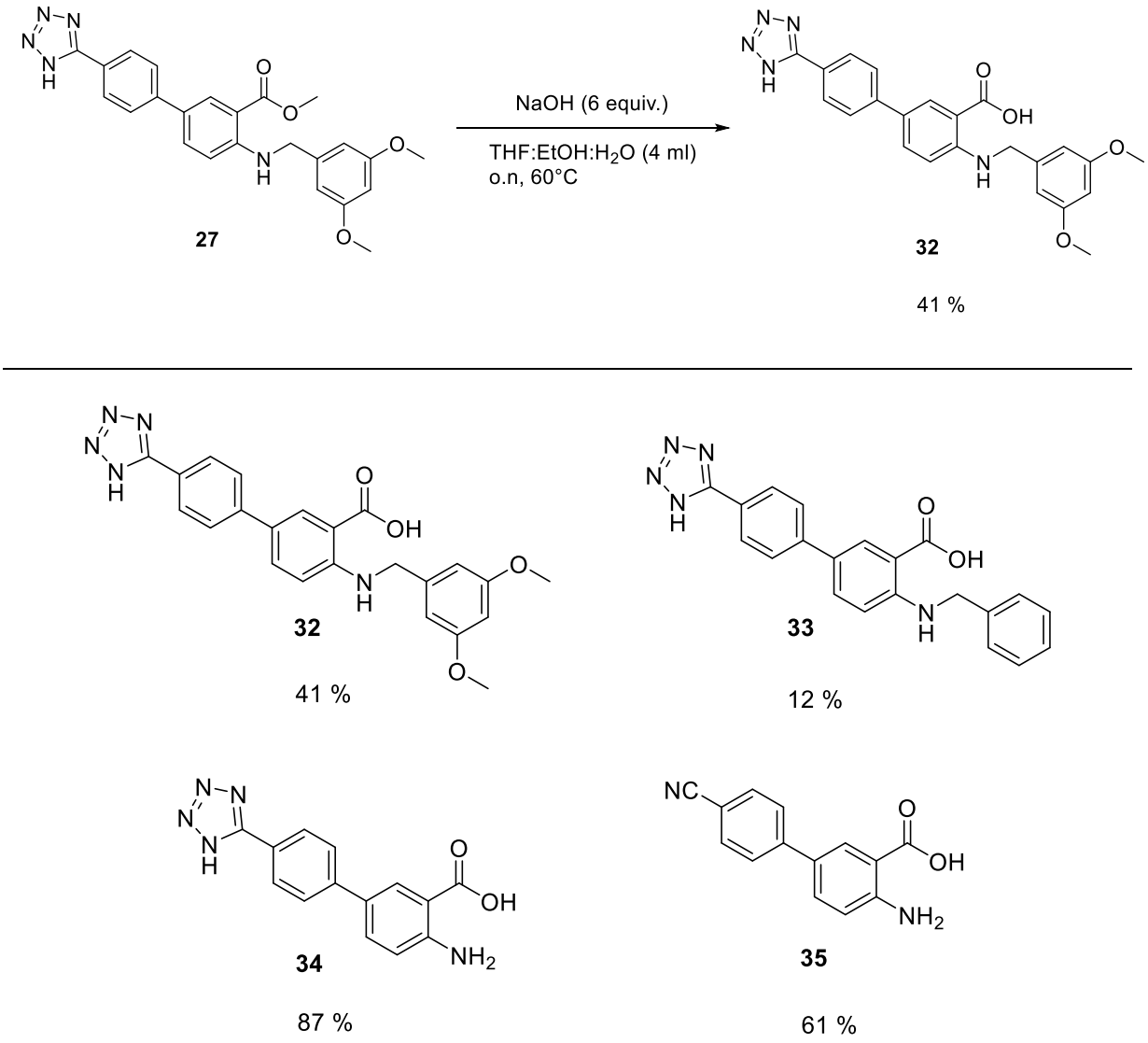

Scheme 26. Overview of ester hydrolysis reactions.

The four compounds **32**-**35** (Scheme 26) were obtained by dissolving starting material in THF:EtOH:H_2O and adding sodium hydroxide (6 equiv.). Initial attempts were made at ambient temperature but observing no change (TLC) the reaction temperature was increased to 60°C and left overnight. The mixture was purified with C-18 flash chromatography yielding poor to good yields (12% - 87%). The columns were flushed with 100 % water as a desalting step, before eluting with acetonitrile. The acids **32**, **33**, **34** and **35** were obtained in 41%, 12%, 87%, and 61% yields, respectively. The low yields can be explained by poor separation on the column. The solvent combination of THF:EtOH:H_2O was suggested by Wei et al.[120] for dissolving amino acids, and was applied with success as several other solvent combination failed.

For compound **34** a different work-up method was attempted in hopes that flash chromatography could be excluded to save time. For compounds soluble in organic solvents, the salts after hydrolysis (either HCl, sodium hydroxide etc) can be washed away into the aqueous phase of an extraction. The problem with the extraction of our charged compounds was that they were insoluble in most of the common organic solvents, resulting in the compound and the salt from sodium hydroxide (or other salts used) being inseparable in the aqueous phase. An attempt to remedy this was carried out by extracting with 2-methyl-THF and acidifying the aqueous phase. Crude NMR of the organic phase showed the product and butylated hydroxytoluene (BHT). BHT is probably introduced through the 2-methyl THF as it is a commonly used stabilizer to prevent the formation of peroxides in organic ethers.[121] C-18 flash chromatography was thereby needed nonetheless, yielding 87 % product (**34**).

Acid ester hydrolysis (Scheme 27) was envisioned as HCl could simply be evaporated under reduced pressure yielding the Cl adduct of the hydrolyzed product without any further work-up

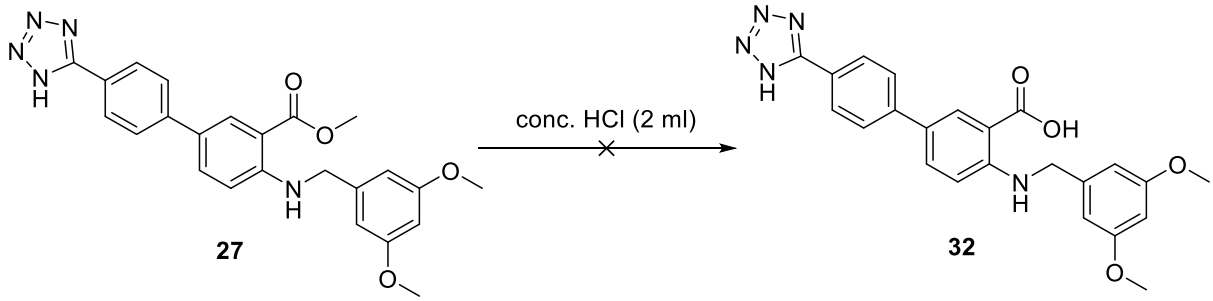

*Scheme 27. Attempted synthesis of methyl 4-((3,5-dimethoxybenzyl)amino)-4'-(1H-tetrazol-5-yl)-[1,1'-biphenyl]-3-carboxylate (**32**) by acid catalyzed hydrolysis.*

Having dissolved several of the tetrazole structures in acetic acid, it was suspected that stirring in concentrated HCl would dissolve and hydrolyze the compound yielding the desired product. The reaction was set up with 20 mg of **27** in 2 mL HCl but showed only partial dissolution. It was monitored by TLC, but after six hours there was no change and HRMS showed only starting material. To mediate this, the reaction temperature was increased to 60°C, which looked to dissolve the compound, and it was left overnight. TLC and HRMS showed no further signs of product so as a last attempt on the acidic hydrolysis, the reaction mixture was submitted to microwave irradiation for 30 min at 100°C. This resulted in the starting material decomposing and further attempts on acidic hydrolysis were discontinued.

4. Biological Results

All the biological testing was performed in collaboration with The Norwegian Structural Biology Centre (NorStruct) and Universitetssykehyset Nord-Norge (UNN) and performed by Susann Skagseth. The compounds were tested towards OXA-48 using Nitrocefin as reporter substrate. The OXA-48 will hydrolyse the β-lactam ring of Nitrocefin, which shifts the ultraviolet absorption of Nitrocefin and allows for visual detection of β-lactamase activity. A diluted series of the inhibitor provides a quantitative measurement indicating how much of the inhibitor is needed to inhibit OXA-48s ability to hydrolyse Nitrocefin by 50%. From this data an IC_{50} can be determined. Due to time management only two compounds were submitted for biological testing. The purity of the compounds submitted was determined by SFC to be **>99%**. The IC_{50} values for compound **32** and **35** were found to be 128 µM and 3.3 µM respectively. The compounds can be seen in Figure 20:

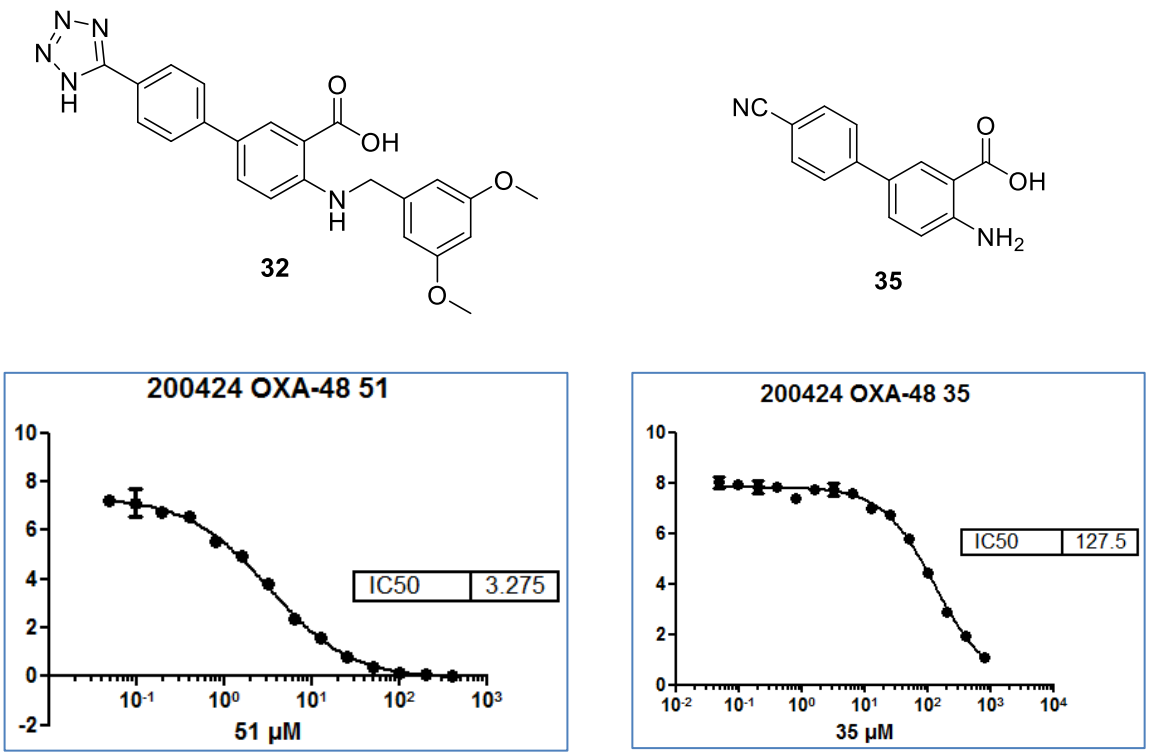

Figure 20. Compounds for biological testing with corresponding IC50 graphs.

Based on evaluation of the previous library presented by our group it was expected that compound **32** would have a better IC_{50} value than compounds **35**. The tetrazole moiety had shown the best affinity of all the previously tested fragments in the *meta*-position, and it was hypothesized that the cyano moiety of compound **35** would not reach far enough into the pocket

for a strong interaction with arginine 214. The *meta* substituents had previously mainly shown interaction with arginine 214, which can form one donating and one accepting hydrogen bonds. Tetrazole can accept one and donate one hydrogen bond, and it was thereby suspected that the interactions could be strong. Nitrile can just accept a hydrogen bond and was thereby predicted to have a lower IC_{50}. Compound **32** additionally has an aryl substituted on its *ortho* positioned amine, which could create more interactions with the binding site. The starting scaffold without any *ortho* substituents (**1**) had an IC_{50} = 36 µM, which was improved by the *ortho* substituent on compound **32** to an IC_{50} = 3.3 µM. There is not enough data to conclude whether 2,5-substituents are better than 3,5-*dimeta* substituents, but the results are promising.

To gauge the application of SeeSAR, the two compounds are compared in Figure 21.

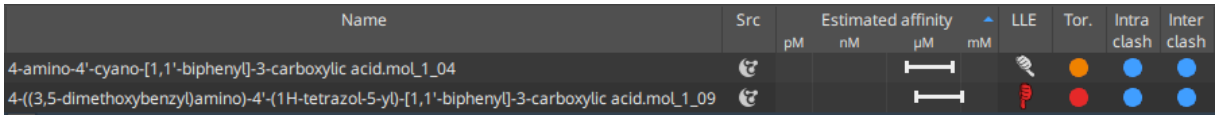

Figure 21.SeeSAR's evaluation of the two biologically tested fragments

As we used SeeSAR in the planning of the compound library, it was interesting to compare the estimated affinities and experimental inhibitor activity. The estimated affinity proposed by SeeSAR is not directly comparable to IC_{50} values and must be considered thusly. As can be seen in Figure 21, SeeSAR estimated compound **35** to have a higher estimated affinity than compound **32**. Since the results deviated a lot, we had a closer look at the SeeSAR models to understand how the software evaluated the compounds. SeeSAR evaluates that the tetrazole and two carbons give negative contributions to the overall affinity due to desolvation (carbons with red corona in Figure 22). Furthermore, it is estimated that one of the methoxy groups contributes positively to hindering desolvation but does not show any interactions between the new *ortho*-addition and the binding site. SeeSAR identified that compound **32** and **35** showed the following interactions: arg214, arg250, thr209 Compound **35** also interacted with ser118.

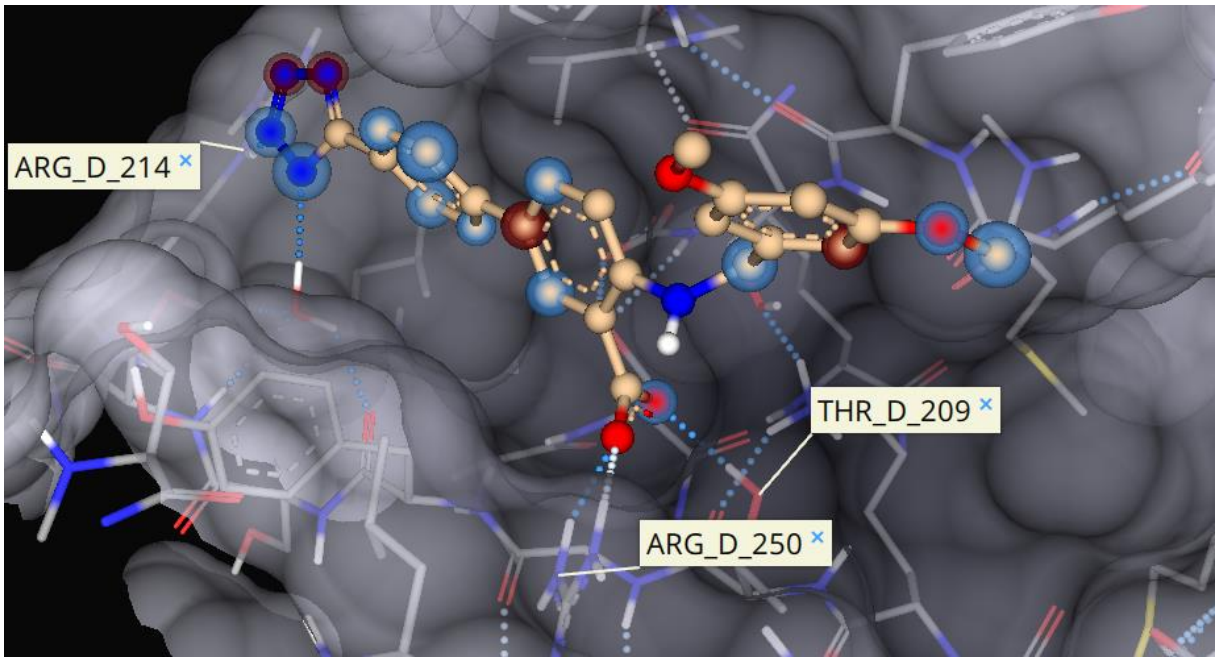

Figure 22. SeeSAR representation of compound 51 in the binding site of OXA-48.

Compound **35,** however, does not show any negative contributions in SeeSAR, as shown in Figure 23, and that is the reason why it is being ranked above compound **32** for estimated affinity. A possible explanation is that SeeSAR does not account for π-π stacking which might allow the fragment to reach further into the binding site compared to what might happen in the actual inhibition. Furthermore, SeeSAR models the enzyme to be static, which may also skew the estimated affinity in favor of compound **35**.

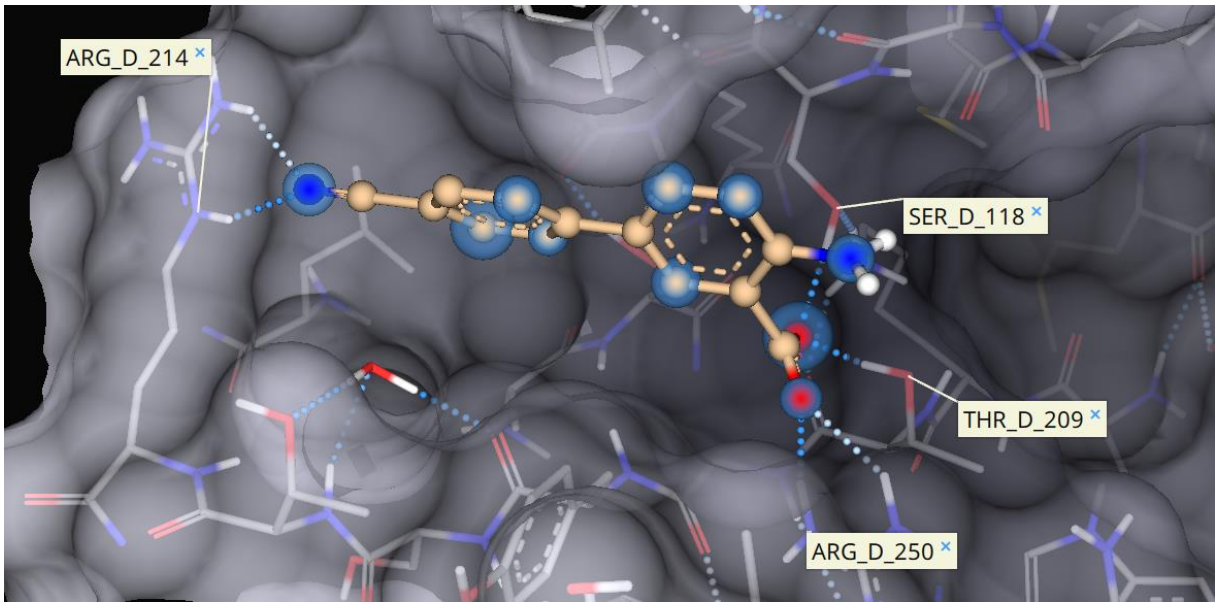

Figure 23. SeeSAR representation of compound 35 in the binding site of OXA-48.

This comparison underlines what was specified in the result and discussion section of this thesis; the utilized version of SeeSAR is missing important parameters for accurate estimations and estimated affinities should be considered carefully. SeeSAR did however identify trends which lead to the synthesis of compounds **32**, which turned out to have a good IC_{50}. No conclusion can be drawn due to the limited amount of data, but the inspiration from SeeSAR in combination with the knowledge of the program's limitations can still be a powerful tool in SBDD.

5. Future Outlook

Due to time management and the interference of the COVID-19 pandemic, the project was cut short. Finishing the fragments already started and finalizing them for biological testing would be the primary objective for the future. As shown in the biological data, compound **32** inhibited OXA-48 with an IC_{50} of 3.3 µM, which is an improvement on the previously reported mono substituted fragments from our group and similar value to di-*meta*-substituted ones (2.9 µM). This inhibition could be an outlier but could also suggest good potential for new inhibitors with an *ortho* substituted functionalisation and should be further investigated. Attempting to synthesize the elongated molecules would be a high priority, given more time. The trend was apparent from the SeeSAR results that elongated molecules would reach new potential binding residues in the binding site and could provide increased inhibition.

Furthermore, it would be interesting to co-crystalize the inhibitors and the OXA-48 enzyme for X-ray analysis to gauge whether the amine contributed to the inhibition. If, as hypothesized through the computational work, it does contribute, the synthetic route herein could be used to synthesize a larger library. If the amine does not contribute to the inhibition of OXA-48, substituting it for a functionality that does not introduce zwitterionic/charged/amphiphile characteristics, would be favourable. Additionally, the computational results presented herein could be of great guidance to future fragment design either by expanding the proposed library or creating new ones.

Lastly, for a new series of inhibitors, it could be interesting to investigate a benzhydrylamine (**36**) scaffold and develop it using structure-based drug design (Figure 24). Based on SeeSAR docking, benzhydrylamine could obtain an estimated affinity in the micro molar range and interact with the all-important serine 70 as well as serine 118, shown in Figure 25. A *di-meta* substituted scaffold (**37**) looks especially promising as SeeSAR suggest that the compounds could directly interact with serine 70, tyrosine 211, whilst *di-meta* substituents like carboxylic acid, tetrazole and phosphonic acid could reach threonine 209, serine 118 and arginine 250 and 214 (shown in Figure 26). The combination of these interactions shows a trend in all submitted fragments of consistent nanomolar inhibition. A preliminary biological test with commercially available benzhydrylamine could be attempted, to gauge the validity of the hypothesis.

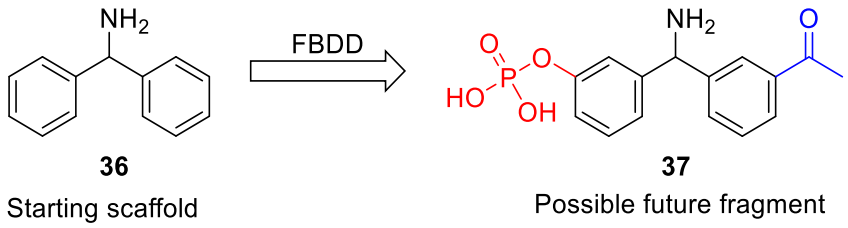

*Figure 24. Benzhydrylamine (**36**) scaffold transformation to new possible future fragment (**37**).*

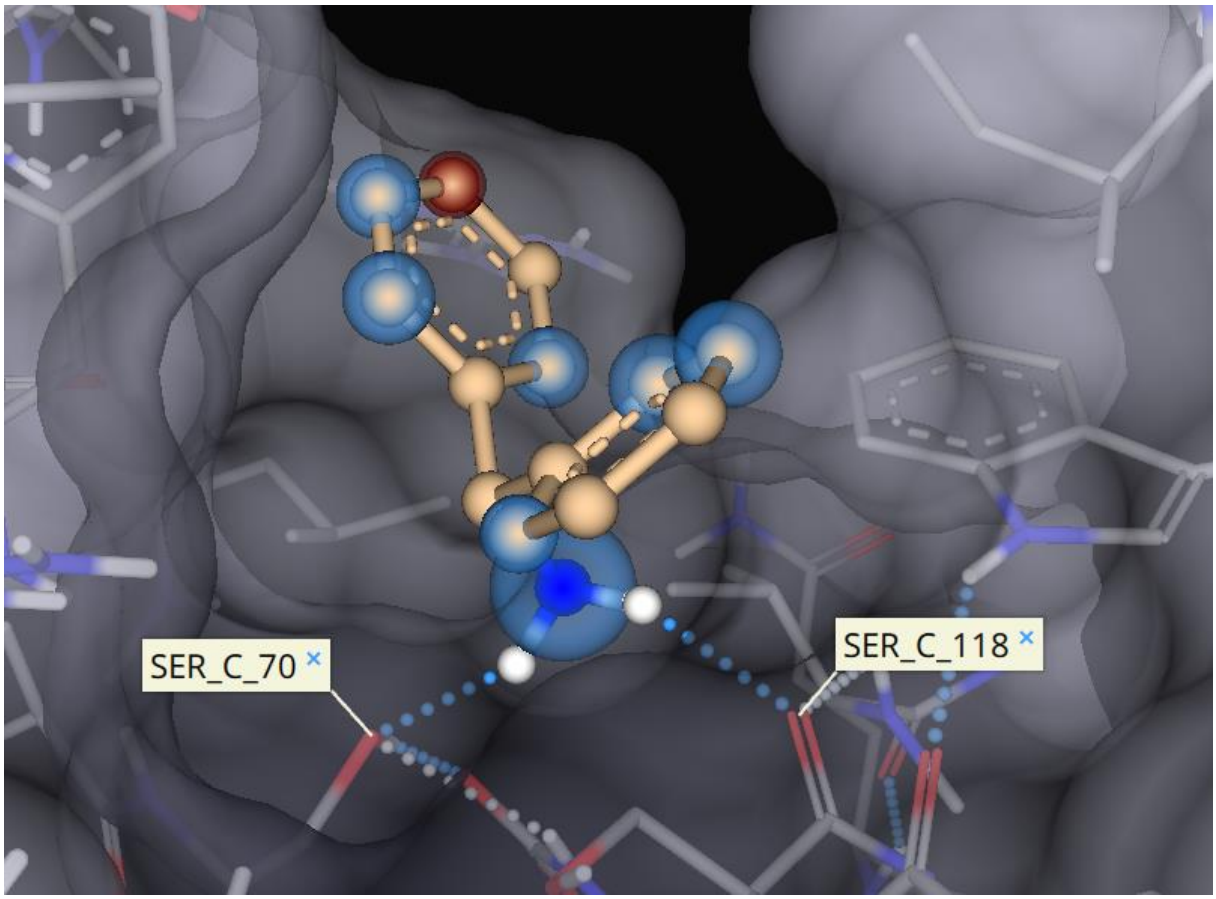

*Figure 25. Benzhydrylamine (**36**) in the active site of OXA-48, showing interactions with ser 70 and ser 118.*

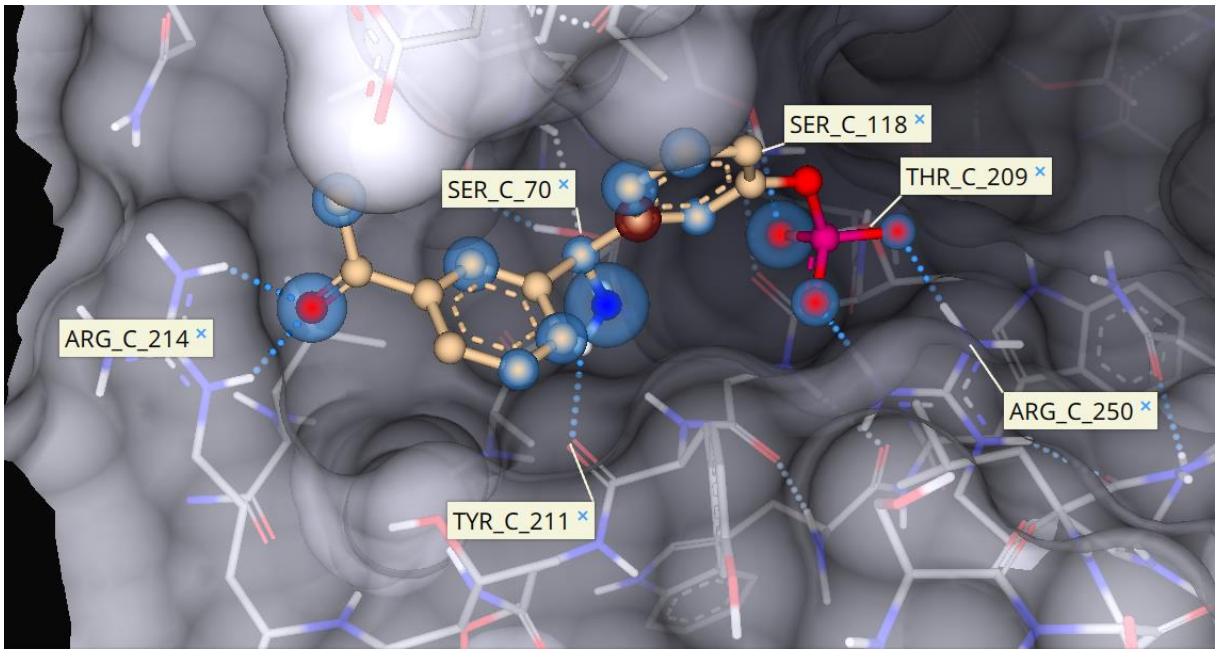

*Figure 26. Possible future fragment (**37**) based on benzhydrylamine in OXA-48 binding site, with nano-molar interaction.*

6. Conclusion

The spread of bacteria possessing antibiotic-deactivating enzymes is a major threat to society and is a growing problem. As the spread continue, it will be increasingly important to have new inhibitors and scaffolds in the pipeline. Our contribution is summarized below.

Three main objectives were identified for this thesis. First, designing new fragments for OXA-48 inhibition, focusing mainly on the 2-*ortho* position (Y) of 4'-(1*H*-tetrazol-5-yl)-[1,1'-biphenyl]-3-carboxylic acid (**1**). In chapter 3.1 We show that SeeSAR was used to explore the active site of OXA-48 and design a library of potential OXA-48 inhibitors. The work herein can be used for further inspiration in future projects by expanding the library proposed in this thesis or for new libraries.

In chapter 3.2 we show our efforts towards the second aim; to develop a synthetic strategy for the target fragments. The molecules identified in the computational section can be synthesized using the synthetic strategy 2 presented in Scheme 14, which was preferable to synthetic strategy 1 (Scheme 13) due to the difficulties of handling the proposed compounds. The synthesis developed here consisted of Suzuki-Miyaura cross coupling, reductive amination, tetrazole formation and ester hydrolysis.

The third and last aim was to synthesize a library of fragments for biological testing. The synthesis results and discussion can be seen in chapter 3.3 and the biological testing can be seen chapter 4. Two compounds (**32** and **35**) were delivered for biological testing (performed by Susann Skagseth) against the OXA-48 enzyme, with IC_{50} of 3.3 µM and 127 µM. The inhibition is very promising, and more analogs are desirable and in the pipeline. In total, 15 new compounds were synthesized and characterized by ^{1}H NMR, ^{13}C NMR, HR-MS, SFC*, IR* and melting point* (* = not for all the compounds)

All the initial aims were met and yielded a potent inhibitor towards OXA-48, with micromolar inhibition. The results herein can be used for further inhibitor optimization and inspiration.

7. References

1. World Health Organization, 5/02/2015, (accessed May 2020). https://www.who.int/news-room/fact-sheets/detail/antibiotic-resistance.
2. Kurz, S.G., Furin, J.J. & Bark, C.M. Drug-Resistant Tuberculosis: Challenges and Progress. *Infectious Disease Clinics of North America* **30**, 509-522 (2016).
3. Watkins, R.R. & Van Duin, D. Current trends in the treatment of pneumonia due to multidrug-resistant Gram-negative bacteria. *F1000 Research* **8**, Faculty Review-1121 (2019).
4. Seung, K.J., Keshavjee, S. & Rich, M.L. Multidrug-Resistant Tuberculosis and Extensively Drug-Resistant Tuberculosis. *Cold Spring Harbor Perspectives in Medicine* **5**, a017863-a017863 (2015).
5. Kong, K.-F., Schneper, L. & Mathee, K. β-lactam antibiotics: from antibiosis to resistance and bacteriology. *APMIS Journal of Pathology, Microbiology and Immunology* **118**, 1-36 (2010).
6. Bush, K. & Bradford, P.A. Interplay between β-lactamases and new β -lactamase inhibitors. *Nature Reviews Microbiology* **17**, 295-306 (2019).
7. Akhter, S., *et al.* A focused fragment library targeting the antibiotic resistance enzyme - Oxacillinase-48: Synthesis, structural evaluation and inhibitor design. *European Journal of Medicinal Chemistry* **145**, 634-648 (2018).
8. N, P. & Cascella, M. β-Lactam Antibiotics. (2019).
9. Palzkill, T. Metallo-β-lactamase structure and function. *Annals of the New York Academy of Sciences* **1277**, 91-104 (2013).
10. Blair, J.M., Webber, M.A., Baylay, A.J., Ogbolu, D.O. & Piddock, L.J. Molecular mechanisms of antibiotic resistance. *Nature Reviews Microbiology* **13**, 42-51 (2015).
11. Bush, K. Past and Present Perspectives on β-Lactamases. *Antimicrobial Agents and Chemotherapy* **62**, e01076-01018 (2018).
12. Bush, K. & Jacoby, G.A. Updated functional classification of β-lactamases. *Antimicrobial agents and chemotherapy* **54**, 969-976 (2010).
13. Mossakowska, D., Ali, N.A. & Dale, J.W. Oxacillin-hydrolysing β-lactamases. *European journal of biochemistry* **180**, 309-318 (1989).
14. Sgrignani, J., Grazioso, G. & De Amici, M. Insight into the Mechanism of Hydrolysis of Meropenem by OXA-23 Serine-β-lactamase Gained by Quantum Mechanics/Molecular Mechanics Calculations. *Biochemistry* **55**, 5191-5200 (2016).
15. Verma, V., *et al.* Hydrolytic mechanism of OXA-58 enzyme, a carbapenem-hydrolyzing class D β-lactamase from Acinetobacter baumannii. *Journal of Biological Chemistry* **286**, 37292-37303 (2011).
16. Evans, B.A. & Amyes, S.G.B. OXA β-lactamases. *Clinical Microbiololgy Reviews* **27**, 241-263 (2014).
17. Stewart, A., Harris, P., Henderson, A. & Paterson, D. Treatment of Infections by OXA-48-Producing Enterobacteriaceae. *Antimicrobial agents and chemotherapy* **62**, e01195-01118 (2018).
18. Poirel, L., Heritier, C., Tolun, V. & Nordmann, P. Emergence of oxacillinase-mediated resistance to imipenem in Klebsiella pneumoniae. *Antimicrobial Agents Chemotherapy* **48**, 15-22 (2004).
19. Mansour, W., *et al.* Outbreak of colistin-resistant carbapenemase-producing Klebsiella pneumoniae in Tunisia. *Journal of Global Antimicrobial Resistance* **10**, 88-94 (2017).

20. Pfeifer, Y., *et al.* Emergence of OXA-48-type carbapenemase-producing Enterobacteriaceae in German hospitals. *Antimicrobial agents and chemotherapy* **56**, 2125-2128 (2012).
21. Iacchini, S., *et al.* Bloodstream infections due to carbapenemase-producing Enterobacteriaceae in Italy: results from nationwide surveillance, 2014 to 2017. *Euro Surveillance* **24**, 1800159 (2019).
22. Nordmann, P., Naas, T. & Poirel, L. Global spread of Carbapenemase-producing Enterobacteriaceae. *Emerging Infectious Diseases* **17**, 1791-1798 (2011).
23. Villacís, J.E., *et al.* OXA-48 Carbapenemase in Klebsiella pneumoniae Sequence Type 307 in Ecuador. *Microorganisms* **8**, 435 (2020).
24. Albiger, B., *et al.* Carbapenemase-producing Enterobacteriaceae in Europe: assessment by national experts from 38 countries, May 2015. *Eurosurveillance* **20**, 30062 (2015).
25. Ahmed, A., Azim, A., Gurjar, M. & Baronia, A.K. Current concepts in combination antibiotic therapy for critically ill patients. *Indian Journal of Critical Care Medicine* **18**, 310-314 (2014).
26. Coates, A.R.M., Hu, Y., Holt, J. & Yeh, P. Antibiotic combination therapy against resistant bacterial infections: synergy, rejuvenation and resistance reduction. *Expert Review of Anti-infective Therapy* **18**, 5-15 (2020).
27. Tyers, M. & Wright, G.D. Drug combinations: a strategy to extend the life of antibiotics in the 21st century. *Nature Reviews Microbiology* **17**, 141-155 (2019).
28. Butler, M.S. & Paterson, D.L. Antibiotics in the clinical pipeline in October 2019. *The Journal of Antibiotics* **73**, 329-364 (2020).
29. Lee, Y.R. & Baker, N.T. Meropenem-vaborbactam: a carbapenem and β-lactamase inhibitor with activity against carbapenem-resistant Enterobacteriaceae. *European Journal of Clinical Microbiology & Infectious Diseases* **37**, 1411-1419 (2018).
30. Liscio, J.L., Mahoney, M.V. & Hirsch, E.B. Ceftolozane/tazobactam and ceftazidime/avibactam: two novel β-lactam/β-lactamase inhibitor combination agents for the treatment of resistant Gram-negative bacterial infections. *International Journal of Antimicrobial Agents* **46**, 266-271 (2015).
31. Zasowski, E.J., Rybak, J.M. & Rybak, M.J. The β-Lactams Strike Back: Ceftazidime-Avibactam. *Pharmacotherapy* **35**, 755-770 (2015).
32. Lahiri, S.D., *et al.* Molecular basis of selective inhibition and slow reversibility of avibactam against class D carbapenemases: a structure-guided study of OXA-24 and OXA-48. *American Chemical Society Chemical Biology* **10**, 591-600 (2015).
33. Livermore, D.M., *et al.* Activities of NXL104 combinations with ceftazidime and aztreonam against carbapenemase-Producing Enterobacteriaceae. *Antimicrobial Agents Chemotherapy* **55**, 390-394 (2011).
34. Kazmierczak, K.M., Bradford, P.A., Stone, G.G., de Jonge, B.L.M. & Sahm, D.F. In Vitro Activity of Ceftazidime-Avibactam and Aztreonam-Avibactam against OXA-48-Carrying Enterobacteriaceae Isolated as Part of the International Network for Optimal Resistance Monitoring (INFORM) Global Surveillance Program from 2012 to 2015. *Antimicrobial Agents Chemotherapy* **62**(2018).
35. Ehmann, D.E., *et al.* Avibactam is a covalent, reversible, non-β-lactam β-lactamase inhibitor. *Proceedings of the National Acadamy of Sciences of the United States of America* **109**, 11663-11668 (2012).

36. Shields, R.K., *et al.* Emergence of Ceftazidime-Avibactam Resistance Due to Plasmid-Borne blaKPC-3 Mutations during Treatment of Carbapenem-Resistant Klebsiella pneumoniae Infections. *Antimicrobial Agents Chemotherapy* **61** (2017).
37. Hecker, S.J., *et al.* Discovery of a Cyclic Boronic Acid β-Lactamase Inhibitor (RPX7009) with Utility vs Class A Serine Carbapenemases. *Journal of Medical Chemistry* **58**, 3682-3692 (2015).
38. Hamrick, J.C., *et al.* VNRX-5133 (Taniborbactam), a Broad-Spectrum Inhibitor of Serine- and Metallo-β-Lactamases, Restores Activity of Cefepime in Enterobacterales and Pseudomonas aeruginosa. *Antimicrobial Agents Chemotherapy* **64**(2020).
39. Pattanaik, P., *et al.* Strategic design of an effective β -lactamase inhibitor LN-1-255, A 6-alkylidene-$2'$ -substituted penicillin sulfone. *The Journal of biological chemistry* **284**, 945-953 (2008).
40. Vallejo, J.A., *et al.* LN-1-255, a penicillanic acid sulfone able to inhibit the class D carbapenemase OXA-48. *Antimicrobial Agents Chemotherapy* **71**, 2171-2180 (2016).
41. Lund, B.A., Christopeit, T., Guttormsen, Y., Bayer, A. & Leiros, H.-K.S. Screening and Design of Inhibitor Scaffolds for the Antibiotic Resistance Oxacillinase-48 (OXA-48) through Surface Plasmon Resonance Screening. *Journal of Medicinal Chemistry* **59**, 5542-5554 (2016).
42. Danielson, U.H. Fragment library screening and lead characterization using SPR biosensors. *Current Topics in Medical Chemistry* **9**, 1725-1735 (2009).
43. Congreve, M., Chessari, G., Tisi, D. & Woodhead, A.J. Recent developments in fragment-based drug discovery. *Journal of Medicinal Chemistry* **51**, 3661-3680 (2008).
44. Taylor, D.M., *et al.* Identifying Oxacillinase-48 Carbapenemase Inhibitors Using DNA-Encoded Chemical Libraries. *American Chemical Society Infectious Diseases* (2020).
45. Leonard, D.A., Bonomo, R.A. & Powers, R.A. Class D β-Lactamases: A Reappraisal after Five Decades. *Accounts of Chemical Research* **46**, 2407-2415 (2013).
46. Meng, X.-Y., Zhang, H.-X., Mezei, M. & Cui, M. Molecular docking: a powerful approach for structure-based drug discovery. *Current Computer-Aided Drug Dessign* **7**, 146-157 (2011).
47. Yusuf, M., Hardianto, A., Muchtaridi, M., Nuwarda, R.F. & Subroto, T. Introduction of Docking-Based Virtual Screening Workflow Using Desktop Personal Computer. *Encyclopedia of Bioinformatics and Computational Biology* 688-699 (2019).
48. SeeSAR version 10.0; BioSolveIT GmbH, Sankt Augustin, Germany, 2020, www.biosolveit.de/SeeSAR
49. Morgan, P. & Mdluli, V. Fragment-Based Design of a Potential TNF-α Inhibitor Inspired by Castanospermine and Methyl Phenylacetate. *American Chemical Society Infectious Diseases* **5**, 9-18 (2018).
50. Brethon, A., *et al.* New Caspase-1 inhibitor by scaffold hopping into bio-inspired 3D-fragment space. *Bioorganic & Medicinal Chemistry Letters* **27**, 5373-5377 (2017).
51. Miyaura, N., Yamada, K. & Suzuki, A. A new stereospecific cross-coupling by the palladium-catalyzed reaction of 1-alkenylboranes with 1-alkenyl or 1-alkynyl halides. *Tetrahedron Letters* **20**, 3437-3440 (1979).
52. Buchspies, J. & Szostak, M. Recent Advances in Acyl Suzuki Cross-Coupling. *Catalysts* **9**, 53 (2019).
53. Maluenda, I. & Navarro, O. Recent Developments in the Suzuki-Miyaura Reaction: 2010–2014. *Molecules* **20**, 7528-7557 (2015).

54. Hatakeyama, T., *et al.* Iron-Catalyzed Suzuki−Miyaura Coupling of Alkyl Halides. *Journal of the American Chemical Society* **132**, 10674-10676 (2010).
55. Almond-Thynne, J., Blakemore, D.C., Pryde, D.C. & Spivey, A.C. Site-selective Suzuki–Miyaura coupling of heteroaryl halides – understanding the trends for pharmaceutically important classes. *Chemical Science* **8**, 40-62 (2017).
56. Hooshmand, S.E., Heidari, B., Sedghi, R. & Varma, R.S. Recent advances in the Suzuki–Miyaura cross-coupling reaction using efficient catalysts in eco-friendly media. *Green Chemistry* **21**, 381-405 (2019).
57. Biteau, N., Hervin, V., Roy, V. & Agrofoglio, L.A. Chapter 3 - Suzuki-Miyaura Cross-Coupling as a Synthetic Tool for Nucleoside and Nucleotide Modification. Book title: *Palladium-Catalyzed Modification of Nucleosides, Nucleotides and Oligonucleotides* (eds. Kapdi, A.R., Maiti, D. & Sanghvi, Y.S.) 37-74, (Elsevier, (2018).
58. Martin, R. & Buchwald, S.L. Palladium-catalyzed Suzuki-Miyaura cross-coupling reactions employing dialkylbiaryl phosphine ligands. *Accounts of Chemical Research* **41**, 1461-1473 (2008).
59. Dolliver, D.D., *et al.* Stereospecific Suzuki, Sonogashira, and Negishi Coupling Reactions of N-Alkoxyimidoyl Iodides and Bromides. *The Journal of Organic Chemistry* **78**, 3676-3687 (2013).
60. Littke, A.F., Dai, C. & Fu, G.C. Versatile Catalysts for the Suzuki Cross-Coupling of Arylboronic Acids with Aryl and Vinyl Halides and Triflates under Mild Conditions. *Journal of the American Chemical Society* **122**, 4020-4028 (2000).
61. Pan, C., *et al.* Palladium catalyzed ligand-free Suzuki cross-coupling reaction. *Catalysis Communications* **9**, 508-510 (2008).
62. Asachenko, A.F., Sorochkina, K.R., Dzhevakov, P.B., Topchiy, M.A. & Nechaev, M.S. Suzuki–Miyaura Cross-Coupling under Solvent-Free Conditions. *Advanced Synthesis & Catalysis* **355**, 3553-3557 (2013).
63. Casalnuovo, A.L. & Calabrese, J.C. Palladium-catalyzed alkylations in aqueous media. *Journal of the American Chemical Society* **112**, 4324-4330 (1990).
64. Amatore, C., Le Duc, G. & Jutand, A. Mechanism of Palladium-Catalyzed Suzuki–Miyaura Reactions: Multiple and Antagonistic Roles of Anionic "Bases" and Their Countercations. *Chemistry – A European Journal* **19**, 10082-10093 (2013).
65. Chun To, S. & Yee Kwong, F. Highly efficient carbazolyl-derived phosphine ligands: application to sterically hindered biaryl couplings. *Chemical Communications* **47**, 5079-5081 (2011).
66. Yin, J., Rainka, M.P., Zhang, X.-X. & Buchwald, S.L. A Highly Active Suzuki Catalyst for the Synthesis of Sterically Hindered Biaryls: Novel Ligand Coordination. *Journal of the American Chemical Society* **124**, 1162-1163 (2002).
67. Barder, T.E., Walker, S.D., Martinelli, J.R. & Buchwald, S.L. Catalysts for Suzuki−Miyaura Coupling Processes: Scope and Studies of the Effect of Ligand Structure. *Journal of the American Chemical Society* **127**, 4685-4696 (2005).
68. Harkal, S., *et al.* Dialkylphosphinoimidazoles as New Ligands for Palladium‐Catalyzed Coupling Reactions of Aryl Chlorides. *Advanced Synthesis & Catalysis* **346**, 1742-1748 (2004).
69. Fu, G.C. The development of versatile methods for palladium-catalyzed coupling reactions of aryl electrophiles through the use of P(t-Bu)3 and PCy3 as ligands. *Accounts of chemical research* **41**, 1555-1564 (2008).

70. Itoh, T. & Mase, T. Direct Synthesis of Hetero-Biaryl Compounds Containing an Unprotected NH2 Group via Suzuki—Miyaura Reaction. *Cheminform* **36**(2005).
71. Thompson, A.E., *et al.* Palladium-Catalyzed Cross-Coupling Reactions of Pyridylboronic Acids with Heteroaryl Halides Bearing a Primary Amine Group: Synthesis of Highly Substituted Bipyridines and Pyrazinopyridines. *The Journal of Organic Chemistry* **70**, 388-390 (2005).
72. Schulz, T., *et al.* A General Palladium-Catalyzed Amination of Aryl Halides with Ammonia. *Chemistry – A European Journal* **15**, 4528-4533 (2009).
73. Bruno, N.C., Tudge, M.T. & Buchwald, S.L. Design and Preparation of New Palladium Precatalysts for C-C and C-N Cross-Coupling Reactions. *Chemical science* **4**, 916-920 (2013).
74. Okuyama, T. & Maskill, H. *Organic chemistry : a mechanistic approach*, Oford University Press, Oxford (2014). a) page 190 b) page 191
75. Ranu, B.C., Majee, A. & Sarkar, A. One-Pot Reductive Amination of Conjugated Aldehydes and Ketones with Silica Gel and Zinc Borohydride. *The Journal of Organic Chemistry* **63**, 370-373 (1998).
76. Abdel-Magid, A.F. & Mehrman, S.J. A Review on the Use of Sodium Triacetoxyborohydride in the Reductive Amination of Ketones and Aldehydes. *Organic Process Research & Development* **10**, 971-1031 (2006).
77. Panfilov, A.V., *et al.* Sodium borohydride in reductive amination reactions. *Pharmaceutical Chemistry Journal* **34**, 76-78 (2000).
78. Alinezhad, H., Tajbakhsh, M. & Zamani, R. One-Pot Reductive Amination of Aldehydes and Ketones Using N- Methyl-piperidine Zinc Borohydride (ZBNMPP) as a New Reducing Agent. *Synlett* **37**, 0431-0434 (2006).
79. Podyacheva, E., Afanasyev, O.I., Tsygankov, A.A., Makarova, M. & Chusov, D. Hitchhiker's Guide to Reductive Amination. *Synthesis* **51**, 2667-2677 (2019).
80. Steinhuebel, D., Sun, Y., Matsumura, K., Sayo, N. & Saito, T. Direct Asymmetric Reductive Amination. *Journal of the American Chemical Society* **131**, 11316-11317 (2009).
81. Mizuta, T., Sakaguchi, S. & Ishii, Y. Catalytic Reductive Alkylation of Secondary Amine with Aldehyde and Silane by an Iridium Compound. *The Journal of Organic Chemistry* **70**, 2195-2199 (2005).
82. Kadyrov, R. & Riermeier, T.H. Highly Enantioselective Hydrogen-Transfer Reductive Amination: Catalytic Asymmetric Synthesis of Primary Amines. *Angewandte Chemie International Edition* **42**, 5472-5474 (2003).
83. Hoffmann, S., Nicoletti, M. & List, B. Catalytic Asymmetric Reductive Amination of Aldehydes via Dynamic Kinetic Resolution. *Journal of the American Chemical Society* **128**, 13074-13075 (2006).
84. Guo, X., Okamoto, Y., Schreier, M.R., Ward, T.R. & Wenger, O.S. Reductive Amination and Enantioselective Amine Synthesis by Photoredox Catalysis. *European Journal of Organic Chemistry*, 1288-1293 (2020).
85. Borch, R.F., Bernstein, M.D. & Durst, H.D. Cyanohydridoborate anion as a selective reducing agent. *Journal of the American Chemical Society* **93**, 2897-2904 (1971).
86. McLaughlin, M., Palucki, M. & Davies, I.W. Efficient Access to Azaindoles and Indoles. *Organic Letters* **8**, 3307-3310 (2006).
87. Kawase, Y., *et al.* Reductive Alkylation of Hydrazine Derivatives with α-Picoline-Borane and Its Applications to the Syntheses of Useful Compounds Related to Active Pharmaceutical Ingredients. *Synthesis* **46**, 455-464 (2014).

88. Nayal, O.S., Bhatt, V., Sharma, S. & Kumar, N. Chemoselective Reductive Amination of Carbonyl Compounds for the Synthesis of Tertiary Amines Using SnCl2·2H2O/PMHS/MeOH. *The Journal of Organic Chemistry* **80**, 5912-5918 (2015).
89. McGonagle, F.I., *et al.* Development of a solvent selection guide for aldehyde-based direct reductive amination processes. *Green Chemistry* **15**, 1159-1165 (2013).
90. Singh, H., Chawla, A.S., Kapoor, V.K., Paul, D. & Malhotra, R.K. Medicinal chemistry of tetrazoles. *Progress in Medicinal Chemistry* **17**, 151-183 (1980).
91. Vignesh, A., Bhuvanesh, N.S.P. & Dharmaraj, N. Conversion of Arylboronic Acids to Tetrazoles Catalyzed by ONO Pincer-Type Palladium Complex. *The Journal of Organic Chemistry* **82**, 887-892 (2017).
92. Heravi, M.M., Fazeli, A., Oskooie, H.A., Beheshtiha, Y.S. & Valizadeh, H. Click Synthesis of 5-Substituted 1H-Tetrazoles from Aldehydes, Hydroxyl-amine, and [bmim]N_3 via One-Pot, Three-Component Reaction. *Synlett* **23**, 2927-2930 (2012).
93. Su, W.-K., Hong, Z., Shan, W.-G. & Zhang, X.-X. A Facile Synthesis of 1-Substituted-1H-1,2,3,4-Tetrazoles Catalyzed by Ytterbium Triflate Hydrate. *European Journal of Organic Chemistry*, 2723-2726 (2006).
94. Patil, P., Zhang, J., Kurpiewska, K., Kalinowska-Tłuścik, J. & Dömling, A. Hydrazine in the Ugi Tetrazole Reaction. *Synthesis* **48**, 1122-1130 (2016).
95. Ishihara, K., Kawashima, M., Matsumoto, T., Shioiri, T. & Matsugi, M. A Practical Synthesis of 5-Substituted 1H-Tetrazoles from Aldoximes Employing the Azide Anion from Diphenyl Phosphorazidate. *Synthesis* **50**, 1293-1300 (2018).
96. Imai, T., Harigae, R., Moriyama, K. & Togo, H. Preparation of 5-Aryl-2-Alkyltetrazoles with Aromatic Aldehydes, Alkylhydrazine, Di-tert-butyl Azodicarboxylate, and [Bis(trifluoroacetoxy)iodo]benzene. *The Journal of Organic Chemistry* **81**, 3975-3980 (2016).
97. Das, B., Reddy, C.R., Kumar, D.N., Krishnaiah, M. & Narender, R. A Simple, Advantageous Synthesis of 5-Substituted 1H-Tetrazoles. *Synlett* 391-394 (2010).
98. Fleming, A., Gaire, J., Kelleher, F., McGinley, J. & McKee, V. Synthesis and characterisation of macrocycles containing both tetrazole and pyridine functionalities. *Tetrahedron* **67**, 3260-3266 (2011).
99. Cantillo, D., Gutmann, B. & Kappe, C.O. Mechanistic Insights on Azide−Nitrile Cycloadditions: On the Dialkyltin Oxide−Trimethylsilyl Azide Route and a New Vilsmeier−Haack-Type Organocatalyst. *Journal of the American Chemical Society* **133**, 4465-4475 (2011).
100. Ruiz-Castillo, P. & Buchwald, S.L. Applications of Palladium-Catalyzed C–N Cross-Coupling Reactions. *Chemical Reviews* **116**, 12564-12649 (2016).
101. Heravi, M., Kheilkordi, Z., Zadsirjan, V., Heydari, M. & Malmir, M. Buchwald-Hartwig reaction: An overview. *Journal of Organometallic Chemistry* **861**(2018).
102. Wu, A., Gao, Y. & Zheng, L. Zwitterionic amphiphiles: their aggregation behavior and applications. *Green Chemistry* **21**, 4290-4312 (2019).
103. Manolikakes, G., Schade, M.A., Hernandez, C.M., Mayr, H. & Knochel, P. Negishi Cross-Couplings of Unsaturated Halides Bearing Relatively Acidic Hydrogen Atoms with Organozinc Reagents. *Organic Letters* **10**, 2765-2768 (2008).
104. Bailey, H.V., Heaton, W., Vicker, N. & Potter, B.V.L. Rapid microwave-assisted reductive amination of ketones with anilines. *Synlett*, 2444-2448 (2006).

105. Too, P.C., Chan, G.H., Tnay, Y.L., Hirao, H. & Chiba, S. Hydride Reduction by a Sodium Hydride-Iodide Composite. *Angewandte Chemie International Edition* **55**, 3719-3723 (2016).
106. Levesque, P. & Fournier, P.-A. Synthesis of Substituted Indole from 2-Aminobenzaldehyde through [1,2]-Aryl Shift. *The Journal of Organic Chemistry* **75**, 7033-7036 (2010).
107. Zhao, Y., Huang, B., Yang, C., Chen, Q. & Xia, W. Sunlight-Driven Forging of Amide/Ester Bonds from Three Independent Components: An Approach to Carbamates. *Organic Letters* **18**, 5572-5575 (2016).
108. Holzschneider, K., Tong, M.L., Mohr, F. & Kirsch, S.F. A Synthetic Route Toward Tetrazoles: The Thermolysis of Geminal Diazides. *Chemistry* **25**, 11725-11733 (2019).
109. Ramanathan, M., Wang, Y.-H. & Liu, S.-T. One-Pot Reactions for Synthesis of 2,5-Substituted Tetrazoles from Aryldiazonium Salts and Amidines. *Organic Letters* **17**, 5886-5889 (2015).
110. Verma, F., *et al.* Visible-light driven regioselective synthesis of 1H-tetrazoles from aldehydes through isocyanide-based [3 + 2] cycloaddition. *Green Chemistry* **20**, 3783-3789 (2018).
111. Neochoritis, C.G., Zhao, T. & Dömling, A. Tetrazoles via Multicomponent Reactions. *Chemical Reviews* **119**, 1970-2042 (2019).
112. Aureggi, V. & Sedelmeier, G. 1,3-Dipolar Cycloaddition: Click Chemistry for the Synthesis of 5-Substituted Tetrazoles from Organoaluminum Azides and Nitriles. *Angewandte Chemie International Edition* **46**, 8440-8444 (2007).
113. Demko, Z.P. & Sharpless, K.B. A click chemistry approach to tetrazoles by Huisgen 1,3-dipolar cycloaddition: synthesis of 5-acyltetrazoles from azides and acyl cyanides. *Angewandte Chemie International Edition* **41**, 2113-2116 (2002).
114. Zhou, Y., Yao, C., Ni, R. & Yang, G. Amine Salt–Catalyzed Synthesis of 5-Substituted 1H-Tetrazoles from Nitriles. *Synthetic Communications* **40**, 2624-2632 (2010).
115. Nasrollahzadeh, M., Jaleh, B. & Jabbari, A. Synthesis, characterization and catalytic activity of graphene oxide/ZnO nanocomposites. *RSC Advances* **4**, 36713-36720 (2014).
116. Razavi, N. & Akhlaghinia, B. Cu (II) immobilized on aminated epichlorohydrin activated silica (CAES): as a new, green and efficient nanocatalyst for preparation of 5-substituted -1H-tetrazoles. *RSC Advances.* **5**(2015).
117. Speight, J.G. Chapter 6 - Hydrolysis. Book title: *Reaction Mechanisms in Environmental Engineering* 203-229 (Butterworth-Heinemann, 2018).
118. A. Alemán, P., Boix, C. & Poliakoff, M. Hydrolysis and saponification of methyl benzoates. *Green Chemistry* **1**, 65-68 (1999).
119. Theodorou, V., Skobridis, K., Tzakos, A.G. & Ragoussis, V. A simple method for the alkaline hydrolysis of esters. *Tetrahedron Letters* **48**, 8230-8233 (2007).
120. Wei, Z., Zhang, J., Yang, H. & Jiang, G. Brønsted Acid-Catalyzed Asymmetric Ring-Closing Alkylation of Inert N-substituted Pyrroles with α, β-Unsaturated Ketones. *Advanced Synthesis & Catalysis* **361**, 3694-3697 (2019).
121. Sigma Aldritch. (access date May 2020) https://www.sigmaaldrich.com/chemistry/solvents/learning-center/stabilizer-systems.html

8. Experimental Procedures

Unless otherwise noted, purchased chemicals were used as received without further purification. Solvents were dried according to standard procedures over molecular sieves 4 Å. Flash chromatography was carried out on silica gel 60 (230−400 mesh) or by automated normal phase flash chromatography (n-heptane/EtOAc) with the sample preloaded on a Biotage Samplet cartridge (SP-1 Biotage system). Purification by reversed phase (RP) C_{18} column chromatography (H_2O with 0.1% TFA/MeCN with 0.1% TFA) was performed on an automated purification PuriFlash Biotage module with the sample preloaded on a Samplet cartridge. Thin layer chromatography was carried out using Merck TLC Silica gel 60 F_{254} and visualized by short-wavelength ultraviolet light or by treatment with an appropriate stain. GC-MS chromatograms were recorded on a Thermo Scientific Trace GC Ultra with a Thermo Scientific ITQ 110 detector (Column: Supelco SLB-5 ms, 30m x 0 ,2 mm x 0,2 µm film thickness, flow 1.0 ml/min helium). Microwave reactions were conducted with Anton Paar Monowave 300 microwave synthesis reactor. NMR spectra were obtained on a Bruker Advance 400 MHz NMR spectrometer at 20 °C. The chemical shifts are reported in ppm relative to the solvent residual peak ($CDCl_3$: δH 7.26 and δC 77.16; MeOH-*d*4: δH 3.31 and δC 49.00; D_20: δH 4.79; DMSO-*d*6: δH 2.51 and δC 39.52, THF-d_8: δH 3.58, δH 1.73 and δC 67.57, δC 25.37; acetic-acid-d_4: δH 11.65, 2.04 and δC 178.99, 20.0). ^{13}C NMR spectra were obtained with ^{1}H decoupling. Data are represented as follows: chemical shift, multiplicity (s = singlet, d = doublet, t = triplet, q = quartet, dt = double triplet, m = multiplet), coupling constant (J, Hz) and corresponding amount of protons. High-resolution mass spectra (HRMS) were recorded from MeOH solutions on an LTQ Orbitrap XL (Thermo Scientific) either in negative or in positive electrospray ionization (ESI) mode. Melting points were measured using Stuart SMP50 automatic melting point detector. The purity of all compounds submitted to biological testing was determined to be ≥ 97%, measured on a WATERS UPC^2 SFC column system.

Unless otherwise noted, the following gradient was used on the Waters UPC, SFC system:

	Time (min)	Flow (mL/min)	% A	%B
1	Initial	1.000	75.0	25.0
2	2.00-3.50	1.000	60.0	40.0
4	3.70-4.50	1.000	75.0	25.0

A: CO_2 B: 0.1% NH_3 in MeOH.

8.1 Suzuki-Miayura Cross coupling

8.1.1 General Procedure 1

The aryl halide (1.0 eq), boronic acid (1.5 eq) and tripotassium phosphate (2.0 – 4.5 eq) were mixed together in anhydrous THF. Before and after adding the air sensitive catalyst, Xphos Pd G2 (0.02 eq), the mixture was degassed with argon. The mixture was stirred at 70°C for 16 hours under argon atmosphere. The resulting mixture was diluted with water and filtered through Celite, before adding additional water and extracting the aqueous phase with $CHCl_3$ (3 times). The combined organic phases were dried over $MgSO_4$, filtered and concentrated under reduced pressure before the crude material was purified by flash chromatography with EtOAc and n-hexane or water and acetonitrile, to yield the pure biaryl product.

8.1.1.1 4'-Amino-3'-(methoxycarbonyl)-[1,1'-biphenyl]-4-sulfonic acid (16)

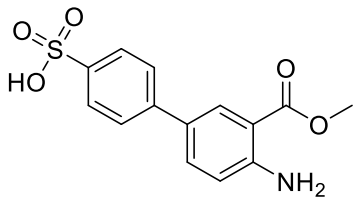

16

Methyl 2-amino-5-bromobenzoate **9** (15.2 mg, 0.07 mmol), 4-boronobenzenesulfonic acid **15** (20 mg, 0.10 mmol), tripotassium phosphate (63 mg, 0.3 mmol) and Xphos Pd G2 (3.1 mg, 0.004 mmol) in water:dioxane (2 mL,1:1) and purified with reverse phase C-18 flash chromatography, yielded **16** (10 mg, 0.03 mmol, **49%**) as white solid**. ^{1}H NMR** (400 MHz,

DMSO -*d*6) δ 8.00 (t, *J* = 2.3 Hz, 1H), 7.65 – 7.58 (m, 3H), 7.52 – 7.47 (m, 2H), 6.88 (d, *J* = 8.7 Hz, 1H), 3.83 (s, 3H). **^{13}C NMR** (101 MHz, DMSO -*d*6) δ 167.7, 150.2, 146.2, 139.5, 132.5, 128.3, 126.6, 126.2 (2C), 124.7 (2C), 117.6, 109.5, 51.6. **HRMS** (ESI) m/z: $[M-H]^-$ calculated for $C_{14}H_{12}O_5NS$ 306.0438; found 306.0431.

8.1.1.2 Methyl 4-amino-4'-cyano-[1,1'-biphenyl]-3-carboxylate (13)

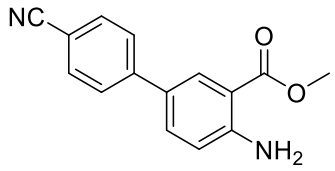

13

Methyl 2-amino-5-bromobenzoate (**9**) (500 mg, 2.17 mmol), 4-cyanophenylboronic acid (**12**) (479 mg, 3.26 mmol) potassium triphosphate (1.38 g, 6.52 mmol) and Xphos Pd G2 (68.4 mg, 0.09 mmol) in anhydrous THF (7 mL) and purified with normal phase flash chromatography, yielded **13** (0.536 g, 2.12 mmol, **98%**) as a beige solid. **m.p.** 146-148°C. **^{1}H NMR**: (400 MHz, $CDCl_3$) δ 8.16 (d, 1H), 7.70 – 7.62 (m, 4H), 7.55 (dd, *J* = 8.6, 2.3 Hz, 1H), 6.81 (d, *J* = 8.6 Hz, 1H), 3.92 (s, 3H). **^{13}C NMR** (101 MHz, $CDCl_3$-*d*) δ 168.3, 150.2, 144.9, 132.8 (2C), 132.7, 130.2, 127.4, 126.7 (2C), 119.3, 117.8, 111.4, 110.0, 52.0. **HRMS** (ESI) m/z: $[M+H]^+$ calculated for $C_{15}H_{13}O_2N_2$ 253.0973; found 253.0972. **IR (cm^{-1}):** 3480, 3365, 2955, 2229, 1681, 1603, 1633, 1495, 1447.

The spectroscopic data is in agreement previously reported data by Manolikakes et al. [103]

8.1.1.3 Methyl 4-(benzylamino)-4'-cyano-[1,1'-biphenyl]-3-carboxylate (18)

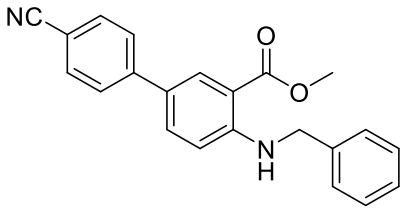

18

Methyl 2-(benzylamino)-5-bromobenzoate (**9**) (185 mg, 0.58 mmol), 4-cyanophenylboronic acid (**12**) (127 mg, 0.87 mmol), potassium triphosphate (367.9 mg, 1.73 mmol) and Xphos Pd G2 (10 mg, 0.01 mmol) in anhydrous THF (7 mL) and purified with normal phase flash chromatography, yielded **18** (131 mg, 0.06 mmol, **66%**) as a white solid. **m.p.** 158.1-165°C. **^{1}H NMR** (400 MHz, $CDCl_3$) δ 8.58 – 8.25 (s, 1H), 8.23 (d, *J* = 2.3 Hz, 1H), 7.69 – 7.59 (m, 4H), 7.57 (dd, *J* = 8.8, 2.4 Hz, 1H), 7.41 – 7.33 (m, 4H), 7.33 – 7.26 (m, 1H), 6.76 (d, *J* = 8.8 Hz, 1H), 4.52 (s, 2H), 3.92 (s, 3H). **^{13}C NMR** (101 MHz, $CDCl_3$) δ 169.0, 151.2, 145.0, 138.5, 133.2, 132.8, 130.6, 129.0, 127.6, 127.3, 126.6, 125.7, 119.5, 112.9, 111.0, 109.8, 52.1, 47.3. **HRMS** (ESI) m/z: $[M+Na]^+$ calculated for $C_{22}H_{18}O_2N_2Na$ and $C_{22}H_{19}O_2N_2$ 365.124 and 343.1443; found 365.1271 and 343.1452 respectively.

8.2 Reductive Amination

8.2.1 Reductive Amination Screening Data

The reductive amination screening was carried out with GCMS with no internal standard, on the following reaction(s):

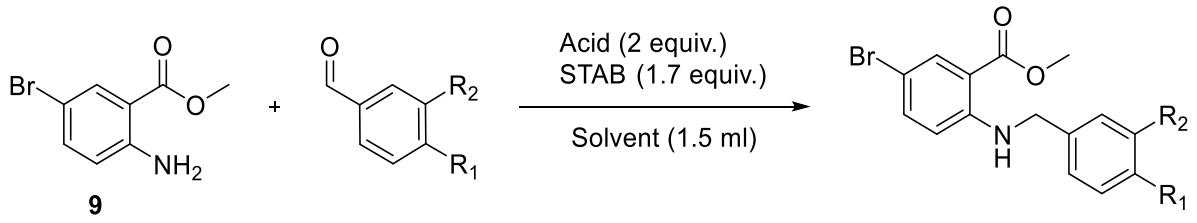

Scheme 28. Reductive amination screening, R1= H or MeOCH3, R2 = H or OH.

The reaction mixture was extracted with $NaHCO_3$ and EtOAc and the organic phase was filtrated through $MgSO_4$. The resulting crude organic phase was diluted with methanol before

submitting for GC-MS analysis. The injection volume used was 1.0 µl. with the following program: GC-Program: 80(1)/25/300(5), Injector 230°C, flow 1.0 ml/min, MS-transfer line 300°C. The results from GCMS analysis provided a graph from, which the area was used to find an estimate of conversion, seen in Figure 27**.**

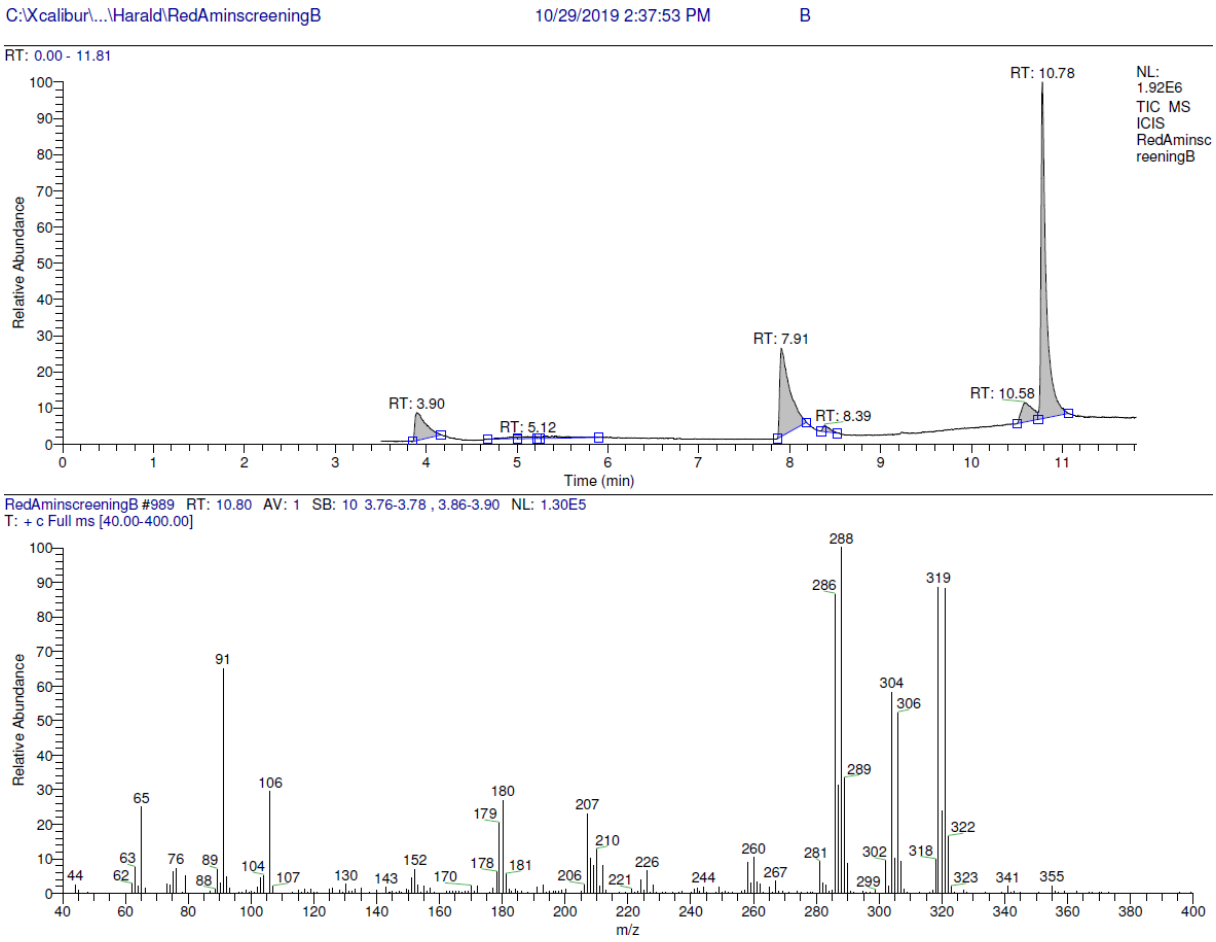

Figure 27. GCMS result of reductive amination screening (entry 2, R_1 = H, R_2 = H)

Compound **9** had a R_f. value of 7.91. Benzaldehyde (**10**) had a R_f. of 3.84. 3-Hydroxy-4-methoxybenzaldehyde had a R_f. value of 7.01 whilst the product (**11**) of entry 2 (R_1 = H, R_2 = H) had a R_f value of 10.78. No internal standard was used, meaning the R_f values deviated slightly for each run. The estimated conversion was based on the area of the curve of the starting material (**9**), compared to the area of the product.

8.2.2 General Procedure 2

The amine (1.0 eq), aldehyde (2.0 eq) and zinc chloride (1.7 –2.0 eq) were mixed in DCE. After 10 minutes of stirring, STAB or $NaBH_3CN$ (1.7 eq) was added and the mixture was left to stir at room temperature overnight. When TLC indicated completion, the resulting crude mixture was quenched with saturated aqueous $NaHCO_3$ solution and extracted with EtOAc (3x), before drying the combined organic phases over $MgSO_4$. The solution was concentrated under reduced pressure and purified by flash chromatography on silica gel (EtOAc and n-hexane) to yield the desired secondary amine.

8.2.2.1 Methyl 2-(benzylamino)-5-bromobenzoate (11)

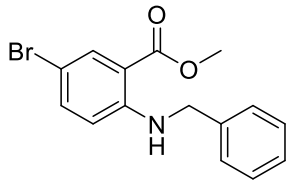

11

Methyl 2-amino-5-bromobenzoate (**9**) (200 mg, 0.87 mmol), zinc chloride (202 mg, 1.48 mmol), $NaBH_3CN$ (92.7 mg, 1.48 mmol) and freshly distilled benzaldehyde (**10**) (177 µL, 1.74 mmol) were refluxed for additional 20 hours after stirring at room temperature overnight, as starting material was still present according to TLC. After purification this yielded a beige solid, compound **11** (0.194 g, 0.61 mmol, **70%**). **^{1}H NMR** (400 MHz, $CDCl_3$) δ 8.19 (s, 1H), 8.04 (d, *J* = 2.5 Hz, 1H), 7.39 – 7.31 (m, 5H), 6.52 (d, *J* = 9.0 Hz, 1H), 4.43 (d, *J* = 5.6 Hz, 2H), 3.87 (s, 3H). **^{13}C NMR** (101 MHz, $CDCl_3$) δ 168.1, 149.9, 138.4, 137.3, 133.9, 128.9, 127.4, 127.1, 113.7, 111.7, 106.3, 51.9, 47.1. **HRMS** (ESI) m/z: $[M+H]^+$ calculated for $C_{15}H_{15}O_2N^{81}Br$ 322.0263; found 322.0271.

8.2.2.2 Methyl 4'-cyano-4-((3-methoxybenzyl)amino)-[1,1'-biphenyl]-3-carboxylate (22)

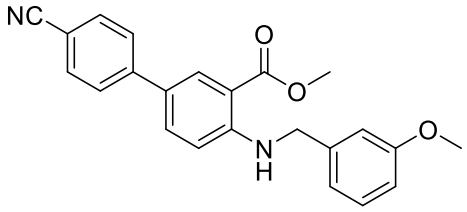

22

Methyl 4-amino-4'-cyano-[1,1'-biphenyl]-3-carboxylate (**13**) (140 mg, 0.55 mmol) and 3-methoxybezaldehyde (134.9 µl, 1.11 mmol), zinc chloride (151 mg, 1.11 mmol) and STAB (200 mg, 0.94 mmol) in DCE (3.5 mL) yielded thin, beige, solid sheets of **22** (198 mg, 0.53 mmol, **96%**). **m.p.** 162-166°C. **^{1}H NMR** (400 MHz, $CDCl_3$) δ 8.38 (d, *J* = 2.3 Hz, 1H), 8.19 (d, *J* = 2.4 Hz, 1H), 7.65 – 7.56 (m, 4H), 7.53 (dd, *J* = 8.8, 2.4 Hz, 1H), 7.25 – 7.21 (m, 1H), 6.96 – 6.90 (m, 1H), 6.88 (s, 1H), 6.81 – 6.76 (m, 1H), 6.72 (d, *J* = 8.8 Hz, 1H), 4.46 (s, 2H), 3.88 (s, 3H), 3.77 (s, 3H). **^{13}C NMR** (101 MHz, $CDCl_3$) δ 168.9, 160.1, 151.0, 145.0, 140.1, 133.1, 132.7, 130.5, 130.0, 126.5, 125.7, 119.4, 119.3, 113.0, 112.9, 112.7, 110.9, 109.7, 55.4, 52.0, 47.2. **HRMS** (ESI) m/z: $[M+Na]^+$ calculated for $C_{23}H_{20}O_3N_2Na$ 395.1369; found 395.1377.

8.2.2.3 Methyl 4'-cyano-4-((3,5-dimethoxybenzyl)amino)-[1,1'-biphenyl]-3-carboxylate (26)

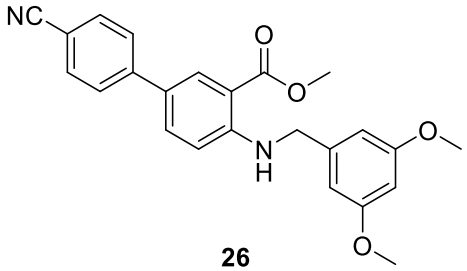

26

Methyl 4-amino-4'-cyano-[1,1'-biphenyl]-3-carboxylate (**13**) (200 mg, 0.79 mmol) and 3,5-dimethoxybenzaldehyde (263 mg, 1.59 mmol), zinc chloride (216.1 mg, 1.59 mmol) in DCE (4 mL) yielded **26** (259 mg, 0.64 mmol, **81%**) as a white solid. . **m.p.** 135-142°C. **^{1}H NMR** (400

MHz, $CDCl_3$) δ 8.28 (t, *J* = 5.8 Hz, 1H), 8.12 (d, *J* = 2.4 Hz, 1H), 7.59 – 7.50 (m, 4H), 7.46 (dd, *J* = 8.8, 2.4 Hz, 1H), 6.63 (d, *J* = 8.8 Hz, 1H), 6.43 (d, *J* = 2.3 Hz, 2H), 6.28 (t, *J* = 2.3 Hz, 1H), 4.35 (d, *J* = 5.7 Hz, 2H), 3.82 (s, 3H), 3.69 (s, 6H). **^{13}C NMR** (101 MHz, $CDCl_3$)δ 168.8, 161.3, 151.1, 144.9, 141.1, 133.1, 133.0, 130.4, 126.4, 125.5, 119.3, 112.7, 110.7, 109.6, 105.0, 99.0, 55.4, 51.9, 47.2. **HRMS** (ESI) m/z: $[M+Na]^+$ calculated for $C_{24}H_{22}O_4N_2Na$ 425.1472; found 425.1472. **IR(cm^{-1}):** 3357, 2948, 2847, 2221, 1685, 1596, 1503.

8.2.2.4 Methyl 4'-cyano-4-((thiophen-2-ylmethyl)amino)-[1,1'-biphenyl]-3-carboxylate (23)

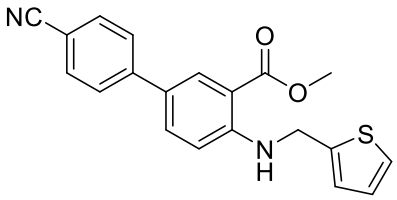

23

Methyl 4-amino-4'-cyano-[1,1'-biphenyl]-3-carboxylate (**13**) (150 mg, 0.59 mmol), 3,5-thiophene-2-carbaldehyde (111 µl, 1.19 mmol), zinc chloride (162.1 mg, 1.19 mmol) and STAB (214.2 mg, 1.01 mmol) in DCE (3.5 mL), yielded **23** (71 mg, 0.20 mmol, **34%**) as a white solid. **^{1}H NMR** (400 MHz, DMSO) δ 8.30 (t, *J* = 5.9 Hz, 1H), 8.18 (d, *J* = 2.2 Hz, 1H), 7.87 – 7.73 (m, 5H), 7.41 (d, *J* = 5.2 Hz, 1H), 7.10 (d, *J* = 3.4 Hz, 1H), 7.01 – 6.95 (m, 2H), 4.75 (d, *J* = 5.8 Hz, 2H), 3.85 (s, 3H). **^{13}C NMR** (101 MHz, $CDCl_3$) δ 168.8, 150.7, 144.9, 142.0, 133.1, 132.7, 130.5, 127.1, 126.5, 125.9, 125.2, 124.8, 119.3, 112.5, 111.0, 109.8, 52.0, 42.4. **HRMS** (ESI) m/z: $[M+H]^+$ calculated for $C_{20}H_{16}O_2N_2S$ 371.0830; found 371.0836.

8.2.2.5 Methyl 4-((2-bromo-6-fluorobenzyl)amino)-4'-cyano-[1,1'-biphenyl]-3-carboxylate (25)

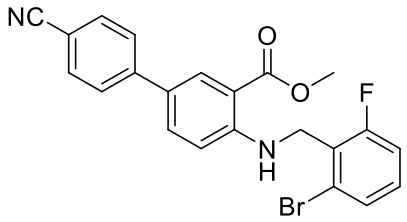

25

Methyl 4-amino-4'-cyano-[1,1'-biphenyl]-3-carboxylate (**13**) (150 mg, 0.59 mmol), 2-bromo-6-fluorobenzaldehyde (241.4 mg, 1.19 mmol), zink chloride (162.1 mg, 1.19 mmol) and STAB (224.3 mg, 1.01 mmol) in DCE(3.5 mL), yielded **25** (67 mg, 0.15 mmol, **26%**) as a white solid.**^{1}H NMR** (400 MHz, $CDCl_3$) δ 8.37 (s, 1H), 8.20 (d, *J* = 2.3 Hz, 1H), 7.65 (m, 5H), 7.46 – 7.35 (m, 1H), 7.17 (q, *J* = 7.5 Hz, 1H), 7.10 – 7.02 (m, 2H), 4.64 (s, 2H), 3.88 (d, 3H).**^{13}C NMR** (101 MHz, $CDCl_3$). δ 168.64, 161.4 (d, *J* = 250.3 Hz), 150.5, 144.8, 133.1, 132.6, 130.5, 130.3 (d, *J* = 9.5 Hz) ,129.1 (d, *J* = 3.6 Hz), 126.39, 125.9 – 125.7 (m), 125.6, 119.2, 115.2, 114.9, 112.1 (d, *J* = 2.8 Hz), 110.9, 109.6, 51.8,40.5 (d, *J* = 3.4 Hz). **HRMS** (ESI) m/z: $[M+H]^+$ calculated for $C_{22}H_{17}O_2N_2F^{81}Br$ 441.0430; found 441.0431 112.14.

8.3 Tetrazole formation

8.3.1 General Procedure 3

The nitrile (1.0 eq) was dissolved in anhydrous dioxane or DCE in a 10 ml microwave vial. Dibutyltin (IV) oxide (0.1 eq) and trimethylsilyl azide (1.0 eq) were added and the vial was flushed with argon. The reaction was heated in the microwave at 150°C for 1 hour. A second portion of dibutyltin (IV) oxide (0.1 eq) and trimethylsilyl azide (1.0 eq) was added before the vial was flushed with argon and resubmitted to the microwave for 1 more hour at 150°C. The resulting mixture was concentrated under reduced pressure before dissolving in diethyl ether. The organic phase was extracted with 2 N aqueous sodium hydroxide (3x). The aqueous phase was acidified with 4N aqueous HCl to pH = 1 and extracted with EtOAc. The organic layer was washed with brine and dried over $MgSO_4$ before concentrating under reduced pressure and purified with C-18 flash chromatography. Due to the unpredictable nature of amino-acid compounds, the purification method had to be adapted for each compound.

8.3.1.1 Methyl 4-amino-4'-(1*H*-tetrazol-5-yl)-[1,1'-biphenyl]-3-carboxylate (14)

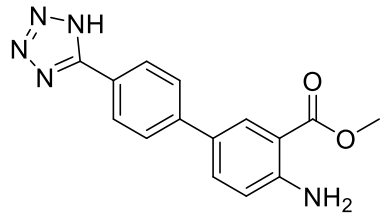

14

Methyl 4-amino-4'-cyano-[1,1'-biphenyl]-3-carboxylate (**13**) (100 mg, 0.40 mmol), dibutyltin (IV) oxide (19.7 mg, 0.08 mmol) and trimethylsilyl azide (104.9 µl, 0.79 mmol) in dioxane (3 mL), yielded **14** as a white solid (100 mg, 0.34 mmol, **86%**). **m.p.** 132-135°C. **^{1}H NMR** (400 MHz, DMSO-d_6) δ 8.11 – 8.03 (m, 3H), 7.77 (d, J = 8.3 Hz, 2H), 7.72 (dd, J = 8.7, 2.4 Hz, 1H), 6.92 (d, J = 8.7 Hz, 1H), 6.88 (s, 2H), 3.84 (s, 3H). **^{13}C NMR** (101 MHz, DMSO-d_6) δ 167.7, 151.2, 141.4, 132.4, 128.5, 127.3, 126.0, 125.4, 123.5, 117.4, 109.0, 51.6. **HRMS** (ESI) m/z: $[M-H]^-$ calculated for $C_{15}H_{12}O_2N_5$ 294.0978; found 294.0986.

8.3.1.2 Methyl 4-((3,5-dimethoxybenzyl)amino)-4'-(1*H*-tetrazol-5-yl)-[1,1'-biphenyl]-3-carboxylate (27)

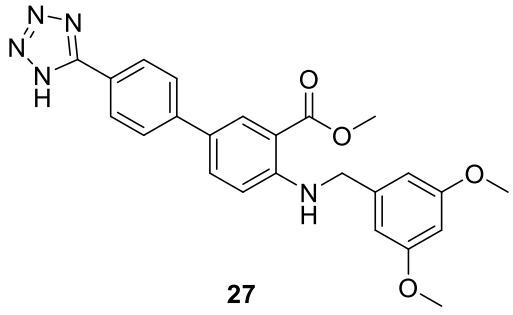

27

Methyl 4'-cyano-4-((3,5-dimethoxybenzyl)amino)-[1,1'-biphenyl]-3-carboxylate (**26**) (165 mg, 0.41 mmol), dibutyltin (IV) oxide (20.4 mg, 0.08 mmol) and trimethylsilyl azide (108.6 µl, 0.82 mmol) in DCE (4 mL), yielded **27** as a yellow solid (170 mg, 0.38 mmol, **93%**). This reaction deviated from the general procedure. The product precipitated from the reaction mixture and filtration was attempted. The residue was washed with 2-methyl THF, followed by dioxane, $CHCl_3$, cold-heptane and lastly DCE. It was attempted several times as product was found in

both filtrate and precipitate. The residue that did not pass through with DCE was pure and yielded 170 mg, and further purification of filtrate was not attempted. **m.p.** 190-193°C. **^{1}H NMR** (400 MHz, THF-d_8) δ 8.28 (t, *J* = 5.7 Hz, 1H), 8.16 (d, *J* = 2.4 Hz, 1H), 7.99 – 7.90 (m, 2H), 7.66 – 7.52 (m, 3H), 6.69 (d, *J* = 8.9 Hz, 1H), 6.43 (d, *J* = 2.3 Hz, 2H), 6.24 (t, *J* = 2.2 Hz, 1H), 4.34 (d, *J* = 5.7 Hz, 2H), 3.76 (s, 3H), 3.61 (s, 6H). *Residual THF (δ 3.62 (m) and 1.78 (m)) and MeOH (δ 3.28 (s)) is observed.* **^{13}C NMR** (101 MHz, THF-d_8) δ 169.5, 162.5, 152.0, 143.7, 142.6, 133.7, 130.5, 128.6, 128.5, 128.3 (2C), 127.2 (2C), 127.1, 113.6, 111.5, 105.8, 99.7 (2C), 55.6, 52.0, 47.9. **HRMS** (ESI) m/z: $[M-H]^-$ calculated for $C_{24}H_{22}O_4N_5$ 322.0263; found 322.0271. **IR (cm^{-1}):** 3357, 2929, 2840, 1685, 1603. **SFC Purity: 97%**.

8.3.1.3 Methyl 4-(((1-methyl-1*H*-imidazol-5-yl)methyl)amino)-4'-(1*H*-tetrazol-5-yl)-[1,1'-biphenyl]-3-carboxylate (20)

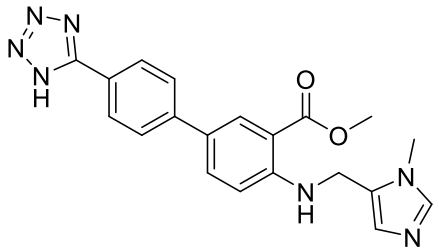

20

Methyl 4-amino-4'-cyano-[1,1'-biphenyl]-3-carboxylate (**13**) (200 mg, 0.79 mmol) 1-methyl-1*H*-imidazole-5-carbaldehyde (175 mg, 1.59 mmol), zinc chloride (216 mg, 1.59 mmol) and STAB (286 mg, 1.35 mmol) in 4 ml DCE, yielded a crude mixture of methyl 4'-cyano-4-(((1-methyl-1*H*-imidazol-5-yl)methyl)amino)-[1,1'-biphenyl]-3-carboxylate (**24**), which was used for tetrazole formation without any further purification. 344 mg crude mixture, dibutyltin (IV) oxide (49.4 mg, 0.20 mmol) and trimethylsilyl azide (263 µl, 2.00 mmol) yielded the title compound (**20**) over two steps after purification with reverse phase flash chromatography, as a white solid (56.9 mg, 0.15 mmol, **18%**). **^{1}H NMR** (400 MHz, DMSO-d_6) δ 8.18 (d, *J* = 2.4 Hz, 1H), 8.06 (d, *J* = 8.1 Hz, 2H), 7.98 (t, *J* = 5.6 Hz, 1H), 7.83 (dd, *J* = 8.7, 2.5 Hz, 1H), 7.78 – 7.68 (m, 3H), 7.07 (d, *J* = 8.9 Hz, 1H), 6.96 (s, 1H), 4.56 (d, *J* = 5.5 Hz, 2H), 3.85 (s, 3H), 3.66 (s, 3H).**^{13}C NMR** (101 MHz, acetic acid-d_4) δ 170.0, 157.0, 150.7, 144.0, 137.9, 134.2, 132.9, 131.1, 129.1, 128.4, 127.6, 122.8, 119.5, 113.5, 112.5, 52.6, 37.2, 34.4. **HRMS** (ESI) m/z: $[M-H]^-$ calculated for $C_{20}H_{18}O2N_7$ 388.1520; found 388.1527. **IR (cm^{-1}):** 3528, 3510, 3353, 1670,

1190. **SFC Purity: 87%.** Structure is proven with additional 2D NMR (see appendix). Residual acetone can be observed. There are 4 aliphatic carbons impurities which is highly likely the dibutyltin (IV) oxide.

8.3.1.4 Methyl 4'-(1*H*-tetrazol-5-yl)-4-((thiophen-2-ylmethyl)amino)-[1,1'-biphenyl]-3-carboxylate (28)

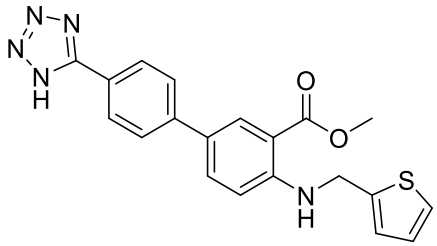

28

Methyl 4'-cyano-4-((thiophen-2-ylmethyl)amino)-[1,1'-biphenyl]-3-carboxylate (**23**) (70 mg, 0.20 mmol), Dibutyltin (IV) oxide (10 mg, 0.04 mmol) and trimethylsilyl azide (53.2 µl, 0.40 mmol) in anhydrous dioxane, yielded **28** as white solid (22 mg, 0.06 mmol, **30%**) after washing the precipitate with $CHCl_3$, deviating from the general procedure. **m.p.** 122.3-224.5°C. **^{1}H NMR** (400 MHz, THF-d_8) δ 8.41 (t, *J* = 5.9 Hz, 1H), 8.28 (d, *J* = 2.4 Hz, 1H), 8.09 (d, *J* = 8.0 Hz, 2H), 7.88-7.74 (m, 3H), 7.28 (d, *J* = 5.1 Hz, 1H), 7.05 (d, *J* = 3.4 Hz, 1H), 6.98 – 6.90 (m, 2H), 4.73 (d, *J* = 5.3 Hz, 2H), 3.87 (s, 3H). **^{13}C NMR** (101 MHz, THF-d_8) δ 169.4, 151.5, 143.8, 143.6, 133.8, 130.5, 128.3 (2C), 127.7, 127.5, 127.3(2C), 125.9, 125.4, 124.7, 113.5, 111.8, 52.0, 42.9. **HRMS** (ESI) m/z: $[M-H]^-$ calculated for $C_{20}H_{16}O_2N_5S$ 390.1026; found 390.1019. **IR:** 3353, 2951, 2843, 2370, 1685, 1611, 1573, 1503. **SFC Purity: 93%**.

8.3.1.5 Methyl 4-((3-methoxybenzyl)amino)-4'-(1*H*-tetrazol-5-yl)-[1,1'-biphenyl]-3-carboxylate (29)

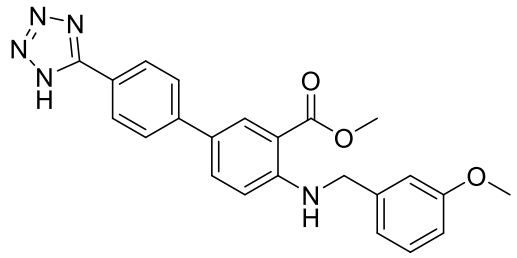

29

Methyl 4'-cyano-4-((3-methoxybenzyl)amino)-[1,1'-biphenyl]-3-carboxylate (**22**) (198 mg, 0.53 mmol), dibutyltin (IV) oxide (26.5 mg, 0.12 mmol) and trimethylsilyl azide (140.8 µl, 1.06 mmol) in DCE (3 mL), yielded 29, as a white solid (165 mg, 0.40 mmol, **75%**). Deviating from the general procedure in that both organic and aqueous layer was combined and purified with reverse-phase flash chromatography. **m.p.** 201-204°C. **^{1}H NMR** (400 MHz, THF-d_8) δ 8.42 (t, *J* = 5.8 Hz, 1H), 8.29 (d, *J* = 2.3 Hz, 1H), 7.90 (m, 4H), 7.70 (dd, *J* = 8.7, 2.2 Hz, 1H), 7.21 (t, *J* = 7.9 Hz, 1H), 6.94 (d, *J* = 6.9 Hz, 2H), 6.85 – 6.75 (m, 2H), 4.52 (d, *J* = 5.2 Hz, 2H), 3.88 (s, 3H), 3.75 (s, 3H). **^{13}C NMR** (101 MHz, THF-d_8) δ 169.6, 161.4, 152.0, 143.7, 141.9, 133.8, 130.5, 130.5, 128.3, 127.2, 127.2, 124.6, 120.0, 113.7, 113.6, 113.3, 111.5, 55.5, 52.0, 47.7.**HRMS** (ESI) m/z: $[M-H]^-$ calculated for $C_{23}H_{20}O_3N_5$ 414.1570; found 414.1561. **IR (cm^{-1}):** 3379, 2840, 1681, 1611, 1573, 1499, 1439. **SFC Purity: 98%**.

8.4 Hydrolysis

8.4.1 General procedure 4

The ester (1.0 eq) was dissolved in a 2:1:1 mixture of THF:H_2O:EtOH. Sodium hydroxide (3.0-6.0 eq) was added and the reaction was left to stir overnight at 60°C. The reaction mixture was concentrated and directly purified by C-18 flash chromatography, using 0.1% TFA in water and acetonitrile.

8.4.1.1 4-Amino-4'-cyano-[1,1'-biphenyl]-3-carboxylic acid (35)

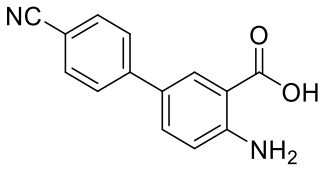

35

Methyl 4-amino-4-cyano- [1, 1-biphenyl]-3-carboxylate (**13**) (40 mg, 0.16 mmol) in a 2 ml 2:1:1 mixture of THF:H_2O:EtOH (2 mL, 1:0.5:0.5) and sodium hydroxide (20 mg, 0.48 mmol) yielded **35** as a white solid (23 mg, 0.10 mmol, **61%**). **m.p.** 214.7-215°C. **^{1}H NMR** (400 MHz, D_2O) δ 8.21 (s, 1H), 8.15 (d, *J* = 8.4 Hz, 2H), 7.75 (d, *J* = 8.4 Hz, 2H), 7.69 (dd, *J* = 8.7, 2.3 Hz, 1H), 6.95 (d, *J* = 8.7 Hz, 1H). **^{13}C NMR** (101 MHz, D_2O) δ 170.9, 158.2, 152.1, 142.7, 132.9, 130.0, 128.0, 127.1 (2C), 126.6 (2C), 124.6, 118.2, 111.0. **HRMS** (ESI) m/z: $[M-H]^-$ calculated for $C_{14}H_9O_2N_2$ 237.0665; found 237.0670. **IR (cm^{-1}):** 3312, 3476, 3365, 2229, 1678, 1622, 1603. **SFC Purity: < 99%.** The SFC method deviated from the standard (method used is shown in the appendix).

8.4.1.2 4-Amino-4'-(1*H*-tetrazol-5-yl)-[1,1'-biphenyl]-3-carboxylic acid (34)

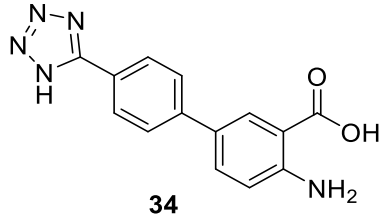

34

Methyl 4-amino-4'-(1*H*-tetrazol-5-yl)-[1,1'-biphenyl]-3-carboxylate (23 mg, 0.08 mmol), in a THF:H_2O:EtOH (4 mL, 2:1:1)and sodium hydroxide (9.36 mg, 0.23 mmol) yielded **4b** as a white solid (19 mg, 0.10 mmol, **87%**). **m.p.** > 300°C. **^{1}H NMR** (400 MHz, D_2O + THF-d_8) δ 8.30 (d, *J* = 2.3 Hz, 1H), 8.24 (d, 2H), 7.84 (d, 2H), 7.78 (dd, *J* = 8.7, 2.4 Hz, 1H), 7.04 (d, *J* = 8.7 Hz, 1H). *Residual THF (δ 3.80 (m) and 1.93 (m)) is observed.* **^{13}C NMR** (101 MHz, D_2O + THF-d_8) δ 170.9, 158.2, 152.1, 142.7, 132.9, 130.0, 128.0, 127.1, 126.6, 124.6, 118.2, 111.0. **HRMS** (ESI) m/z: $[M-H]^-$ calculated for $C_{14}H_{10}O_2N_5$ 280.0832; found 280.0840.

8.4.1.3 4-(Benzylamino)-4'-(1*H*-tetrazol-5-yl)-[1,1'-biphenyl]-3-carboxylic acid (33)

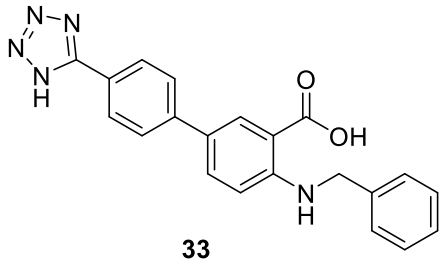

33

Methyl 4-(benzylamino)-4'-cyano-[1,1'-biphenyl]-3-carboxylate (24 mg, 0.10 mmol), dibutyltin (IV) oxide (5 mg, 0.02 mmol) and trimethylsilyl azide (26.2 µl, 0.20 mmol) in DCE (2 mL), yielded methyl 4-(benzylamino)-4'-(1*H*-tetrazol-5-yl)-[1,1'-biphenyl]-3-carboxylate, which was directly stirred in sodium hydroxide (1M, 9 ml) and diethyl ether (5 mL) for 20 minutes for hydrolysis to occur. The mixture was concentrated under reduced pressure and purified by a C-18 column, yielding **33**, as a sand-white solid (3 mg, 0.01 mmol, over two steps **12%**). **^{1}H NMR** (400 MHz, MeOH-d_4) δ 8.28 (d, J = 2.4 Hz, 1H), 8.04 (d, 2H), 7.72 – 7.66 (m, 3H), 7.41 – 7.31 (m, 5H), 7.29 – 7.20 (m, 1H), 6.81 (d, J = 8.8 Hz, 1H), 4.52 (s, 2H). *Residual acetone (δ 2.2 (s) is observed* **^{13}C NMR** (101 MHz, MeOH-d_4) δ 172.1, 160.1, 152.1, 143.5, 140.5, 133.8, 131.3, 129.7, 128.5, 128.2, 128.2, 127.7, 127.3, 126.1, 113.6, 112.3, 47.7. *Residual acetone (30.6 ppm) (s) is observed*. **HRMS** (ESI) m/z: $[M-H]^-$ calculated for $C_{21}H_{16}O_2N_5$ 370.1308; found 370.1309.

8.4.1.4 4-((3,5-Dimethoxybenzyl)amino)-4'-(1*H*-tetrazol-5-yl)-[1,1'-biphenyl]-3-carboxylic acid (32)

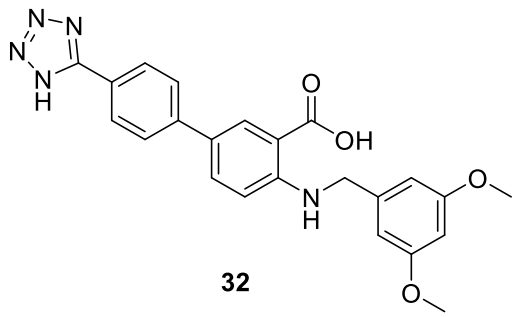

32

Methyl 4-((3,5-dimethoxybenzyl)amino)-4'-(1*H*-tetrazol-5-yl)-[1,1'-biphenyl]-3-carboxylate (**27**) (80 mg, 0.18 mmol). in a 4 ml 2:1:1 mixture of THF:H_2O:EtOH and sodium hydroxide (43.1 mg, 1.08 mmol) yielded **32** as a white solid (32 mg, 0.07 mmol, **41%**). . **m.p:** decomposed. **HRMS** (ESI) m/z: $[M-H]^-$ calculated for $C_{23}H_{20}O_4N_5$ 430.1517; found 430.1510. **^{1}H NMR** (400 MHz, DMSO-d_6) δ 8.21 (d, *J* = 2.4 Hz, 1H), 8.06 (d, *J* = 8.3 Hz, 2H), 7.85 – 7.73 (m, 3H), 6.80 (d, *J* = 8.9 Hz, 1H), 6.53 (d, *J* = 2.3 Hz, 2H), 6.39 (t, *J* = 2.3 Hz, 1H), 4.47 (s, 2H), 3.72 (s, 6H). **^{13}C NMR** (101 MHz, DMSO-d_6) δ 169.8, 160.7, 150.5, 142.0, 141.8, 132.6, 129.6, 127.5, 126.1, 124.9, 121.8, 112.7, 110.8, 105.0, 98.4, 55.1, 45.9. **IR (cm^{-1}):** 3365, 2929, 2843, 1681, 1581, 1432. **SFC Purity: > 99%. IC_{50} = 3.3 µM**.

.

9. Appendices

9.1 Suzuki Miyaura cross coupling Spectra

9.1.1 4'-amino-3'-(methoxycarbonyl)-[1,1'-biphenyl]-4-sulfonic acid (16)

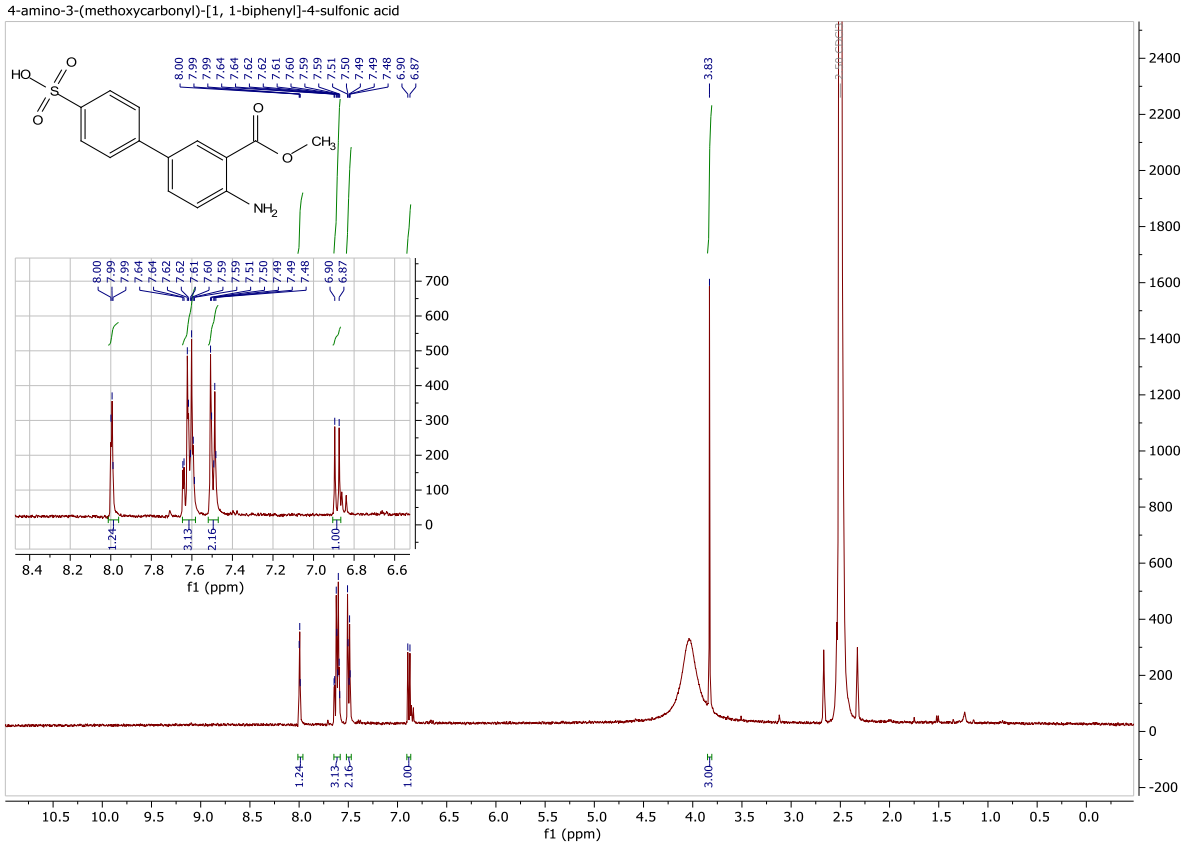

4'-amino-3'-(methoxycarbonyl)-[1,1'-biphenyl]-4-sulfonic acid

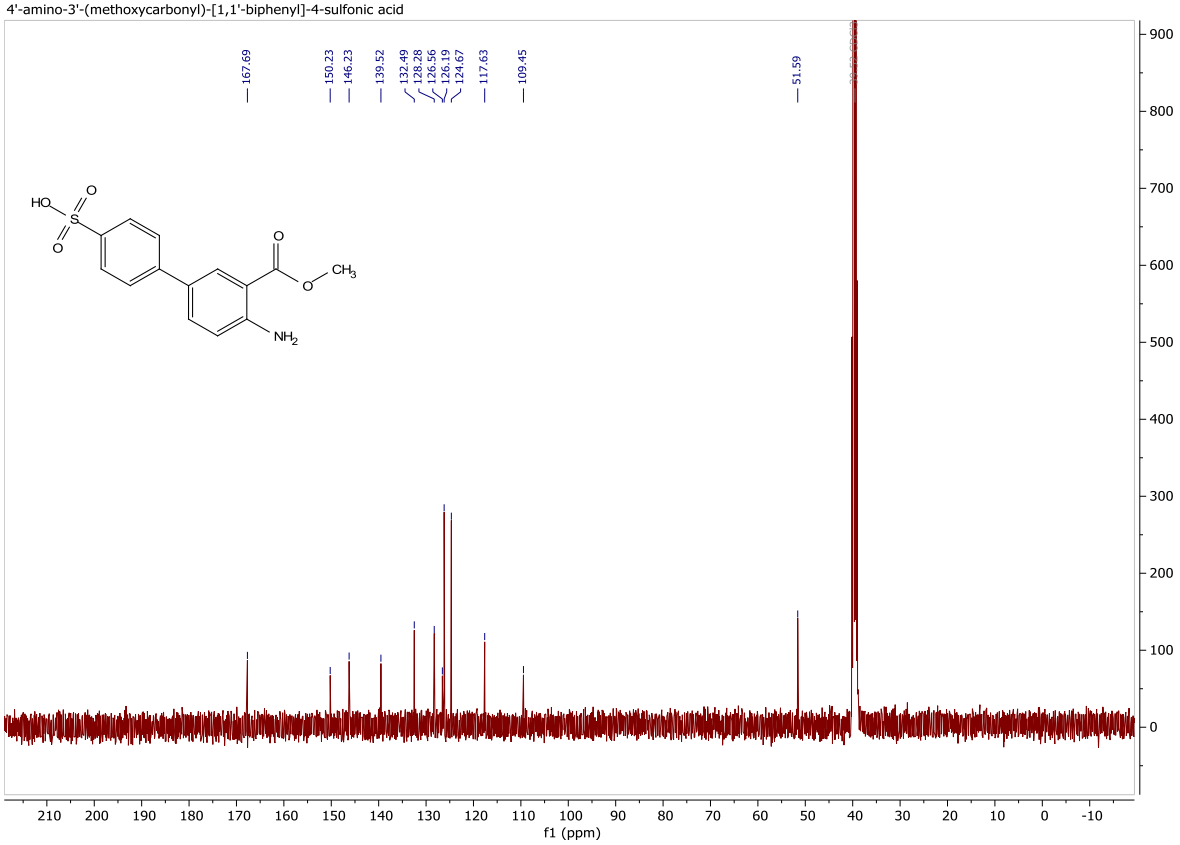

abhm100634frag5finalester_neg #1-9 RT: 0.02-0.24 AV: 9 NL: 1.40E8
T: FTMS - p ESI Full ms [100.00-800.00]

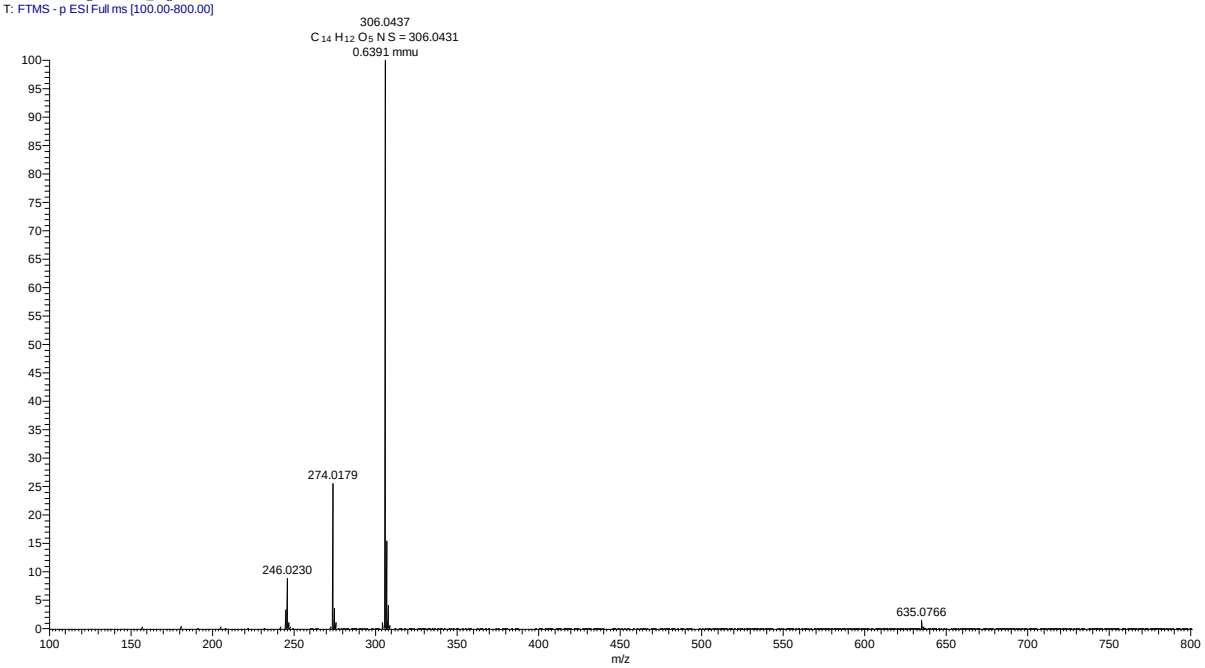

9.1.2 Methyl 4-amino-4'-cyano-[1,1'-biphenyl]-3-carboxylate (13)

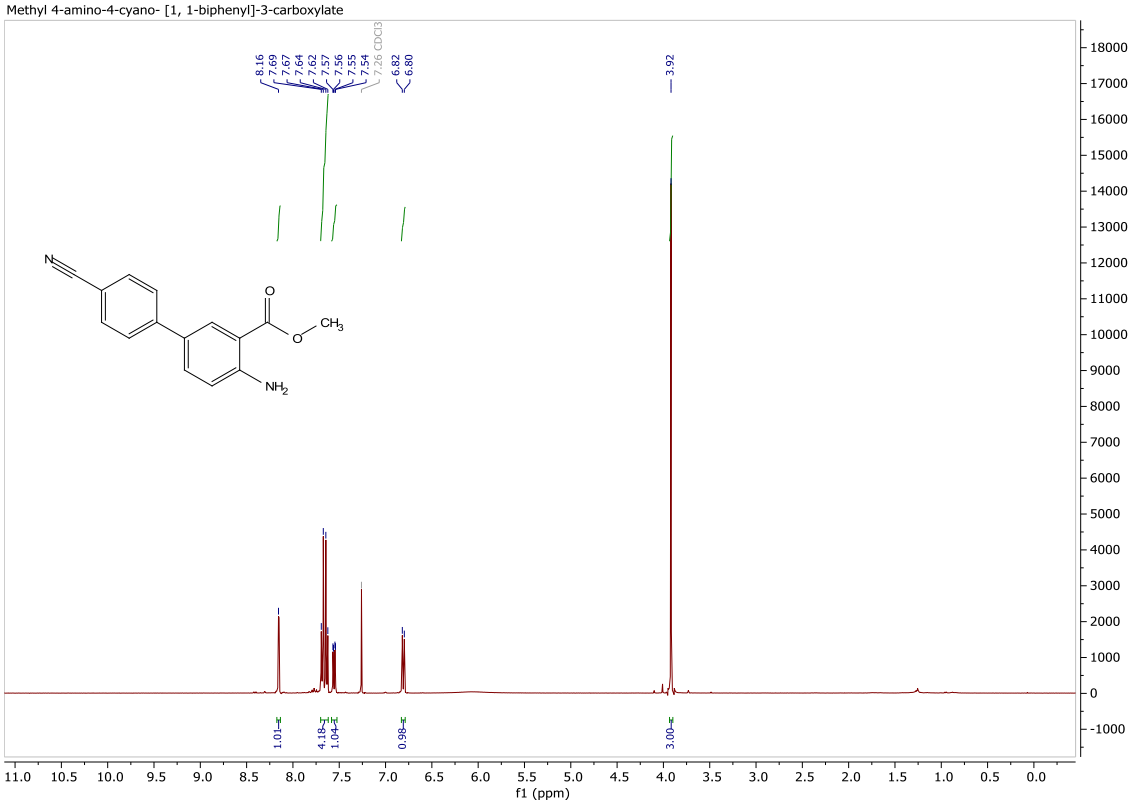

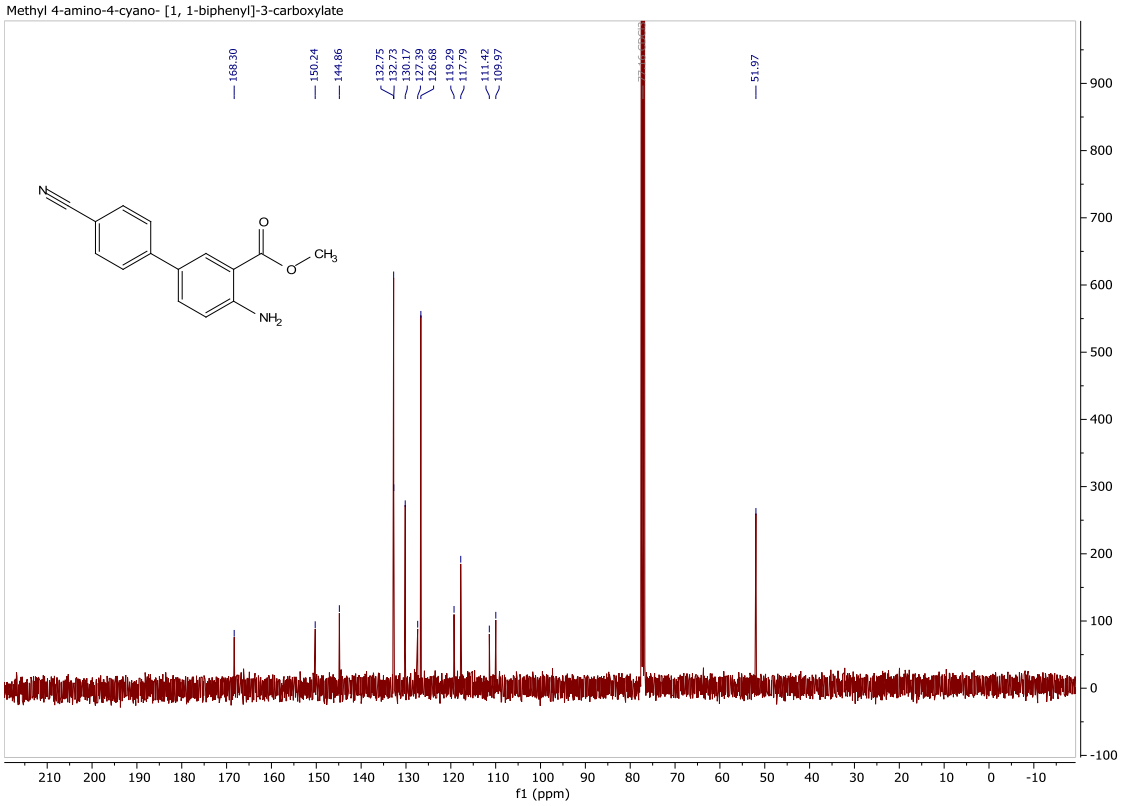

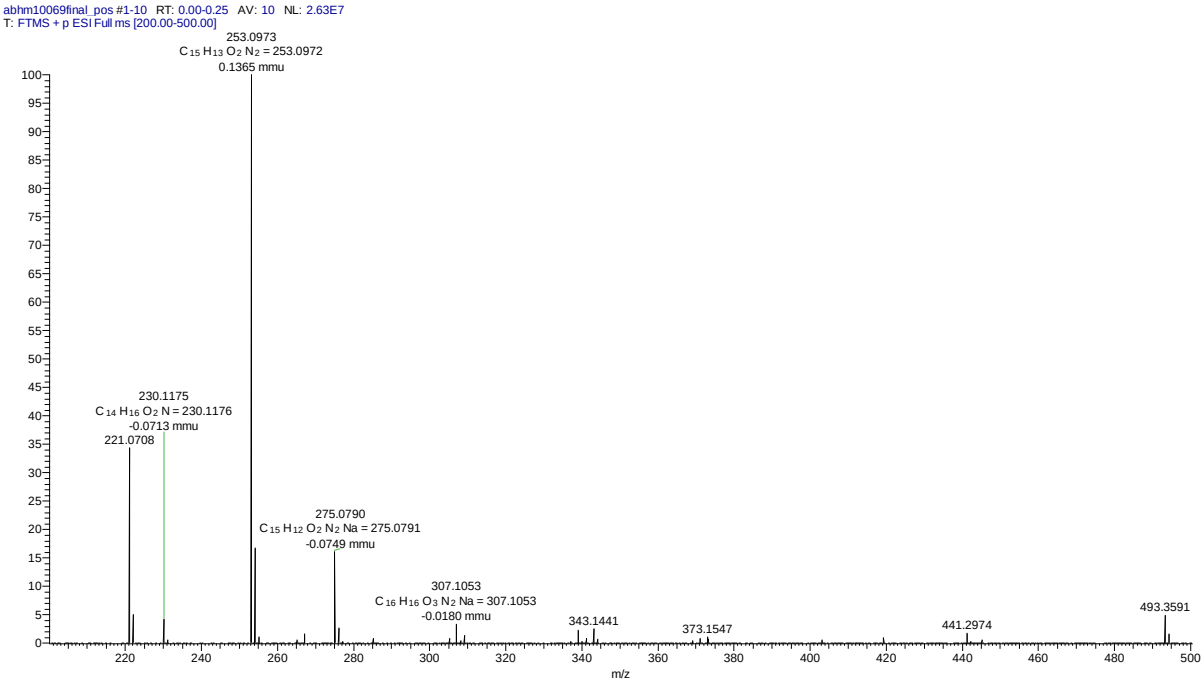

Agilent Technologies

Sample ID:	sm	Method Name:	ATR-default
Sample Scans:	4	User:	IK
Background Scans:	4	Date/Time:	4/7/2020 11:15:47AM
Resolution:	8 cm-1	Range:	4,000.00 - 650.00
System Status:	Good	Apodization:	Happ-Genzel
File Location:	C:\Program Files\Agilent\MicroLab PC\Results\Rune\sm_2020-04-07T11-17-46.a2r		

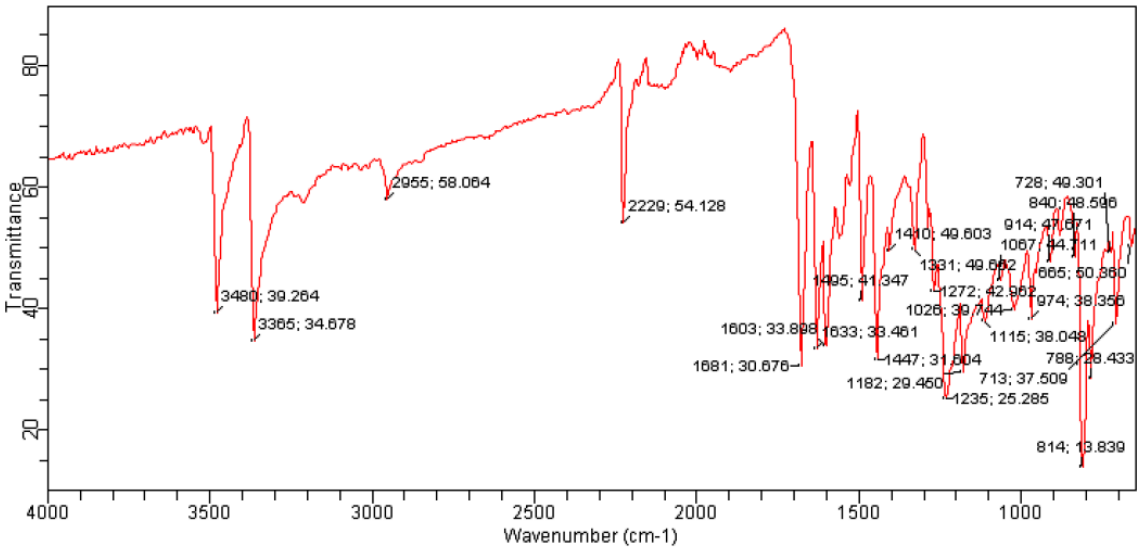

9.1.3 Methyl 2-(benzylamino)-5-bromobenzoate (11)

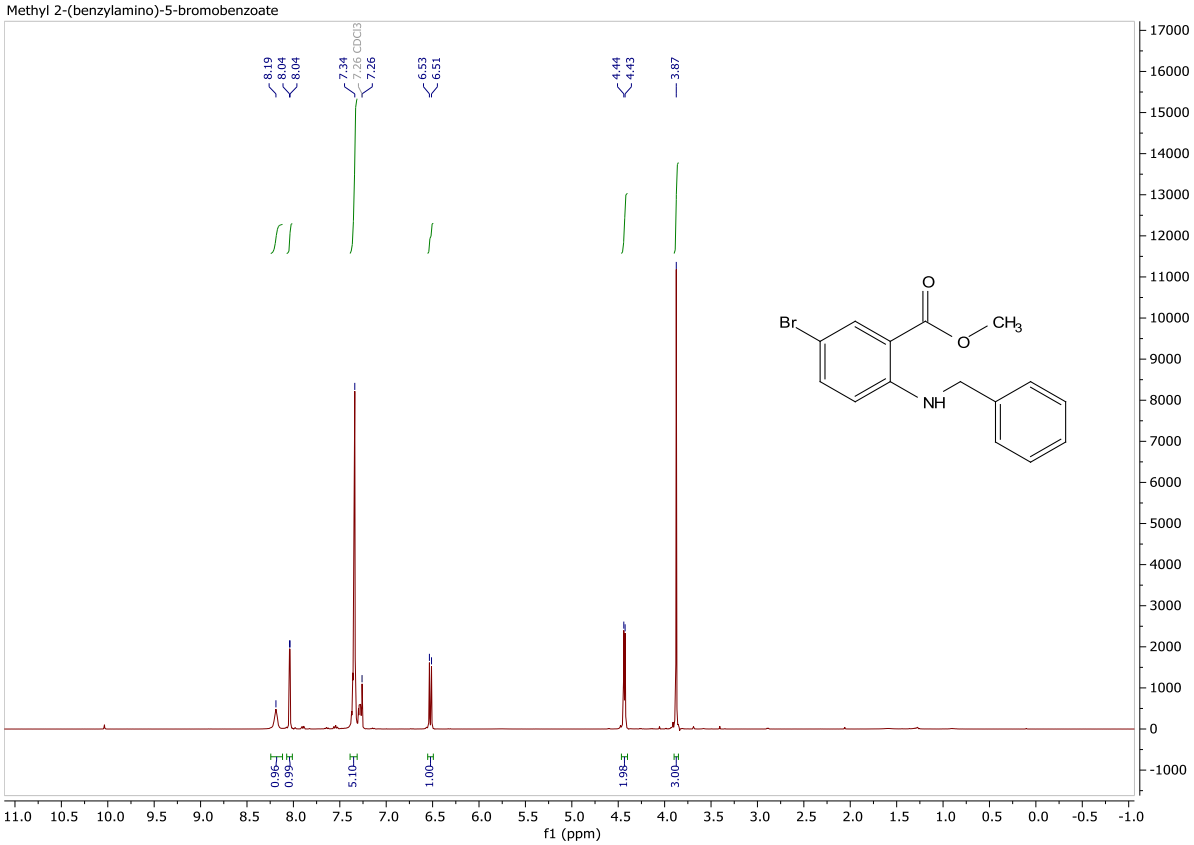

CARBON Methyl 2-(benzylamino)-5-bromobenzoate

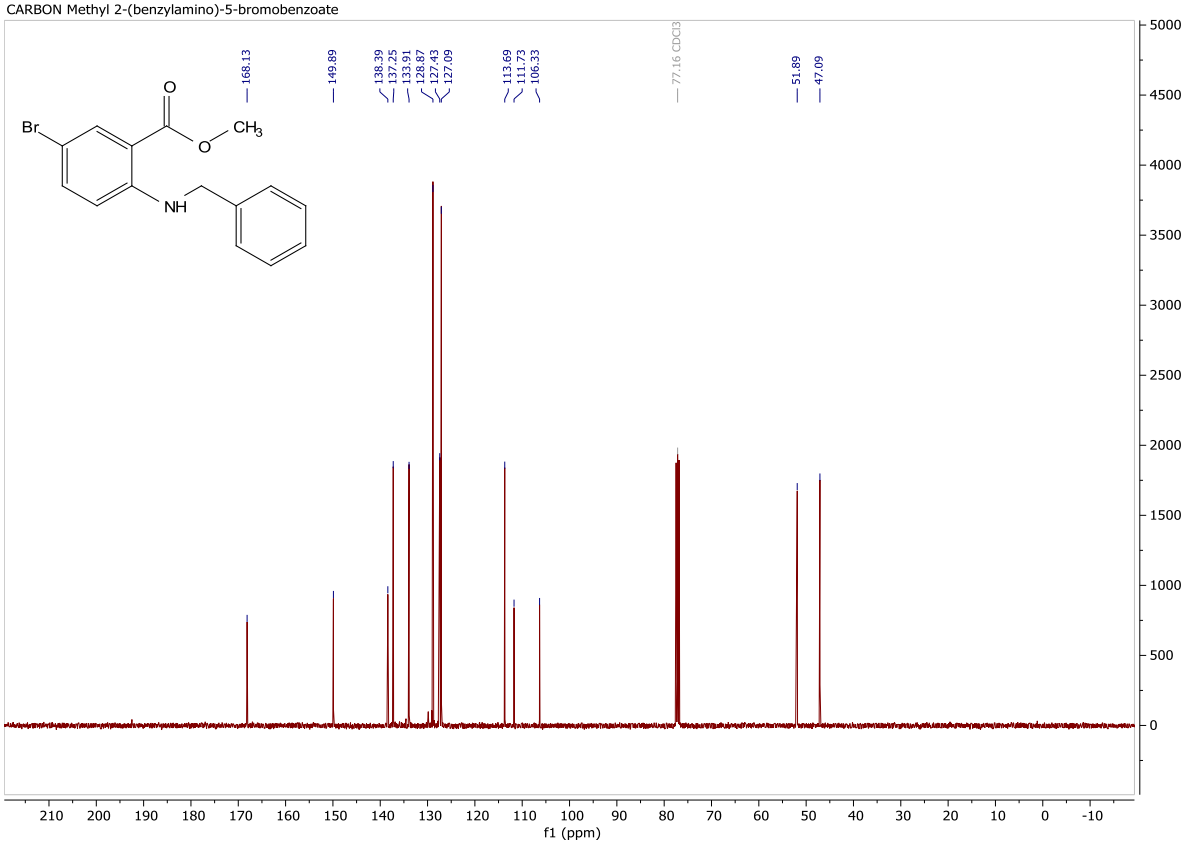

abhm100617spot2_pos2 #1-9 RT: 0.02-0.24 AV: 9 NL: 2.87E7
T: FTMS + p ESI Full ms [100.00-600.00]

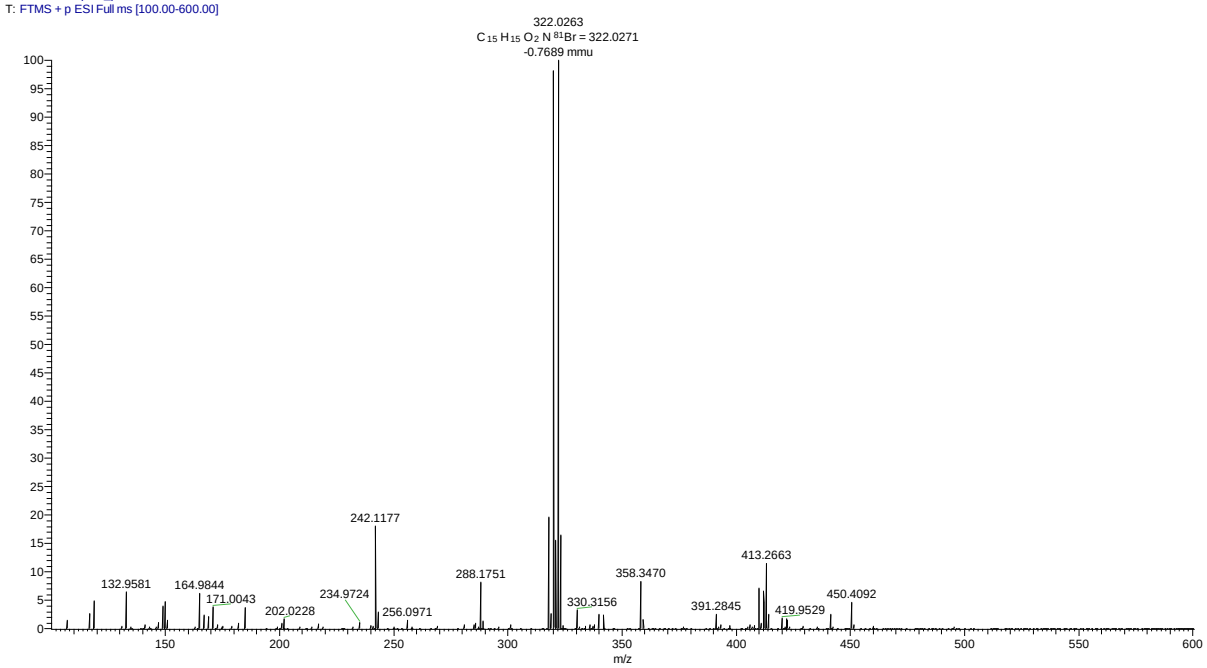

9.2 Reductive amination Spectra

9.2.1 Methyl 4-(benzylamino)-4'-cyano-[1,1'-biphenyl]-3-carboxylate (18)

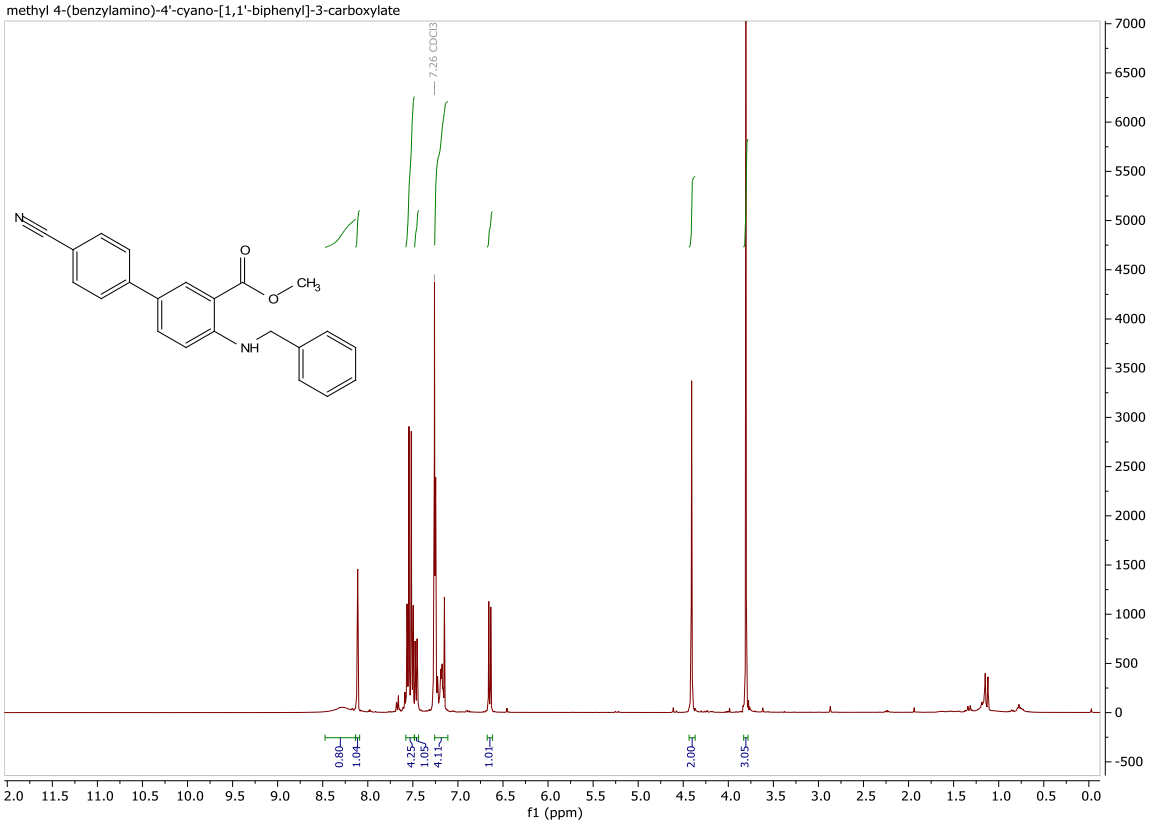

methyl 4-(benzylamino)-4'-cyano-[1,1'-biphenyl]-3-carboxylate

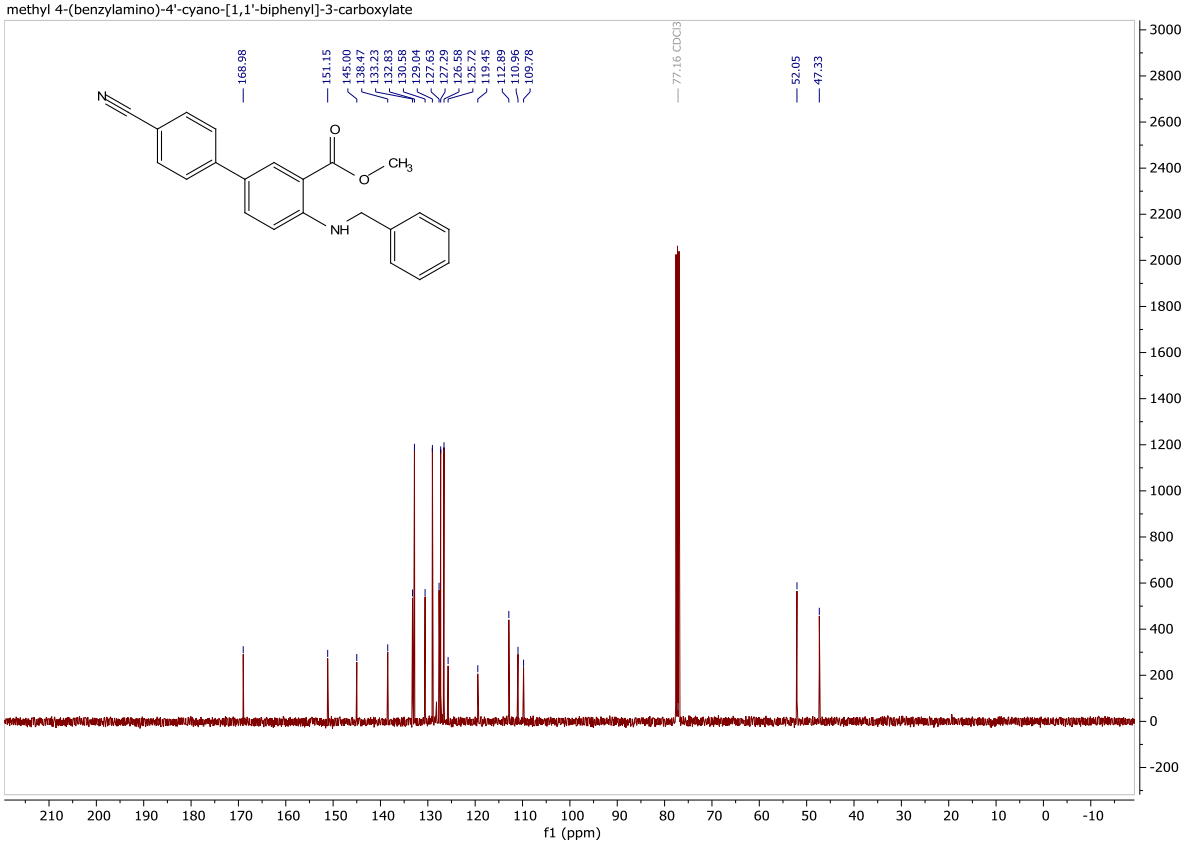

abhm100621final_pos #1-9 RT: 0.02-0.26 AV: 9 NL: 1.68E6
T: FTMS + p ESI Full ms [200.00-500.00]

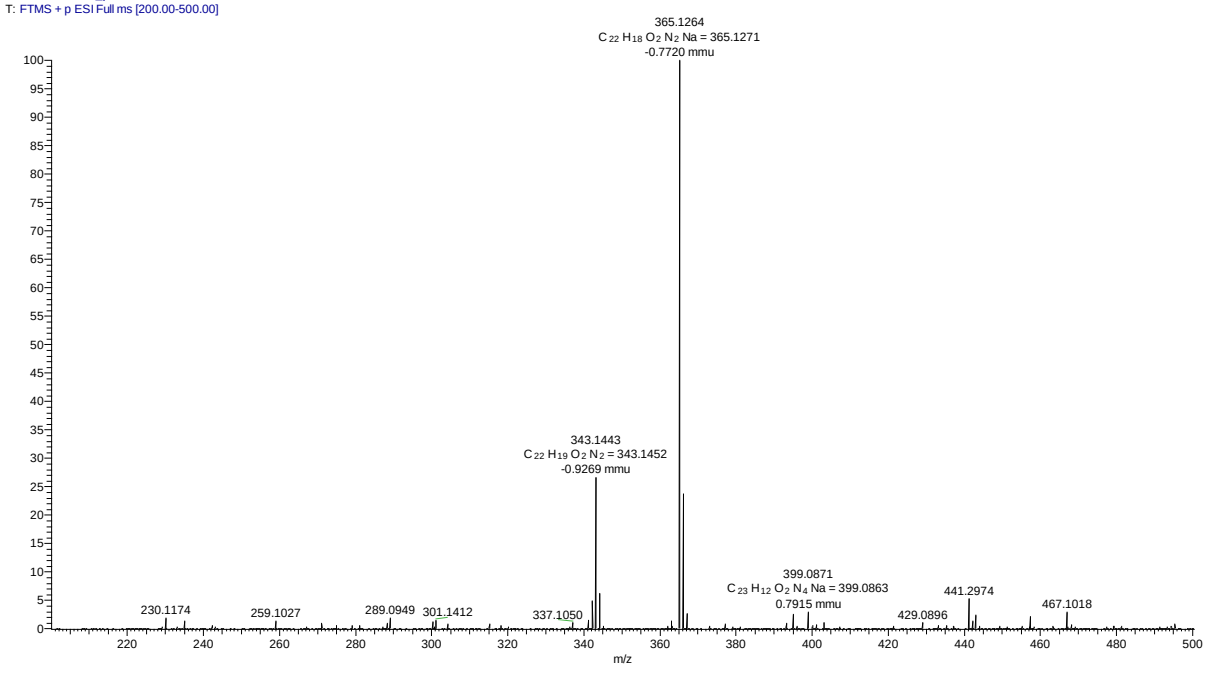

9.2.2 Methyl 4'-cyano-4-((3-methoxybenzyl)amino)-[1,1'-biphenyl]-3-carboxylate (22)

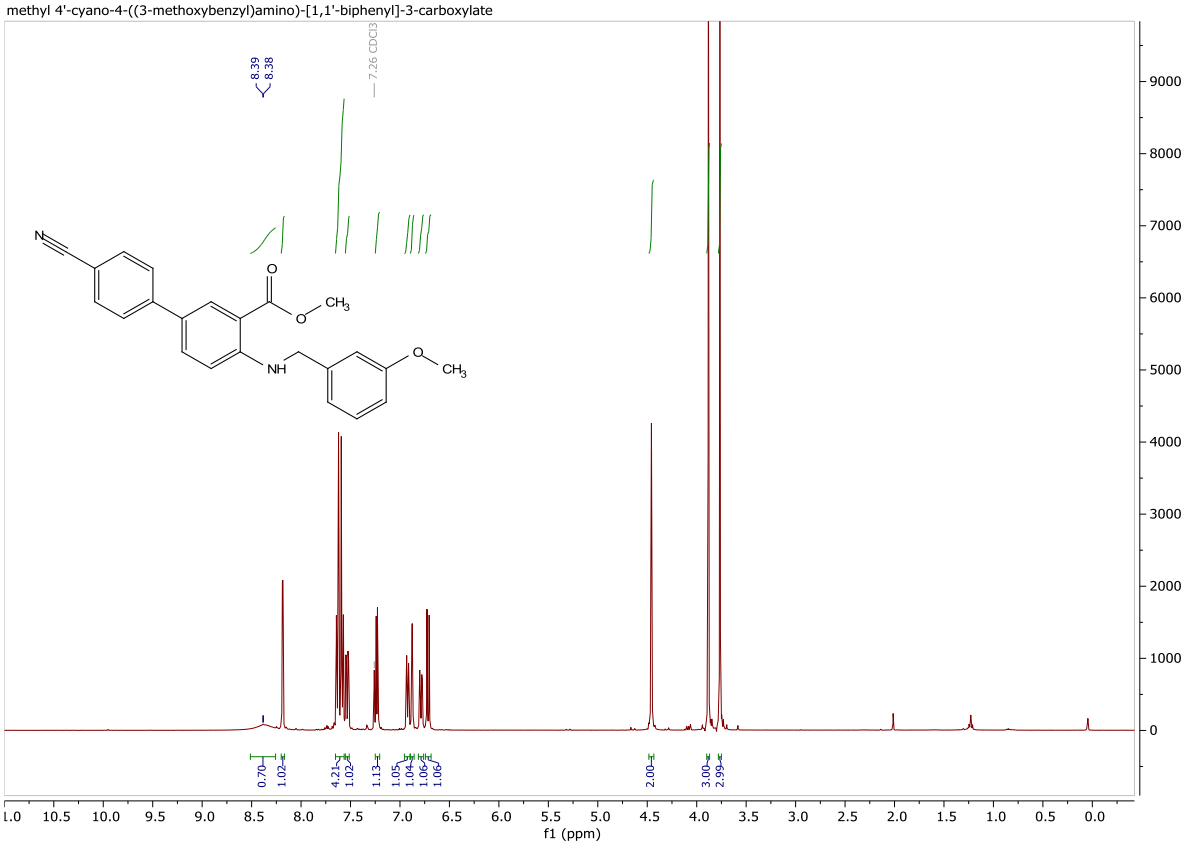

methyl 4'-cyano-4-((3-methoxybenzyl)amino)-[1,1'-biphenyl]-3-carboxylate

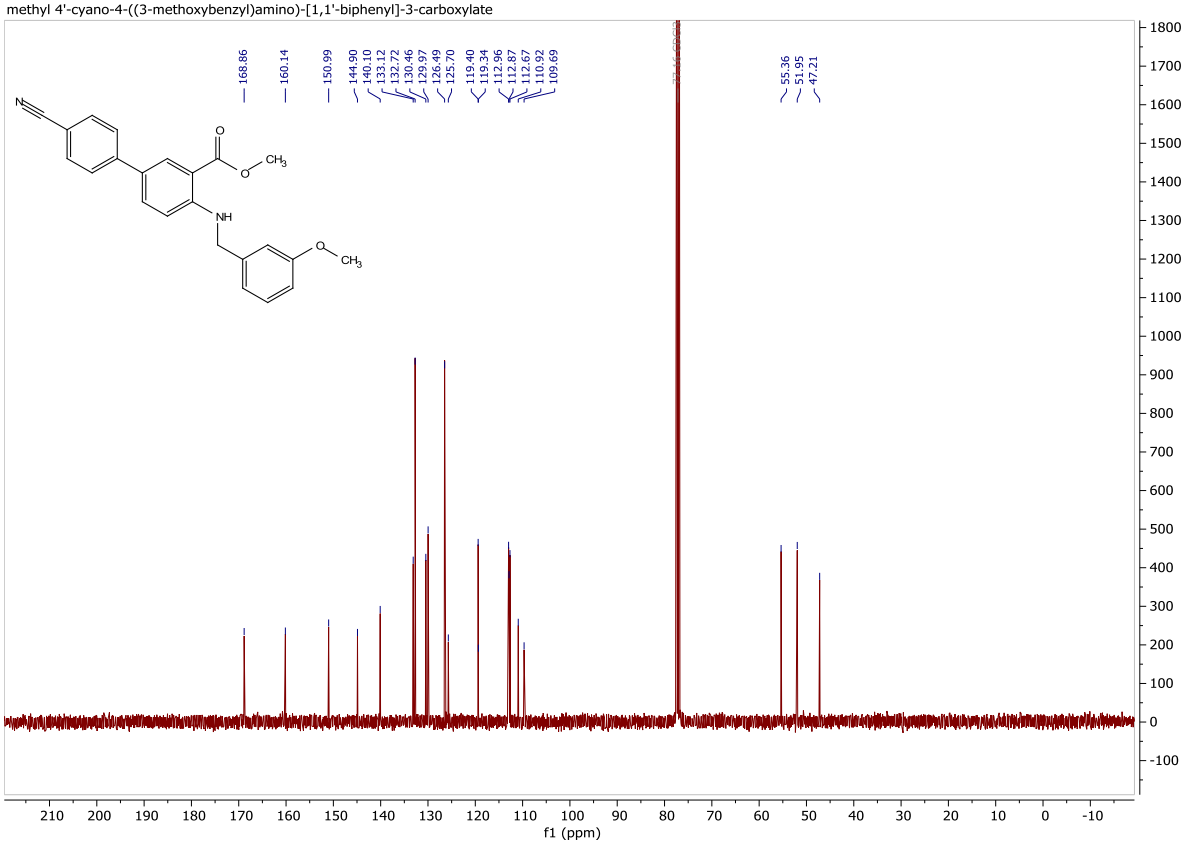

ABHM100644_final_pos #1-8 RT: 0.01-0.26 AV: 8 NL: 5.36E4
T: FTMS + p ESI Full ms [100.00-600.00]

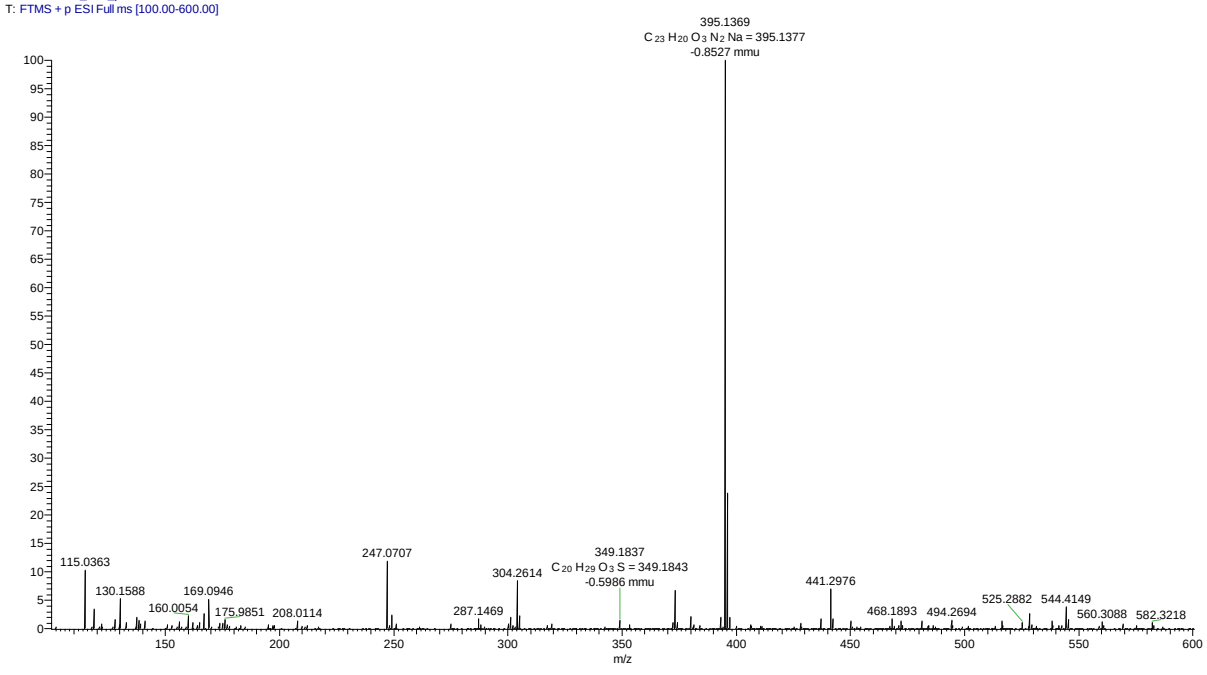

9.2.3 Methyl 4'-cyano-4-((3,5-dimethoxybenzyl)amino)-[1,1'-biphenyl]-3-carboxylate (26)

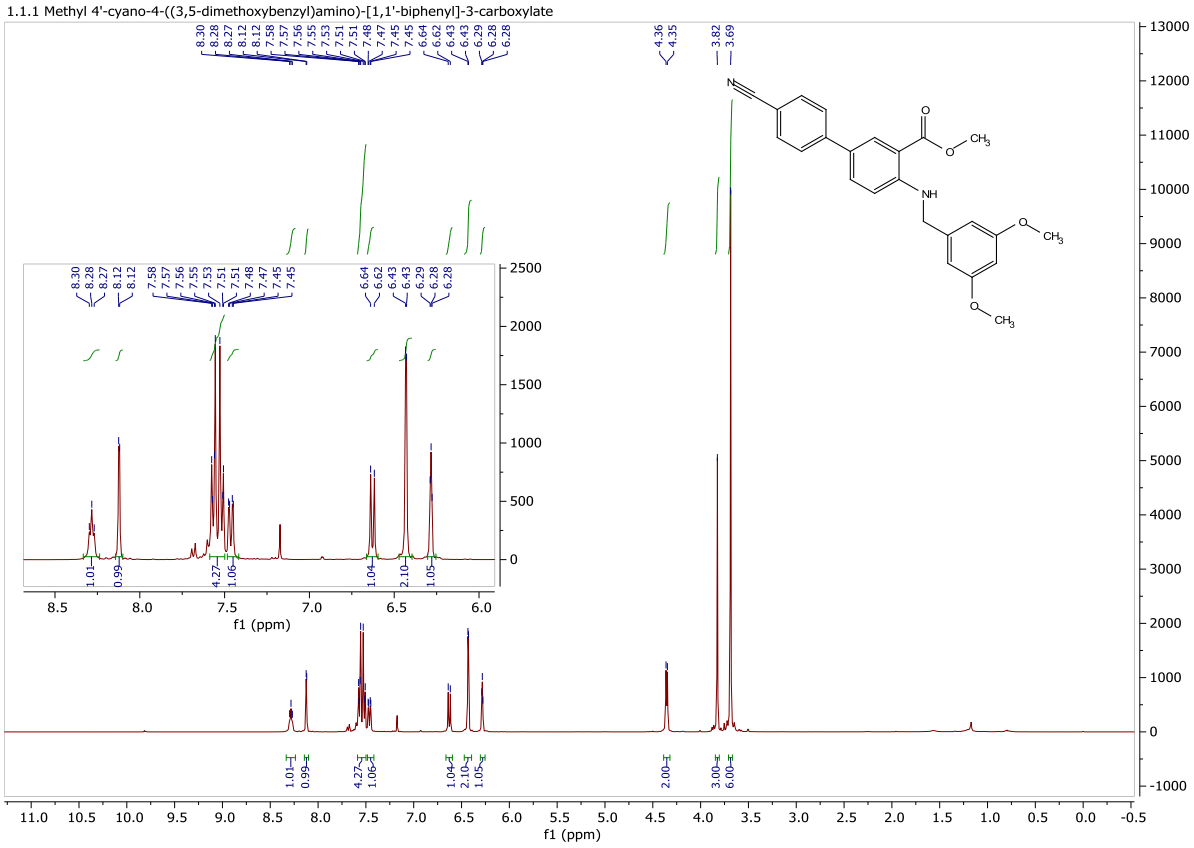

methyl 4'-cyano-4-((3,5-dimethoxybenzyl)amino)-[1,1'-biphenyl]-3-carboxylate

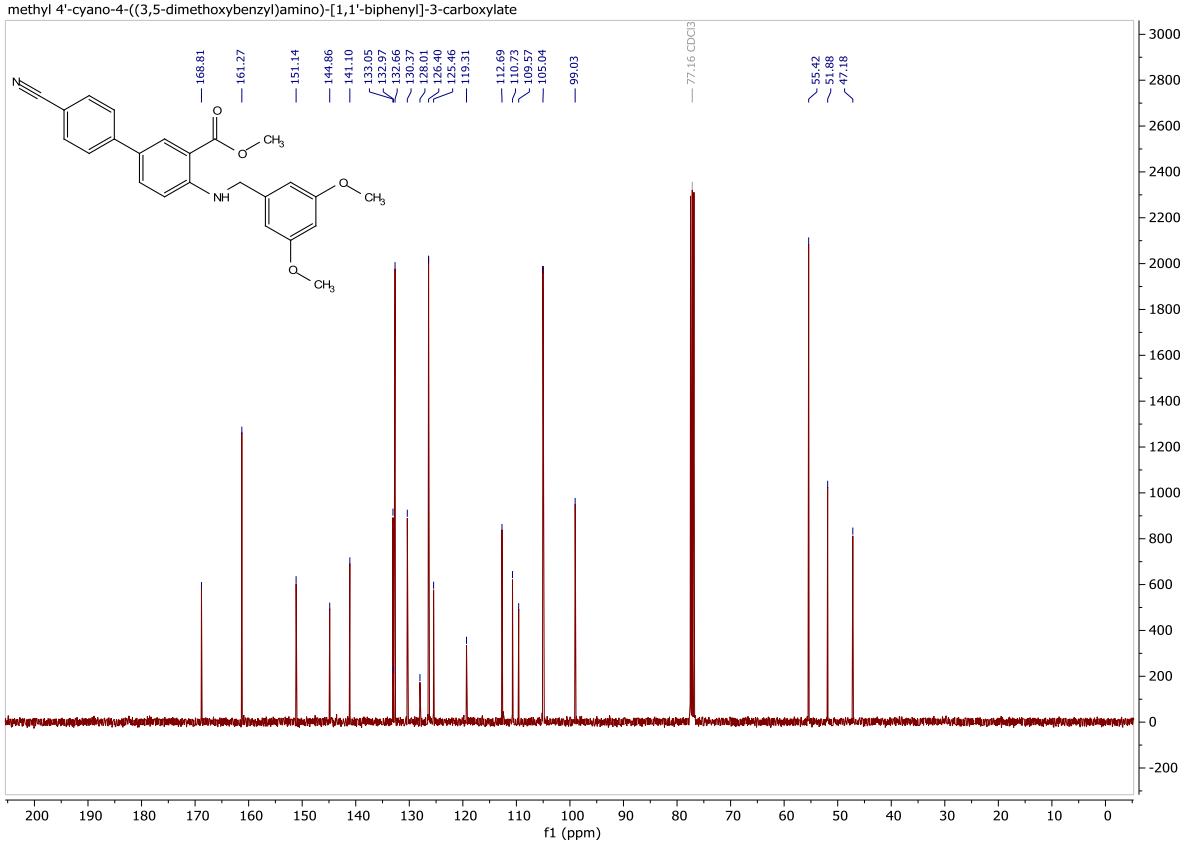

ABHM100638_CRUDE_2_final_pos #1-7 RT: 0.02-0.24 AV: 7 NL: 3.29E4
T: FTMS + c ESI Full ms [100.00-700.00]

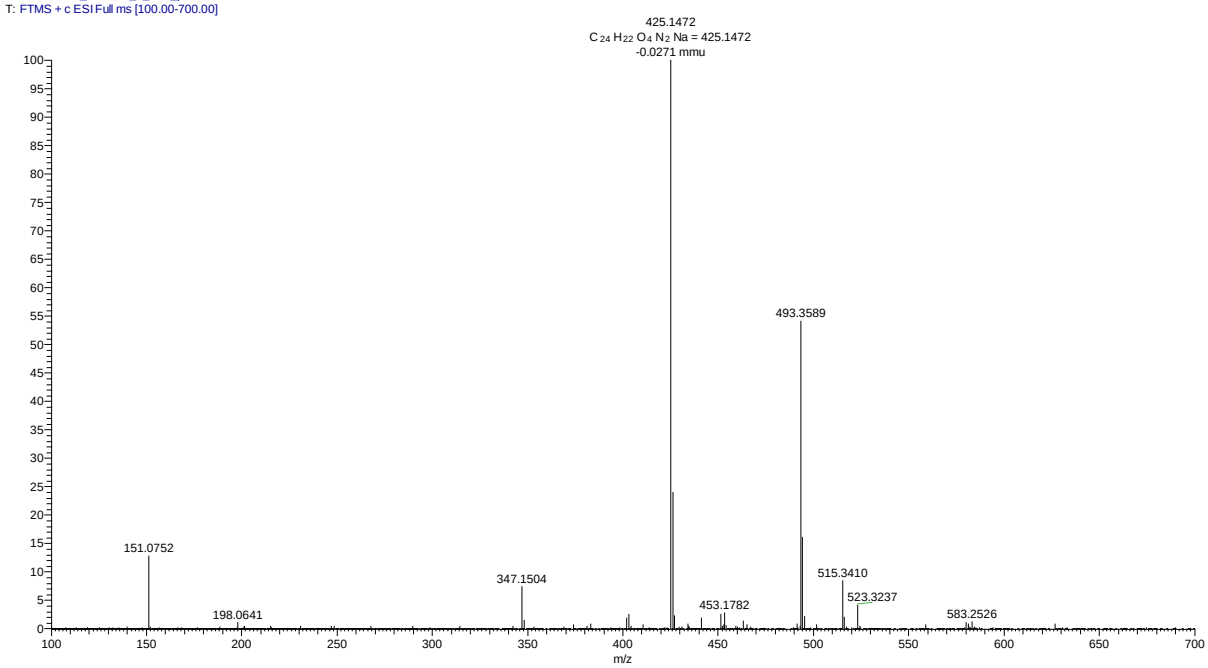

Agilent Technologies

Sample ID:	abhm100638	Method Name:	ATR-default
Sample Scans:	4	User:	IK
Background Scans:	4	Date/Time:	4/7/2020 11:12:36AM
Resolution:	8 cm-1	Range:	4,000.00 - 650.00
System Status:	Good	Apodization:	Happ-Genzel
File Location:	C:\Program Files\Agilent\MicroLab PC\Results\Rune\abhm100638_2020-04-07T11-13-45.a2r		

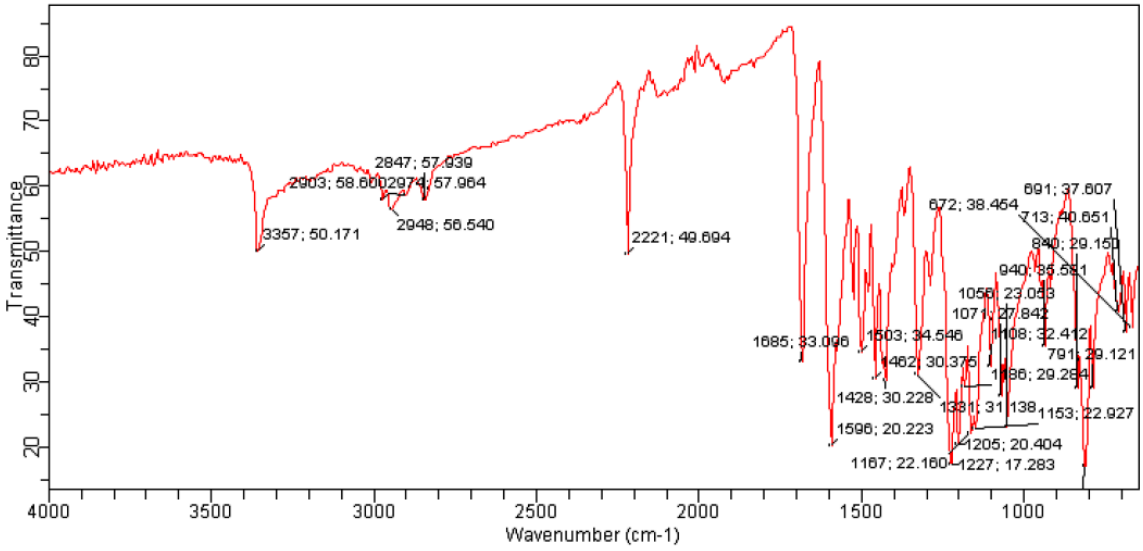

9.2.4 Methyl 4'-cyano-4-((thiophen-2-ylmethyl)amino)-[1,1'-biphenyl]-3-carboxylate (23)

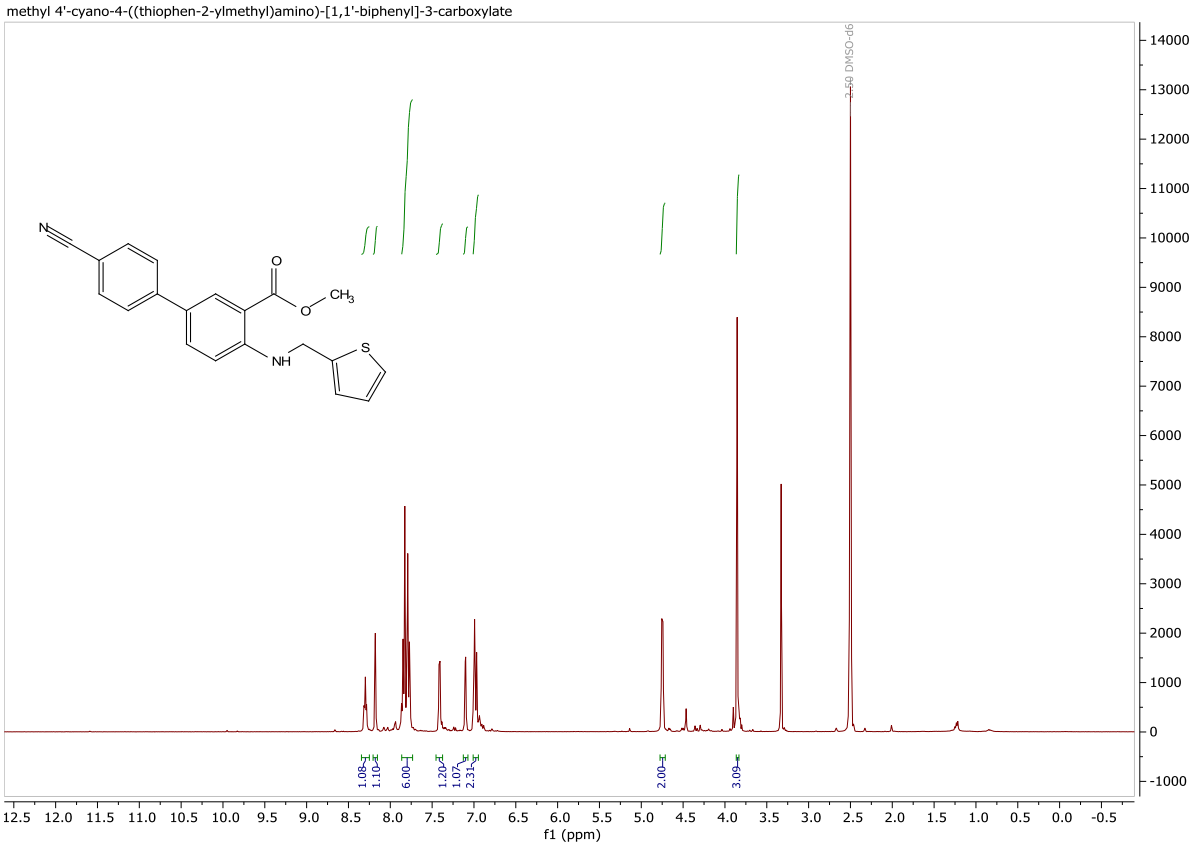

methyl 4'-cyano-4-((thiophen-2-ylmethyl)amino)-[1,1'-biphenyl]-3-carboxylate

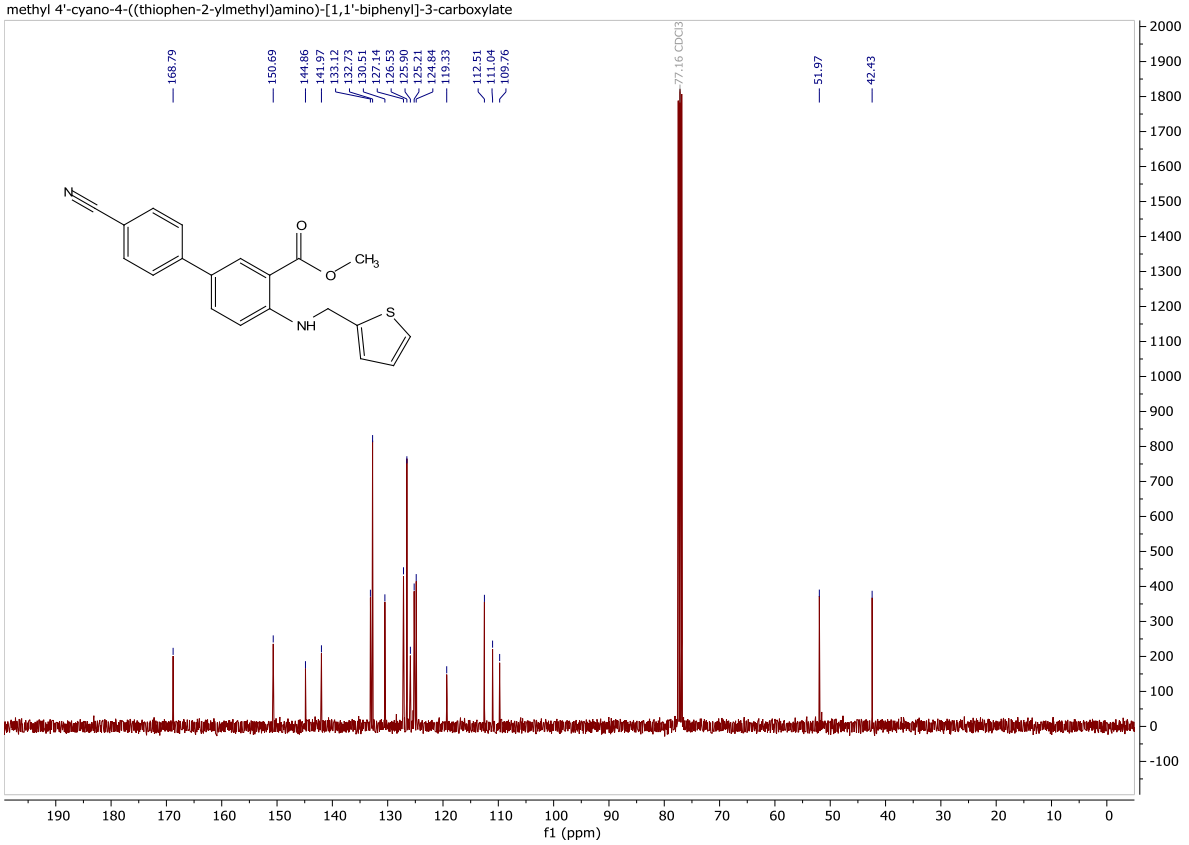

abhm100645possibly_pos #1-5 RT: 0.01-0.07 AV: 5 NL: 7.76E6
T: FTMS + p ESI Full ms [115.00-500.00]

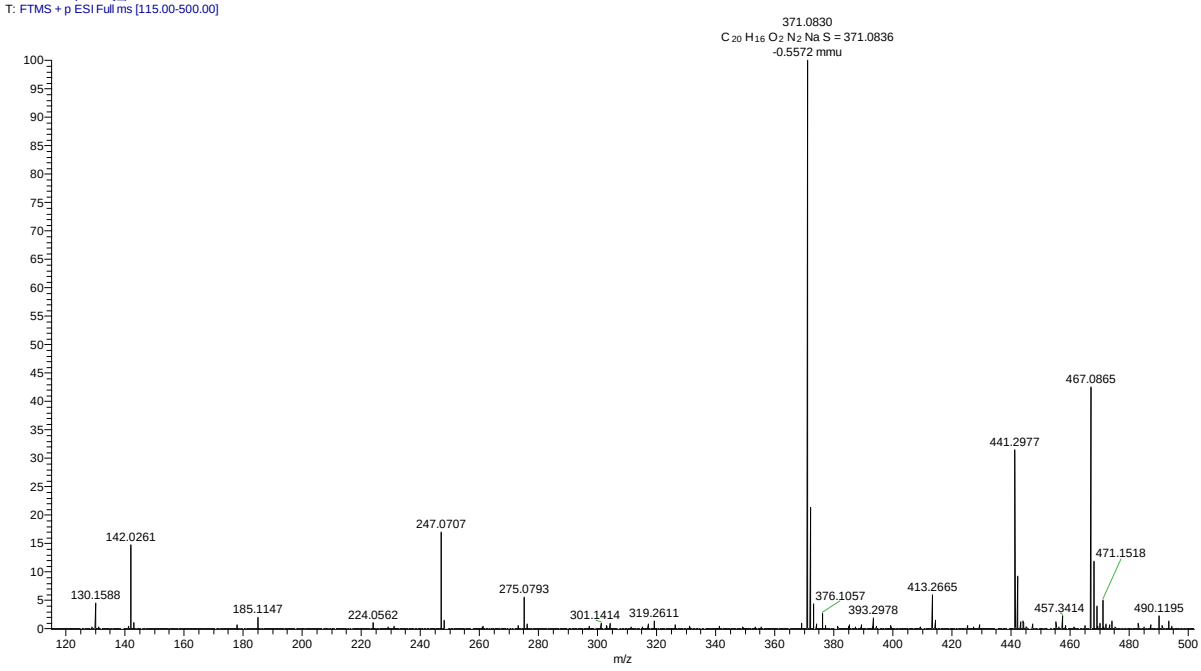

9.2.5 Methyl 4-((2-bromo-6-fluorobenzyl)amino)-4'-cyano-[1,1'-biphenyl]-3-carboxylate (25)

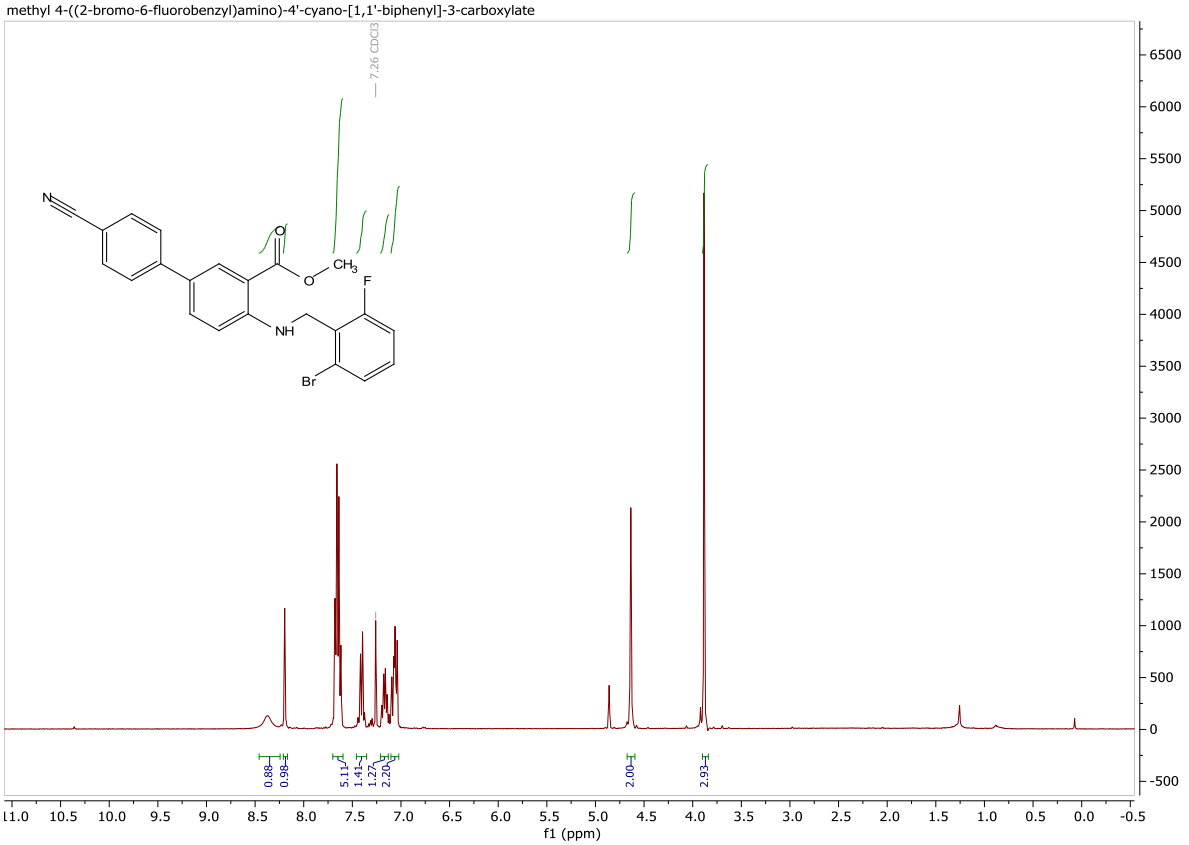

methyl 4-((2-bromo-6-fluorobenzyl)amino)-4'-cyano-[1,1'-biphenyl]-3-carboxylate

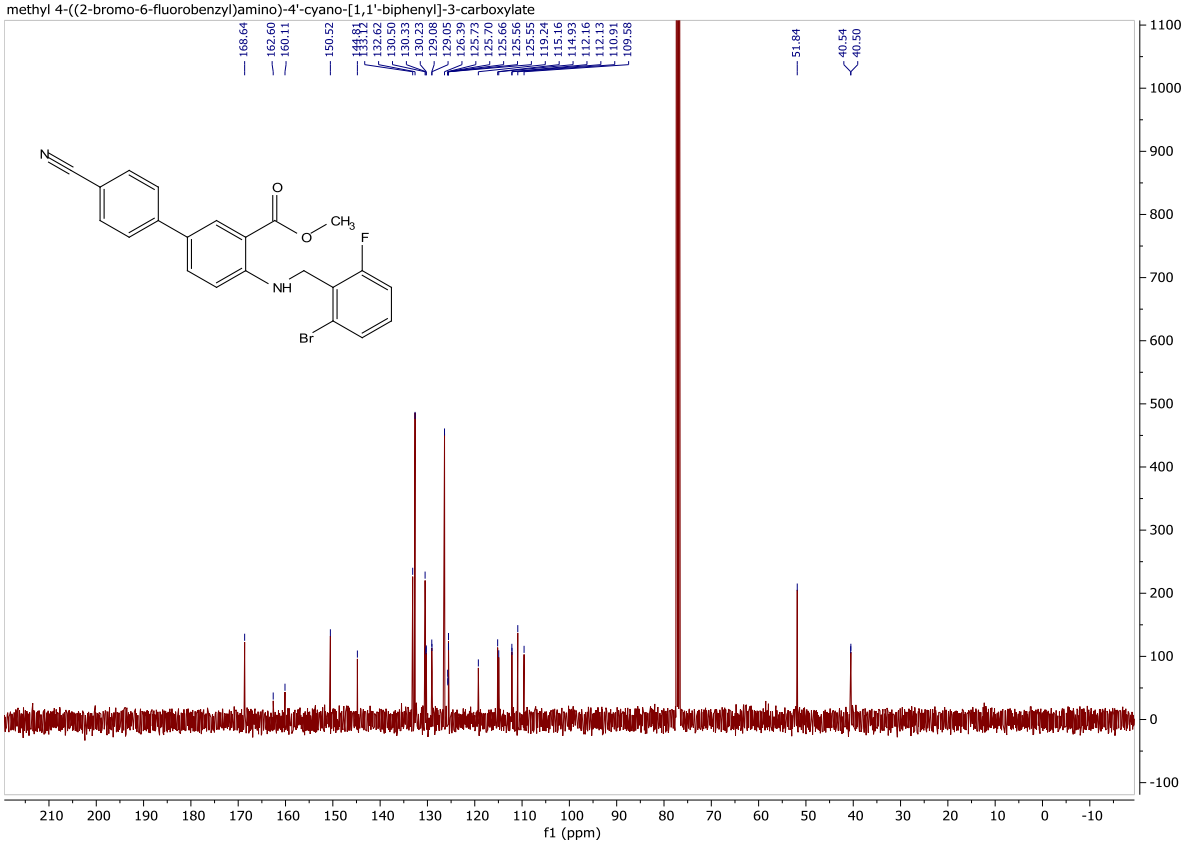

abhm100649_final_good_pos #1-9 RT: 0.02-0.25 AV: 9 NL: 6.04E6
T: FTMS + p ESI Full ms [100.00-650.00]

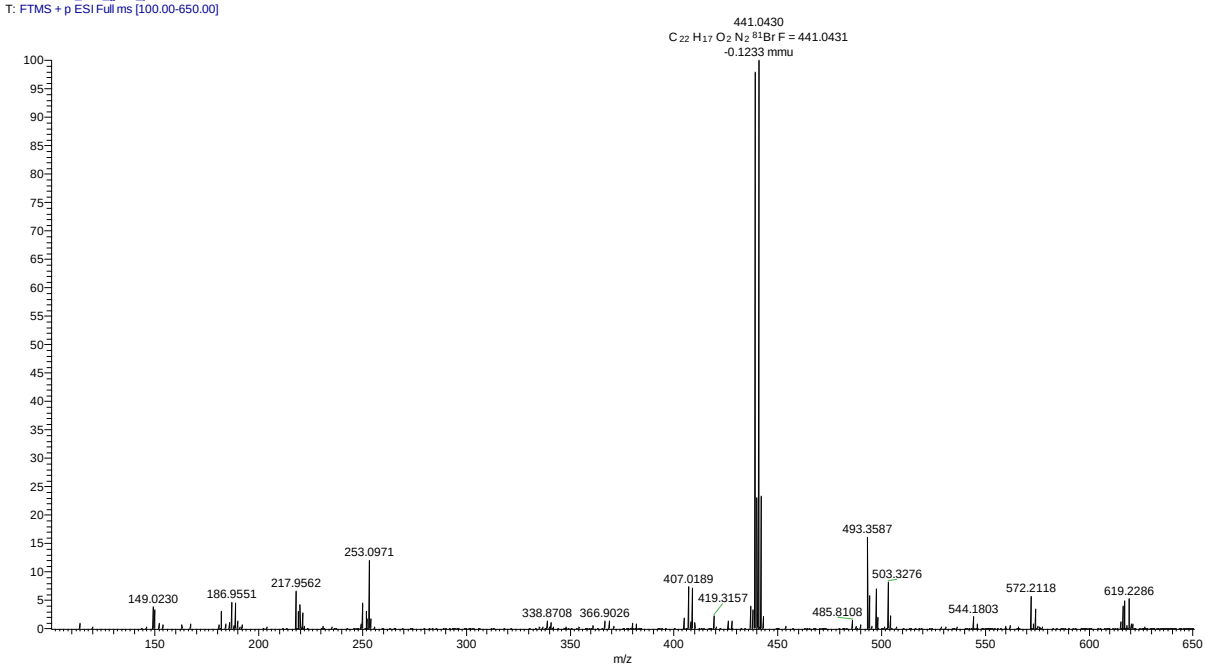

9.3 Tetrazole formation

9.3.1 Methyl 4-amino-4'-(1*H*-tetrazol-5-yl)-[1,1'-biphenyl]-3-carboxylate (14)

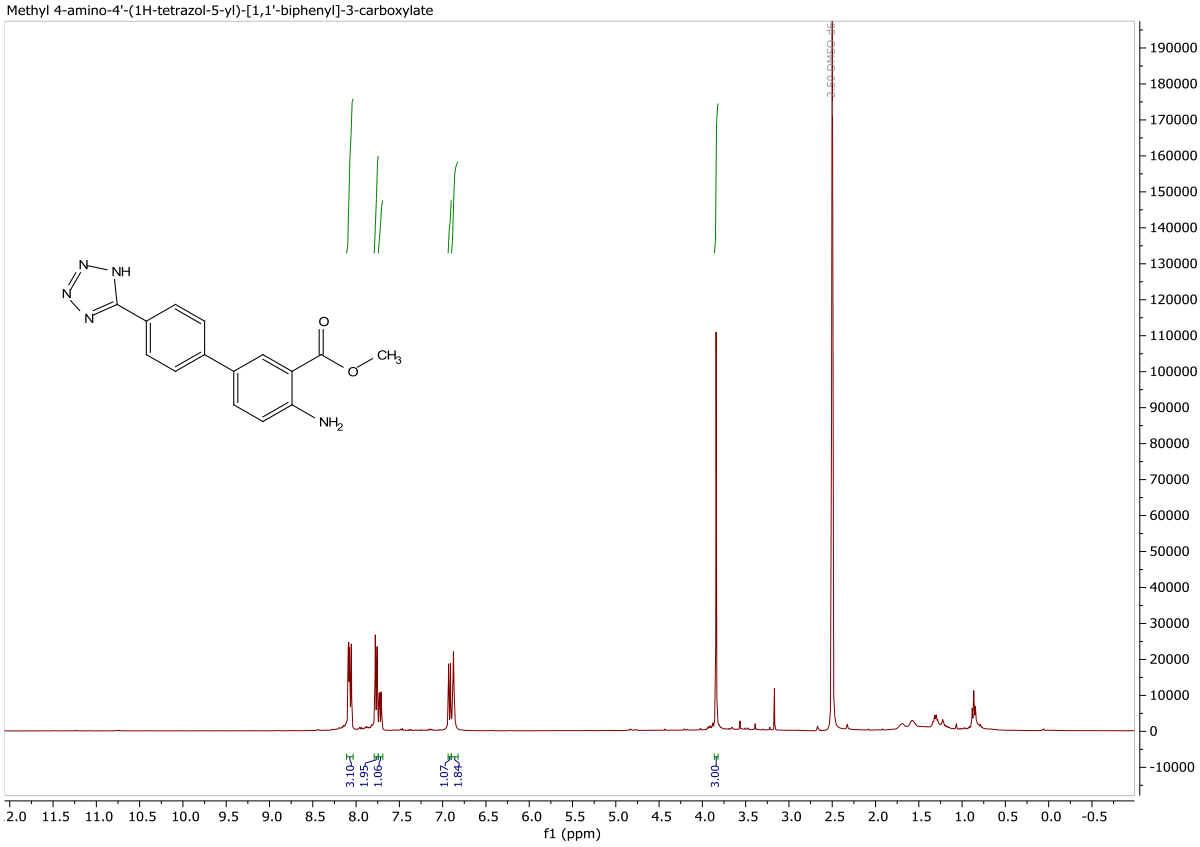

Methyl 4-amino-4'-(1H-tetrazol-5-yl)-[1,1'-biphenyl]-3-carboxylate

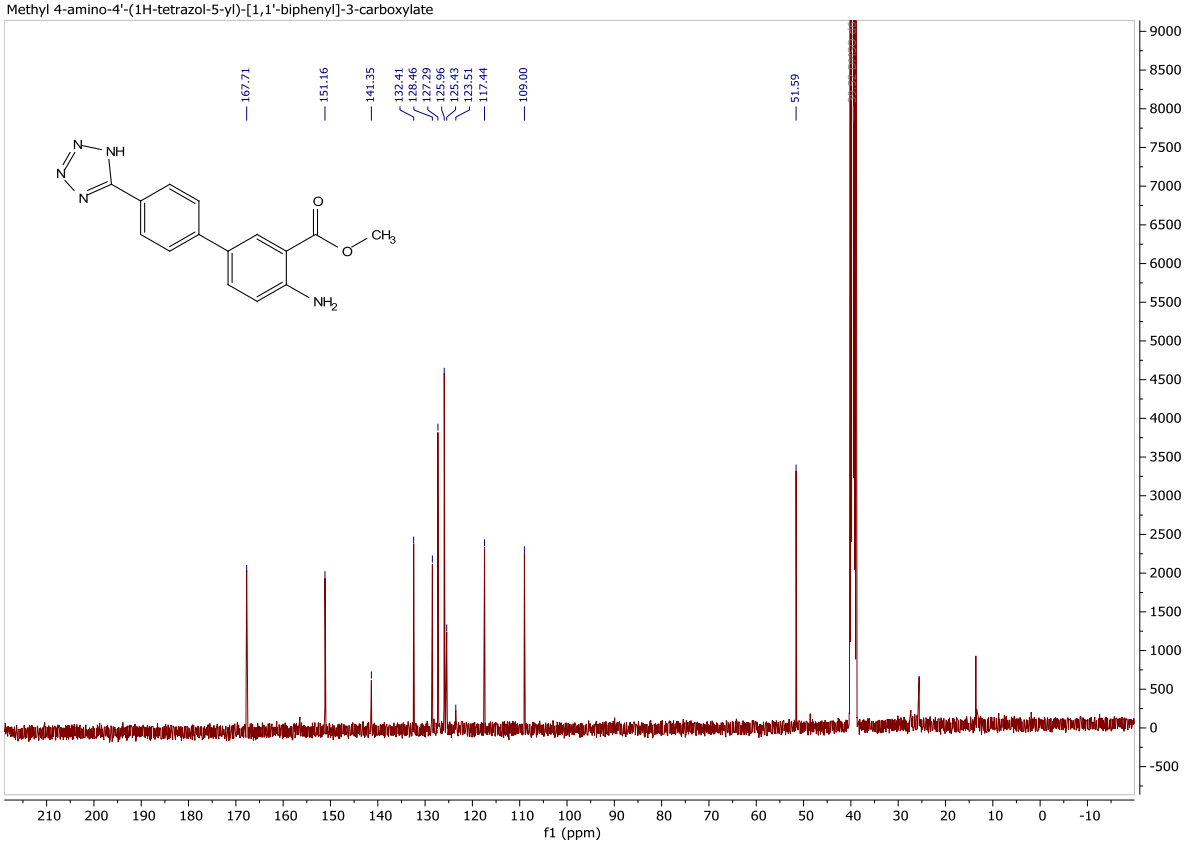

abhm10066final_neg #1-9 RT: 0.02-0.25 AV: 9 NL: 4.10E7
T: FTMS - p ESI Full ms [200.00-500.00]

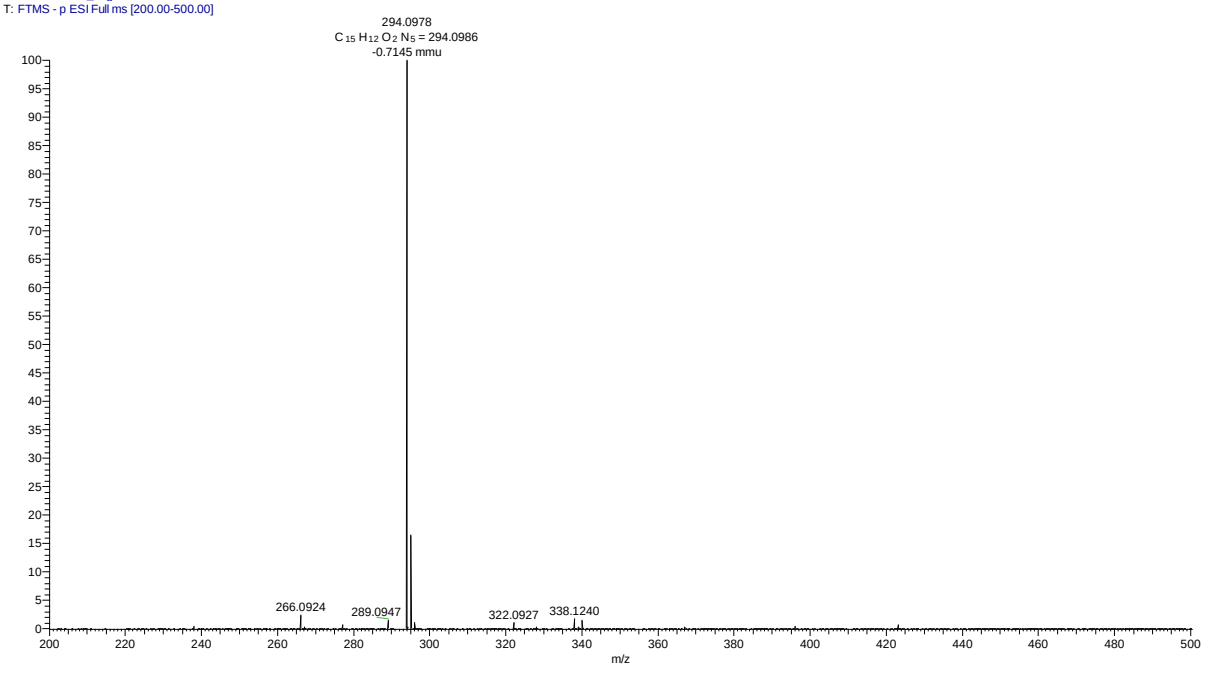

9.3.2 Methyl 4-((3,5-dimethoxybenzyl)amino)-4'-(1*H*-tetrazol-5-yl)-[1,1'-biphenyl]-3-carboxylate (27)

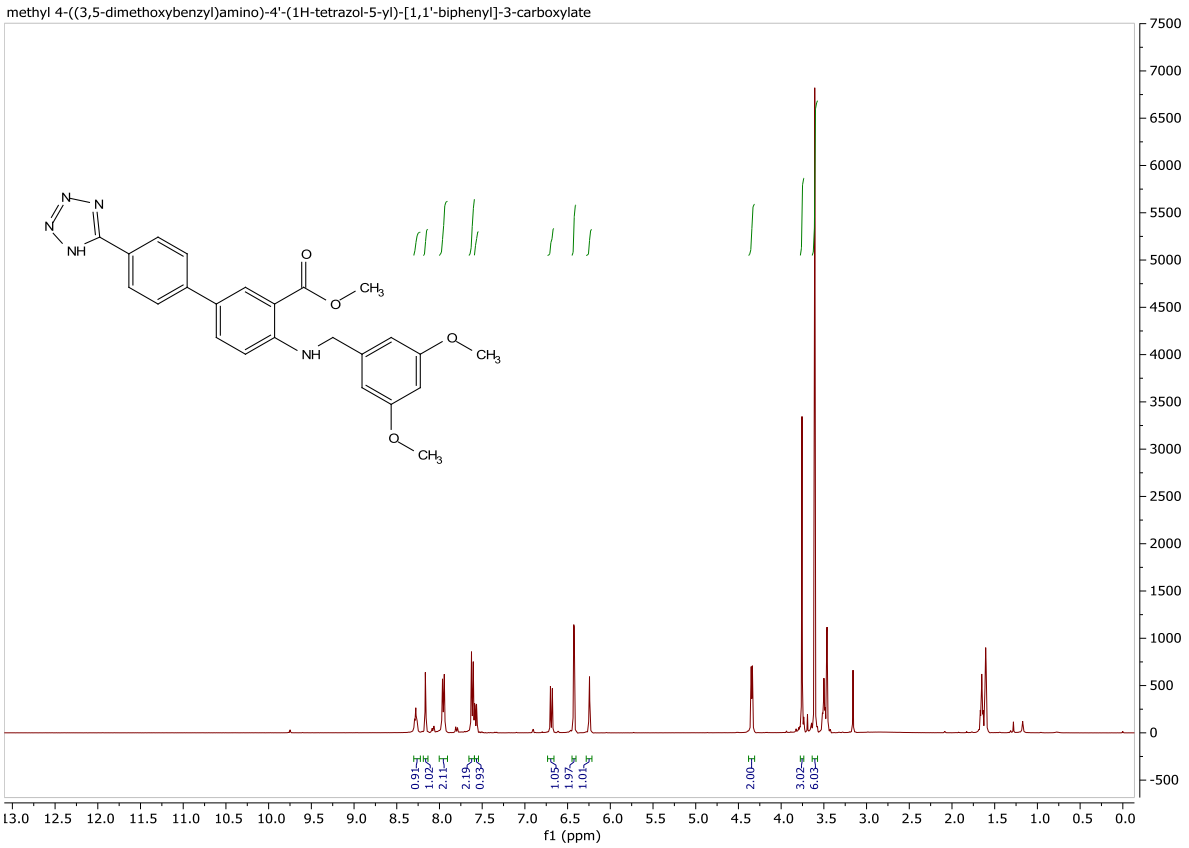

methyl 4-((3,5-dimethoxybenzyl)amino)-4'-(1H-tetrazol-5-yl)-[1,1'-biphenyl]-3-carboxylate

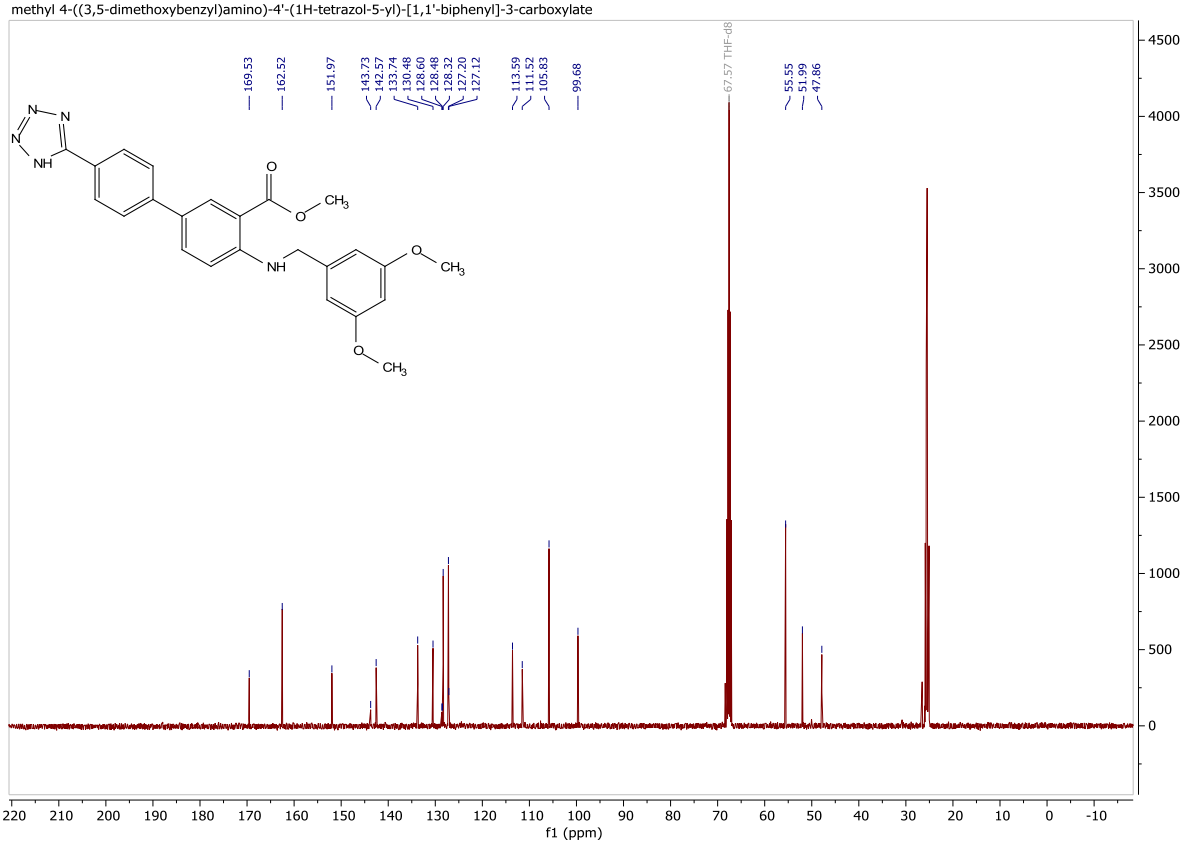

abhm100639_Final_neg #1-9 RT: 0.01-0.25 AV: 9 NL: 6.64E7
T: FTMS - p ESI Full ms [100.00-800.00]

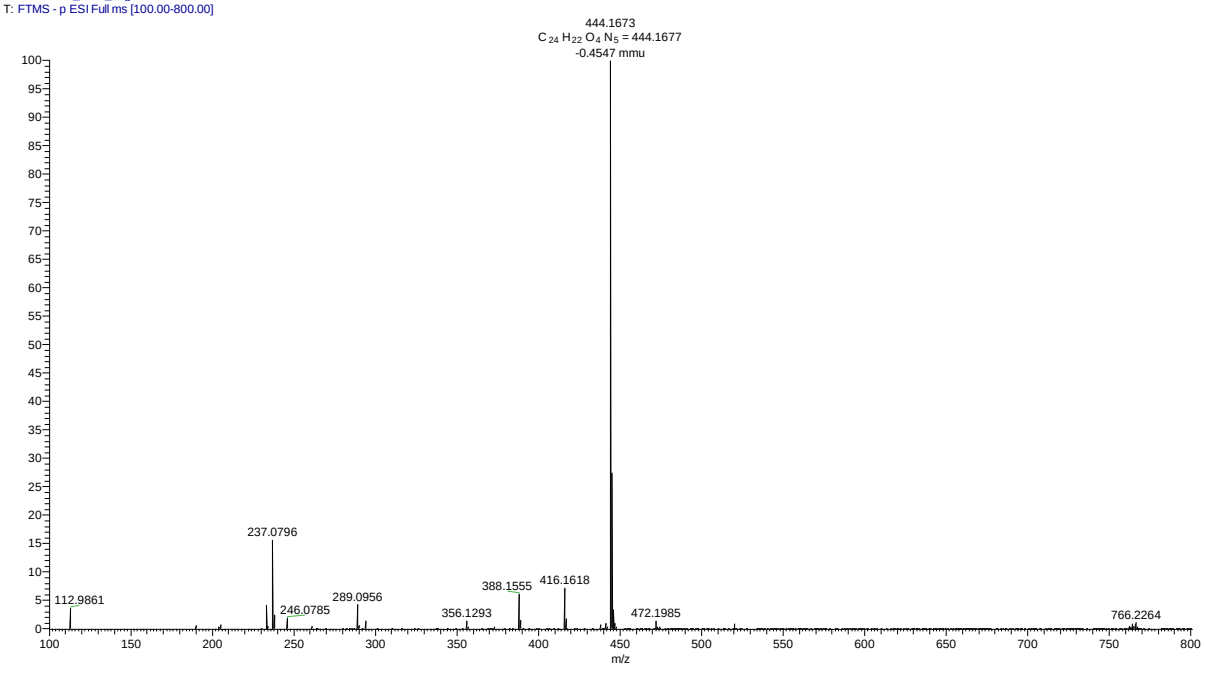

Agilent Technologies

Sample ID:	abhm100639	Method Name:	ATR-default
Sample Scans:	4	User:	IK
Background Scans:	4	Date/Time:	4/7/2020 11:01:57AM
Resolution:	8 cm-1	Range:	4,000.00 - 650.00
System Status:	Good	Apodization:	Happ-Genzel
File Location:	C:\Program Files\Agilent\MicroLab PC\Results\Rune\abhm100639_2020-04-07T11-06-03.a2r		

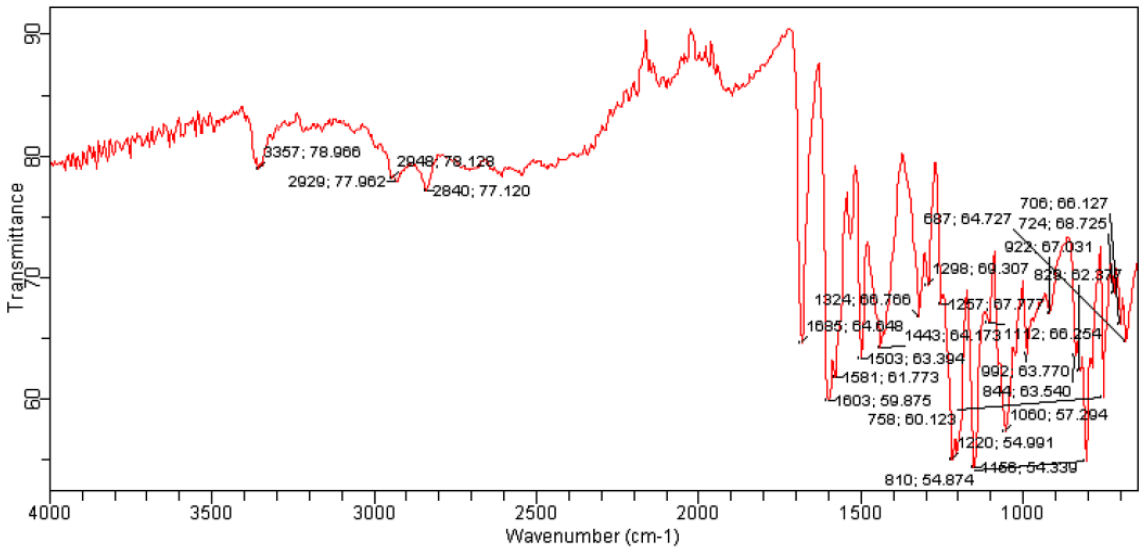

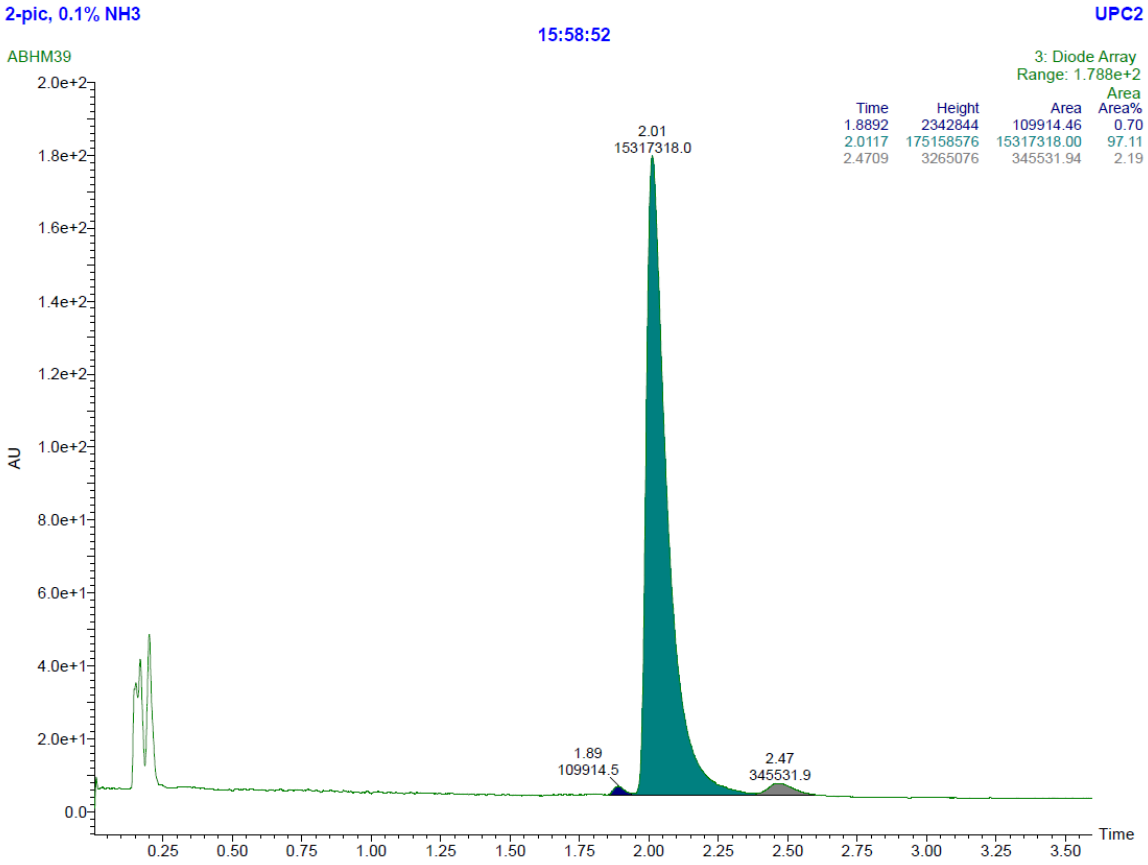
2-pic, 0.1% NH3
15:58:52
UPC2
ABHM39
3: Diode Array
Range: 1.788e+2
Time Height Area Area%
1.8892 2342844 109914.46 0.70
2.0117 175158576 15317318.00 97.11
2.4709 3265076 345531.94 2.19
2.01
15317318.0
1.89
109914.5
2.47
345531.9
AU
Time
2.0e+2
1.8e+2
1.6e+2
1.4e+2
1.2e+2
1.0e+2
8.0e+1
6.0e+1
4.0e+1
2.0e+1
0.0
0.25 0.50 0.75 1.00 1.25 1.50 1.75 2.00 2.25 2.50 2.75 3.00 3.25 3.50

9.3.3 Methyl 4-(((1-methyl-1*H*-imidazol-5-yl)methyl)amino)-4'-(1*H*-tetrazol-5-yl)-[1,1'-biphenyl]-3-carboxylate (28)

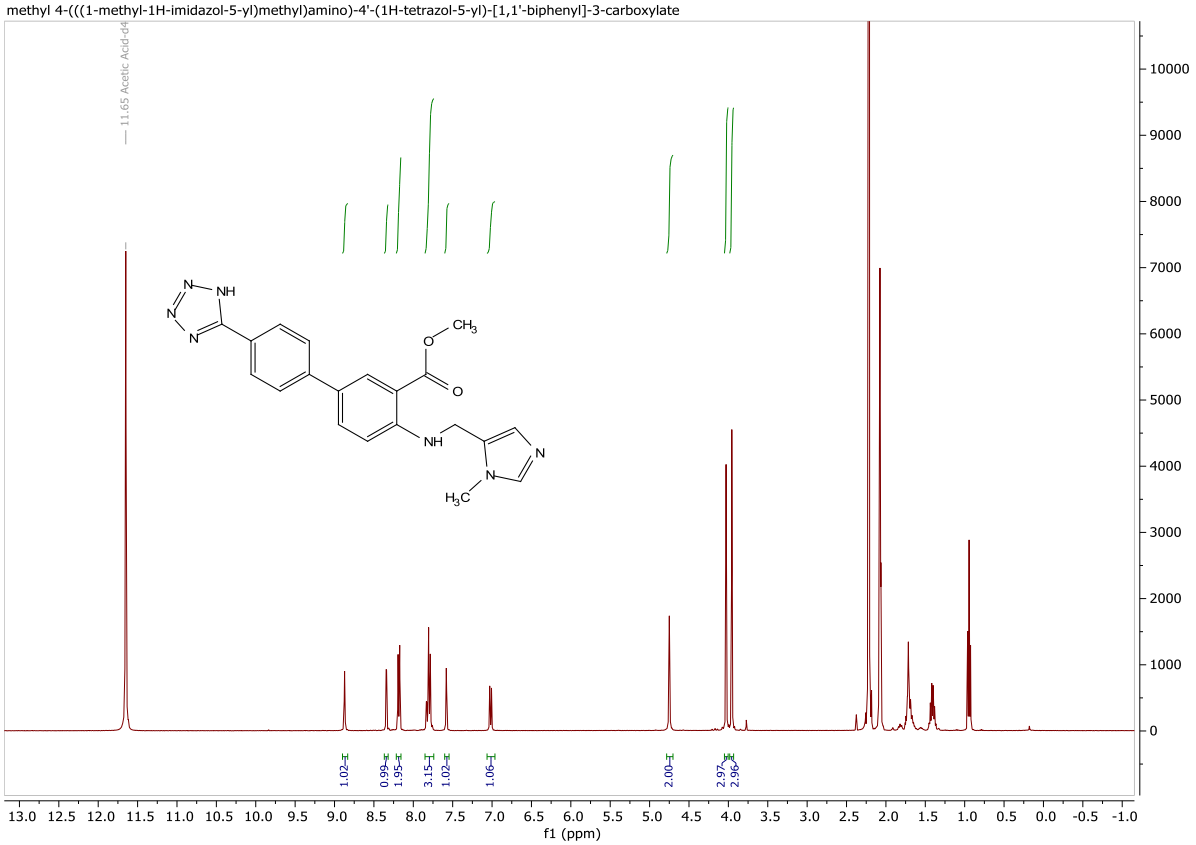

Methyl 4-(((1-methyl-1H-imidazol-5-yl)methyl)amino)-4'-(1H-tetrazol-5-yl)-[1,1'-biphenyl]-3-carboxylate

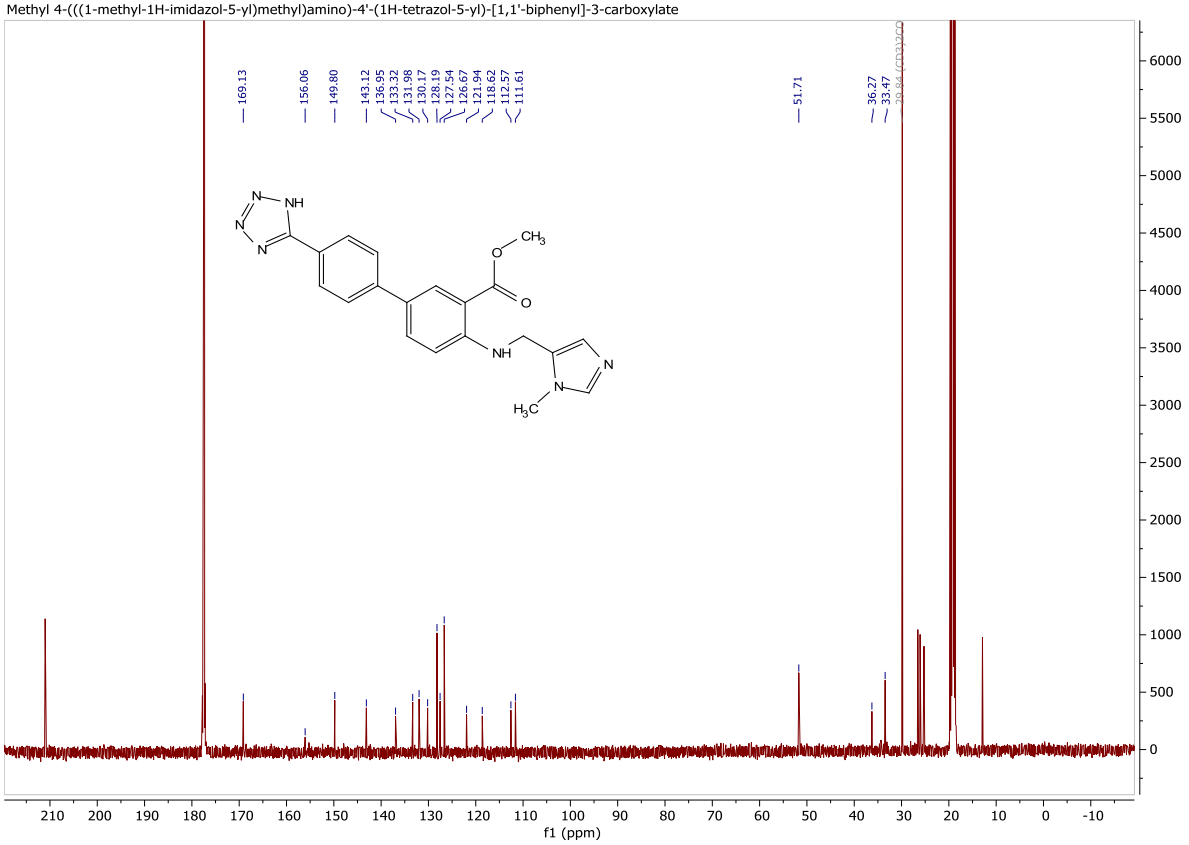

ABHM100640_FINAL_neg #1-7 RT: 0.02-0.25 AV: 7 NL: 3.64E5
T: FTMS - p ESI Full ms [120.00-700.00]

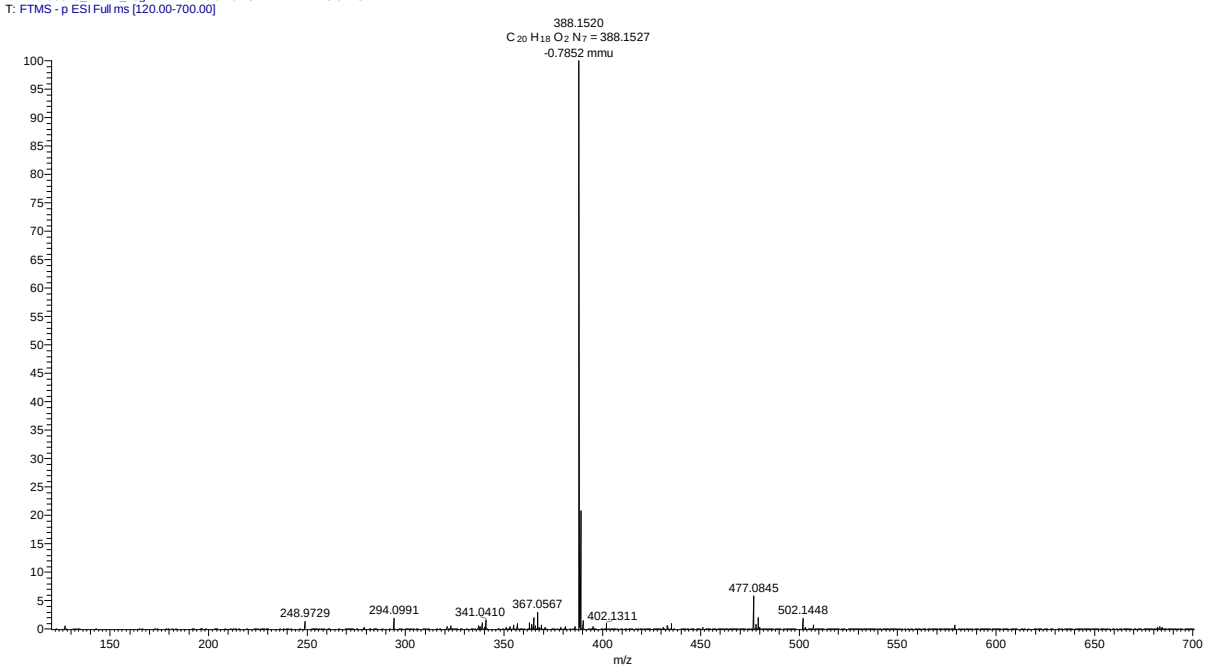

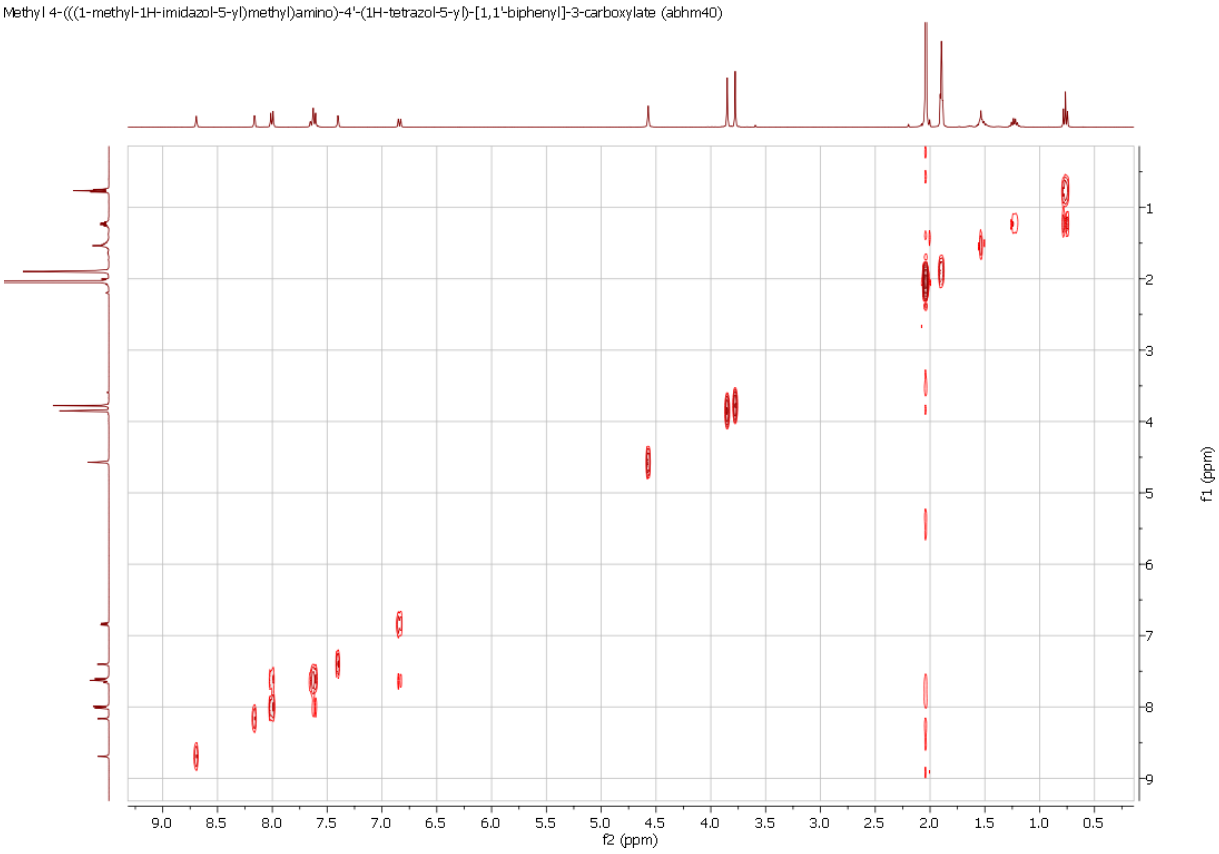
Methyl 4-(((1-methyl-1H-imidazol-5-yl)methyl)amino)-4'-(1H-tetrazol-5-yl)-[1,1'-biphenyl]-3-carboxylate (abhm40)
f2 (ppm)
f1 (ppm)

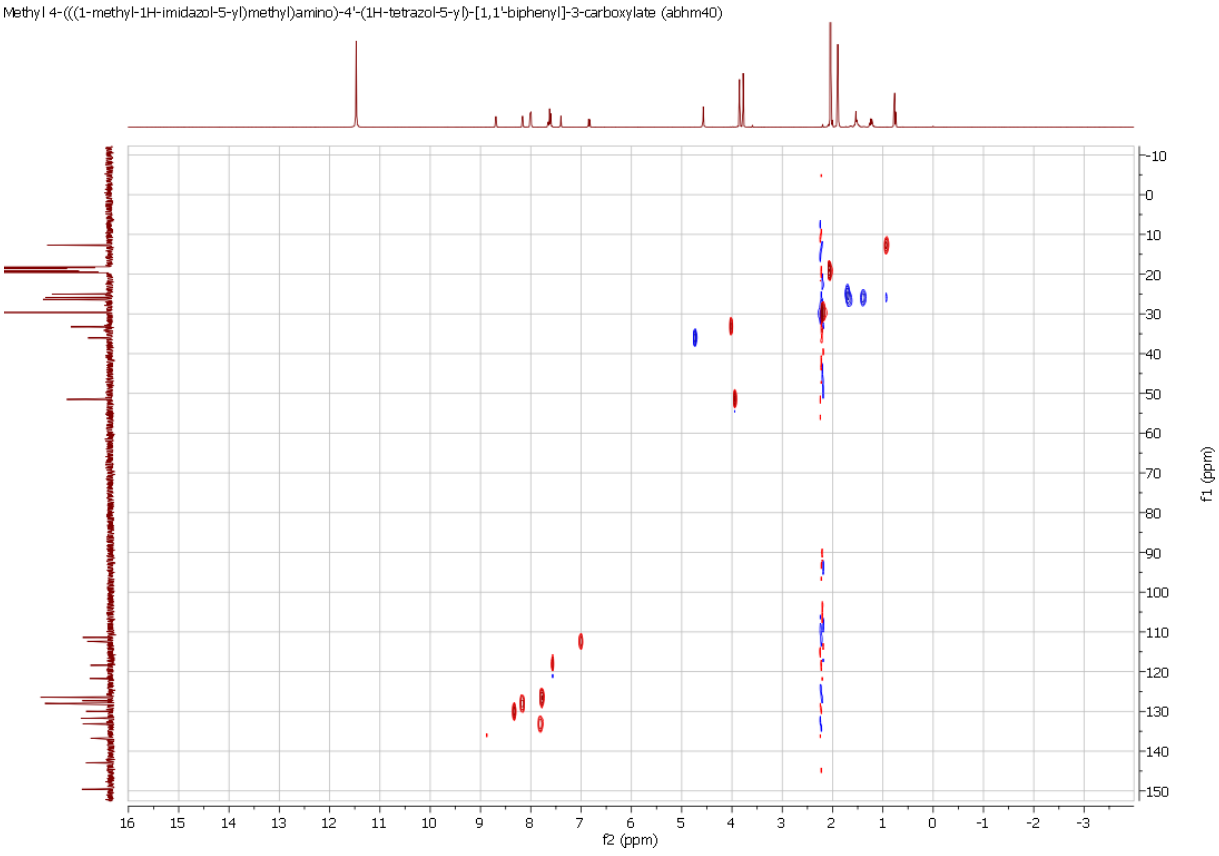
Methyl 4-(((1-methyl-1H-imidazol-5-yl)methyl)amino)-4'-(1H-tetrazol-5-yl)-[1,1'-biphenyl]-3-carboxylate (abhm40)
f2 (ppm)
f1 (ppm)

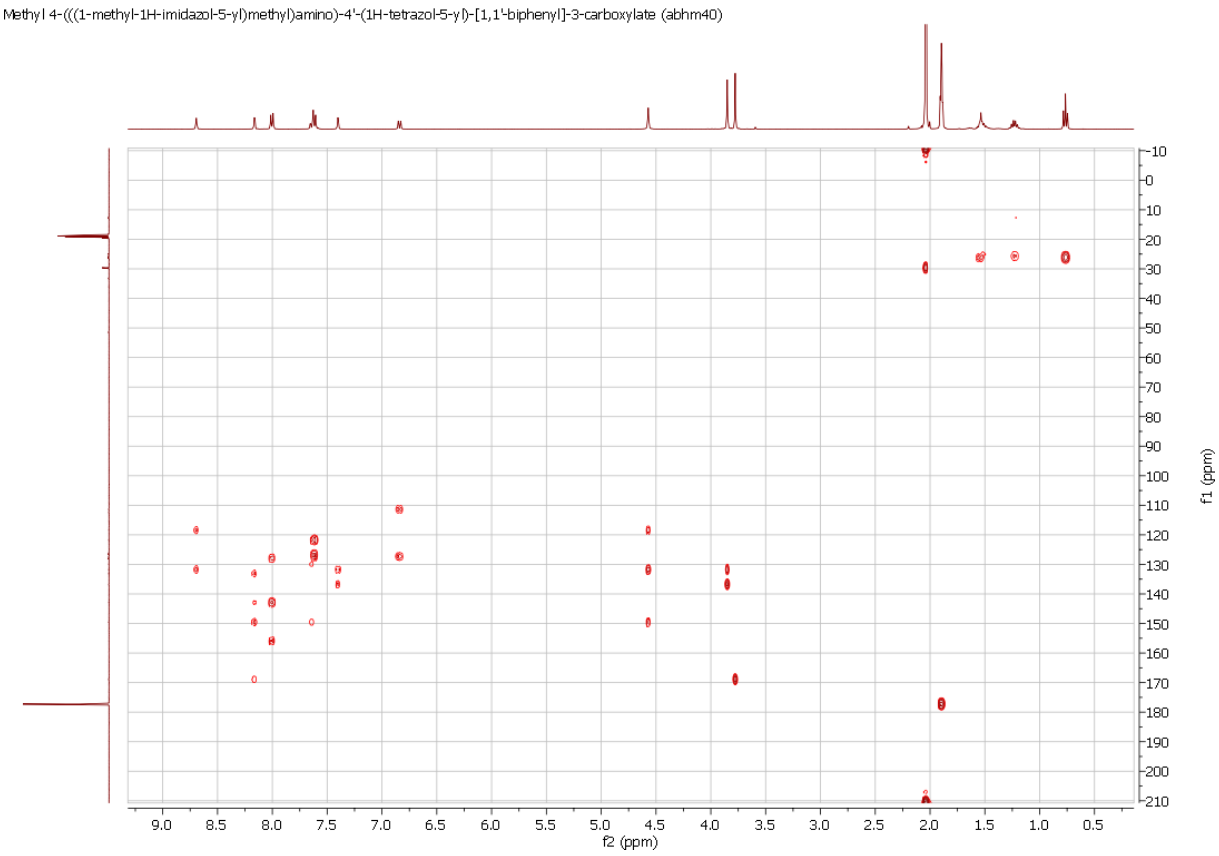
Methyl 4-(((1-methyl-1H-imidazol-5-yl)methyl)amino)-4'-(1H-tetrazol-5-yl)-[1,1'-biphenyl]-3-carboxylate (abhm40)
f2 (ppm)
f1 (ppm)

Agilent Technologies

Sample ID:	abhm100640	Method Name:	ATR-default
Sample Scans:	4	User:	IK
Background Scans:	4	Date/Time:	4/7/2020 11:08:04AM
Resolution:	8 cm-1	Range:	4,000.00 - 650.00
System Status:	Good	Apodization:	Happ-Genzel
File Location:	C:\Program Files\Agilent\MicroLab PC\Results\Rune\abhm100640_2020-04-07T11-10-21.a2r		

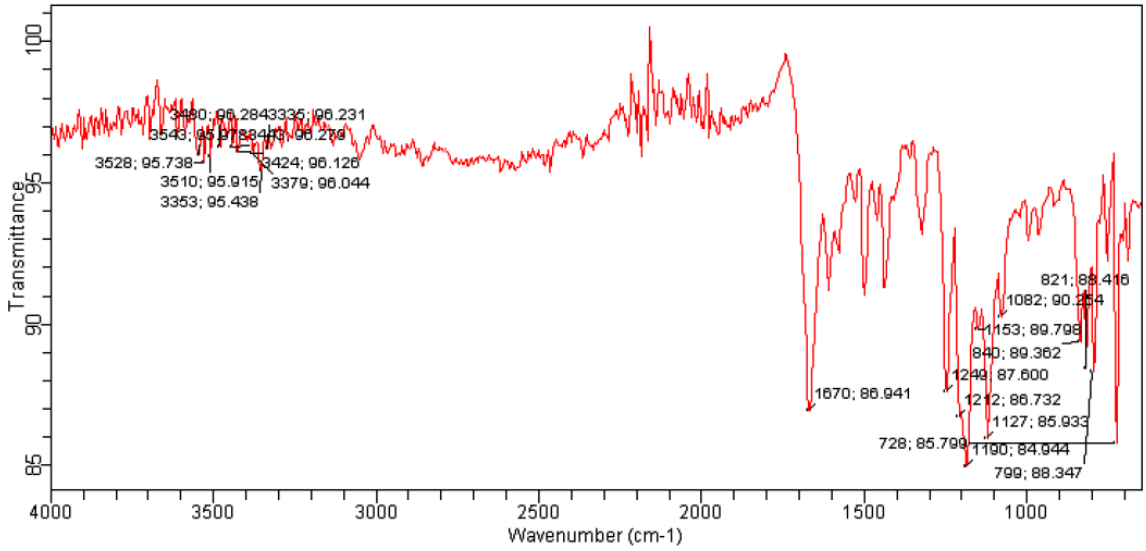

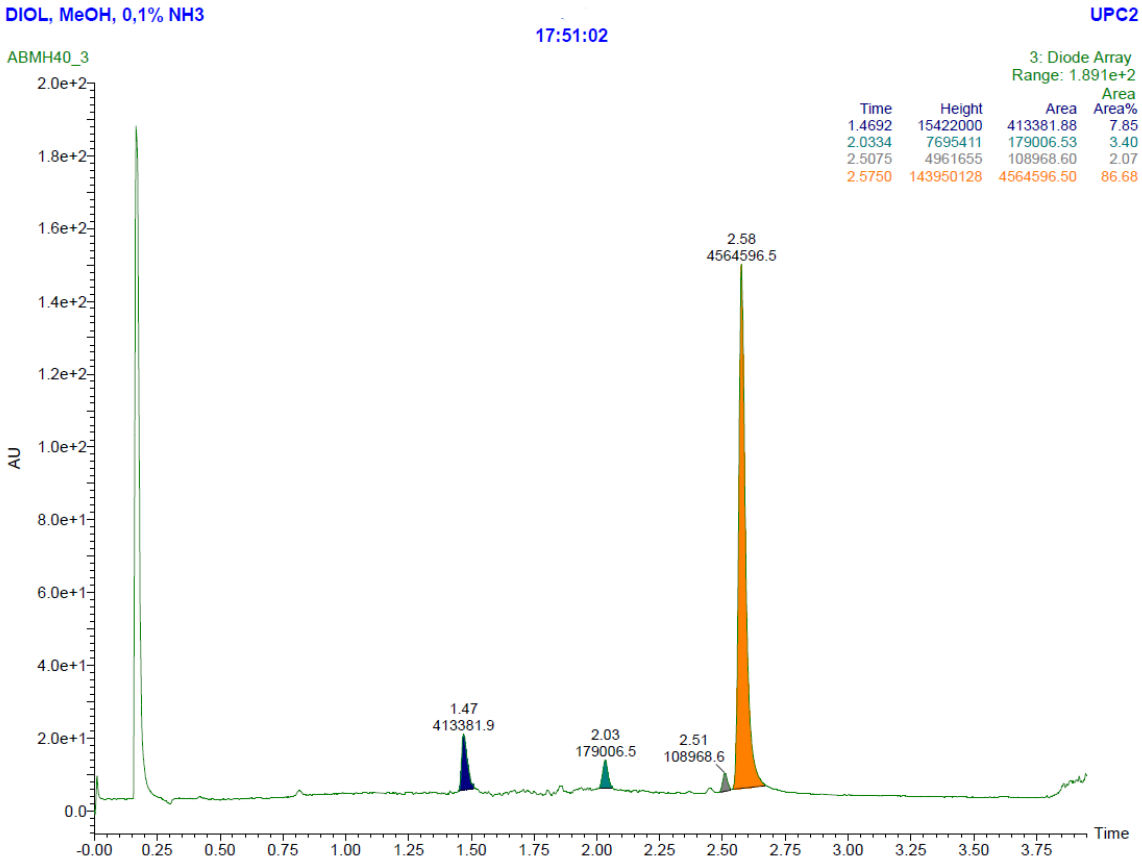
DIOL, MeOH, 0,1% NH3
17:51:02
UPC2
ABMH40_3
3: Diode Array
Range: 1.891e+2
Time Height Area Area%
1.4692 15422000 413381.88 7.85
2.0334 7695411 179006.53 3.40
2.5075 4961655 108968.60 2.07
2.5750 143950128 4564596.50 86.68
2.58
4564596.5
1.47
413381.9
2.03
179006.5
2.51
108968.6
AU
Time

9.3.4 Methyl 4'-(1*H*-tetrazol-5-yl)-4-((thiophen-2-ylmethyl)amino)-[1,1'-biphenyl]-3-carboxylate (28)

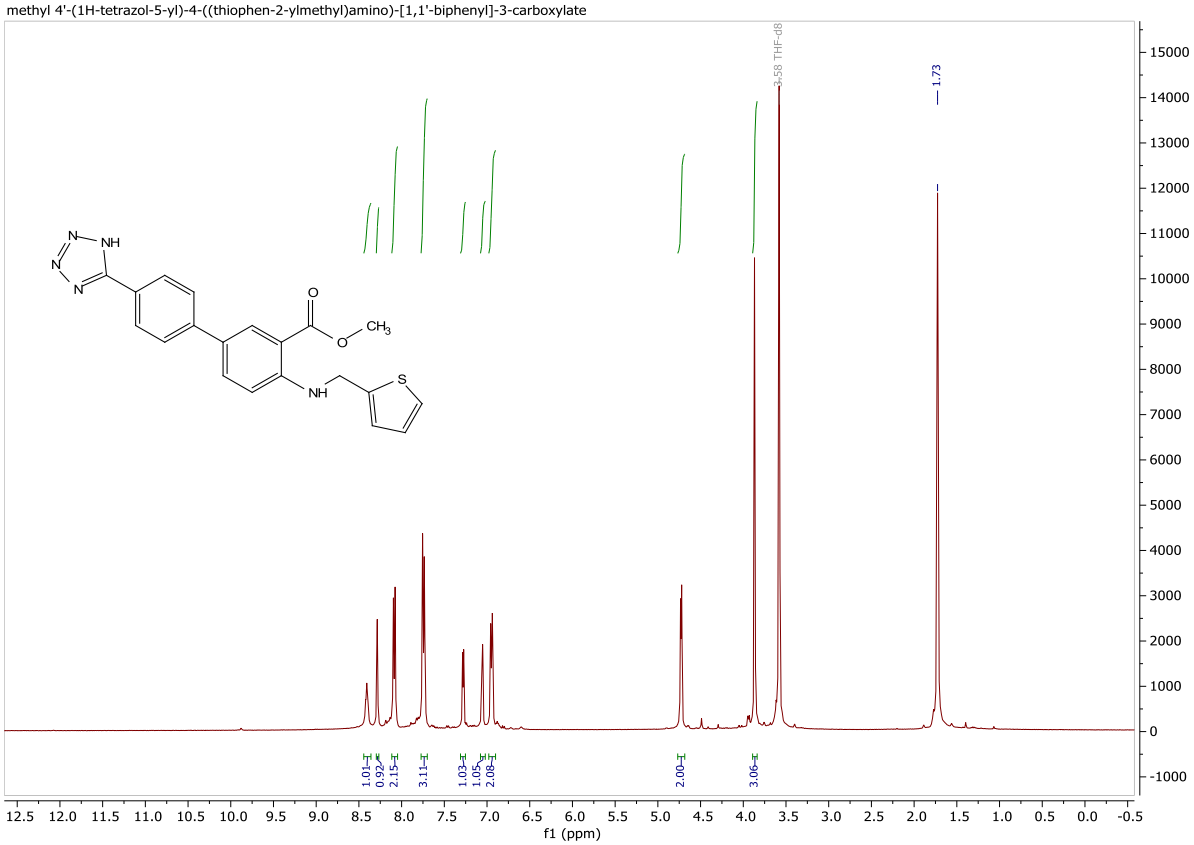

methyl 4'-(1H-tetrazol-5-yl)-4-((thiophen-2-ylmethyl)amino)-[1,1'-biphenyl]-3-carboxylate

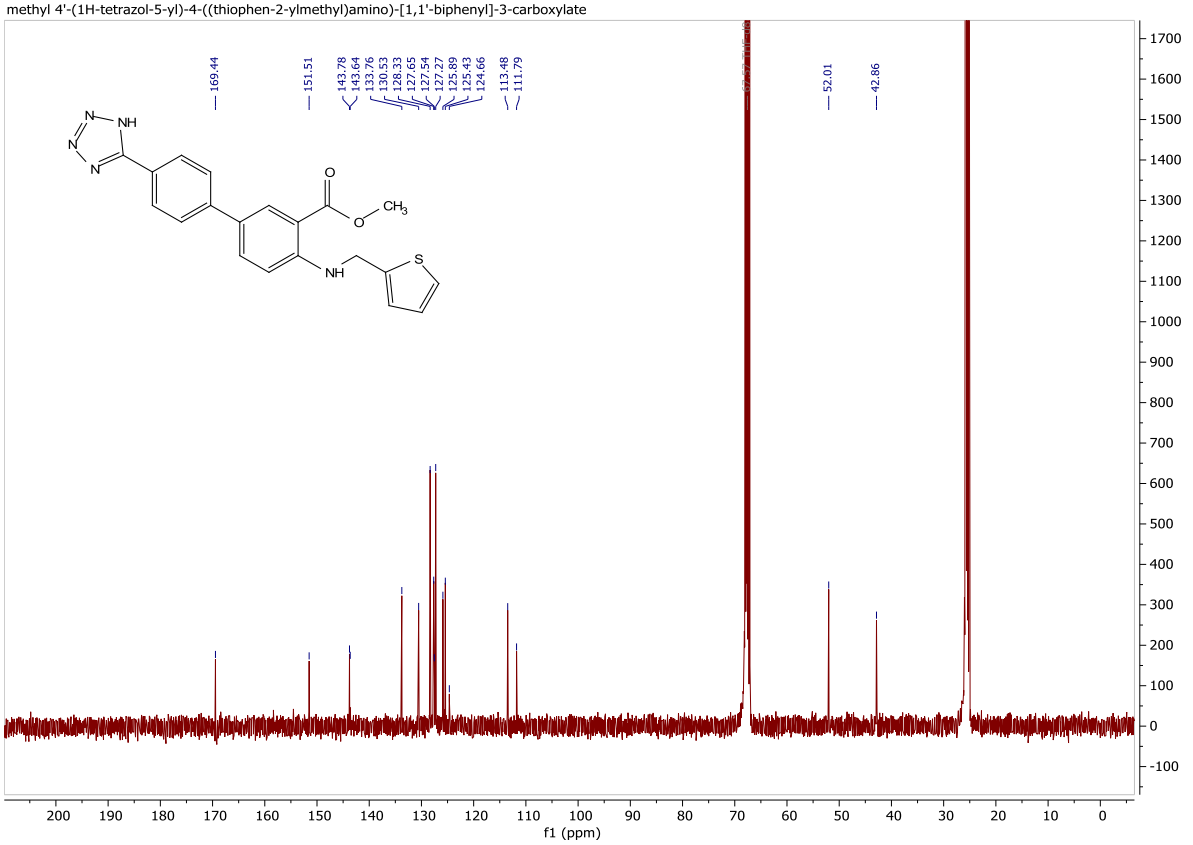

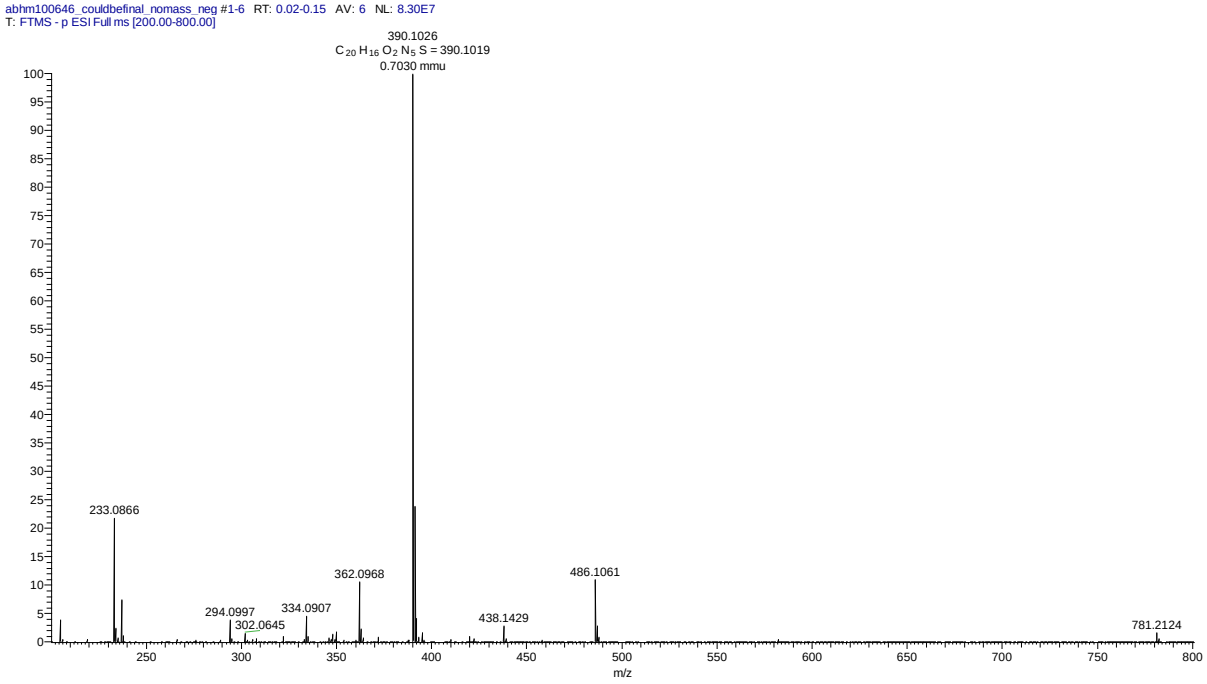

Agilent Technologies

Sample ID:	abhm100646	Method Name:	ATR-default
Sample Scans:	4	User:	IK
Background Scans:	4	Date/Time:	4/7/2020 10:52:27AM
Resolution:	8 cm-1	Range:	4,000.00 - 650.00
System Status:	Good	Apodization:	Happ-Genzel
File Location:	C:\Program Files\Agilent\MicroLab PC\Results\Rune\abhm100646_2020-04-07T10-53-43.a2r		

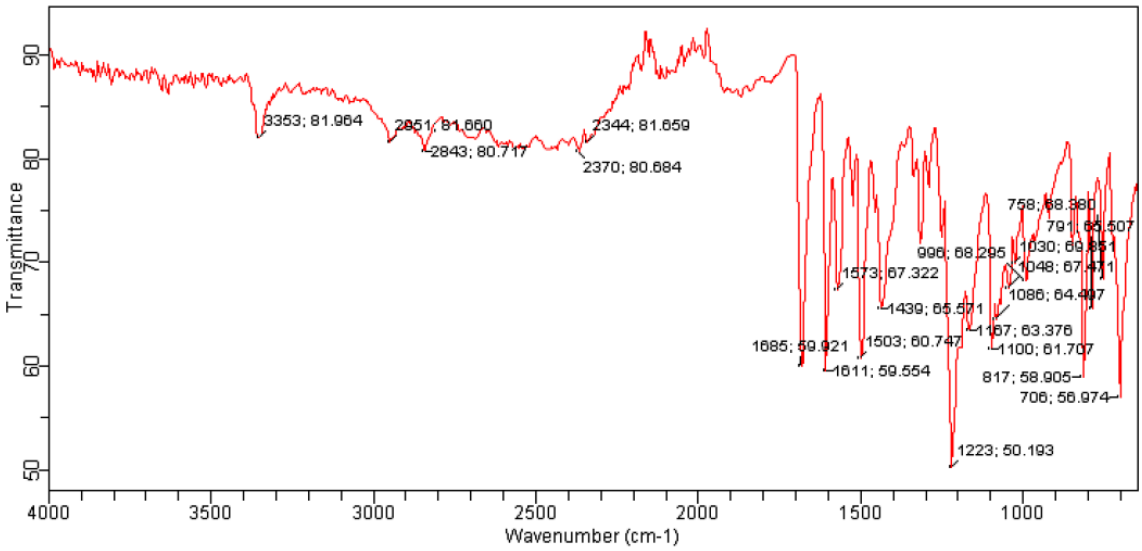

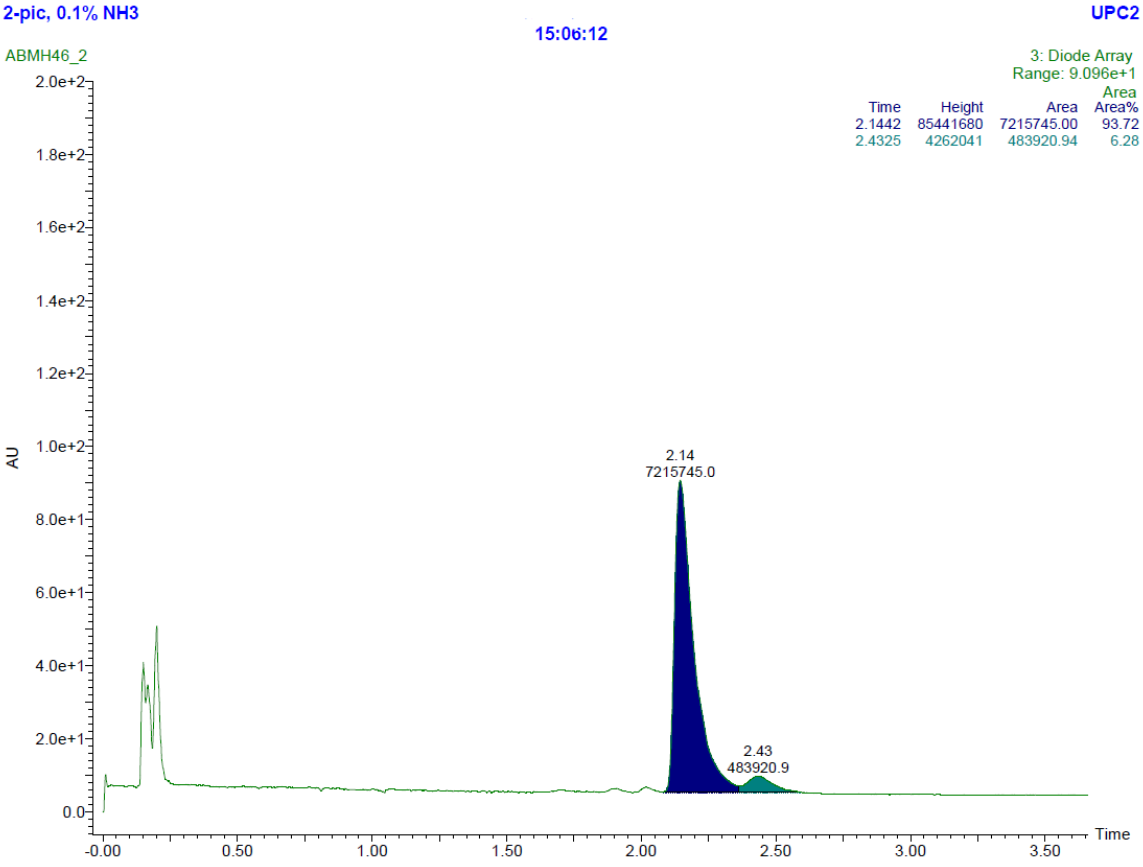
2-pic, 0.1% NH3
15:06:12
UPC2
ABMH46_2
3: Diode Array
Range: 9.096e+1
Time Height Area Area%
2.1442 85441680 7215745.00 93.72
2.4325 4262041 483920.94 6.28
2.14
7215745.0
2.43
483920.9
AU
Time
2.0e+2
1.8e+2
1.6e+2
1.4e+2
1.2e+2
1.0e+2
8.0e+1
6.0e+1
4.0e+1
2.0e+1
0.0
-0.00
0.50
1.00
1.50
2.00
2.50
3.00
3.50

9.3.5 Methyl 4-((3-methoxybenzyl)amino)-4'-(1*H*-tetrazol-5-yl)-[1,1'-biphenyl]-3-carboxylate (29)

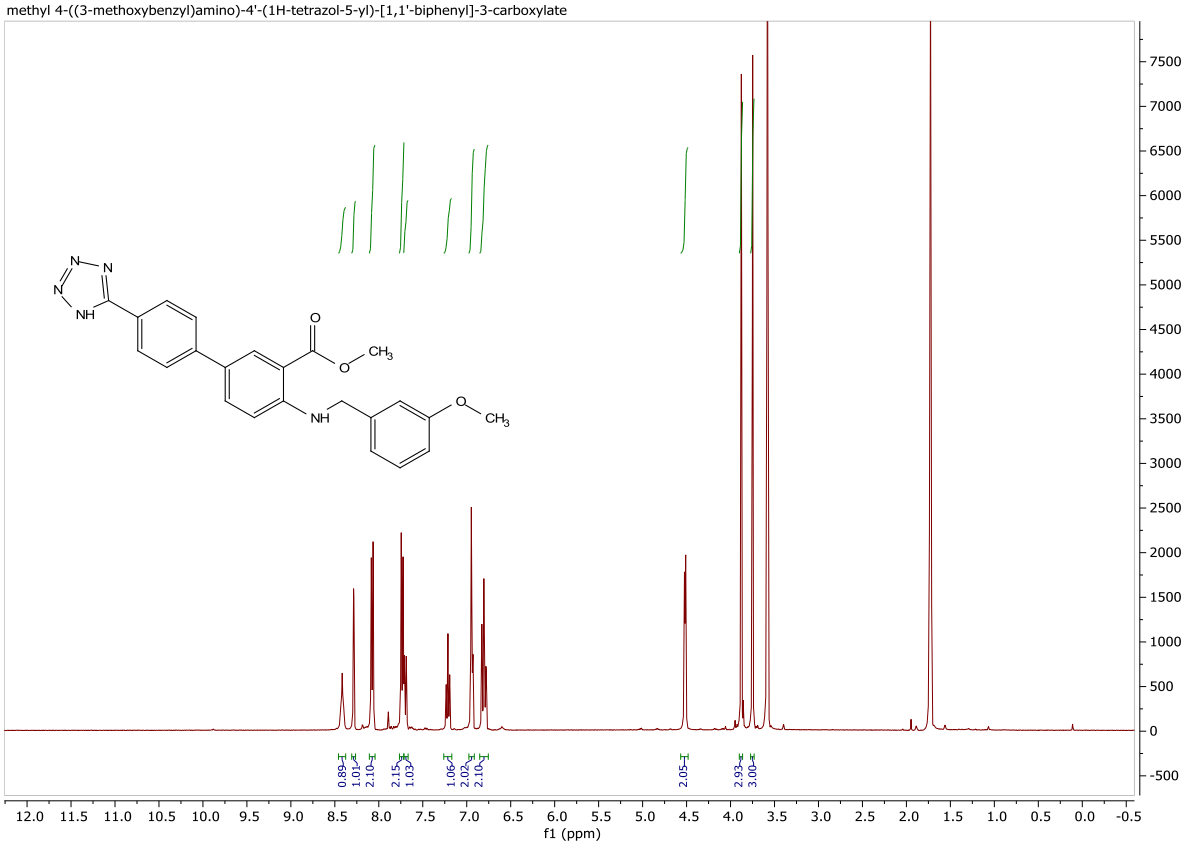

methyl 4-((3-methoxybenzyl)amino)-4'-(1H-tetrazol-5-yl)-[1,1'-biphenyl]-3-carboxylate

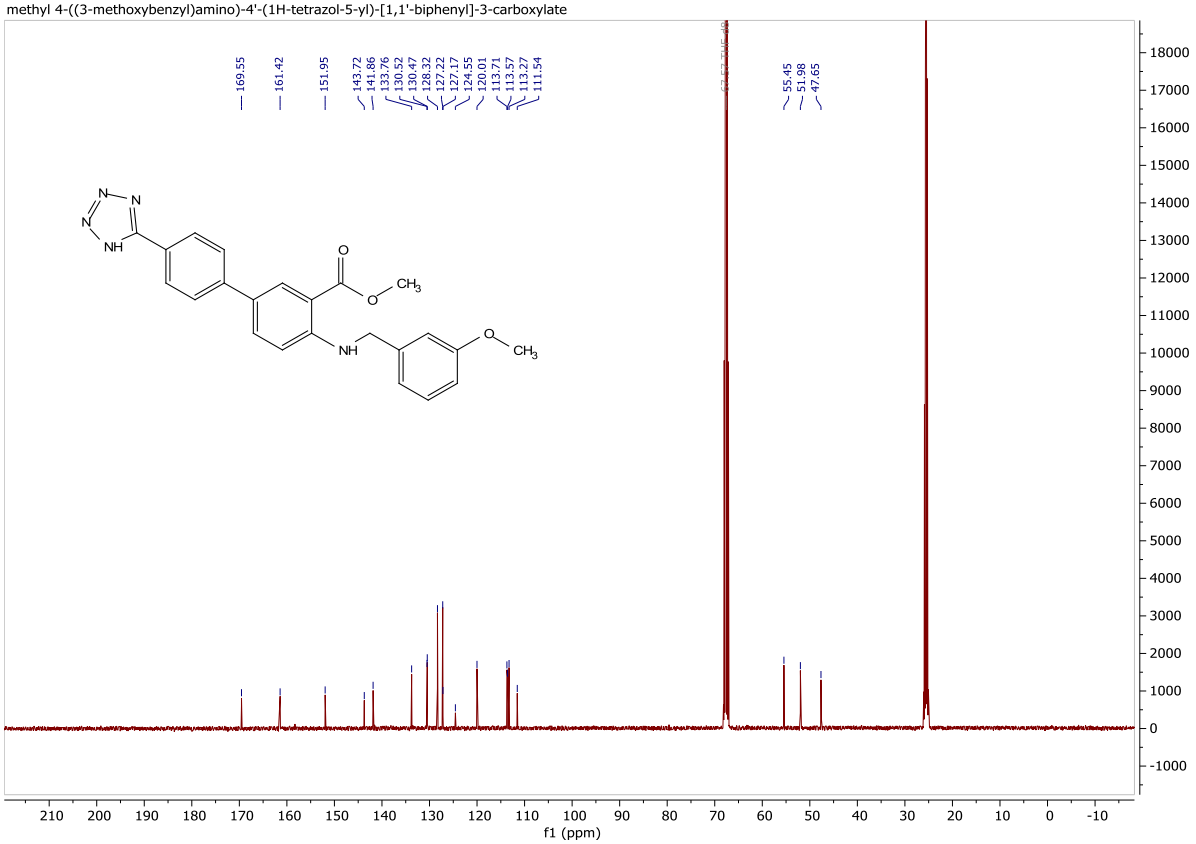

abhm100647_aqphase_final_neg #1-9 RT: 0.01-0.25 AV: 9 NL: 1.62E6
T: FTMS - p ESI Full ms [120.00-800.00]

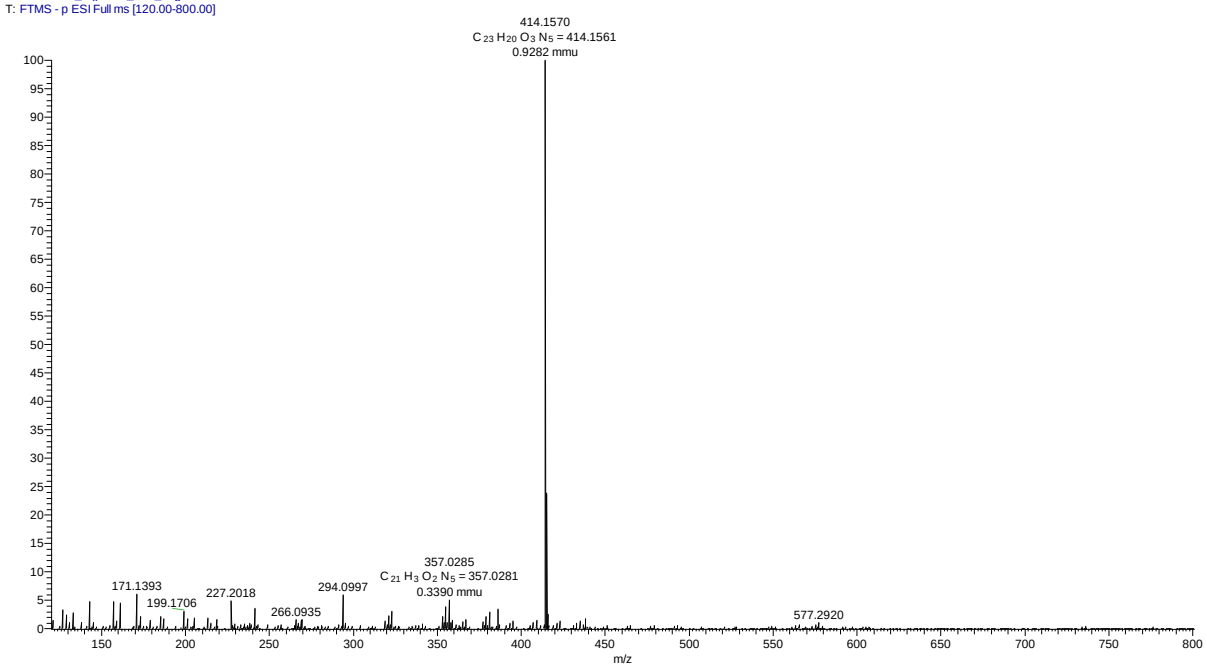

Agilent Technologies

Sample ID:	abhm100647	Method Name:	ATR-default
Sample Scans:	4	User:	IK
Background Scans:	4	Date/Time:	4/7/2020 10:55:45AM
Resolution:	8 cm-1	Range:	4,000.00 - 650.00
System Status:	Good	Apodization:	Happ-Genzel
File Location:	C:\Program Files\Agilent\MicroLab PC\Results\Rune\abhm100647_2020-04-07T11-00-08.a2r		

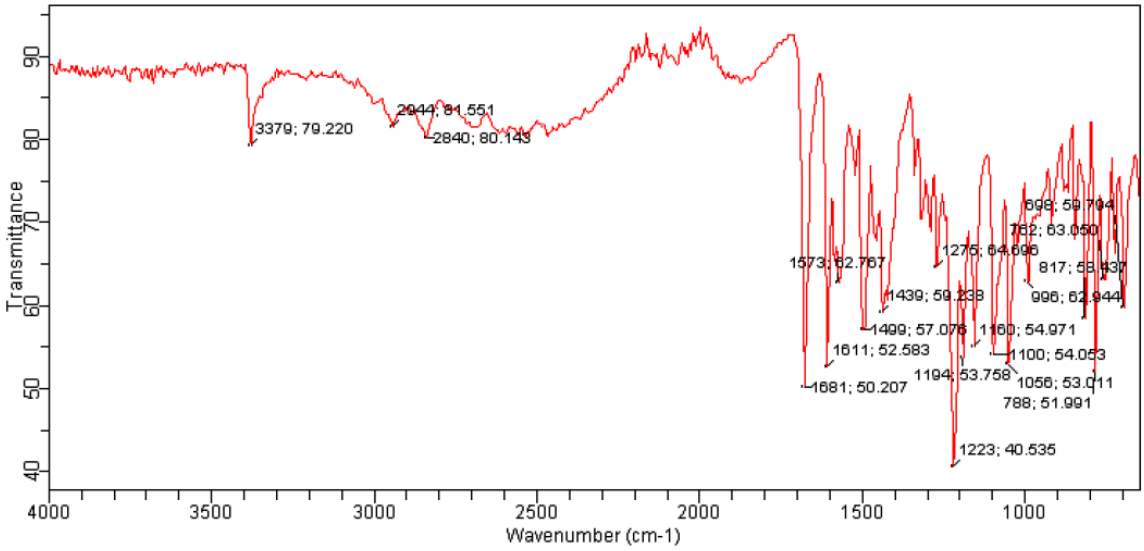

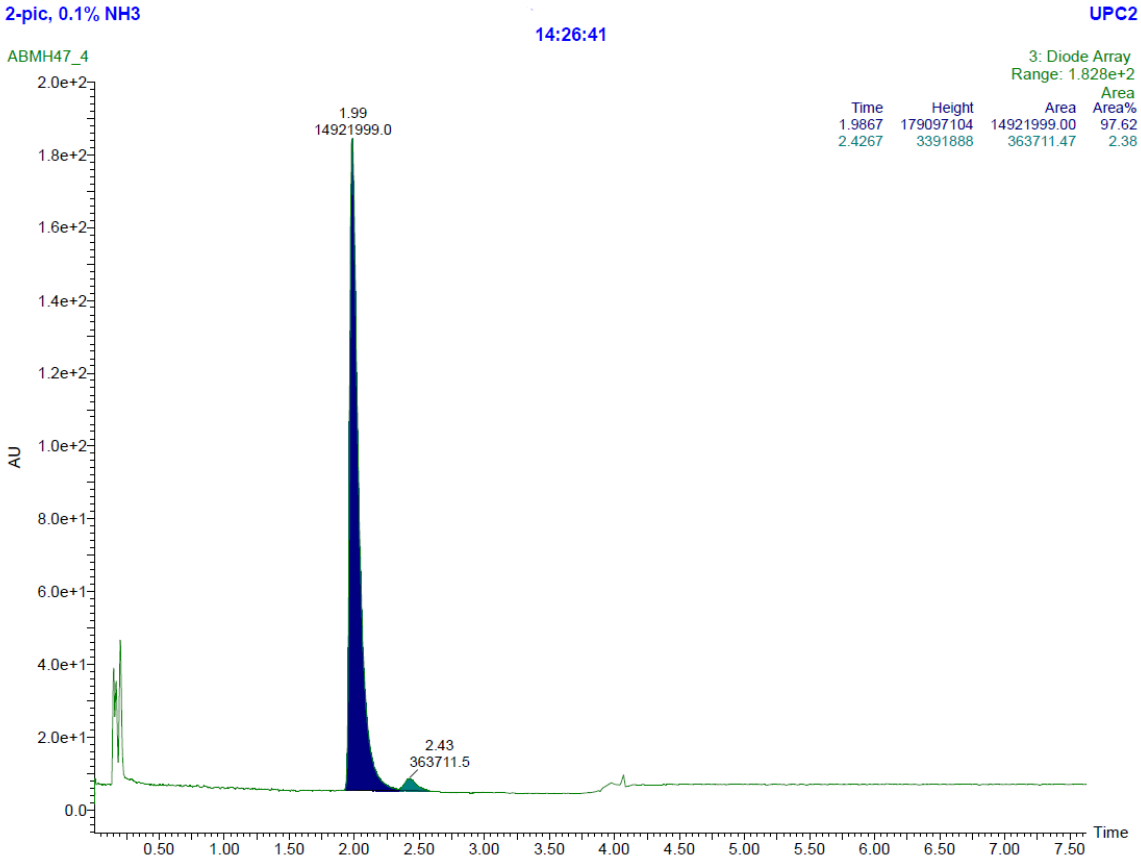
2-pic, 0.1% NH3
14:26:41
UPC2
ABMH47_4
3: Diode Array
Range: 1.828e+2
Time Height Area Area%
1.9867 179097104 14921999.00 97.62
2.4267 3391888 363711.47 2.38
1.99
14921999.0
2.43
363711.5
AU
Time
2.0e+2
1.8e+2
1.6e+2
1.4e+2
1.2e+2
1.0e+2
8.0e+1
6.0e+1
4.0e+1
2.0e+1
0.0
0.50 1.00 1.50 2.00 2.50 3.00 3.50 4.00 4.50 5.00 5.50 6.00 6.50 7.00 7.50

9.4 Hydrolysis Spectra

9.4.1 4-amino-4'-cyano-[1,1'-biphenyl]-3-carboxylic acid (35)

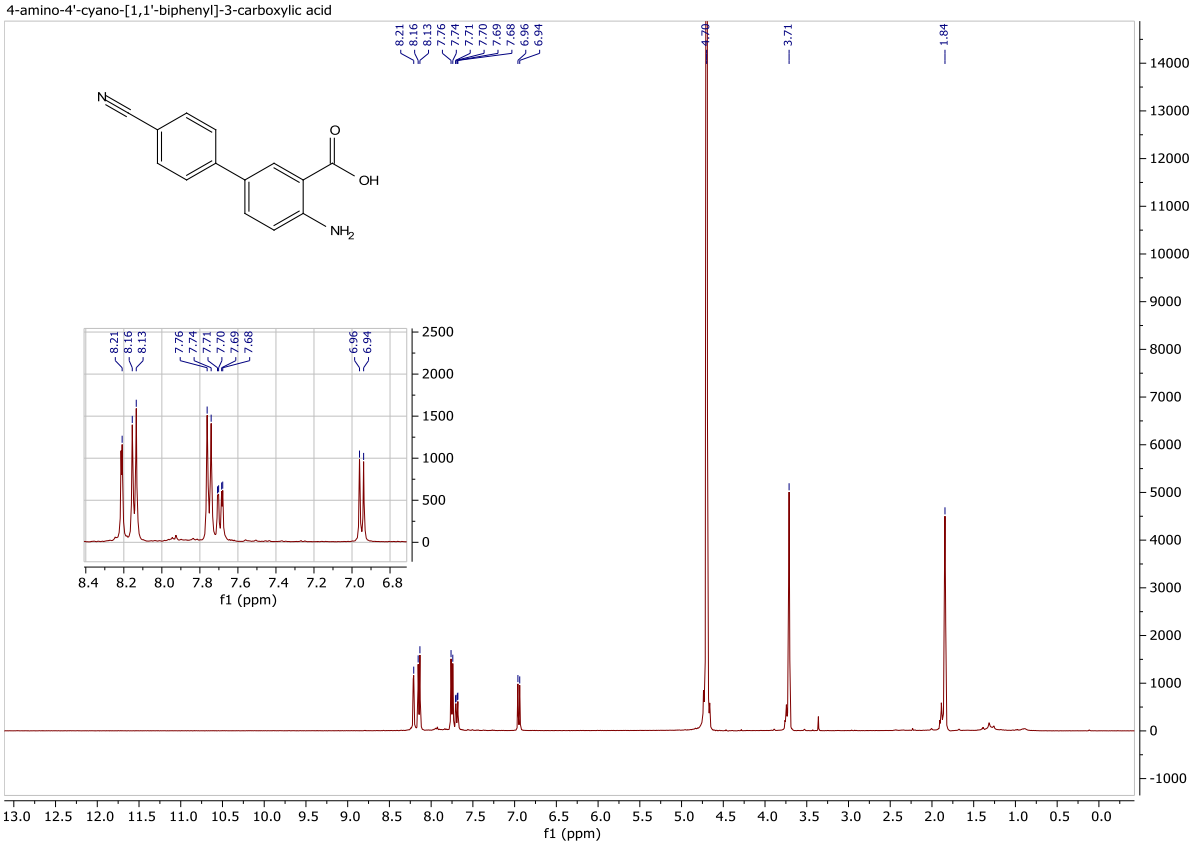

4-amino-4'-cyano-[1,1'-biphenyl]-3-carboxylic acid

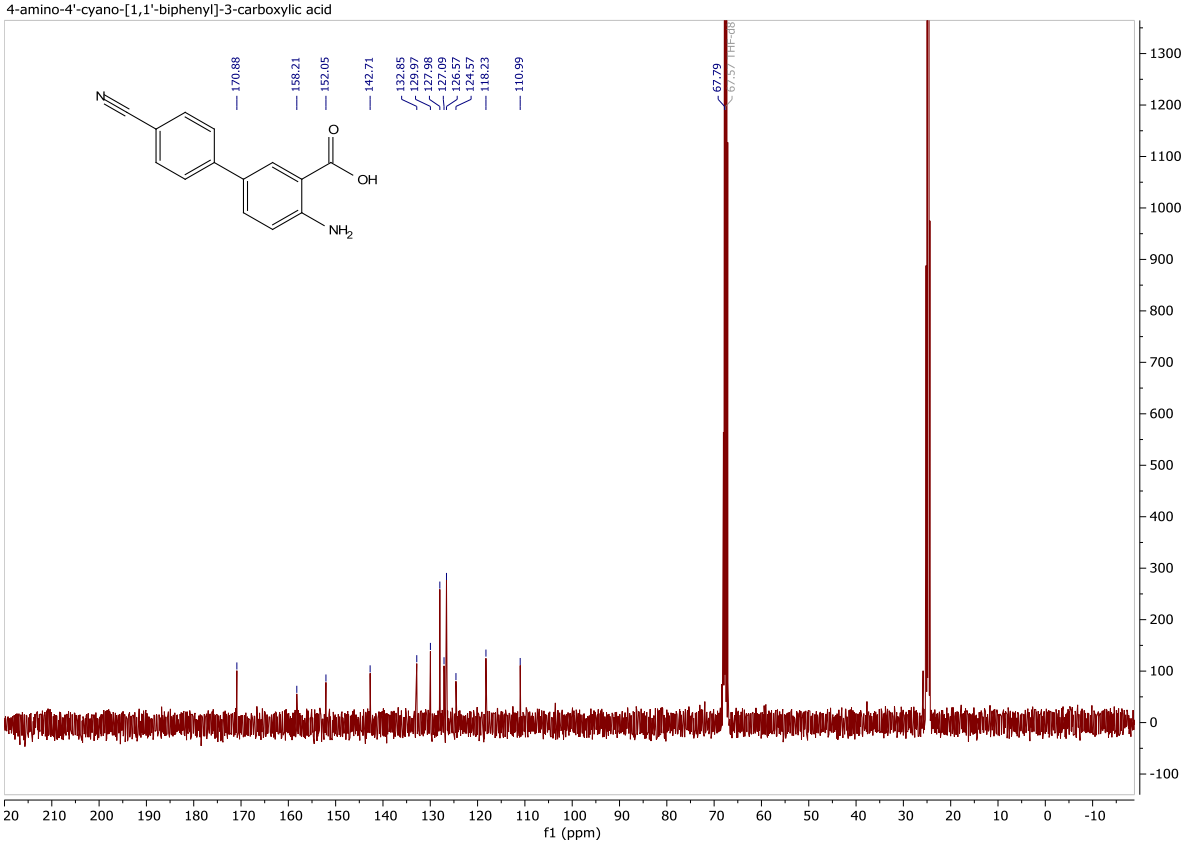

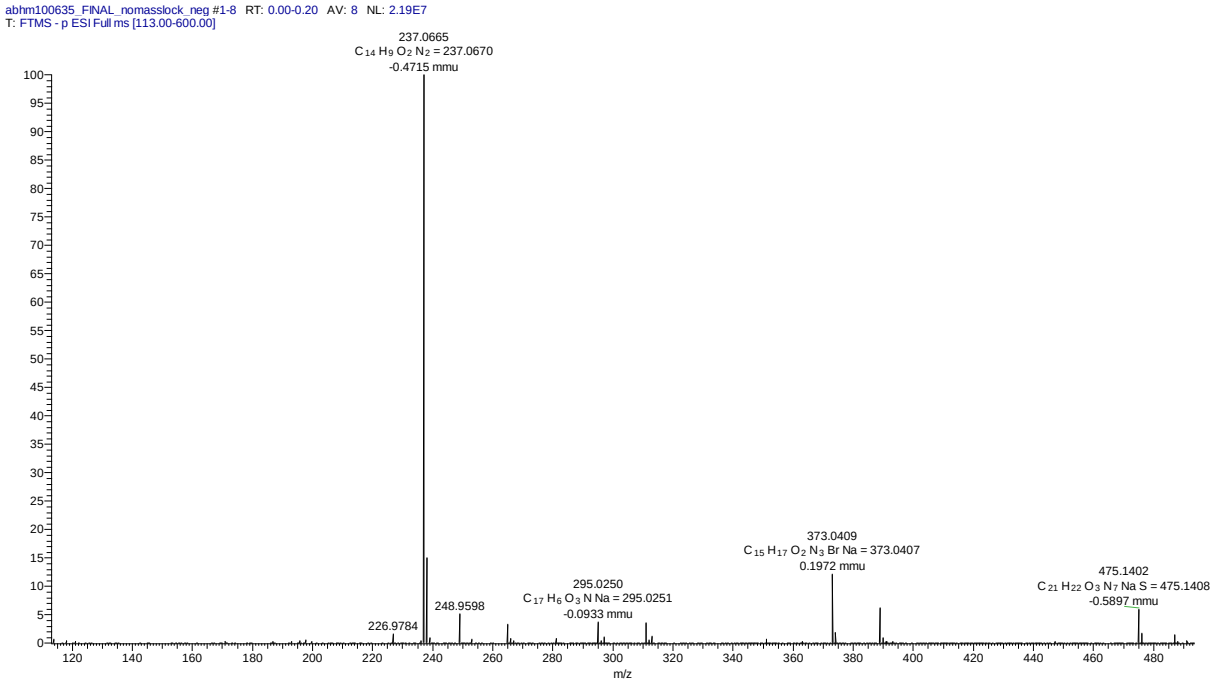

Agilent Technologies

Sample ID:	abhm100635	Method Name:	ATR-default
Sample Scans:	4	User:	IK
Background Scans:	4	Date/Time:	4/7/2020 10:28:20AM
Resolution:	8 cm-1	Range:	4,000.00 - 650.00
System Status:	Good	Apodization:	Happ-Genzel
File Location:	C:\Program Files\Agilent\MicroLab PC\Results\Rune\abhm100635_2020-04-07T10-30-29.a2r		

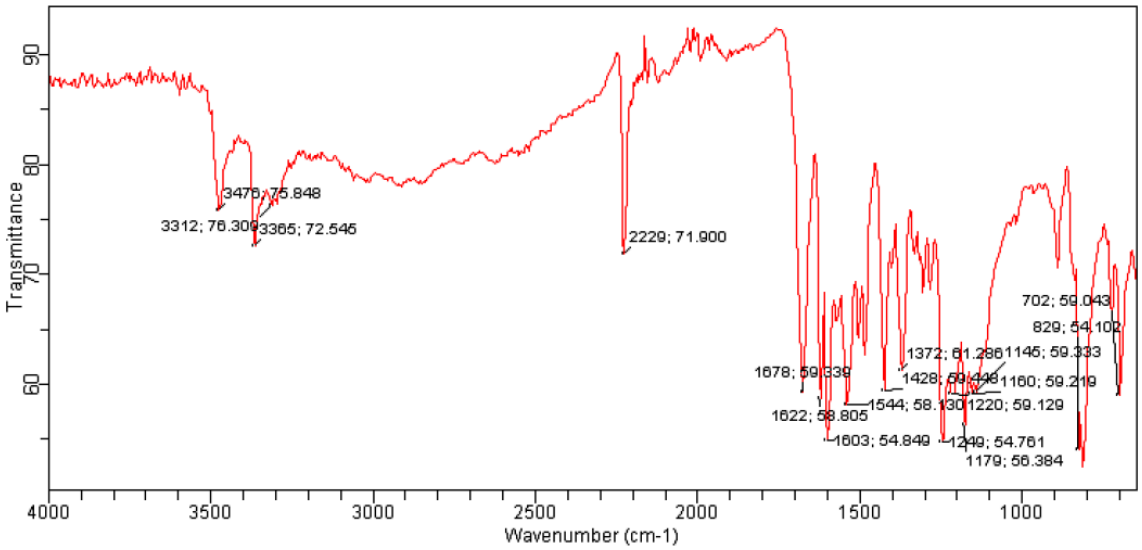

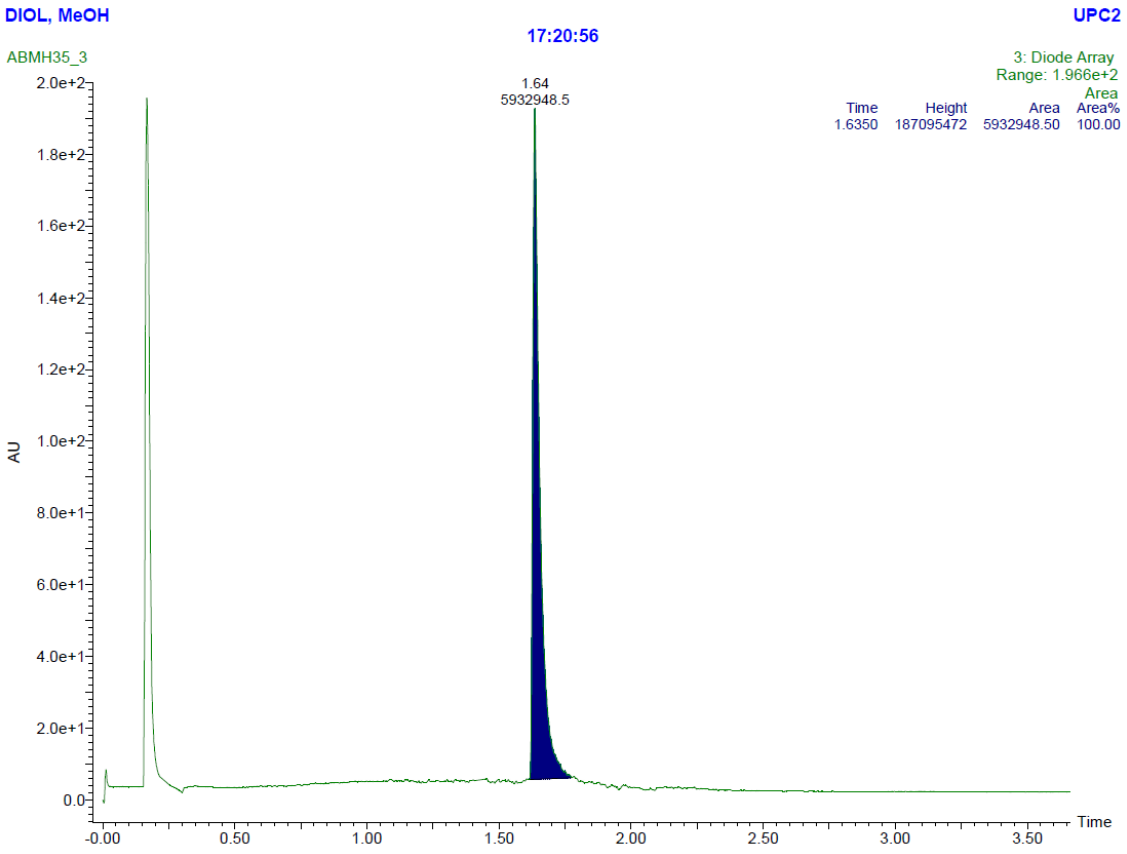

Waters UPC, SFC system, deviating from standard gradient:

	Time (min)	Flow (mL/min)	% A	%B
1	Initial	1.000	98.0	2.0
2	2.00-3.50	1.000	60.0	40.0
4	3.70-4.50	1.000	98.0	2.0

A: CO_2 B: 0.1% NH_3 in MeOH.

9.4.2 4-amino-4'-(1*H*-tetrazol-5-yl)-[1,1'-biphenyl]-3-carboxylic acid (34)

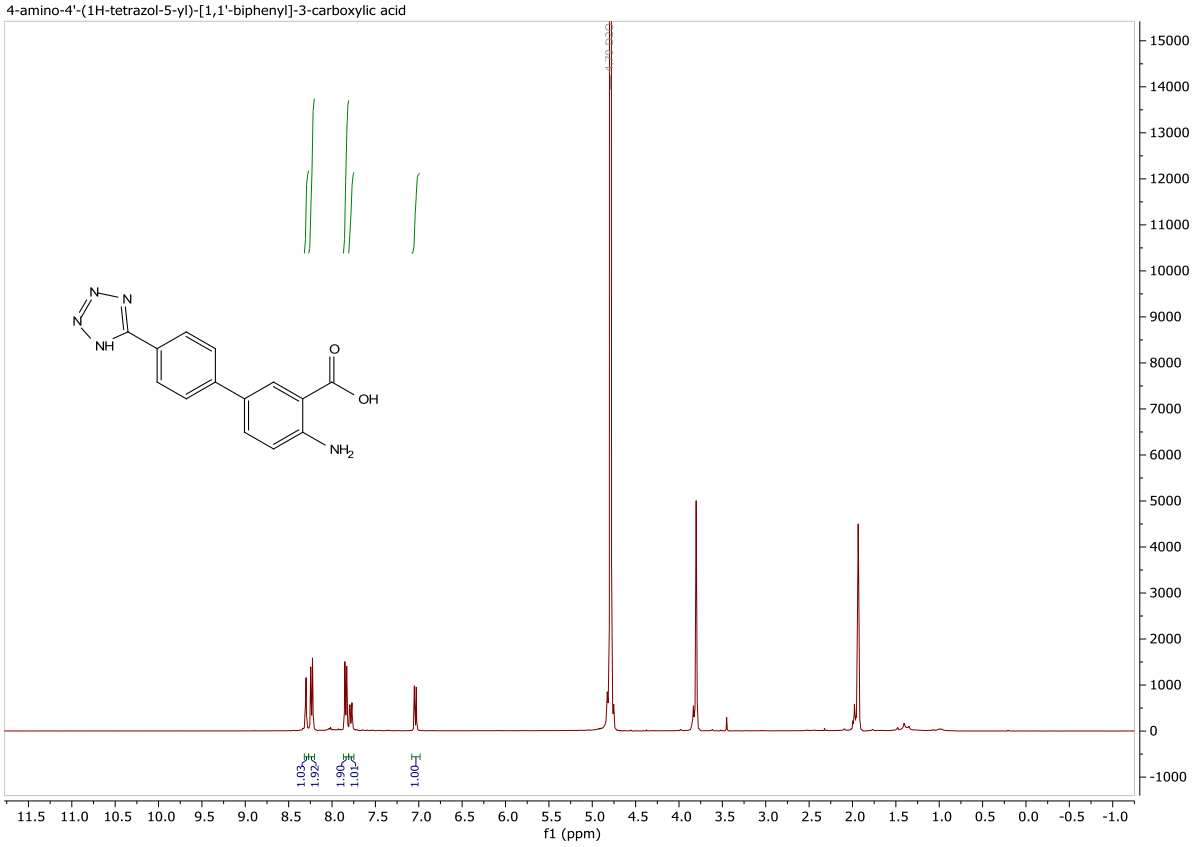

4-amino-4'-(1H-tetrazol-5-yl)-[1,1'-biphenyl]-3-carboxylic acid

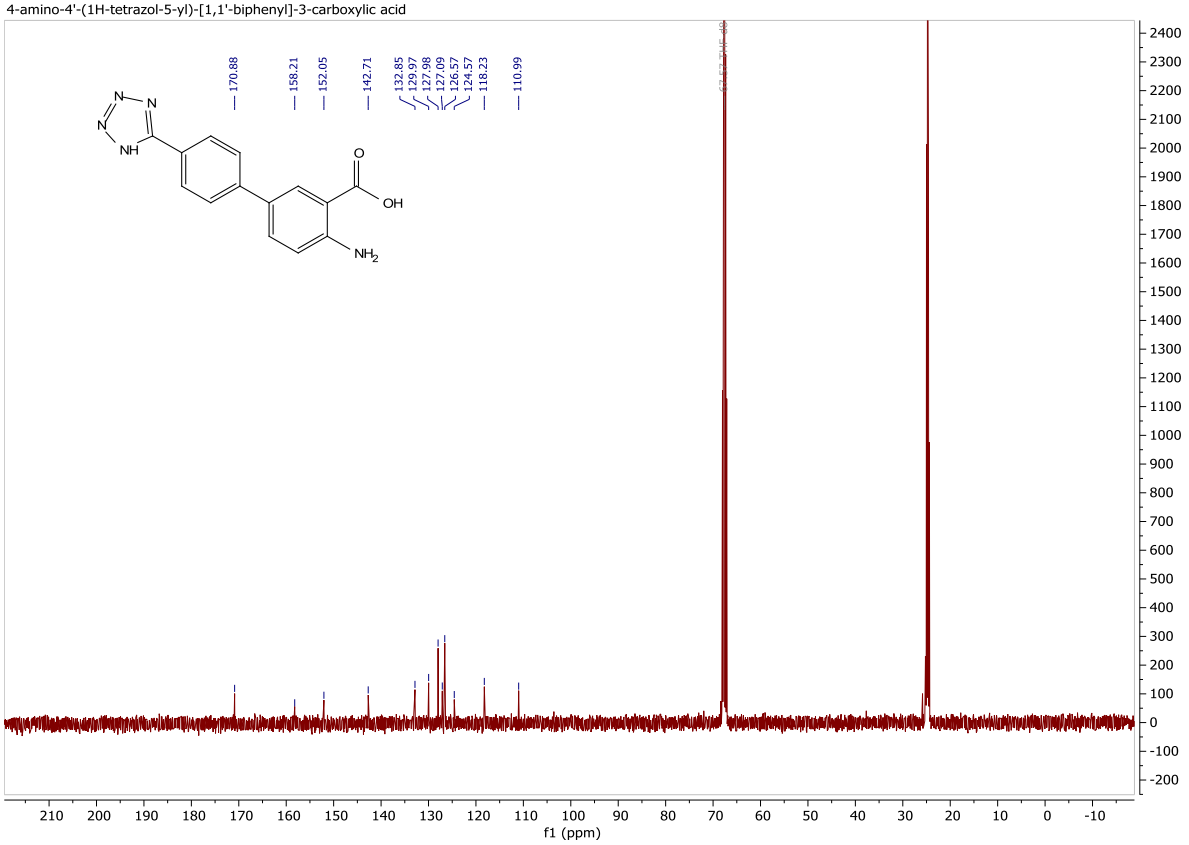

abhm100606HACTUALfinal_neg #1-10 RT: 0.01-0.24 AV: 10 NL: 1.13E6
T: FTMS - p ESI Full ms [100.00-500.00]

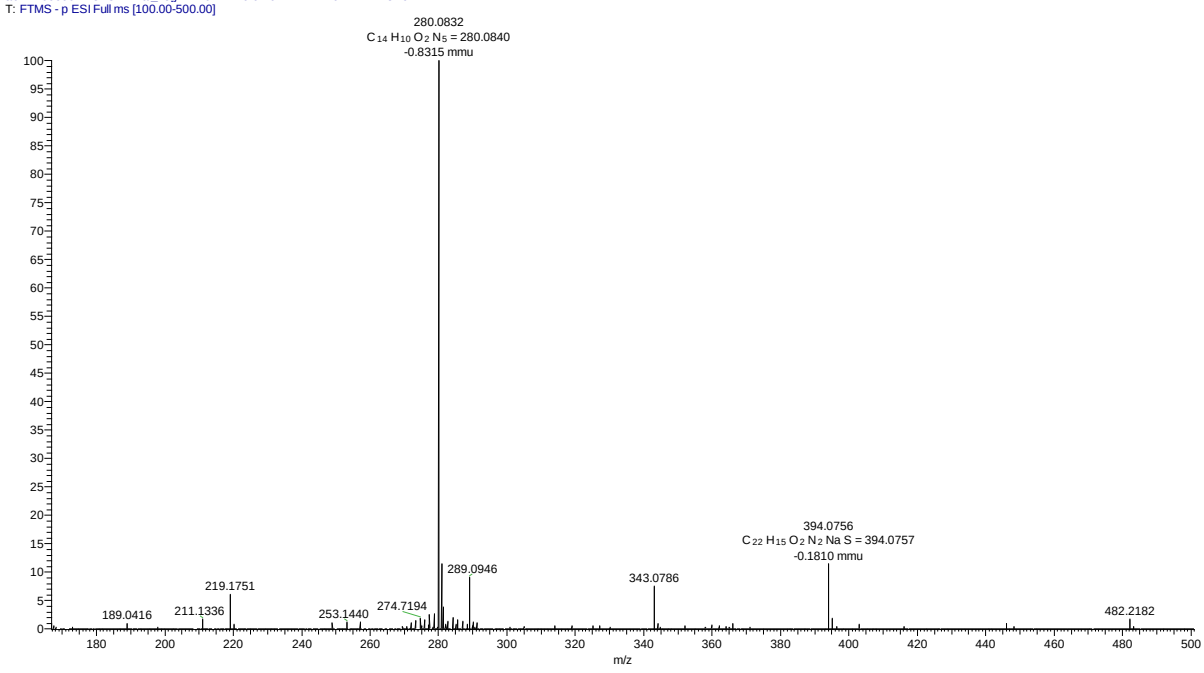

Agilent Technologies

Sample ID:	abhm100606hydrolyzed	Method Name:	ATR-default
Sample Scans:	4	User:	IK
Background Scans:	4	Date/Time:	4/7/2020 10:46:08AM
Resolution:	8 cm-1	Range:	4,000.00 - 650.00
System Status:	Good	Apodization:	Happ-Genzel
File Location:	C:\Program Files\Agilent\MicroLab PC\Results\Rune\abhm100606hydrolyzed_2020-04-07T10-47-44.a2r		

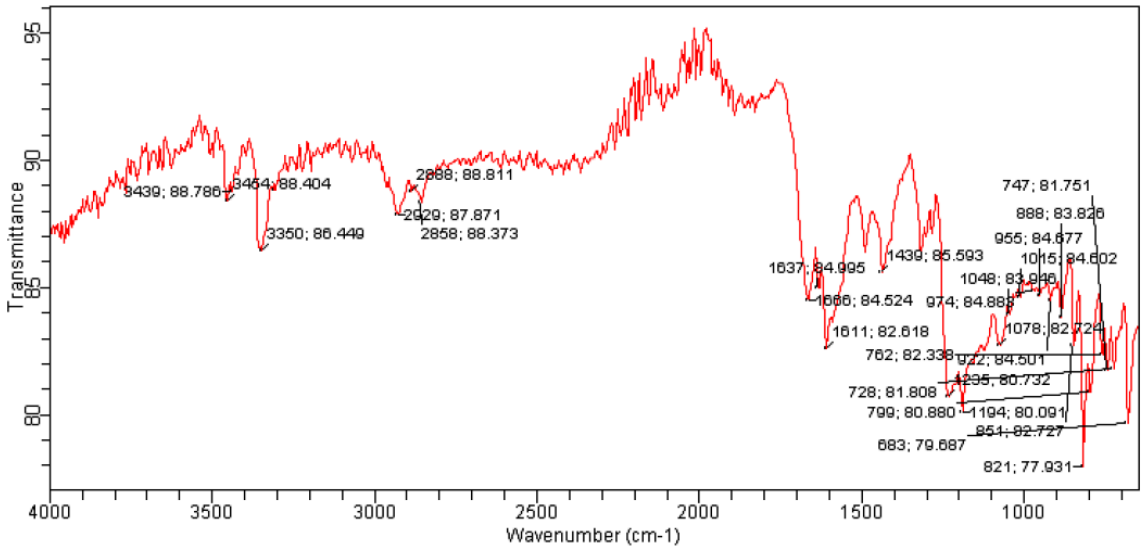

9.4.3 4-(benzylamino)-4'-(1*H*-tetrazol-5-yl)-[1,1'-biphenyl]-3-carboxylic acid (33)

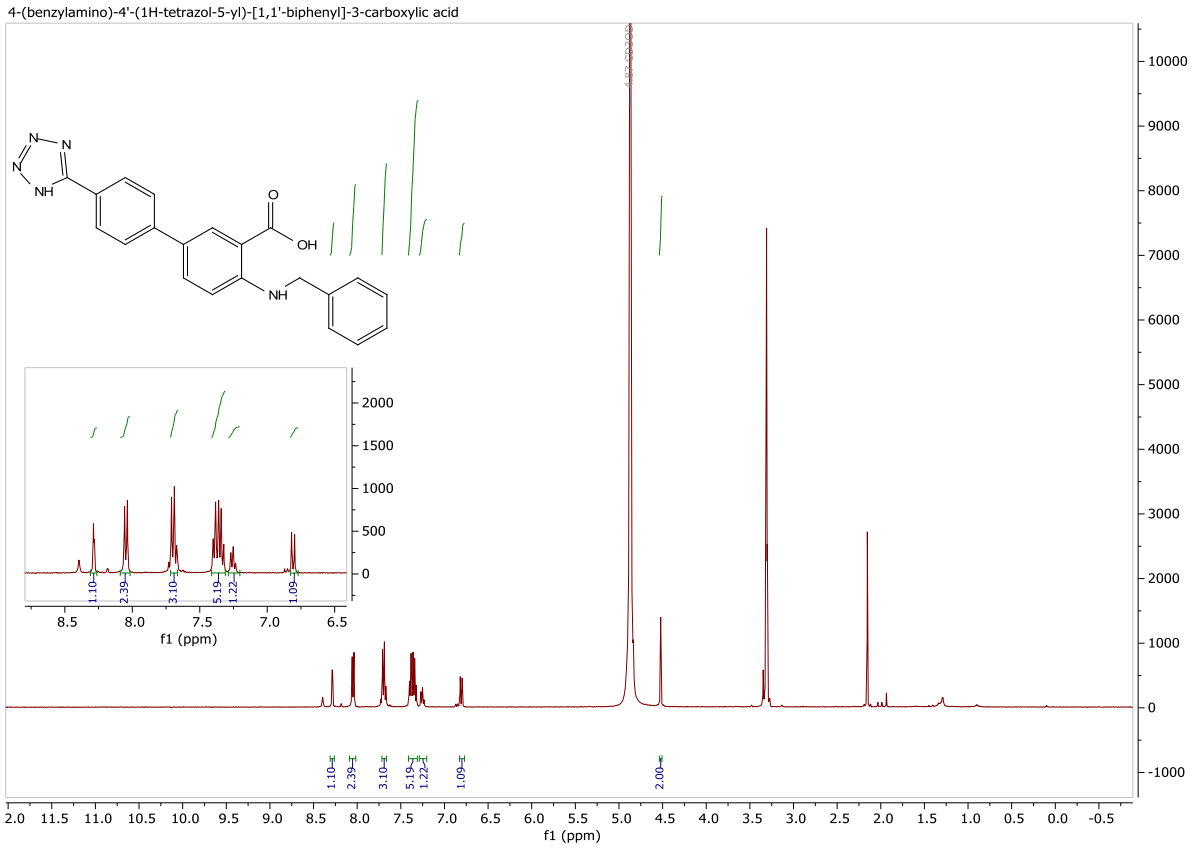

4-(benzylamino)-4'-(1H-tetrazol-5-yl)-[1,1'-biphenyl]-3-carboxylic acid

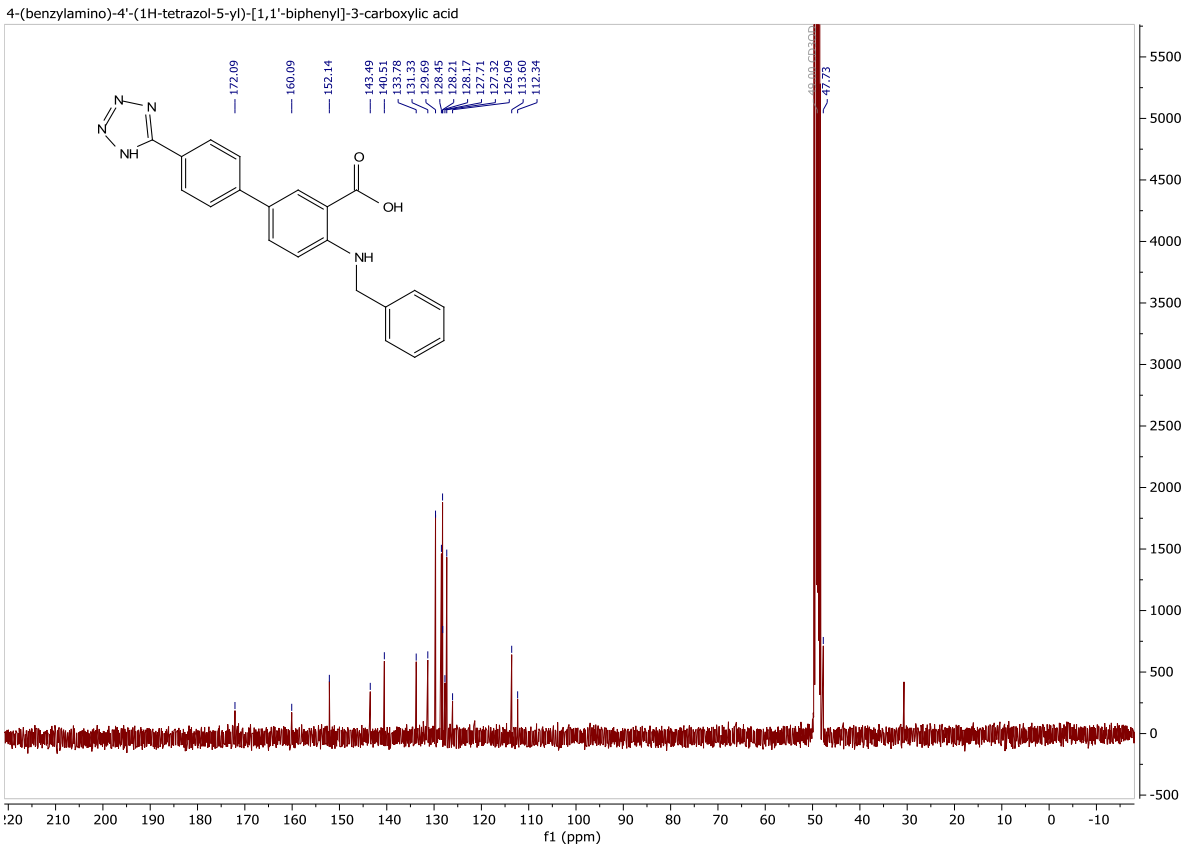

ABHM100630muligfinal_neg #1-6 RT: 0.01-0.15 AV: 6 NL: 2.17E6
T: FTMS - p ESI Full ms [100.00-800.00]

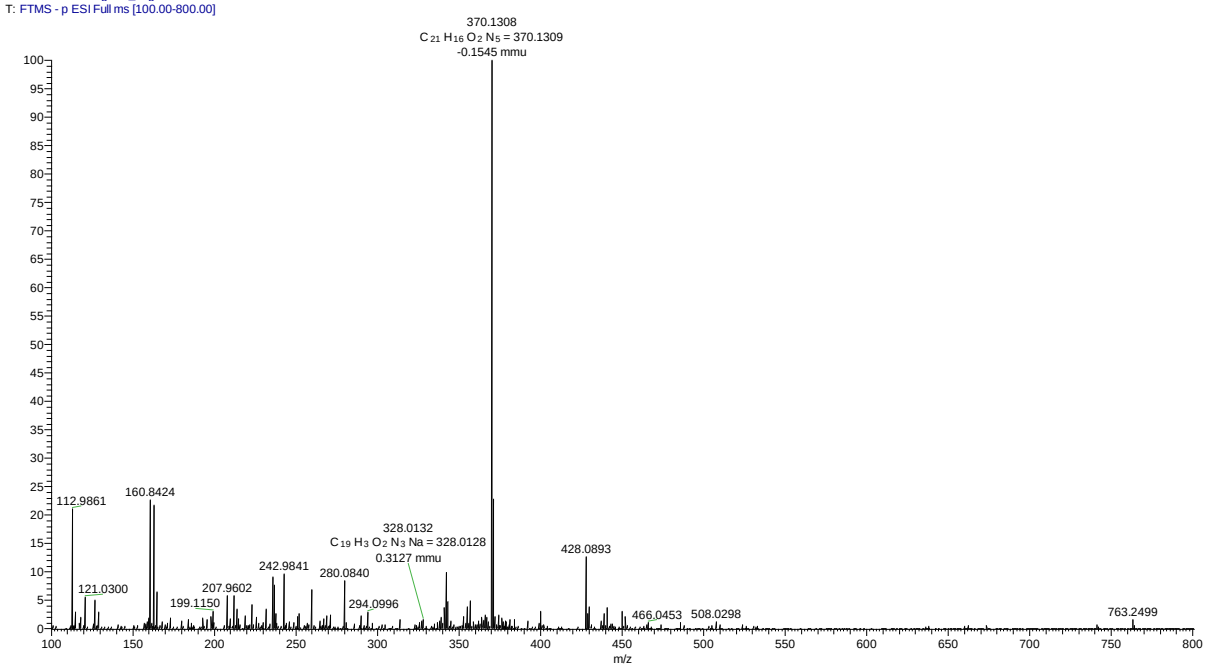

9.4.4 4-((3,5-dimethoxybenzyl)amino)-4'-(1*H*-tetrazol-5-yl)-[1,1'-biphenyl]-3-carboxylic acid (32)

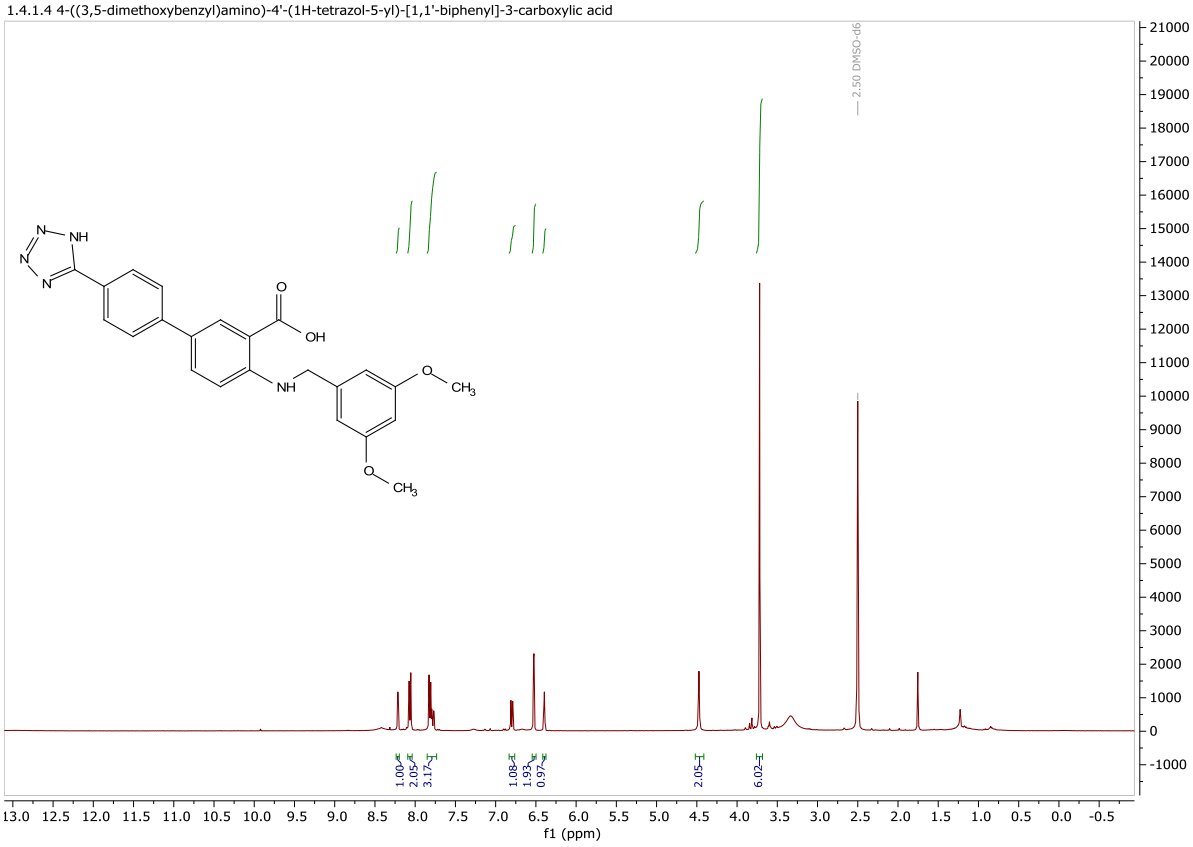

1.4.1.4 4-((3,5-dimethoxybenzyl)amino)-4'-(1H-tetrazol-5-yl)-[1,1'-biphenyl]-3-carboxylic acid

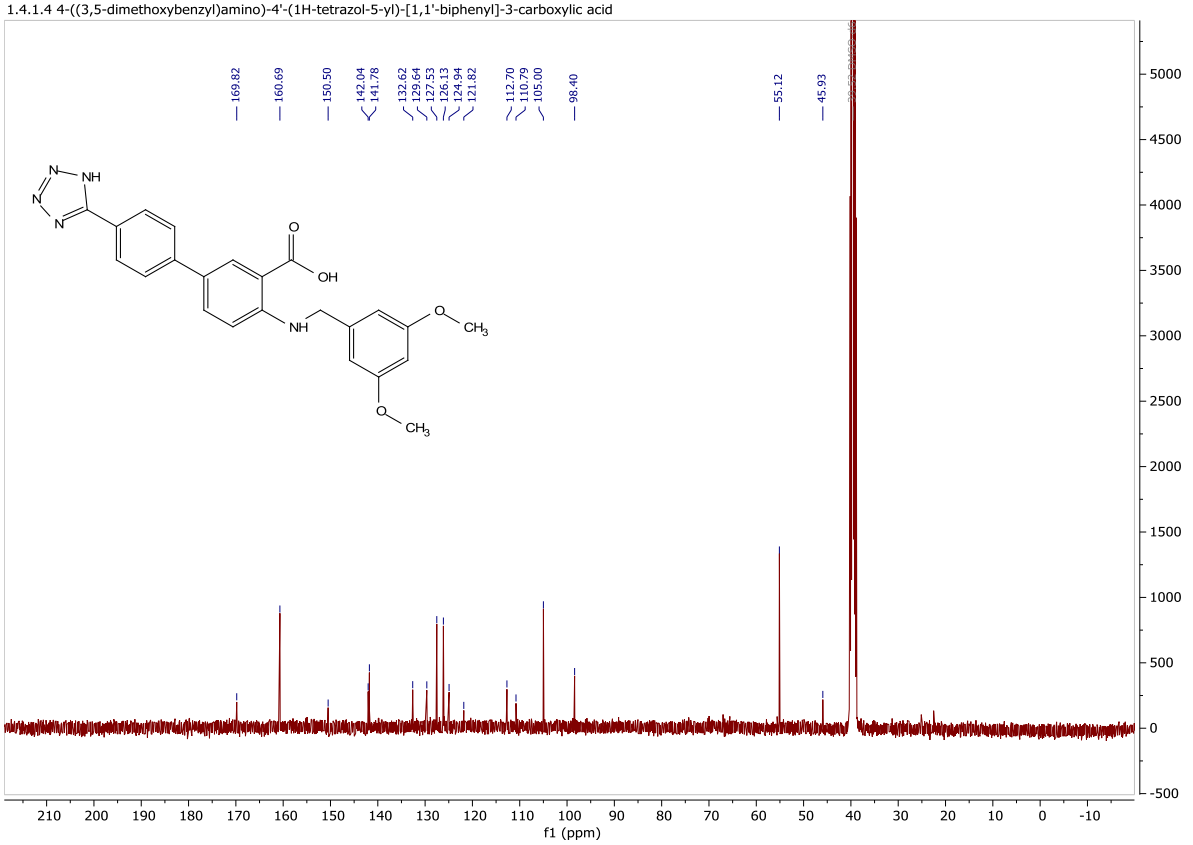

abhm100651good_neg #1-8 RT: 0.01-0.24 AV: 8 NL: 1.72E6
T: FTMS - p ESI Full ms [113.00-700.00]

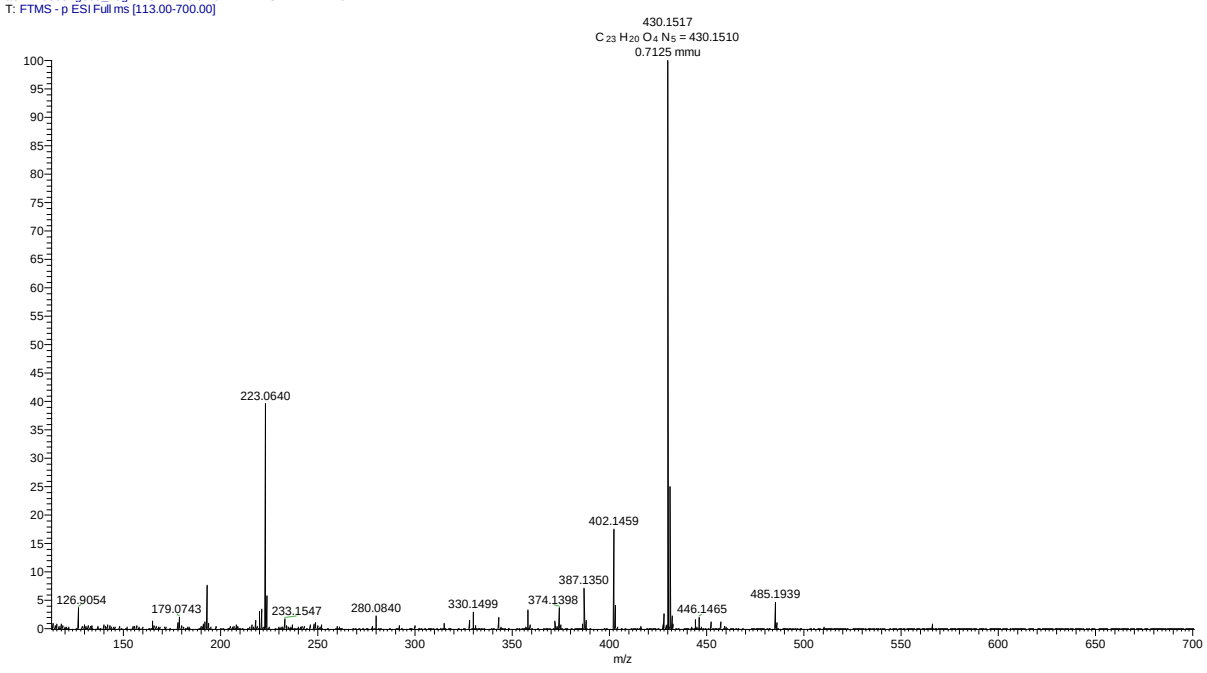

Agilent Technologies

Sample ID:	abhm100651	Method Name:	ATR-default
Sample Scans:	4	User:	IK
Background Scans:	4	Date/Time:	4/13/2020 2:37:30PM
Resolution:	8 cm-1	Range:	4,000.00 - 650.00
System Status:	Good	Apodization:	Happ-Genzel
File Location:	C:\Program Files\Agilent\MicroLab PC\Results\Rune\abhm100651_2020-04-13T14-39-10.a2r		

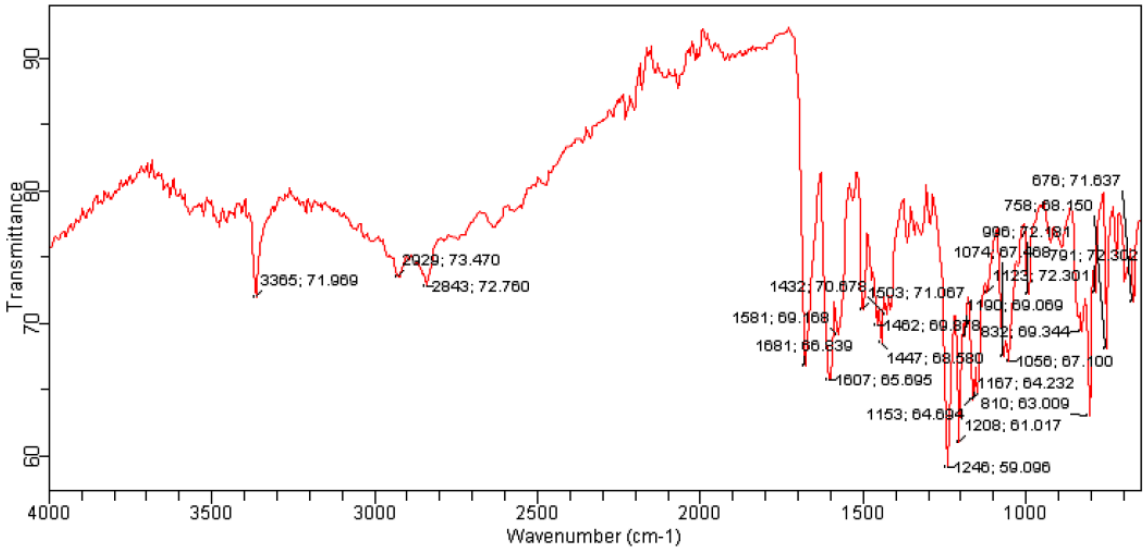

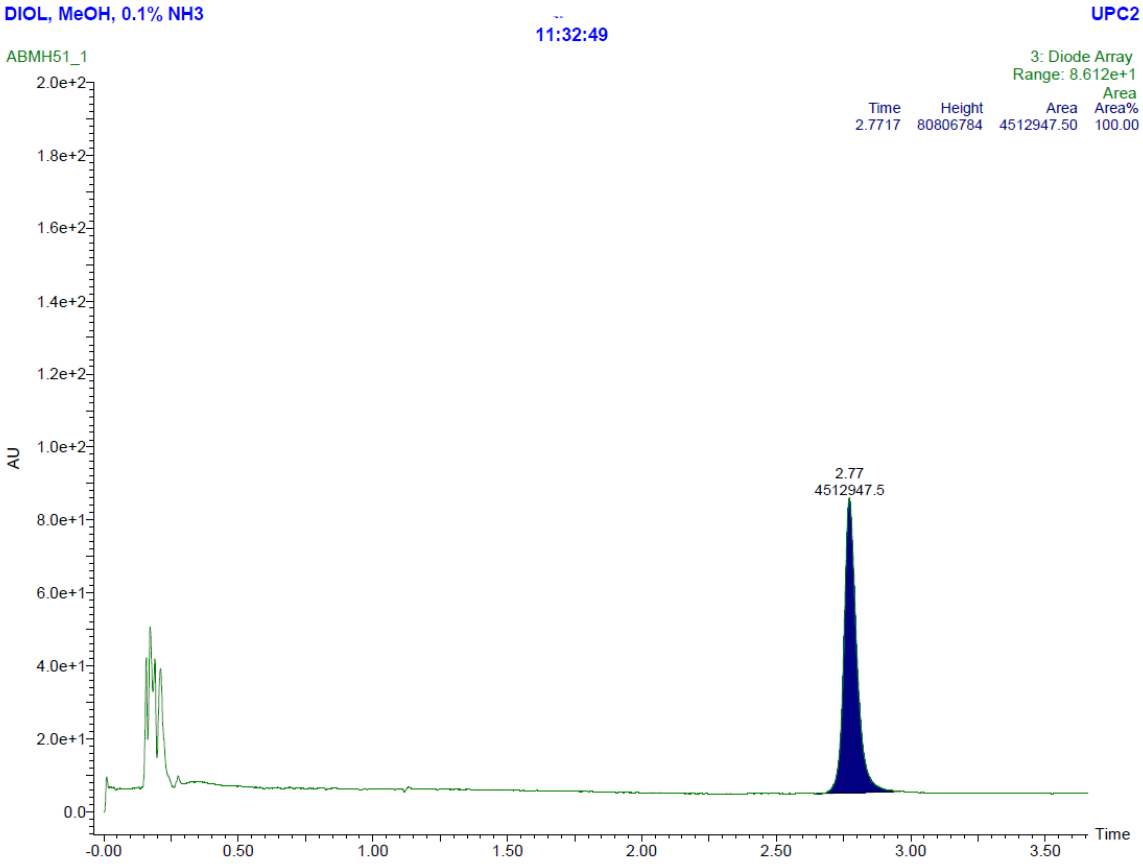
DIOL, MeOH, 0.1% NH3
11:32:49
UPC2
ABMH51_1
3: Diode Array
Range: 8.612e+1
Time Height Area Area%
2.7717 80806784 4512947.50 100.00
2.77
4512947.5
AU
Time
2.0e+2
1.8e+2
1.6e+2
1.4e+2
1.2e+2
1.0e+2
8.0e+1
6.0e+1
4.0e+1
2.0e+1
0.0
-0.00
0.50
1.00
1.50
2.00
2.50
3.00
3.50

9.5 Suzuki-Miyaura Screening Spectra

The SMC screening was carried out based on the following crude ^{1}H NMR spectra.

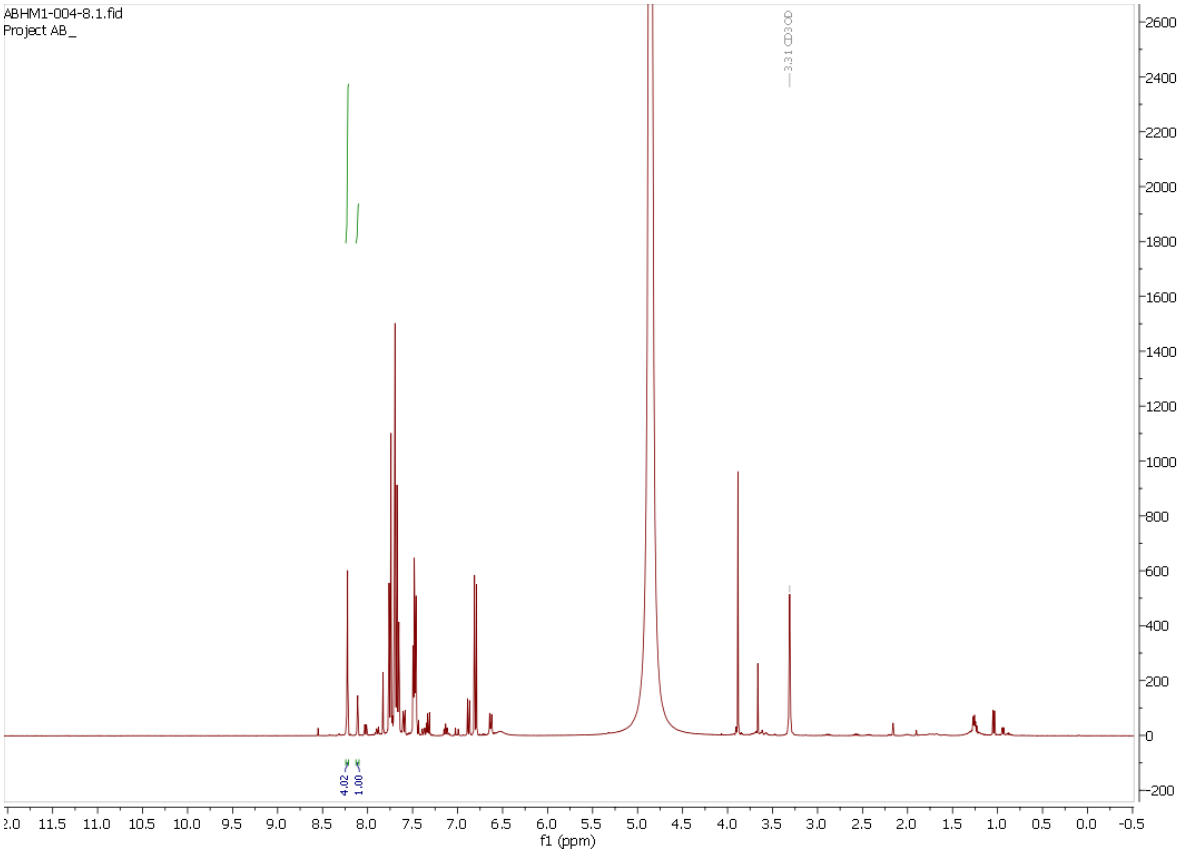

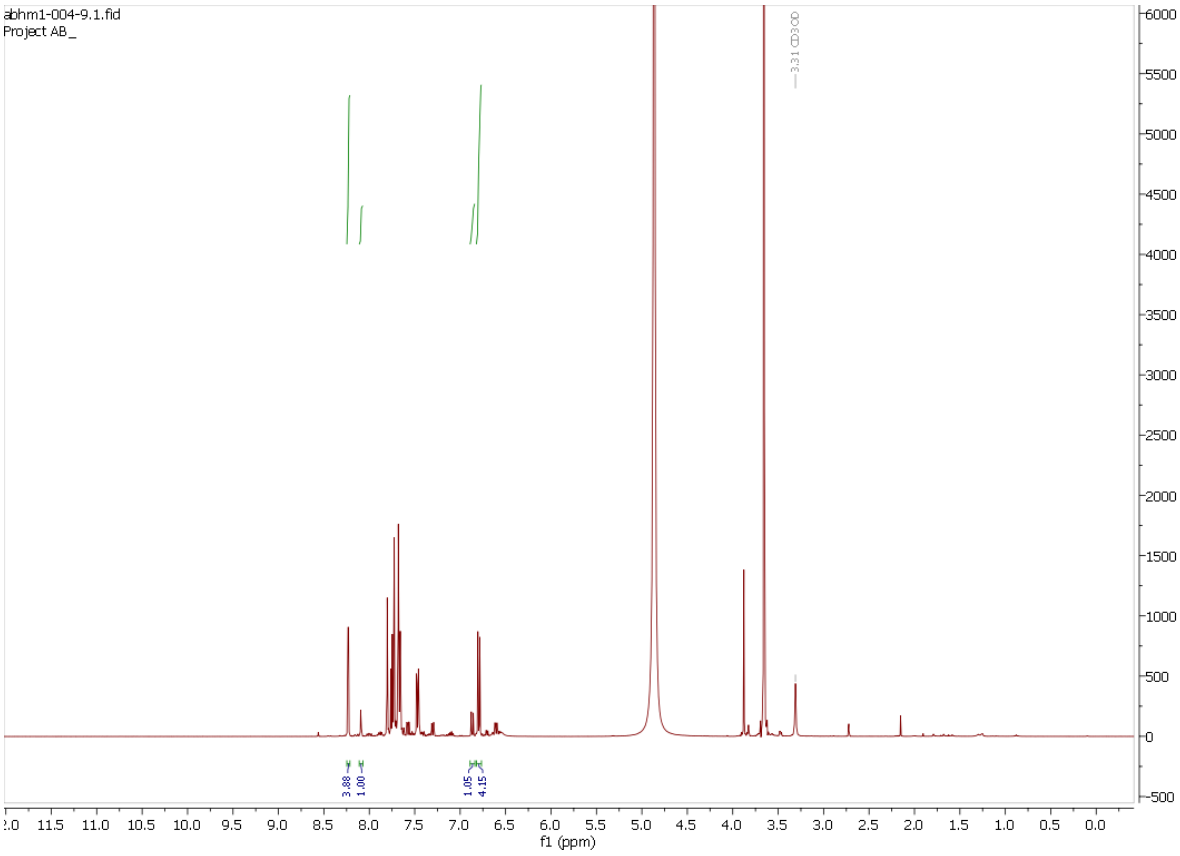
abhm1-004-9.1.fid
Project AB_
3.31 CD3OD
3.88
1.00
1.05
4.15
f1 (ppm)

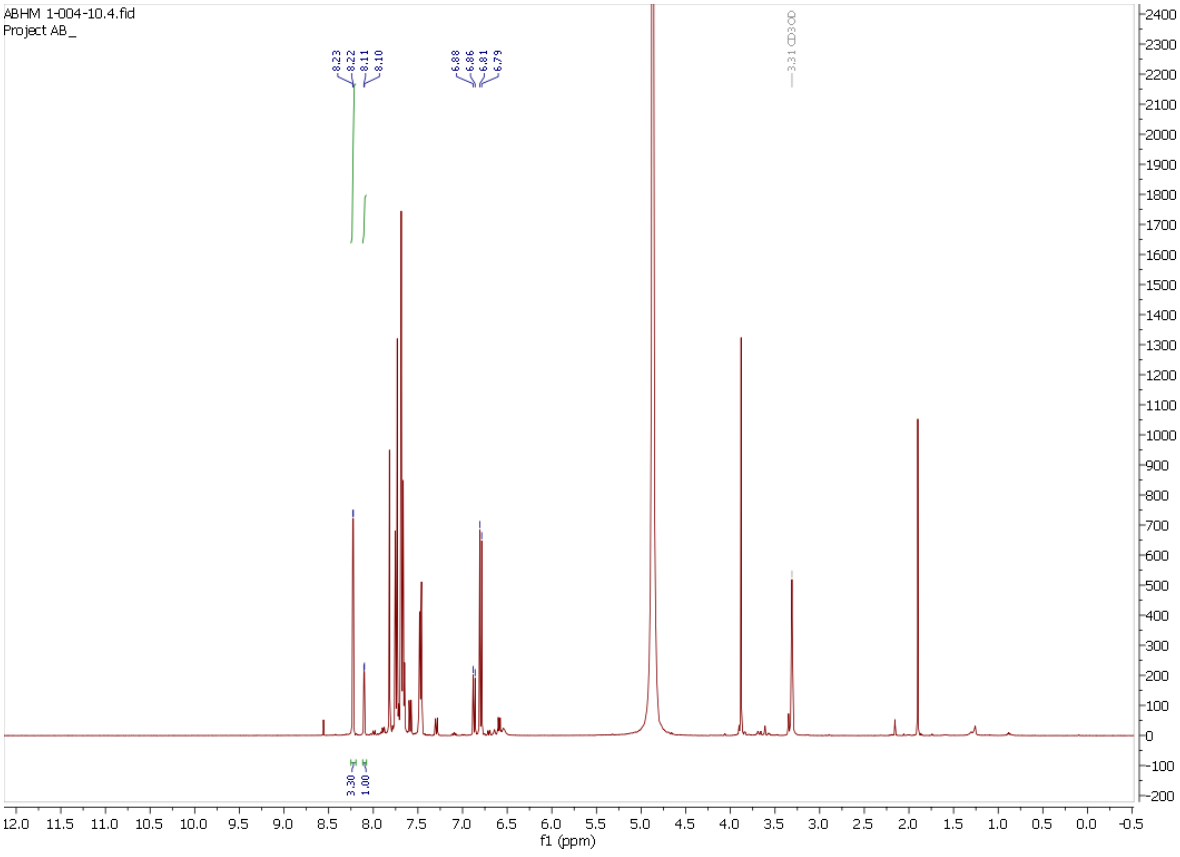
ABHM 1-004-10.4.fid
Project AB_
8.23
8.22
8.11
8.10
6.88
6.86
6.81
6.79
3.31 CD3OD
3.30
1.00
f1 (ppm)

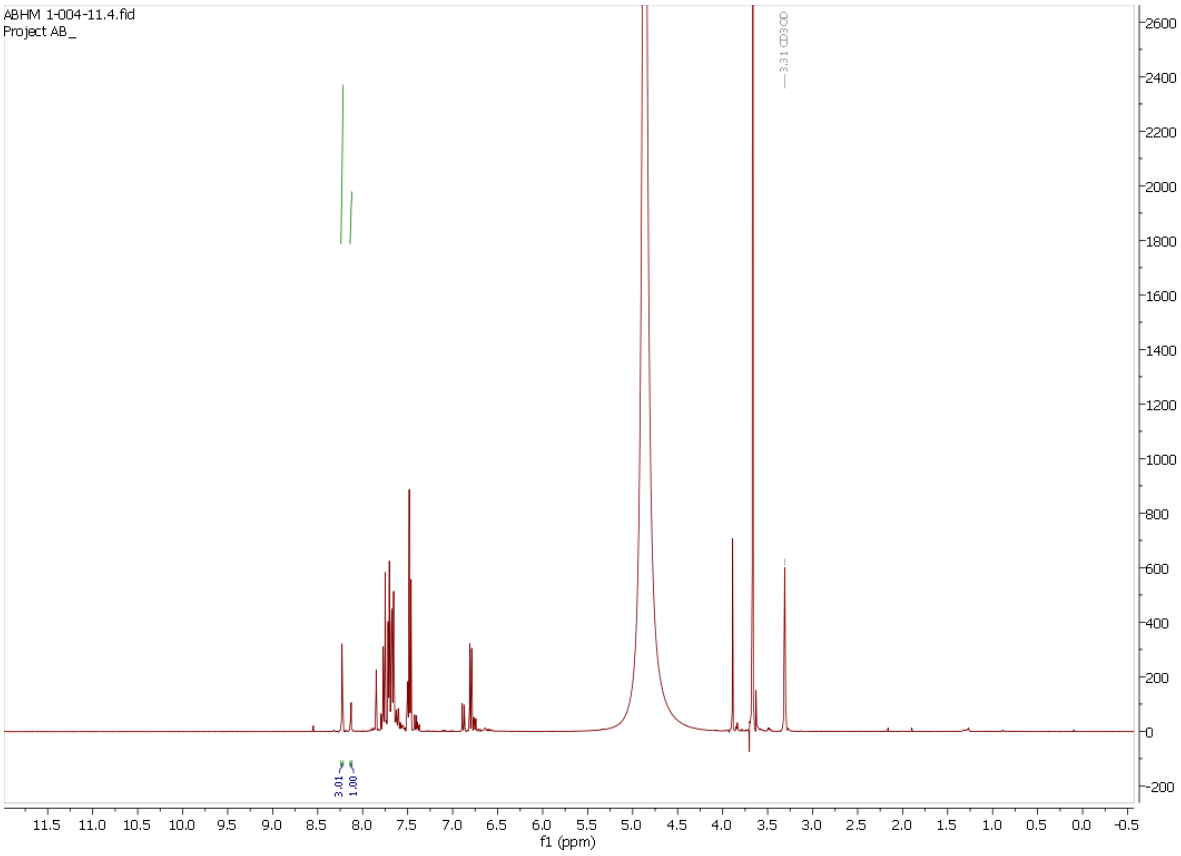
ABHM 1-004-11.4.fid
Project AB_
3.31 CD3OD
3.01
1.00
f1 (ppm)

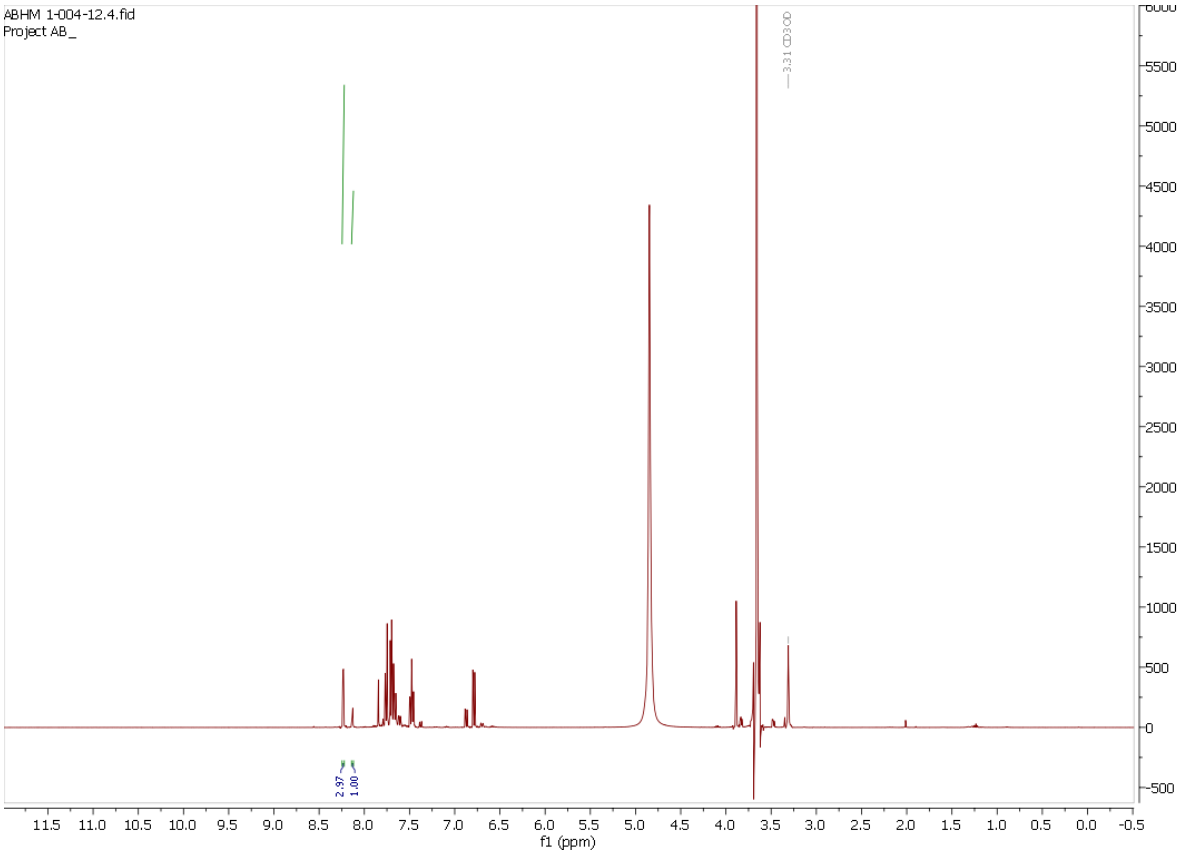
ABHM 1-004-12.4.fid
Project AB_
3.31 CD3OD
2.97
1.00
f1 (ppm)

9.6 SeeSAR experimental

The version of the software used was SeeSAR version 9.2; BioSolveIT GmbH, Sankt Augustin, Germany, 2019, https://www.biosolveit.de/SeeSAR.

The enzyme used was 5QAV from PDB, which is the OXA-48 enzyme in complex with compound **1**. SeeSAR defines compound **1** with the following name: L43_D_301, which was used to define the binding site automatically by SeeSAR. The binding site was lacking enough dept in the OUT pocket and additional residues were thereby added, for a total of 39, which can be seen in Figure 28.

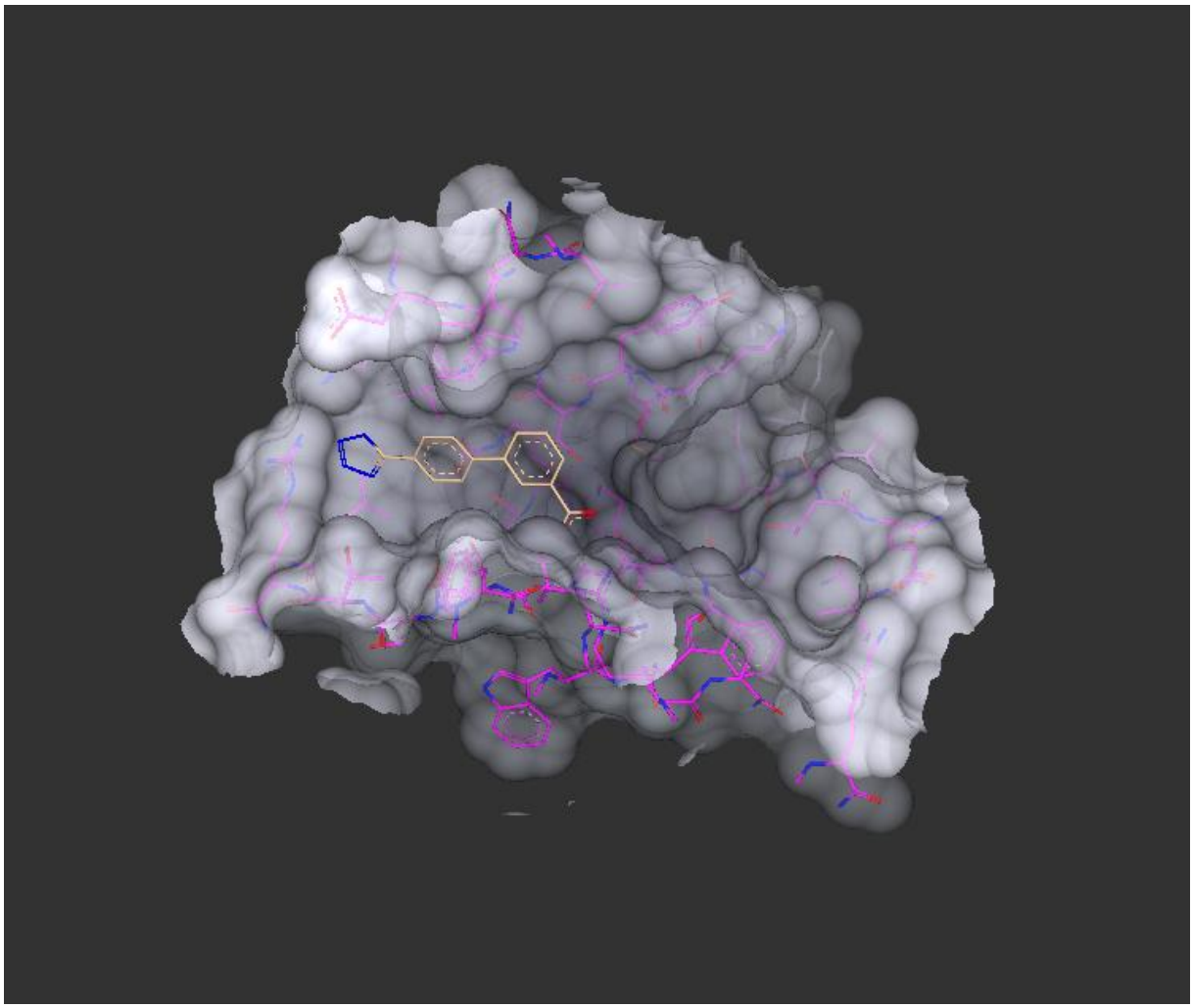

Figure 28. Custom defined binding site around L43_D_301 inhibitor

By using the "docking mode" molecules were drawn and imported from Chemdraw. On average ten poses was generated for each molecule, before calculating the estimated affinity,

torsion quality, molecular clashes, optibrium properties, Ligand lipophilic efficiency (LLE) and more. The results were resulted in a list, seen in Figure 29.

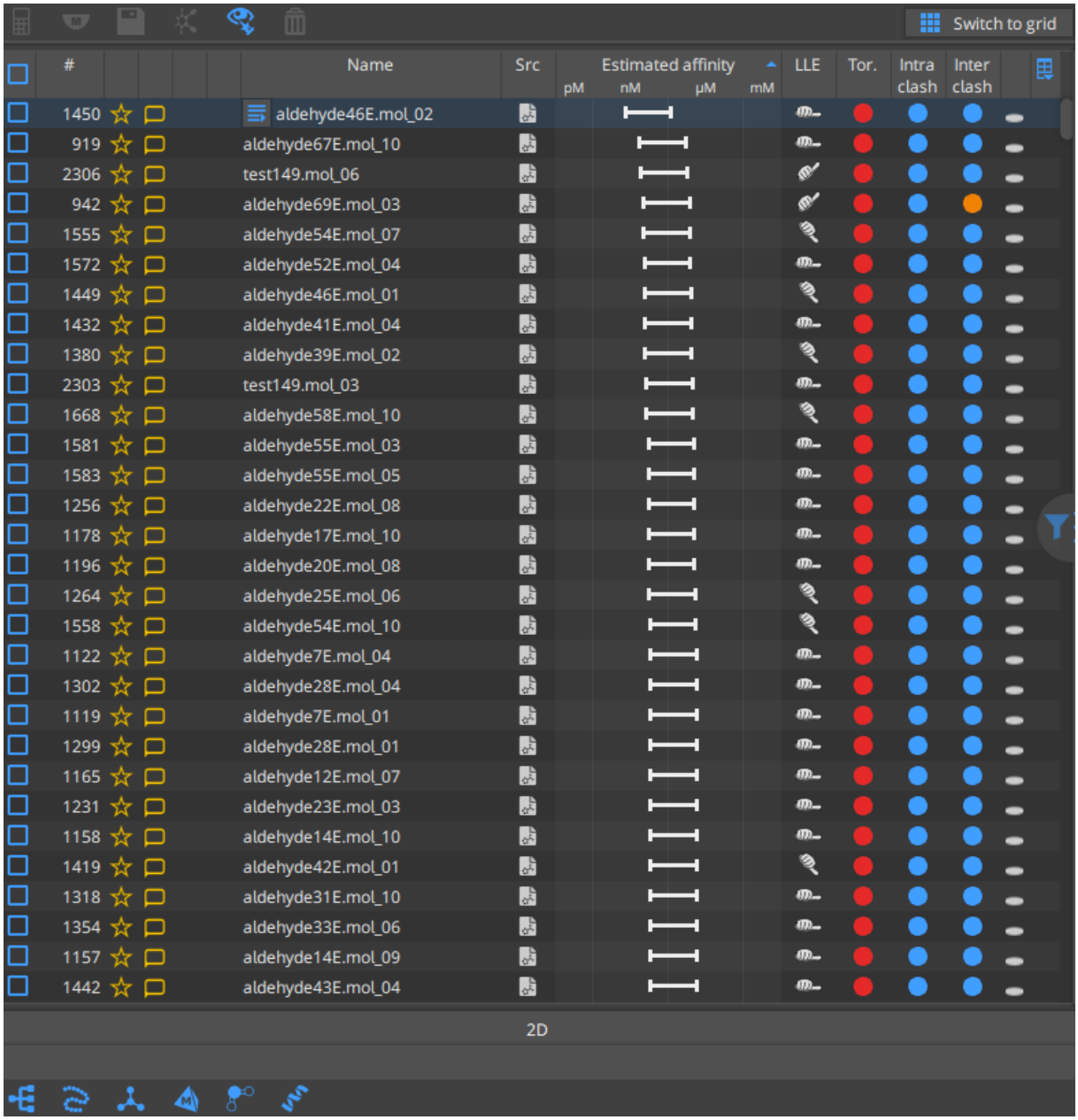

Figure 29. Example list of SeeSAR results